Cranfield University

Richard Dudeney

Electrochemical Method for the Determination of Arsenic *in the field* using Screen-printed Gold Electrodes

Cranfield Health

PhD Thesis

2007/2008

Cranfield University

Cranfield Health

Analytical Science and Informatics

Doctor of Philosophy

Academic Years 2005-2008

Richard Dudeney

Electrochemical Method for the Determination of Arsenic *in the field* using Screen-printed Gold Electrodes

Supervisors: Dr S.J. Setford (2005-2006), Dr J.D. Newman (2007-2008),
Dr I.E. Tothill (2007-2008)

February 2008

This thesis is submitted in partial fulfilment of the requirements for the Degree of PhD

Abstract

This project describes development and problem solving efforts to realise a viable portable sensor for arsenic, applicable to drinking water. The work is the first dedicated effort towards this goal, after the preliminary investigations previously conducted at Cranfield University (Cooper, 2004 and Noh, 2005). Using polymeric gold ink BQ331 (DuPont Microcircuit Materials, Bristol, UK) as working electrode on screen printed strips, the electrochemical procedure was studied. Due to the wealth of research on electrochemical and non electrochemical methods for arsenic determination, this project attempts to capitalise on the unique advantages of the screen-printed gold surface.

In particular, the issues surrounding the performance of the sensor were evaluated by electrochemical and spectroscopic means (including infrared, nuclear magnetic resonance and X-ray photoelectron spectroscopy). A number of custom screen printed electrodes were prepared *in house* comparing sensor performance on compositional factors. An interference coming from silver interaction with chloride in the reference electrode was identified. As such, the design of the sensor needs to change to include either an immobilising layer, such as Nafion, over the silver, or to omit screen-printed silver altogether. The Nafion was presumed to work by excluding (or at least much reducing) the passage of negatively charged chloride ions to the silver surface preventing formation of soluble silver chloride complexes.

The design of the sensor was considered in light of performance and sensitivity. The screen-printed electrodes were cut to facilitate a microband design lending favourable diffusive to capacitive current characteristics. With this design, As(III) detection was demonstrated comfortably at 5 ppb (in a copper tolerant 4 M HCl electrolyte) without electrode need for additional preparation procedures. This is below the World Health Organisation (WHO) guideline and United States Environmental Protection Agency (USEPA) regulation level of 10 ppb in drinking water. The electrode materials are already mass manufacturable at an estimated cost less than £ 0.5 per electrode. The

microband design could, in principle, be applied to mercury and other metal ions. The procedure for As(V) either with chemical or electrochemical reduction and determination still needs to be assessed. However, the presented electrode system offers a viable alternative to the colorimetric test kits presently employed around the world for arsenic in drinking water.

Also, the Nicholson Method (Nicholson, 1965a), used for characterising electron transfer kinetics at electrode surfaces, was extended for application to rough surfaces using a fractal parameter introduced by Nyikos and Pajkossy (1988). This work includes mathematical derivation and numerical evaluation and gives a number of predictions for electrochemical behaviour. These predictions could not be tested experimentally, as yet, since the physical conditions must be carefully controlled.

Acknowledgements

The author would like to thank:

Dr Steve Setford for advice and supervision during the first two years of this project. Dr Jeff Newman and Dr Sam Tothill for supervision during the final year. Vince Arancio, Trevor Combes and Keith Stanley of DuPont Microcircuit Materials (Bristol, UK) for the advice and supply of the sensors used in the project, often free of charge.

Dr Ramin Pirzad for business oriented advice and willingness to push the project forward. Also, kind help and advice in the laboratory from Dr C. Walton, D. Pitts, P. Knight, Dr L. Ritchie, Dr M. Whitecombe, Dr M. Cauchi, Dr I. Sanchez and Dr G. Saint-Pierre. Professor T. Pajkossy (Budapest University of Technology and Economics, Hungary) for advice and reading through a draft paper on electrochemistry of rough surfaces.

Finally, I would like to thank my parents for their support and my mum, in particular for reading through a majority of this thesis.

Contents

List of Tables

List of Figures

Abbreviations and Symbols

AAS – atomic absorption spectroscopy
AES – Auger Electron Spectroscopy
ASTM – American Society for Testing and Materials
ASV/CSV - anodic / cathodic stripping voltammetry
ATAAS – Atomic trapping atomic absorption spectroscopy
ATR – Attenuated total reflectance
BAS - Bio Analytical Systems (West Lafayette, US)
BHT – butylated hydroxytoluene, common anti oxidant
BCR - Bureau Commun de Reference, soil extraction protocols
BQ164 – DuPont polymeric Silver-silver chloride ink
BQ221 – DuPont polymeric carbon ink
BQ242 – DuPont polymeric carbon ink
BQ331 - 'Biomedical Quality' polymeric gold ink for medical electrodes (DuPont Microcircuit Materials, Bristol, UK)
C2041206D2 – Gwent Gold polymeric ink
CCAS – Constant current anodic stripping
CE – counter electrode
CV – cyclic voltammetry
CVAAS – Cold vapour atomic absorption spectroscopy
DCAAS – Direct atomic absorption spectroscopy
DMF – Dimethyl formamide
DMSO – dimethylsulfoxide
DPASV/DPCSV – differential pulse anodic stripping voltammetry/ differential pulse cathodic stripping voltammetry
DTGS – Dueterated triglycine sulphate (infrared detector)
EDX – Energy dispersive x-ray spectroscopy (also EDAX)
Electrodag 423 ss– Acheson polymeric carbon ink
Electrodag 6038 ss – Acheson polymeric silver-silver chloride ink
Elvacite 2048 – Trade name for methyl methacrylate resin
EMF – electro motive force
EPA – Environmental Protection Agency (US)
ESCA – Electron spectroscopy for chemical analysis
ETAAS – Electrothermal atomic absorption spectroscopy
EXAFS – Extended X-ray absorption fine structure
FAAS – Flame atomic absorption spectroscopy
FTIR – Fourier transform infrared spectroscopy
GC – gas chromatography
GDE – gold disk electrode
GPES – Software for controlling Autolab (Windsor Scientific, Slough, UK)
HDME – Hanging drop mercury electrode
HGAAS – Hydride generation spectroscopy
HPLC – High performance liquid chromatography
ICP – Inductively coupled plasma
INAA – Instrumental neutron activation analysis
iR – potential correction due to current I through resistance R

IR – infrared
LF141 – Trade name for high temperature screen- printed gold ink (DuPont, Bristol)
MCT – Mercury cadmium telluride (infrared detector)
MS – mass spectroscopy
NHE – Normal hydrogen electrode
NMR – Nuclear magnetic resonance
PDMS – polydimethylsiloxane (silicone oil)
PEO – polyethylene oxide (or poly ethylene glycol)
PET – polyethyleneterephthalate
PF – potassium ferrocyanide
Pgstat xx – Autolab potentiostat model (Windsor Scientific, UK)
PMMA – polymethylmethacrylate
PSAN – polystyrene-co-acrylonitrile
PSA – potentiometric stripping voltammetry
PTF – polymer thick film
PVA – polyvinylacetate
PVC – polyvinylchloride
PVOH – polyvinylalcohol
PVP – polyvinylpyrrolidone
R-464 (DPM-78) – Ercon polymeric gold ink
R430 – DuPont polymeric carbon ink
R471 – DuPont polymeric carbon ink
RE – reference electrode
RSD – relative standard deviation
SAM – self assembling monolayer
SCE – Saturated Calomel Electrode
SCEM – Scanning Electrochemical Microscopy
SEM – Scanning electron microscopy
SHE – Standard hydrogen electrode
SPE – screen- printed electrode; referring to < 200 ºC curing on flexible substrate as opposed to high temperature ceramic based electrodes
SS – solid state (referring to standard gold/platinum/carbon/silver-silver chloride electrodes as opposed to screen- printed electrodes)
SWASV – Square wave anodic stripping voltammetry
TEOS – Tetra ethoxysilane
UCAR VAGH – trade name for vinyl resin (Union Carbide, UK)
UNICEF – United Nations International Children's Emergency Fund
US EPA – United States Environmental Protection agency
UV – ultra violet
WDX wavelength dispersive X-ray
WE – working electrode
WHO – World Health Organisation
XANES – X-ray absorption near edge spectroscopy
XPS – X-ray photoelectron spectroscopy (also ESCA)
XRF – X-ray fluorescence spectroscopy

Mathematical Symbols

α	electron transfer constant
β	fractal parameter
γ	square root of the ratio of oxidised and reduced diffusion constants
δ	(i) size of integration step; (ii) diffusion length
ε	alternate fractal parameter equal to twice β
θ	initial concentration ratio
λ;	(i) length scale; (ii) time for one half scan
λ_i; λ_O	inner cut off length for roughness; outer cut off length
ξ	dimensionless parameter dependent only on fractal parameter β
ρ	(i)density
σ	coefficient
τ	(i) characteristic time scale (ii)substitute time variable
υ	(i) scan rate; (ii) number of integration/summation unit from 0 to n
χ (chi)	dimensionless current function
ψ (psi)	dimensionless kinetic parameter
ΔE_p (also dEp)	peak to peak separation
Γ	gamma function
Φ	particle flux
a	scan rate dimensionless parameter
dE	potential step of integration
g	dimensionless geometrical constant
i	(i) current (ii) integration/summation counter
j	current density
k	constant
k_f; k_b	rate constant for forward and backward reactions
k_s	standard rate constant
l	length
n	(i) number of electrons (ii) discrete integration counter
n_e	number of electrons
n_s	Scan number
r	radial spatial coordinate
v	scan rate
y	dimensionless time parameter
z	substitute dimensionless time parameter
A	area

C; C^*; C_O;C_R;C^s	concentration; initial concentration; concentration of oxidised species; and for reduced species; surface concentration
C_p	Capacitance
D; D_O; D_R	diffusion constant; for oxidised species; and for reduced species
D_f	Hausdorff dimension
E; E^0; E_i; E_f; E_λ	electrode potential; formal potential; initial; and final potential; switching potential
F	Faraday constant
J	particle flux density
M	range of integration
N	number of integration steps
R	(i) resistance; (ii) spherical/ cylindrical electrode radius; (iii) molar gas constant
T	temperature
S_λ	dimensionless parameter for potential sweep

Chapter 1 Introduction and Literature Review

1.1 Introduction

The perception of environmental issues and health and safety is complex. It often undermines the physical reality with a variety of visceral opinions (for example, Pimm and Harvey, Nature, 414, p149, 2001: Book review on The Skeptical Environmentalist, Measuring the Real State of the World by Bjorn Lomborg). Fortunately, issues such as contamination by heavy metals of land and groundwater are straightforward by comparison with the projections of global warming or the effects of deforestation. There is no mention of arsenic by Lomborg (2001). That is not to say that arsenic and perception of its dangers have not been subject to controversy. The Bush administration was the last to delay the implementation of the 10 ppb limit for arsenic in drinking water, first proposed by the United States Environmental Protection Agency (US EPA) in 1962, implemented in 2002 and requiring compliance from 2006 (Smith *et al.*, 2002), citing cost-risk benefit, not out of place in the style of Lomborg (2001). This was in stark contrast to the estimated cancer related risks of drinking water at the previous compliance level of 50 ppb when compared with other high priority pollutants (Smith *et al.*, 2002).

The Blacksmiths Institute (an international charity, working with available information from governments and non governmental organisations) has published a report (Blacksmiths Institute, 2008) of the ten most heavily contaminated sites, for which it obtains funds to help remediation. These sites are in poorer regions of the world: Russia, China and India each have two sites; Azerbaijan, Peru, Zambia and the Ukraine each have one site. It is clear that, although large numbers of people are at risk, the majority are relatively poor, and so less likely to provide the market demand needed for commercial research and development in the developed world. Arsenic, along with mercury and lead, is amongst the highest priority pollutants at these sites. Whilst remediation is evidently the main priority, effective analysis is also required.

Initially for this project, the intention was to use prefabricated screen-printed sensors to detect a range of metals in soil and water samples. It was thought that the principle difficulty would be the complexity of the matrices, considering the range of aqueous extraction procedures and availability of metals to those fractions. Using mercury and/or bismuth coated carbon electrodes for copper, cadmium and lead on the one hand, and the newer gold sensors for arsenic and mercury on the other, coupled to a 4-channel portable potentiostat, (designed *in-house*, to be used with a PDA or inbuilt display) would facilitate the development of a rapid screening device for multiple metals *in-situ*. However these intentions were not addressed in this work for reasons that will become apparent.

Prior to this work, the recently introduced gold polymeric ink, BQ331 (DuPont Microcircuit Materials, Bristol, UK) was assessed for the determination of arsenic and mercury. Excellent sensitivity was reported (Cooper, 2004) and a patent was published (Bolbot *et al.*, 2007). However, it has been found that gold polymeric inks are also produced by, Ercon, Inc. and Gwent Electronic Materials; at least one other researcher was working on the detection of arsenic (Noh, 2005).

During the course of this project the focus centred on arsenic due to the world wide problem and associated market demand for a reliable analytical method.

According to anecdotal evidence at Cranfield, the perception among some funding bodies is that technology for screen-printed sensors has matured. Also, according to a review by Hart *et al.,* (2004), *Designs and developments of Screen-Printed Carbon Sensors/Biosensors for Biomedical, Environmental and Industrial Analyses*, many electrode systems have reached *proof of concept* but not necessarily commercial application.

1.2 Environmental Law and Regulation

The law must account for human safety as well as the environment itself. The Act for punishing nuisances which cause corruption of the air near cities and great towns,1388, contained the following (Lane & Peto, 1995):

"For that so much Dung and Filth of the Garbage and Intrails as well of Beasts killed…be put in Rivers and other Waters…the Air there is greatly corrupt…and if any do he shall be called before the Chancellor…and shall be punished after the discretion of the Chancellor."

This early English example shows that the system of law threatened to punish those who compromised the safety of others through negligent acts. The preface to an undergraduate text for law students includes the following insight,

"…environmental problems are first and foremost problems of the affluent society, which is very complex and complicated. And the number of environmental standards is increasing, simply by the fact that the emission of pollutants into the air, the water or the soil can no longer be seen as an activity which can take place uncontrolled" (Thornton & Beckwith, 1997).

Though we cannot ascribe pollution to a particular cause or wrong doing, managing the problems of pollution is the responsibility of society as a whole. Society's affluence is rarely unconnected with its infringement on the environment which sustains it. Often the burden to remediate depends on the ability to both recognise the problem and then remediate. Intentions where we do not have, or are able to acquire, proof, inevitably reflect uncertainty:

'Like many legal terms, the term "environmental law" may be seen as having a central "core of meaning" surrounded by what may be called a "penumbra of uncertainty"' (Thornton & Beckwith, 1997).

Practical restrictions on pollution into the environment have developed since the 1970s, as its effects, due to anthropogenic activity, have become clear. Where as safeguards for health and sanitation have existed for centuries, the law has, more recently, come to safeguard the natural environment in its own right.

Legislation provides a framework of broader principles in which an organisation such as the Environment Agency serves to implement specific environmental requirements. These requirements may be demanded of individuals or organisations. In relation to contaminated land the Contaminated Land Act 1995 (in the UK) establishes the framework.

"Contaminated land is defined in the Act by reference to 'significant possibility' of such harm being caused to human health or property or the health of other living organisms or the pollution of controlled waters." (Lane & Peto, 1995)

Polluted land requires clean up or containment which may include methods such as: soil removal, separation or washing; physical containment with a barrier, cementing or vitrification; electrochemical treatment; phytoremediation or covering. The costs were compared in a study in 2001 by Mulligan *et al.* The cheaper methods, per ton of contaminated land included physical containment such as land fill covers and slurry walls (10 - 90 $US/ton) and soil washing with salts and surfactants for leachable components (25 - 300 $US/ton). More expensive methods included pyrometallurgy to drive off volatiles (400 - 700 $US/ton) and vitrification to seal contaminant in glass like containment (200 - 1000 $US/ton). The electrochemical method is in experimental stage. Phytoremediation can only be applied to shallow contamination, long time frames and where the soil is otherwise fertile enough to support growth (Mulligan *et al.*, 2001).

In the UK, the Environment Agency has the task of identifying responsible parties, where they exist. The definition of contaminated land and the harm associated with; who provides guidance and interpretation of the framework; and the potential of the

individual or organisation to respond to demands; all require clarification where legal disputes are involved (Lane & Peto, 1995).

What constitutes harm is open to question. The law is there to moderate human activity which occurs principally in urban and industrial areas. Therefore, human health and safety is normally the primary concern. For protection of the Environment in its own right, further guidance can be found (Lane & Peto, 1995):

"'Harm' includes protection to wildlife but not over and above existing populations. Also does not include offences to the senses such as a smell."

Guidance also must be flexible as perceived dangers change; interpretation of the framework contained within the Environmental Act 1995, is provided by the Secretary of State: what harm is regarded as significant; whether the possibility of significant harm being caused is 'significant'; and whether the pollution of controlled waters is being, or is likely to be caused. When polluted land has been identified guidance is provided regarding action to be taken by the Environment Agency (Lane & Peto, 1995):

Air and water pollution are universally accepted issues, but land contamination receives mixed concerns. USA, The Netherlands and Britain recognise risks and impose legislation; many countries do not recognise a problem. Global warming and the thinning of the ozone layer have overshadowed problems associated with contamination, in part explains why legislation has taken effect only in the last decade (Cairney & Hobson, 1998).

The Dutch have taken a firm line stating action is required to safeguard human and environmental health. Therefore there is a strong driving force in the Netherlands to produce effective systems for identifying and remediating contaminated land; the New Dutch List contains allowable levels of toxic trace substances in soils, as shown for heavy metals in Table 1.1. The attitude adopted in the Netherlands is in part due to

the dense population and the need to keep the shallow groundwater resources clean (Cairney & Hobson, 1998).

Table 1.1 The new Dutch List (1996) regulations for heavy metals in soil and water samples

Contaminant	Soil Sediment (ppm dry weight)		Groundwater (ppb)	
Metals	optimum	action	optimum	action
Arsenic	29	55	10	60
Barium	200	625	50	625
Cadmium	0.8	12	0.4	6
Chromium	100	380	1	30
Cobalt	20	240	20	100
Copper	36	190	15	75
Lead	85	530	15	75
Molybdenum	10	200	5	300
Nickel	35	210	15	75
Mercury	0.3	10	0.05	0.3
Zinc	140	720	65	800

Britain has a less stringent approach and views remediation in terms of safe redevelopment; the term “significant harm”, allows a degree of flexibility whilst maintaining an air of caution. In practice many contaminated industrial sites, as many as 90% (Cairney & Hobson, 1998), do not, by law, require remediation as they would under the Dutch conventions. The contaminated land exposure assessment (CLEA) was brought into effect in 2002; the present guideline limits are shown Table 1.2.

Table 1.2CLEA regulations for heavy metals applicable in the UK (Environment Agency, 2002)

		Arsenic	Mercury[b]	Lead	Chromium	Cadmium
Oral	[c]ppb bw /d	0.3	0.26		2.8	0.77
Inhalation	[c]ppb bw /d	0.002	0.3		0.001	0.001
residential with plant uptake	ppm	20	8	450	130	1;2;8[a]
residential without plant uptake	ppm	20	8	450	200	30
Allotments	ppm	20	15	450	130	1;2;8[a]
Commercial/ industrial	ppm	500	480	750	5000	1400
Blood level				10		

[a] values in triplicate for pH 6, 7 and 8; [b] specified for inorganic mercury; [c] ppb based on body weight, per day

The USA is less certain than the Netherlands as to what constitutes contamination; however, the litigation processes, in what is a wealthy country, are enforced and severe (Cairney & Hobson, 1998). Therefore many of the methodologies for analysis are American in origin; in particular the United States Environmental Protection Agency (US EPA) is a useful source for analytical techniques and protocols. The heavy metal limits for drinking water are given in Table 1.3.

Table 1.3 US EPA Regulations for Heavy Metals in Drinking Water (EPA, 2006)

Metal	**Drinking water (ppb)**
Arsenic	10
Lead	15
Antimony	6
Cadmium	5
Chromium	100
Copper	1300
Mercury	2
Selenium	50
Beryllium	4

The standards utilised have typically been given by absolute metal concentrations for which the USA, Netherlands and UK have had some criticism, particularly in light of the high costs involved. Large disparity maybe seen between actual risks and the

clean up work that is enforced since resources and environmental concerns could be better served with more intelligent standards and the differing responses to contaminated land serve to highlight the inconsistencies. The use of absolute concentrations is not by itself a sufficient indication since the exposure mechanism such as leaching or biological has not been taken into account. The UK legislation, with the elliptical "significant harm" phrase, allows flexibility for making practical decisions as to the potential risks on site. However, in a commercial environment appropriate safeguards may not be enforceable.

1.3 Arsenic in the environment

The word arsenic is thought to date back to ancient Greece, the word meaning golden, describing the colour of orpiment which is bright yellow (Nriagu, 1994). Arsenic is Ranked 20th in abundance in the Earth's crust and found in many minerals. The prevalence of various metals is shown in Table 1.4. Arsenic occurs in higher concentrations than either cadmium or mercury but less than chromium.

Table 1.4 Presence of various metals in the Earth's Crust (Alloway *et al.*, 1990)

	Crust (mg/kg)	Igneous Rock (mg/kg)	Sedimentary Rocks (mg/kg)
As	1.5	1 - 1.5	1 - 10 (<900)
Cd	0.1	0.09 - 0.1	0.03 - 0.2 (<200)
Cr	100	4 - 3000	10 - 90
Cu	50	10 - 90	6 - 40
Hg	0.05	0.004 - 0.08	0.1 - 0.3
Pb	14	3 - 20	6 - 20

In the vicinity of humans, these metals are at relatively elevated concentrations from consumer electronics, old and residual paints, pesticides and fertilisers, and possibly batteries and many kinds of industrial products. Table 1.5 shows the levels of metals in some relevant situations. Operations such as mining and smelting can produce extremely high levels of all metals.

Table 1.5 Concentrations of metals in various human related materials (Alloway *et al.*, 1990)

	Sewage Sludge (mg/kg)	Fertiliser (mg/kg)	Farmyard Manure (mg/kg)	Compost Refuse (mg/kg)
As	3 – 30	2 – 1200	3 - 25	2 - 50
Cd	1 – 3400	0.05 – 200	0.1 - 0.8	0.01 - 100
Cr	8 – 40000	3 – 250	1 - 55	2 - 400
Cu	50 – 8000	1 – 300	2 - 200	10 - 3500
Hg	0.1 – 55	0.01 – 3	0.01 0.36	0.1 - 20
Pb	30 – 4000	2 – 200	1 - 30	1 - 2200

Arsenic is most associated with Fe, and S. Common minerals include realgar (AsS), orpiment (As_2S_3), arsenopyrite (FeAsS), arsenolite, (As_2O_3), and domeykite (Cu_3As) (Smedley and Kinniburgem, 2002).

A typical natural level of arsenic in soils is 5-6 ppm, though the levels can vary widely from 10 ppb to 1000 ppm depending on the mineral composition. Arsenic occurs predominantly in the valence states arsenate (As^{5+}) and arsenite (As^{3+}) in water and soils, but may also be found as the native As(0) and or as the volatile Arsine (As^{-}_{3}). Arsenic pollution occurs through both natural and anthropogenic causes as summarised in Table 1.6. The use of arsenic in commercial products such as paints, pesticides and preservatives has been virtually phased out. However, residual concentrations still remain in highly affected areas.

Table 1.6 Sources of Arsenic Pollution (Alloway *et al*., 1990)

Source Category	Residual presence	Significance
None	Usual low-level background	1~10 ppm
Natural Minerals	Arsenic associated with sulphide and iron minerals	10~1000 ppm
Volcanoes	Atmospheric deposition	Effect is dispersed,
Industrial	Gaseous residual of Copper, Smelting and Coal Combustion.	Effect is dispersed
	Coal burned ash residual Sewage Sludge, Mining ore-deposits	0~200 ppm
	Wind dispersal (mainly arsenic trioxide) and leaching Ground contamination	Effect dispersed, > 10000 ppm in local hotspots
Agricultural	Pesticides, Phosphate fertiliser, wood preservative, growth promotion animal feed (compounds such as cacodylic acid and lead arsenate)	200~2000 ppm

In water, arsenic forms an aqueous acid As(V) forms $AsO(OH)_3$, depending on the pH each of the hydroxyl groups maybe deprotonated. Similarly, As(III) forms $As(OH)_3$ with varying levels of protonation. At high acidities $As(OH)_2^+$ is also thought to exist (Arcand, 1957). The deprotonated forms of As(III) and As(V) are shown in Figure 1.1. As(III) is generally more soluble than As(V).

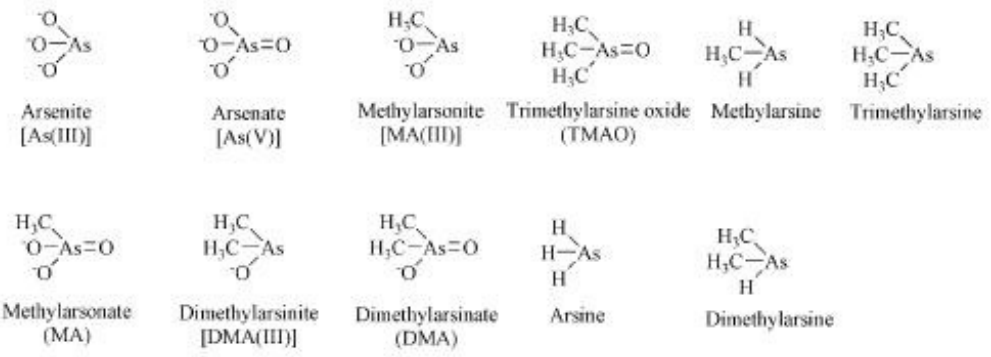

Figure 1.1 Inorganic and organic species of arsenic including -3, 3 and 5 valence states, taken from Francesconi and Kuehnelt (2004)

Whilst arsenic forms compounds with many common elements in clays, such as iron, aluminium, calcium, magnesium, manganese and nickel the solubility of these solids is significant: as high as 50 ppb (Nriagu, 1994). At usual levels arsenic is not affected by Cl^-, NO_3^- or SO_4^{2-} so unlike other metals arsenic forms few complexes in waters (Cullen and Reimer, 1989). But, a fluoride complex can form when F^- exceeds 1 ppm. The amount of solubilised arsenic is affected by pH, eH, biological activity and adsorption. But solubility equilibriums are generally poor indicators since the kinetic factors are slow.

Thermodynamically predicted ratios of As (V)/As(III) are generally very high, but rarely observed in natural waters where this ratio varies between 0.1 and 250. This difference is generally attributed to biological factors such as algae, fungi and bacteria. Low pH and anoxic conditions favours As(III). Addition of H_2S and Fe^{3+} had been noted to effect reduction of arsenate in a time period of about 10 hours (Cullen and Reimer, 1989).

Arsenic is typically immobilised in the presence of sulfur and iron hydroxides, such as those found on high surface area clays. Arsenic maybe mobilised into solution by one of several common processes, such as the example oxidation of arsenopyrite. Arsenic may also be dissolved due to reduction of iron compounds (Nikson *et al.,* 1998), bacterial action (Islam *et al.,* 2004), geothermal action in high Cl^- solutions or by suspension of arsenic bound particulates.

As(III) maybe immobilised by sulphur as orpiment. In reducing conditions sulphur solubility as S^{2-} can vary widely with factors such as precipitation with iron. When sulphur is available with predominating As(III), realgar and orpiment can precipitate in acidic conditions, but solubilise in alkaline conditions (Ferguson and Gavis, 1972, Cullen and Reimer, 1989).

Under strongly reducing conditions or when suitable bacterial activity is present, arsenic compounds can be converted to arsine (AsH_3) and methylated arsines. These compounds are highly volatile. This form easily enters into the atmosphere, but it is

also soluble in water. Volatilisation of arsines is limited by the effect of oxygen in the atmosphere (Planer-Friedrich *et al.*, 2006).

Cacodylic acid (comes from the Greek for stink) is one of the most common organic forms of arsenate, and can be volatile. Cacodylic acid is dimethylarsenate, $AsO(OH)(CH_3)_2$. This and monomethylarsenate are still used as pesticides. PbAs and Sodium arsenite are no longer used as pesticides due to their acute toxicity. In some cases cacodylic acid predominates in soils. Methylated forms of arsenite also form due to bacterial, plant and fungal action. Nitric acid can usually decompose organoarsenicals but hydrochloric acid cannot (Cullen and Reimer, 1989)

Arsenate is phytotoxic. Some plants, such as Bermuda Grass can withstand high levels of arsenate (> 1% in soils). This is not the case for arsenite, however. Since arsenate is chemically similar to phosphate, excess phosphate can relieve arsenate uptake. Where pesticides have been applied, arsenic is accumulated in the roots of plants such as alfalfa and pasture grass (Cullen and Reimer, 1989).

Some organisms, such as the acidophile archaeon reported by Baker-Austin *et al.* (2007) are able to withstand very high (up to 0.5 % by weight in solution) arsenic concentrations. The evidence presented suggests some alternate mechanism is responsible for the high tolerance other than As(V) reduction and efflux since no arsenic reductase was observed.

Whilst it is well known that the accumulation of methyl mercury in the aquatic food chain it can have lethal consequences, accumulation of arsenic in seafood presents no such problem. Normally non toxic arsenobetaine is identified in as much as 80 % of As found in fish, with concentrations above 100 ppm. Other species are less often reported, but include methylarsonium ion, arsenocholine, trimethylarsine oxide found naturally in fish. Dimethyl arsenate is also found at low concentrations. The variety of arsenic compounds including arsenosugars produced by algae is thought to constitute stages in the biosynthesis of arsenobetaine. Inorganic forms of arsenic accounts for only a few percent of the total (Larsen *et al.*, 1993). The level of total arsenic found in

terrestrial food is generally much less than seafood. Also, the speciation is usually limited to the more toxic inorganic and methylated forms.

Freezing of samples can induce As(III) predominance in water samples and speciation changes more common in non sterilised containers, suggesting bacterial effects. The presence of manganese oxide on solid particulates also influences oxidation. In absence of these factors the oxidation/reduction interchange is slow.

1.4 Worldwide Contamination of Drinking Water with Arsenic

Although exposure to arsenic can occur through occupational exposure, such as mining, pesticide, pharmaceutical, glass and microelectronics, the principal cause of arsenic poisoning is through drinking water at concentrations above 50 ppb (Tchounwou *et al.,* 2003).

Arsenic contamination of ground water supplies is recognised as a worldwide problem. In Bangladesh, West Bengal (Rahmann *et al.,* 2001), Vietnam (Berg *et al.,* 2001), Chile (Smith *et al.,* 1998) and Argentina (HopenhaynRich *et al.,* 1996) arsenic has been found to cause skin lesions and increased risks of cancer in lungs, bladder and urinary tract. Arsenic has also been identified in groundwater in the UK and USA. The numbers thought to be at risk have increased with improving knowledge. Recently the number of countries with significant levels of arsenic pollution exceeds 70 (Bagchi, 2007, citing a press release given by P. Ravenscroft of Cambridge University, UK) risking an estimated 140 million people, according to a safe limit of 10 ppb.

In 1958, the WHO had set the first guideline limit for arsenic at 200 ppb. Although the lung cancer–arsenic connection was realised before 1900 in people (Smith *et al.,* 2002), the lack of decent animal model on which to base human cancer risks caused uncertainty to persist, such that the limits took a long time to drop. In 1963, the recommended limit was lowered to 50 ppb and in 1993 to 10 ppb. This limit reflected both a safeguard and the capability of analytical procedures (WHO, 2001).

Some studies suggest that 10 ppb is too low a limit. Lamm *et al.* (2004) conducted an in depth analyses for arsenic poisoning in the USA based on statistics for bladder cancer over 30 years. The drinking water included arsenic between 3 and 60 ppb. No arsenic related increase in bladder cancer mortality was found. Lamm *et al.,* (2005 and 2006) have begun to reassess statistical data from south west Taiwan showing evidence that lung and bladder cancer risks are relevant at concentrations > 100 ppb, 10 times the EPA recommendation of 10 ppb. However, Lamm *et al.* do not question that prevalence of skin lesions is significantly increased for those drinking water with arsenic above 50 ppb.

This position is in contrast to prevailing opinion that drove the US EPA limit down to 10 ppb. There was backing by political agents in the US government, based on such estimates as 1 in 100 dying due to long term drinking of 50 ppb (Smith *et al.,* 2002). Smith *et al.* (2002) recognise that statistical analyses of border line cases of exposure would be unlikely to prove a 1 in a 100 death toll. They suggest a "margin of safety" to be adopted rather than excessive manipulation of statistical results until better information becomes available. The evidence gives no reason to believe that the carcinogenic action of arsenic has a threshold value. One reason that the implementation of the 10 ppb EPA limit came into effect only in 2002 was due to the high cost of analysis and remediation.

Rahman *et al.,* (2007) presented the results of a study on over 29,000 pregnancies in Bangladesh. The drinking water exposure was compared with the outcome of child birth. A significant dose response for arsenic resulting in infant death was found. Thus the study concluded that pregnant women should be prioritised for 'arsenic mitigation activities'. Although previous studies had shown evidence for arsenic effects on pregnancy, none had shown a significant effect, probably because the number of women involved was too small.

The first cases of skin lesions were identified in 1983 in West Bengal and in 1987 in Bangladesh (Smith *et al.,* 2000), with the primary source of drinking water for these patients being underground wells. The majority of tube wells (in excess of 1 million)

were built by UNICEF and the Department of Public Health Engineering between 1980 and 2000 to provide water free of the disease present at the surface. Arsenic was not believed to be a problem when the wells were constructed. The standard design for the tube wells included a 5 cm diameter pipe drilled less than 200 m into the ground. However, between 1993 and 1996 tests confirmed that widespread arsenic contamination was in evidence. Out of 125 million inhabitants of Bangladesh, a large percentage was thought to be drinking water with > 50 ppb of As present. The number of people showing skin lesions was estimated to be in the order of hundreds of thousands (Smith *et al.,* 2000).

Part of the widespread analysis of the wells using field based kits was later criticised (Ahmed, 2002). Colorimetric kits produced by Merck (Merck KGaA Merckoquant Arsen Test; Darmstadt, Germany), intended only to measure above 100 pbb were used to assess wells (at a cost to UNICEF and the World Bank of 'several million dollars') as safe or hazardous based on a 50 ppb limit resulting in a large number of incorrectly labelled wells. The effort was defended, by arguing that the kits were adequate for assessing the most hazardous wells. Further issues were raised about the test kits due to their semi quantitative nature, unreliability at low concentrations, generation of toxic arsine, problem of colour perception and inactivation of reagents due to high humidity.

The Merck kit uses HCl to acidify the sample and zinc powder to reduce the arsenic to arsine. The arsine reacts with a mercury bromide strip and the colour change is measured. This is a modification of the Gutzeit test. Although shorter times maybe used, 30 minutes is required for the reduction to arsine at the lowest concentrations (< 10 ppb).

In 2004, the Environmental Protection Agency published a report (EPA, 2004) of the then available technologies for detecting arsenic *in situ* including colorimetric and electrochemical kits. In summary, a successful field procedure was lacking. Emerging technologies were also discussed such as those sensors including biological components of which some sensitive (10 ppb) but unstable results could be obtained.

X-ray fluorescence was thought promising for monitoring soils with high ppm concentration, with the advantage of being able to measure many elements simultaneously. The method is still in the early stages, but struggles to function in the presence of water or at concentrations low enough for drinking water and related applications. Laser induced breakdown coupled with a portable spectrometer is an additional possibility, but again it is in early development with high limit of detection (> 100 ppm). Electrochemical techniques involving either ASV or potentiometric stripping analysis (PSA) were discussed. Although electrochemical techniques are, in principle, inexpensive to implement, rapid and able to differentiate oxidation state, problems associated with procedural complexity, maintenance of the electrode requiring skilled operators have inhibited (so far) the adoption of the technique. The PVD 6000 produced by MTI Diagnostics, Ltd. (Cambridge, UK) was evaluated. Again issues of cost and complexity were raised.

Jaunakais *et al.* (2004) describe improvements to the colorimetric methods relative to both the Hach (Hach Lange Ltd., Arsenic Test Kit 0 – 500 ppb, Salford, UK) and Merck test kits in use prior to 2001. In the subject of this patent metal ions, iron and nickel are used to accelerate the reduction process lessening the overall test time. The patent is used as the basis of the Low Range Arsenic Quick test kit (Industrial Test Systems, Inc., USA) advertised to be suitable for detecting 2 ppb arsenic in 12 min. The Arsenic Quick II was evaluated by the EPA (Kaufman *et al.*, 2003) it was found to be easy to use but bias between a technical and non technical operator was found. The Arsenic quick test offered the option to use a scanning device to measure the colour change for improved accuracy. The basic kit cost $ 219 (with quoted method detection limit of 15 ppb) and the computerised scanning method $ 1600, at the time of the report.

The Arsenator is presently produced by Wagtech International, Ltd (Berkshire, UK) and is considered the first adequate test kit for screening arsenic at the EPA limit of 10 ppb. The kit was evaluated by Swash (2003), who tested samples from Myanmar finding good results from 10 ppb to 100 ppb (using a digital spectrometer to measure the colour change strip). There were, however, significant outliers amongst the results

for the five machines tested. A UNICEF report (2006) found that the Arsenator gave excellent performance for monitoring drinking water with an analysis time of 20 min and minimum tested concentration of 5 ppb. The 20 min test time includes the need to run a calibration sample with preloaded arsenic, and retests if the concentration range needs to be altered by dilution. The presented data was the average of triplicate measurements and significant outliers were not visible. A very high correlation between the Arsenator and AAS was found. The report concluded that the Arsenator Kit was '*almost complete in all aspects*', with the kit considered safe to use. An article in Down to Earth (2004) pointed out scepticism due to the high cost (entire kit for $1837) and mentions that the kit uses (as do the Merck and Hach kits) a mercuric bromide colour strip with an error rate of 5 – 10 %.

In a study by Samanta *et al.,* (1999) on speciation in drinking water, no methylated forms of arsenic were detected. The ratio As(V):As(III) was about 1:1 of which about 90 % was inorganic. In the urine of those drinking from the wells, most arsenic is present in methylated forms (Samanta *et al.,* 1999). Chatterjee *et al.,* (1995) studied the speciation of arsenic in drinking water and the urine of those affected using Flow-Injection-Hydride Generation Atomic adsorption Spectroscopy. Only inorganic arsenic could be found in the water. In the urine more than 90 % of the arsenic was inorganic with the rest made up of methylated forms.

Although arsenic contamination of a given aquifer is relatively unusual, because of the high spatial variability, each well, in a given local, needs to be analysed individually (Smedley and Kinniburge, 2002).

The temporal variation of arsenic in tube wells has been subject to some controversy in the way that the findings affect policy (Cheng *et al.,* 2006). A summary of the literature shows that long term studies are lacking for temporal arsenic variation. The majority of wells appear to be stable, some increase and a few decrease. The changes, where information is available, are less than 2 ppb/yr correlating to well age. Some evidence points to seasonal fluctuation, and based on this a given tube well should be tested at least twice a year. Cheng *at al,* (2006) agree that based on the 'dense geo-

referenced data' arsenic distributions are highly variable. Savarimuthu *et al.,* (2006) provide an in depth report for 74 selected tube wells in West Bengal, for the year 2002-2003, measuring in summer, winter and monsoon. The maximum was seen in the monsoon where arsenic was 150 % of the summer season. During the year overall levels had increased substantially. However, Thundiyil *et al.,* (2007) found no seasonal variation on 356 wells in West Nevada (USA) with average concentration of 73 ppb. During the wet season 22 % of the wells had higher concentrations and 21 % were lower. The arsenic concentration and extremity of the wet-dry seasonal variation is likely to be less in West Nevada than in West Bengal. Also, the underlying geology was not included in the studies, for which there may be significant differences.

The occurrence of As has been found to correlate with aquifer type both in depth and age whether Holocene (the last 10000 years) or Pleistocene (before Holocene). Part of the mitigation process has been to build deeper wells where less contamination is expected (Zheng *et al.,* 2004).

There are four mobilisation mechanisms: reductive dissolution, alkali desorption, sulphide oxidation and conditions in geothermal waters (high temperature and Cl^- content). Reductive dissolution is predominant in Bangladesh, Geothermal is prevalent in Himalayan region, areas in China have alkali desorption. Areas in Mexico, Europe and Brazil have As resulting from sulphide oxidation. Arsenic is particularly evident in Holocene alluvial aquifers accounting for 59 % of known As contamination. Reductive dissolution is typical in humid climates and alkali desorption in arid climates. No data has been obtained from most of Africa, Australia, South America and India (away from the Ganges Basin) (Ravenscroft, 2007).

Contaminated ground water contributes to additional modes of exposure including ingestion of rice grown in arsenic rich waters and soils (Rahman *et al.,* 2007b). Although the tolerance for most plants to As in soils is about 2 ppm (dried weight), some plants, rice for example, can tolerate as much as 1000 ppm in the roots and 100 ppm in the plant tops (Kabata-Pendias, 2001). The speciation of arsenic in rice is

principally the toxic inorganic and methylated forms or arsenic (Heitkemper *et al.,* 2001).

Recently, Pal *et al.,* (2007) reported that the burning of arsenic rich cow dung (where cows have drunk from arsenic present groundwater) as a traditional fuel leads to inhalation of high levels of particulates. Burning in unventilated ovens was thought to contribute 1.8 µg/d of arsenic by inhalation (as arsenictrioxide), with an estimated 0.46 µg/d adsorbed in the respiratory tract. Another unexpected effect was the evidence of enhanced radioactivity correlating with arsenic at selected sites in Bangladesh, adding to and confounding the cancer risk associated with arsenic. The element has not been identified (Ghosh *et al.,* 2008).

1.5 Metal Toxicology

The effects of toxins on human physiology are limited by irregular occurence cases and often confounded by multiple toxins, exposure routes or symptoms. The effect of metals in biochemical reactions is only partly understood. In general, metals are small (compared with macromolecules such as proteins) avoiding the immune system. In addition the immune system cannot destroy the metal, unlike organic toxins. In some cases the metal can be converted to less toxic forms such as the methylation of As, or subjected to excretion, as happens with As, or Pb. The metals all cause widespread damage at high levels. Many substitute for benign elements such as Ca, Mg, or P disrupting biochemical reactions. Metals such as As and Hg are suspected carcinogens but Cu is not (Furst, 1981). Many of the differences between toxicities associated with metals can be explained by solubility, oxidation state, absorbability, transport and complexes (Stohs and Bagchi, 2000). The physiological fate of metals is important for analyses of poisoning. Measurements of blood and urine are good indicators for short term (several days) exposure where hair and nails can indicate longer term exposure (3-6 months).

Poisoning due to acute arsenic exposure as opposed to long term effects of low concentrations produces differing physiological results. Historically, there are well

known cases of both intentional and accidental poisoning. In the former case arsenic trioxide was an effective murder weapon because it was both tasteless and efficiently lethal. Until the invention of techniques such as atomic adsorption and mass spectroscopy identification the identification of the poison was not feasible (Cullen and Reimer, 1989). The use of arsenic in paints has also been suspect for long term poisoning particularly when in combination with bacterial agents. Present technology allows hair and nails to be tested for arsenic speciation even on exhumed bodies as long as the hair remians (Francesconi and Kuehnelt, 2004).

Arsenic causes the inactivation of key enzymes, reacting with OH and SH groups. Arsine, and methylated arsines forms are volatile and most toxic. Inorganic forms of arsenic are about100 times as toxic as methylated forms of As(III) and As(V) (Kim *et al.,* 2002). As(V) disrupts phosphate processes due to similar chemistry: preventing adenosintriphosphate (ATP) generation via formation of adenosindiphosphate(ADP) - arsenate (Styblo *et al.*, 2000).

Although, it is common for people to ingest significant amounts of arsenic with their diet, for example in seafood, this is in organic forms, such as arsenobetaine, which are much less toxic. By contrast, organic mercury compounds accentuate toxicity and bioaccumulate in seafood.

Arsenic exposure occurs via inhalation of arsine, methyl arsines and dusts of other oxidation states. Ingestion of aqueous As(III) and As(V) represents the greater risk. Although most therapeutic uses of arsenic have been abandoned, Soignet *et al.,* (1998) showed the effectiveness in treating leukaemia by prescribing low doses of arsenic trioxide. Doses between 60 and 200 μg per kg body weight per day were prescribed for between 12 and 36 days. The leukemic cells in the bone marrow subsided but adverse health effects included rash, light-headedness, fatigue and musculoskeletal pain.

As an aside, some plants accumulate heavy metals. For example the Chinese Brake fern, has been identified as a promising hyper accumulator of arsenic (Ma *et al.,* 2001)

able to accumulate in excess of 1000 ppm As in fronds from a soil spiked at 50 ppm. This fern and other closely related species are promising for phytoremediation. In general phytoextraction involves several mechanisms: removal of metal, accumulating in plant, filtration by the root system removing polluting metals from ground water and phytostabilisation, reducing the bioavailability of metals (Salt *et al.*, 1995). The fern uptakes arsenate with phosphate and reduces it to arsenite. The arsenic is then stored in the vacuoles (part of the function of a vacuole in the cell is to remove harmful substances). Also, some yeast and bacteria, reduce arsenic to As(III) then store the As(III) as a thiol complex in the vacuole, where others extrude the As from the cell (Ellis *et al.,* 2006). Initially, the arsenic is reduced so as to differentiate the toxin from phosphate (Nies, 1999). The toxicity is lessened by methylation. The arsenate reductase enzyme with glutathione acts as the reducing agent (Duan *et al.,* 2005). Arsenite can also be taken up by the plant routes with aquaglyceroporins (Rosen, 2002). Aquaporins are responsible for the transport of water molecules independently of ions. In general, most cells reduce arsenate to arsenite, which is then extruded from the cell via specialised proteins.

Mercury in the common divalent state has a high affinity for binding SH groups, thereby inactivating proteins and enzymes, and interfering with protein synthesis and DNA replication. Metallic forms penetrate throughout the body. Mercury alters cell membrane permeability and calcium homeostasis. Neurologic effects include acetylcholine inhibition leading to impaired motor skills (Stohs and Bagchi, 2000). Any form of mercury is toxic. Adsorption through skin contact with liquid mercury is low. However, mercury is volatile and about 70 % of inhaled mercury adsorbs.

Mercury is particularly dangerous due to bioaccumulation in the food chain, such as the well known incidence in Minamata (Kumamoto Prefecture, Japan) where the Chisso Corporation dumped waste between 1932 and 1968 into Minamata bay, later Minamata River, and subsequently the Shiranui Sea. The first recorded cases of poisoning occurred in 1953 in 1956 the disease was named Minamata disease. Among the pollutants was methyl mercury chloride, used as part of a catalyst for acetaldehyde (used in plastics manufacture). The disease was traced to methyl mercury

accumulating in sea food such as shellfish caught by local fishermen. In 1959, a ban was placed on sea food in the Minamata area curbing the acute cases of Minamata disease, but the widespread contamination of the Shiranui Sea continued. Many people as well as cat and dogs suffered symptoms of sensory impairment and madness (associated with neurological toxicity). Lethal cases included muscle weakness and coma with death occurring within weeks. There have been over 2000 official cases and over 200,000 thought to have been affected. The social and political climate was not conducive to open admission and cessation of pollution. Information was suppressed, in part because of the role played by large industries in providing modernisation, and wealth to the local area (Ekino *et al.*, 2007). A second outbreak of the same disease occurred in Niigata (Kumamoto Prefecture, Japan). A plant run by the Showa Electrical Company used mercury sulphate to catalyse acetaldehyde production, during the mid 1960s, with the waste released into the Agano River.

With no biological function, cadmium accumulates in the liver. The underlying mechanism of toxicity is not well understood. It is thought that the main cause could be oxidative stress or lipid peroxidation of cell membranes (Stohs and Bagchi, 1995). Cadmium stimulates cell proliferation and inhibits DNA repair. Classified as a carcinogen, there is both prostate and lung risk. Prolonged accumulation affects the central nervous system.

The distribution of lead is widespread through organs and systems. Whilst found in blood and soft tissue, the highest concentrations occur in liver lung, spleen and kidneys. Lead mimics and inhibits calcium processes thereby affecting bone cell function. Lead interferes with vital proteins when bound to sulfhydryl, amine, phosphate and carboxyl groups, affecting the neurological system, renal system and cardiovascular system. In the blood, it interferes with haemoglobin synthesis. Lead is excreted as salts by the kidneys; exhalation is a major excretion route for organic Pb compounds (Barile *et al.,* 2004).

Copper is a required element in the diet of most living organisms, but toxic in excess. The toxicity is poorly understood. Copper ions irritate the stomach. There is the

ability, as with other metal ions to facilitate redox reactions, changing between Cu(I) and Cu(II) thereby inducing oxidative stress with the generation of oxy and hydroxyl radicals (Stohs and Bagchi, 1995). Copper causes problems with DNA replication when cofactored with hydroquinone (Barile *et al.,* 2004).

1.6 Methods of Detection for Heavy Metals

In this section various methods for metal determination are discussed. Electrochemical methods will be dealt with separately.

Some metal analysis methods can be applied directly to solid samples such as X-ray fluorescence (XRF), instrumental neutron activation (INAA) or direct current arc atomic emission spectroscopy (DCAAS). Most trace level methods, however, incorporate an aqueous extraction scheme (or organic extraction where the metal is complexed with organics). The extraction serves to separate the analyte of interest from the bulk sample and to help homogenise the analyte speciation for analysis. These methods include, flame, graphite furnace, cold vapour and hydride generation modifications of atomic absorption spectroscopy (FAAS, GFAAS, CVAAS, HGAAS respectively), and also, inductively coupled plasma atomic emission spectroscopy (ICP-AES) and inductively coupled plasma mass spectroscopy (ICP-MS) (Alloway *et al.,* 1990, Fifield and Haines, 2000).

1.6.1 X-ray Techniques

With XRF, either an energetic electron beam or an X-ray source can be used to stimulate X-ray emission within a solid. The system of detection for XRF is either energy dispersive (EDX) using a semiconductor sensor sensitive to energy; or wavelength dispersive (WDX) using a diffraction grating to separate the light (angle of deviation corresponds to wavelength). The WDX form may determine, to a 1 ppm limit, 100 % of As Cr, Cu in a sample, but Cd, Hg require pre-concentration. Energy dispersive modes are poorer in resolution and sensitivity and so less suitable for trace

element analysis. Handheld XRF devices suitable for simultaneous detection of metals including arsenic exist (EPA, 2004) with detection limits of approximately 60 ppm.

Sbarato and Sanchez (2001) adapted XRF to measure the concentration of arsenic in groundwater. Samples of water were taken and dried under a 60 W bulb leaving a fine residue of salt and particulates on a cellophane film. By calibrating with spiked water samples containing arsenite the detection limit was determined to be about 50 ppb. This technique was then used on groundwater samples around the town of La Francia (Cordoba, Argentina).

EDX techniques are often available with scanning electron microscopes and are able to provide elemental information for a sample surface where the X-ray penetration depth is of the order microns. Other X-ray techniques have been used such as X-ray absorption (XAS), extended X-ray absorption fine structure (EXAFS), and X-ray absorption near edge spectroscopy (XANES) (Strawn *et al.* 2002). Modified XANES has been used to find the oxidation state of metals in soil minerals such as arsenic and selenium with micro scale resolution (Strawn *et al.,* 2002). EXAFS provides information on atomic environment of target metals in soil and may also provide oxidation state. EXAFS has been modified for micro scale investigations. Since many elements are detectable by these methods, a high degree of information pertaining to mineral composition is possible. For example, Strawn *et al.*, (2002) demonstrated that arsenic was associated with iron and phosphorus. However, these techniques are not suitable for trace analysis.

X-ray photoelectron spectroscopy (XPS) also known as Electron Spectroscopy for Chemical Analysis (ESCA) can be used for elemental surface analysis. A beam of X-rays incident on a sample surfaces having energy enough to interact and free electrons from the inner shells of atoms on the surface, causes electrons to emit from the surface at energies which characterise the elemental composition and oxidation states. The elements are limited to those with atomic weights between lithium and lawrencium. The detection limit for a metal is typically 1000 ppm on a surface layer only 1-10 nm thick. The process requires ultra high vacuum for the emitted electrons

to reach the detector. Closely related is Auger Electron Spectroscopy (AES), where energetic electrons at the surface give rise to further interaction with elements producing secondary electrons. Often Auger electron emission occurs in parallel with X-ray stimulated emission during XPS measurements (Seah, 1984).

1.6.2 Instrumental neutron activation analysis (INAA)

INAA is a multi trace element technique that can be utilised for soils and biological materials. The method requires the detection of gamma radiation emitted when the sample is irradiated with neutrons (for which a neutron source such as a nuclear reactor is needed). Sample analysis times can take 2-20 days for a 50-100 mg sample. Limitations on detection of trace elements are caused by matrix effects since neutrons are not selective. Thus dissolution is advantageous for reducing matrix effects (Fifield and Haines, 2000). See Table 1.7 for detection limits.

1.6.3 Atomic Absorption and Emission Spectroscopy

Direct Current Atomic Absorption Spectroscopy (DCAAS) is a form of atomic absorption spectrometry. Samples of 10-25 mg finely ground soil are used and 70 elements are detectable but only 30 with sufficient sensitivity for trace levels. The limit of detection is generally 1-10 ppm. Metals such as Hg, Cd and As cannot be measured.

Optical spectrometry is generally less expensive than mass spectrometry. For AAS the sample is prepared such that the material of interest is finely dispersed. For this, a fine spray of aqueous extract and high temperatures, for example, produce an atomised dispersion of analyte. Source light is produced by a hollow cathode lamp. Each element has characteristic absorption spectrum according to the difference in energy levels of the atomic electrons. Absorption follows the Beer-Lambert law. Some peak overlap can occur. In excess of 62 elements can be detected. A key feature of Atomic Absorption spectrometry is the sharpness of the absorption line; these lines are intense and so called resonance lines. AAS is inexpensive in comparison with AES. (Fifield and Haines, 2000)

AES is generally more sensitive. When atoms are heated to sufficient temperatures electrons are released and recaptured by the atom causing emission of light. Incident light from AAS experiments can also cause the same phenomena, but this emission is referred to as fluorescence.

Flame atomic absorption spectroscopy (FAAS) uses flame atomisation: air-acetylene mixtures are commonly used as a consistent fuel. For metals the limit of detection, see Table 1.7. With electro-thermal atomic absorption spectroscopy (ETAAS), atomisation of compounds is achieved by electrical heating of the sample. A common form utilises a carbon tube furnace known as a graphite cylinder: graphite furnace atomic absorption spectroscopy (GFAAS). There is a greater control over production of ground state atoms; an atom trap effect coupled with automated injection of sample solution improves the limit of detection to about 1-10 ppb. Interference has been a problem using this method for trace metals caused by the effects close to the tube wall, been matrix and analyte, and between analyte and graphite wall. Chloride ions present interferences. See Table 1.7 for detection limits. Some elements will form hydrides, such as arsenic and mercury. These are volatile species which can be collected separately from the bulk sample and introduced into the AAS atomiser. FAAS, ICP-AES and GFAAS have been used in conjunction with hydride generation achieving very low limit of detection (Fifield and Haines, 2000, Alloway *et al.,* 1990).

Flow Injection hydride generation atomic absorption spectroscopy (FI-HGAAS) was used by Chatterjee *et al.,* (1995) for the speciation of arsenic in drinking water finding inorganic arsenite and arsenate as well as monomethylarsonic acid and dimethylarsinic acid.

Atomic trapping atomic absorption spectroscopy (ATAAS), is an in-situ pre-concentration technique; the process of atomisation is confined, keeping the analyte in a confined space. ATAAS is sensitive and free of interference by comparison with FAAS. Finds use for determining metals from within the presence of Cl^- ions. Table 1.7 below shows the detection limits (Alloway *et al.,* 1990). Cold vapour atomic absorption spectrometry (CVAAS) is commonly part of hydride generation

procedures. Mercury is an element usually found at lower concentrations and so difficult to detect; the cold vapour method takes advantage of the natural volatility of mercury and by atomising to the gas phase. The limit of detection can be down to the microgram per litre range. Digestion is used to reduce mercury to its elemental form for which an oxidative acid required. Interferences occur from I, Se, Au, Pd and Pt. See table below for detection limits.

As with AAS, in atomic emission spectroscopy (AES) the sample solution is nebulised and sprayed into an atomiser: flame, inductively coupled plasma, direct current arc, or graphite furnace. The energy source in this case, must cause not only atomisation, but also excitation of electrons to elicit electromagnetic emissions. The emission intensity is dependent upon the analyte concentration. The emission spectrum of each element has a unique complex characterisation; a monochromator capable of scanning wavelengths is required. A polychromator may also be used for multiple element analysis. In this sense AES differs from AAS because sequential or simultaneous of multiple elements is possible. AES has advantages over AAS in cost and convenience when the number of elements surpasses ten at a time. Since AES utilises higher energy sources there is greater atomisation of the sample thus matrix interferences are lowered; however, at increased temperatures more elements will emit spectra at higher temperatures so spectrometers must be more elaborate (Alloway *et al.,* 1990, Fifield and Haines, 2000).

1.6.4 Mass Spectroscopy

With mass spectroscopy, the sample is ionised in one of a number of ways. The ions are then separated by passing them through a magnetic field in a vacuum, and detected according to their charge to mass ratio. An inductively coupled plasma (ICP) as ion source is used primarily for the analysis of heavy metals. The plasma is at a temperature of more than 10000 K composed of a mixture of native argon and ions with free electrons. A large fraction of the sample introduced will be ionised in this environment. The sample is usually introduced via nebulisation (a fine spray) after

extraction into a liquid phase such as aqueous acid. The technique is highly sensitive as shown in Table 1.7.

Mass spectroscopy can also be used for molecular identification. If an ionisation process is less severe molecules are broken into ionised fragments in ratios dependent on the molecular structure. These can be separated in the magnetic field and measured together to generate a distinctive spectrum (with a peak for each fragment). For this technique to be feasible complex molecular compositions need to be separated first. For this, gas chromatography (for volatiles) or high performance liquid chromatography (for dissolved species) can be used.

For example, ICP-MS coupled with HPLC (Branch *et al.,* 1994) showed that HPLC-ICP-MS was useful for speciation of arsenic in fish. The occurrence of arsenic in fish was almost entirely due to arsenobetaine (non toxic) with negligible concentrations of arsenate and arsenite were negligible. The authors note that HGAAS, although a good techniques is not suitable to As speciation since arsenobetaine is non reducible (to form a volatile hydride); ICP coupled with AES is not sensitive enough for arsenic detection; and that ETAAS is too difficult to couple for quick analysis times.

Table 1.7 Summary of detection limits. Detection limits in ppb or as indicated. (Fifield and Haines, 2000, Alloway *et al.,* 1990)

	As	Cd	Cr	Cu	Hg	Pb
FAAS	100	0.5	2	1	200	10
HGAAS	0.02				0.008	
GFAAS	0.2	0.003	0.01	0.02	1	0.05
ATAAS	150	0.3		19		1
ICP-AES	20	1	2	0.9	20	20
ICP-MS	0.05	0.02	0.02	0.03	0.03	0.02
DCAAS (ppm)	1000	300	1	1	1000	10
INAA (ppm)	0.5	4	2.5	4	0.6	

1.6.5 Spectroscopic, Colorimetric and Immunoassay Methods

There are several techniques that come under the heading of molecular spectrometry (Fifield and Haines, 2000). Including ultraviolet and visible spectroscopy (UV/VIS),

infrared spectroscopy (IR) and nuclear magnetic resonance (NMR). These techniques are sometimes used for metal determination.

NMR spectra are usually confined to H^1 and C^{13} nuclei. For routine measurements of different nuclei the instrumental setup needs to be tuned. Other nuclei used include isotopes of N, O, F, Na, P, Ca, Fe, Co, Sn, Cs and Pt. Many nuclei have non simple spin arrangements which are not convenient for simple analysis: an electric quadrapole moment causes peaks to broaden and definition is difficult. Some isotopes such as ^{195}Pt and ^{59}Co are very temperature sensitive. (Friebolin 2005) When studying organic compounds a large amount of information is possible regarding molecular composition and structure for isolated or synthesised compounds. NMR is not inherently sensitive enough to be applicable to trace metal detection. The NMR signature of arsenic (^{75}As) has a large quadrapole moment rendering spectra difficult to use (Bowers and Kirkpatrick, 2007).

With Fourier transform infrared spectroscopy (FTIR) and Raman Spectroscopy it is possible to distinguish signals from arsenic oxide minerals in soils (Frost *et al.,* 2003). An AsO stretch appears in Raman spectra between 797 and 852 cm^{-1} with precise value determined by mineral formation. In infrared spectra the AsO appears between 823 and 922 cm^{-1}.

A spectrophotometric method of determination exists for arsenic appropriate to ppm values. Arsenite reacting with Silver-diethyldithiocarbamate forms a red chromophore. As(V) can be reduced with so that As(III) and As(V) maybe determined simultaneously to obtain some speciation information (Lopez *et al.,* 1992)

The colorimetric techniques used in the range of arsenic test kits including the Arsenator (Wagtech International Ltd, Berkshire, UK) uses a reducing agent to generate arsenic hydride which is reacted with mercury bromide. The colour of strip is measured to determine arsenic down to around 5 ppb, when a spectrophotometer is used. More detail is given in Section 1.4.

Trace metal determination may also be determined by immunoassay techniques incorporating selective biological components. Antibody based sensors have been successfully used for toxins pesticides and explosives. There are few antibodies with metal specificity. Sensors for As(III), Cd(II), Pb(II), U(VI) and Co(II) have been developed and show sensitivity down to low ppb levels. The biological components need to be handled carefully and tend to be temperature sensitive. According to Blake *et al.* (2001), these immunoassays are in development and there is apparent high RSD but reasonable performance for the screening of metals. However, other groups have not been able to satisfactorily repeat these results (Bello-Rodriguez, 2004). Other highly sensitive methods have been reported (Bontidean *et al.,* 1998) using biological molecules isolated from cell defence mechanisms. Capacitance measurements were performed on proteins immobilised to electrode surfaces on exposure to metal ion containing solutions. The technique was so sensitive that ICP-MS could not be used for validation in the lower ranges. Sensitivity to Hg^{2+}, Cu^{2+}, Zn^{2+} and Cd^{2+} was demonstrated using proteins extracted from Escherichia Coli, immobilised using a thiol bond onto gold electrodes. The sensors were non specific and had about 2 week stability.

1.7 Extraction Procedures for Heavy metals from Samples

Extraction is used to remove an analyte from a matrix, sometimes simplifying the analyte speciation. For metal ions an aqueous or acidic solution is normally chosen since most metals form soluble positive ions under these conditions (Deltombe *et al.,* 1966). Where organic speciation is needed organic phase extractants may also be used.

To get total ion extractions from solid samples, where a fraction of the analyte is found within the mineral phase, aggressive oxidising solutions are needed, including HF, HCl, HNO_3, $HClO_4$ and H_2SO_4. The acids may need a long period of time >12 hr, high pressure, microwaving, sonication or UV radiation (Davidson *et al.,* 1997) to effectiveness.

Many sequential extraction procedures have been tested in the literature (for example, McLaren and Crawford, 1973, Tessier *et al.,* 1979, Sposito *et al.,* 1982, Miller *et al.,* 1986) designed for ions including Cu, Cd, Pb, Ni and Fe. The number of schemes has lead to efforts towards standardisation, such as the Bureau Commun de Reference, soil extraction protocols (BCR) with the increasing demands for testing contaminated land (Davidson *et al.,* 1998, Rauret, 1999). As noted by Tessier *et al.* (1979), whilst single solvent extractions are rapid, it is difficult to obtain conditions where a solvent will attack one part of the matrix without affecting others. Therefore, the sequential extraction procedures are considered to be 'operationally' defined.

Davidson *et al.,* (1997) looked at a three stage extraction for Cr, Cd, Cu, Pb, Mg, Ni, V and Zn. The three steps were: acetic acid for ions in soil solution carbonates and exchangeable fractions; hydroxyl ammonium chloride for iron and manganese oxyhydroxide bound ions; and hydrogen peroxide and ammonium acetate for metals bound in organic matter and sulfides. Optionally aqua regia could be used for the mineral residual phase. The procedure involved the use of time periods in excess of one day with mechanical shakers, centrifuges and water baths at elevated temperatures. Davidson *et al.*, (1997) report serious analytical difficulties with such procedures on heavily contaminated sites.

Wenzel *et al.,* (2001) report a sequential extraction procedure based on similarity between P and As, rather than other metal ions, because arsenic forms oxyanions in aqueous solutions. Synthetic soils were made, and nine possible solutions were tested for specificity for fractionation of arsenic. A sequential extraction was chosen with five steps: ammonium sulphate (0.05 M); hydrogen ammonium sulphate (0.05 M); 0.2 M ammonium oxalate buffer at pH 3.25; 0.2 M ammonium oxalate and ascorbic acid at pH 3.25; and HNO_3-H_2O_2. These solutions correspond to non-specifically sorbed, specifically sorbed, amorphous poorly crystalline hydrous oxides of Fe and Al, the well crystallised fraction of hydrous Fe and Al , and a the residual crystalline phase (Wenzel *et al.,* 2001, Gong *et al.,* 2002).

In a review of arsenic analysis Gong *et al.,* (2002) noted that for the extraction of arsenic from fish, solvents such as methanol-water or acetone extraction solutions are common, because many of the species are organic. In some experiments orthophosphoric acid extraction is used to estimate uptake due to the arsenate – phosphate similarity (Hutton *et al.*, 2005).

Due to the length and complexity of sequential extraction procedures, single solution procedures are common (Quevauviller, 1998). Particularly for field based analyses, the extraction protocol must be as short and simple as possible. Microwaving, sonication and temperature can be used to speed up extraction. The concept of extraction could be categorised into: (pseudo) total digestion with a mineral acid; the leachable fraction with ligand solution; or a water-salt solution for bioavailable metals. Since regulations of metal ion concentrations are set for total ion concentration, mineral acid extraction is usually favoured (Cairney and Hobson, 1998). However, the metals in the mineral phase are unlikely to pose any short- to mid-term danger to health, so priority to either the leachable fraction or bioavailable fraction could be argued. Also, the less aggressive fractions are less dangerous for the operator in the field.

Cooper (2004) identified the need for an effective protocol for *in the field* extraction of Cd, Cu and Pb. A 3 min procedure was used with HCl-HNO_3 in an ultrasonic bath. Recovery and reproducibility were compromised compared with longer extraction. However, according to the project goal, about 25 % variability due to the extraction in excess of the 10 % irreproducibility of the analyses itself was thought tolerable for screening purposes.

1.8 Description of Electrochemical Processes

Electrochemistry describes the physical phenomena occurring where electrical circuits via electrodes are in contact with chemical phases (usually solution).

1.8.1 The Nernst Equation

Electrical circuits and chemical solutions conduct with free electrons and free ions respectively. Therefore, there must be a surface reaction, if charge is to be exchanged between the phases. An ion in solution exchanges an electron with the electrode, thereby changing its redox state. If O is the oxidised ion and R is the reduced ion with n electrons, e, per reaction, the reaction is written:

$$O + ne \leftrightarrow R \qquad \mathbf{1}$$

Either one or both of O and R is charged. The thermodynamic state of the reaction for the relationship between the potential E of the electrode and the concentration of O and R, C_O and C_R respectively is described by the Nernst equation (Equation 2). The molar gas constant, temperature and Faraday constant are given by R, T and F, respectively.

$$E = E_0 + \frac{RT}{nF}\ln\left(\frac{C_0}{C_R}\right) \qquad \mathbf{2}$$

The Nernst equation describes the reaction at equilibrium. E_O, the formal potential is the potential when the oxidised and reduced species are present at equal surface concentrations. The formal potential comes from the difference between the chemical potentials of O and R. These chemical potentials are based both on the intrinsic quantum structure of the species and also on the electrolyte environment. Thus E_O for a given couple (O/R reaction) is dependent on electrolyte environment particularly where strong complexing occurs. To be general, the concentration of O and R should be replaced by the activity (the effective concentration).

The Nernst equation describes a certain spread associated with the distribution of thermal energies of O and R. The distribution is displayed graphically in Figure 1.2 for suitable values of n, R, T and F. A simple one electron reaction takes place over about a 0.2 V range. In Figure 1.2, the differential of C_O with E shows, effectively, the

exchange of electrons from solution to the electrode as the potential is changed. The exchange of electrons is related to the current. However, as the current is the flow of charge with time, the peak shape depends on how the potential changes with time.

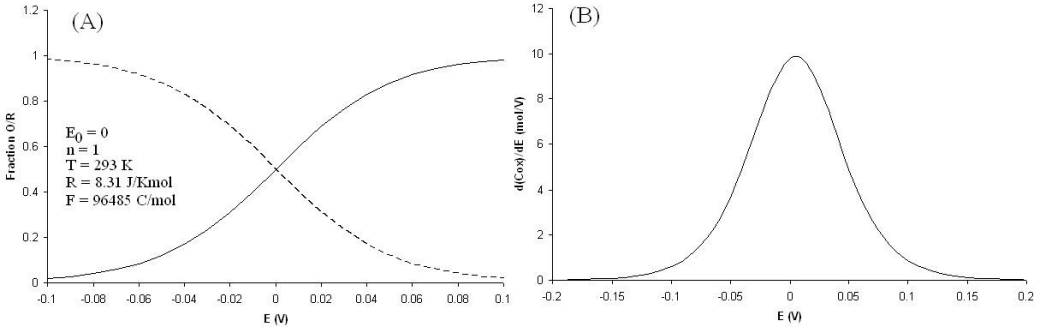

Figure 1.2 A graphic description of the Nernst equation for a one electron reaction: the fractional concentration of R (dotted) and O (line) (A) and differential of O concentration with potential (B)

The formal potential, E_O, for various redox couples can be written down based on the energy of reaction. However, it is necessary to ascertain a zero potential. Although, in principle, the energy to remove an electron from a molecule could be calculated using quantum mechanical techniques, the difficulty of evaluating all the physical parameters in the molecular environment, results in the use of a relative scale. For this scale, the potential of the reaction of the hydrogen couple H_2/H^+ when the activity of the hydrogen molecule and hydrogen ion are unity, is defined as zero.

$$2H^+(aq) + 2e \leftrightarrow H_2(g) \qquad \mathbf{3}$$

This reaction involves the formation (consumption) of hydrogen gas, H_2, from (for) hydrogen ions in aqueous solution (H_3O^+). The reaction is complicated by the necessity of bringing two reduced hydrogen ions together to make one hydrogen molecule. For example, a platinum electrode has the catalytic qualities, forming Pt-H as an intermediate in the formation of hydrogen. In practice, the surface area of the platinum electrode is maximised by depositing platinum salt on the surface. To maintain the hydrogen gas partial pressure in solution, the gas is bubbled through an inlet, close to the surface (Hamann *et al.*, 2007). This system is referred to as the normal or standard hydrogen electrode (NHE or SHE respectively). Table 1.8 shows

the formal potentials of some metallic reactions with respect to the hydrogen electrode. The dependence of some physical parameters, such as halide ions in solution, and in the case of Cu, several oxidation states, can be seen.

Table 1.8 Formal potentials for silver, copper and chloride (Lide *et al.,* 2003)

Reaction	E_O(V) 25 °C (NHE)
$AgCl(s) + e^- = Ag + Cl^-$	0.2223
$AgBr(s) + e^- = Ag + Br^-$	0.071
$Ag^+ + e^- = Ag$	0.799
Hg_2Cl_2, Cl^-/Hg	0.2679
Hg_2Br_2, Br^-/Hg	0.140
$PbSO_4$, SO_4^{2-}/Pb	-0.351
$Cu^{2+} + 2e^- = Cu$	0.337
$Cu^+ + e^- = Cu$	0.52
$CuCl_3^{2-} + e^- = Cu + 3Cl^-$	0.178
$Cl_2 + 2e^- = 2Cl^-$	1.36

The potentials of chemical reactions have been catalogued since the early days of electrochemistry (for example Latimer, 1952, Deltombe *et al.,* 1966, Bard and Parsons, 1973). Known as the electrochemical series, concise lists are available, such as Lide *et al.,* (2003). In some cases, speciation maps for different elements according to pH, redox potential without and without complexing ions are presented (Latimer, 1952, Deltombe *et al.,* 1966).

1.8.2 Three Electrode Cell

To connect a chemical solution to an electrical circuit two electrodes are needed: one as charge sink and the other as source. Usually a third electrode is included to measure the potential of the electrolyte, so that the potential drop at the working electrode surface can be set precisely. Whilst the NHE can provide this, the electrolyte would need to contain hydrogen ions and a supply of hydrogen gas. For practical purposes, other reactions can be used not requiring gas supply or a carefully prepared platinum electrode. The mercury calomel electrode and silver-silver chloride (Ag/AgCl) electrode are two such examples. The potential of the Ag/AgCl electrode is given in Table 1.8 although this depends on the Cl^- ion activity in solution. The silver chloride electrode is chosen because no gas is needed, dissolved chloride ions

are common, AgCl has low solubility, silver has a relatively low toxicity (compared to Hg) and the reaction is fast.

A typical cell is shown with a simplified schematic of the electrical circuit in Figure 1.1. Since dissolved atmospheric oxygen in the electrolyte can result in adverse background reactions for analytical applications, an inlet for inert gas (such as N_2) purging is common. The reference and working electrodes are close minimising the resistivity of the solution. Generally, the counter electrode is larger than the working electrode, allowing the passage of required current without generation of electroactive species. This follows from the potentiostat design, shown in Figure 1.3B. To set the working electrode at a precise potential relative to the solution (inferred from the reference electrode), the potentiostat incorporates a feedback mechanism driving current through the counter electrode until the correct potential is measured between working and counter electrodes. With the use of operational amplifiers the process can be achieved in a short time frame (<< 1 second) as long as the solution resistance is not too high. The time to achieve the set potential is called the rise time. If the counter electrode has a small area then a greater current density is needed. The potential required to generate this current density is more extreme. Extreme potentials are more likely to corrode electrode and adjacent materials introducing electroactive species into the solution. These species may diffuse to the working electrode as contaminants.

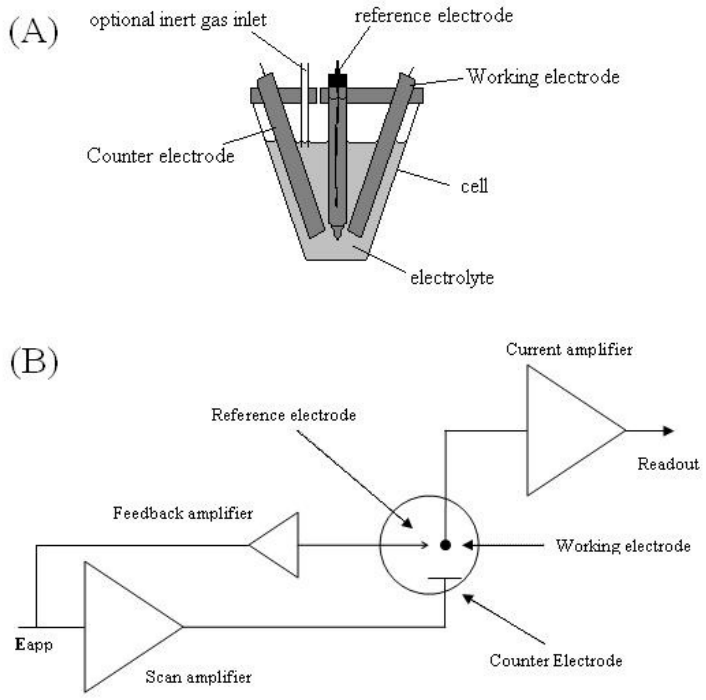

Figure 1.3 (A) Simple electrochemical cell and (B) simplified potentiostat schematic. The potentiostat design is taken from Wang (2000a)

In Figure 1.3A, the reference electrode shown is a silver wire coated in silver chloride inside a glass capillary housing; the bottom of the tube features a ceramic frit. This design allows a chloride solution to be contained inside the tube. The frit slows ion transport to (from) the reference electrode from (to) the electrolyte.

1.8.3 Electrode Capacitance

When the potential is insufficient for charge to be exchanged across at the working electrode surface, there is another physical effect. In aqueous electrode the water molecules are polar. Molecules, local to the surface, align according to the charge forming a compact layer. Also, the electrolyte ions close to the electrode move to oppose the electric field that is generated by the working electrode-solution potential. The movement of ions close to the surface effectively shields the remaining electrolyte from the electrode potential. The displaced ions and aligned water

molecules are referred to as the Helmholtz layer (Bard and Faulkner, 2001, Hamann *et al.,* 2007). Since there is a minimum distance according to the molecular size, the layer is separated into the inner and outer Helmholtz layers for adsorbed and diffuse ions. The arrangement of ions close to the electrode surface is dependent on the micro and nano scale irregularities in the electrode surface. The system is effectively two conducting regions (the electrolyte and electrode) separated by a narrow insulating region (in absence of charge exchange mechanism), therefore behaving like a capacitor, with capacitance, C_p. Thus, when the potential is changed a current, i_c, is expected due to realignment of water and ions (Equation 4). Once the potential is fixed, however, the capacitive current decays to zero, like a conventional capacitor. The speed of the decay in this current depends on the system resistance (He and Faulkner, 1986).

$$i_c = C_p \frac{dE}{dt} \qquad \textbf{4}$$

The capacitance layer in electrochemical experiments is usually less than 10 nm thick for aqueous electrolytes with suitable conductivity (Bard and Faulkner, 2001, Hamann *et al.,* 2007).

For an ideal metal ion sensor, the working electrode would have a low background current density associated with capacitance. Limits on the useful potential range are imposed by: specific interactions, such as electrode electrolyte reactions causing deposition, passivation and/or corrosion of surface layers; or, in aqueous electrolytes, the hydrolysis of water generating either oxygen at positive potentials or hydrogen at negative potentials. The evolution of hydrogen and oxygen are both relatively complex reactions, and dependent on the electrode, having different associated overpotentials. The evolution of hydrogen on mercury and carbon is very slow, allowing capacitive type behaviour for a low potential range of as much as 1 V negative than is possible platinum, gold and silver metals (dependent on H^+ activity in solution). Overpotential is excess potential that is needed beyond the formal potential to drive a kinetically slow reaction. The positive range of mercury is limited by the

oxidation of mercury forming soluble cations. Platinum, gold (and silver in the absence of chloride ions) have larger oxidation ranges where capacitive type behaviour holds. Figure 1.4 (taken from Hamann *et al.,* 2007) shows Pt and Au surfaces in an acid electrolyte; the potential is changed uniformly with time (at 100 mV/s) up from 0.0 to 1.7 V and back. The current has been recorded. This procedure is called cyclic voltammetry (CV). The gold has a low background from 0 to 1.4 V. Pt forms Pt-O and Pt-H owing to its catalytic properties (Hamann *et al.,* 2007).

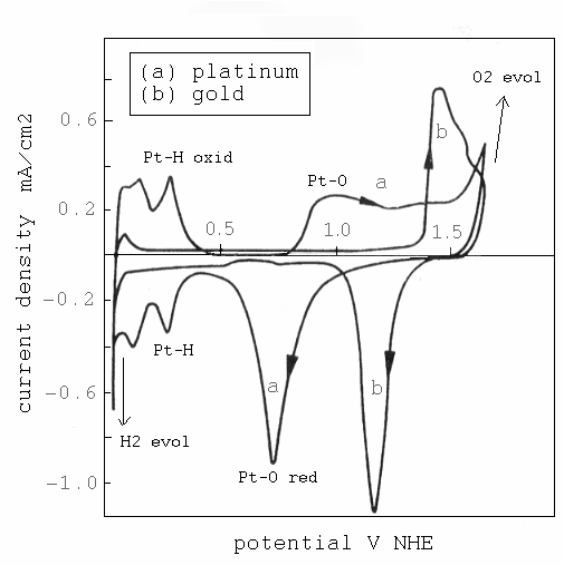

Figure 1.4 Cyclic voltammograms of Pt and Au electrodes in 0.5 M H_2SO_4 with scan rate 100 mV/s and nitrogen purging. Taken and modified from Hamann *et al.,* (2007).

1.8.4 Analyte Diffusion

Ions in solution move by one of three processes: ions disperse evenly within an available phase moving due to the thermal molecular motion, called diffusion; an electrical field moves ions according to their charge toward opposing poles, called migration; and the electrolyte itself may be moving carrying ions by convection. The use of moderate potentials and concentrated electrolytes minimises migration. Stirring is used sometimes to increase ion transport, thereby increasing reaction rates. However, for analytical applications quiescent solutions are common. Thus diffusion is the only process of ion movement (Bard and Faulkner, 2001, Hamann *et al.,* 2007).

Using calculus the diffusion of ions can be described. Shown here for one spatial dimension, x, but easily extended to more dimensions, the flux of particles, J, at x, in the diffusive media is proportional to the difference in concentration of particles. This is Fick's law and the constant of proportion is the diffusion constant, D:

$$J = -D\frac{\partial C}{\partial x} \qquad \textbf{5}$$

There is a negative sign because the particles flow from high to low concentration. The build up or reduction of particle concentration at x is proportional to the difference in flux across the point:

$$\frac{\partial C}{\partial t} = -\frac{\partial J}{\partial x} \qquad \textbf{6}$$

These two equations give the diffusion equation, which is a second order partial differential equation.

$$\frac{\partial C}{\partial t} = D\frac{\partial^2 C}{\partial x^2} \qquad \textbf{7}$$

Qualitatively speaking, if an electrode is set to such a potential as to cause a reaction, converting a species O to R, and the ions near to the electrode react according to the Nernst equation, more particles of O diffuse to the electrode surface as O depletes, thereby extending the reaction. After a while the solution can no longer provide a significant supply of O, forming a concentration gradient from the electrode into the solution. Thus, the peak shape seen in Figure 1.2B, (without diffusion) is changed. If the potential is taken to rise uniformly (as for CV) from a non-reaction inducing potential up to and beyond E_0 for the O/R couple, the initial part of the peak shape will be similar to Figure 1.2B. The tail end will lengthen due to the extra particles diffusing to the surface. However, the shape cannot be described easily by an

analytical expression. The equations can be solved numerically as detailed by Bard and Faulkner (2001), and Nicholson (1965a).

To do this for CV the diffusion of both O and R are considered simultaneously. For every O reduced at the electrode an R must be produced, taking one electron from the electrode. At distances far from the electrode the O and R concentrations are unaffected. By using the Nernst equation for the surface condition of thermodynamic equilibrium, and setting values for the many physical constraints such as electrode area, scan rate and concentration, the ideal voltammogram shape can be calculated, as is shown in Figure 1.5. Although the peak separation shown here is 60 mV (numerically evaluated with a 2 mV interval) the value is known to be slightly less, about 58 mV (Bard and Faulkner, 2001). The precise value depends on the total scan range.

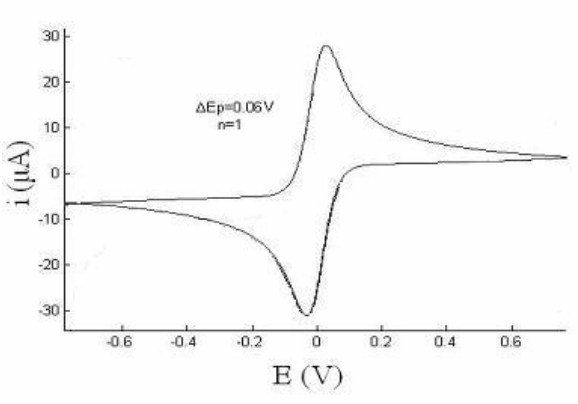

Figure 1.5 The ideal peak shape for one electron reaction obeying the Nernst equation at the electrode surface for two scans in CV, electrode surface area 0.15 cm^2, scan rate 0.1 V/s and total concentration of O and R of 1 mM. Formal potential is zero and the difference in potential of the two peaks is 0.06 V.

The Randles-Sevcik Equation (Equation 8) provides a simple relationship between peak height, i_p, scan rate, v, diffusion constant, D_0 (for O) and electrode area, A for flat electrode surfaces (Wang, 2000a, Bard and Faulkner, 2001, Hamann *et al.,* 2007):

$$i_p = (2.69\times10^5)n^{3/2}AD_0^{1/2}C_0^{*}v^{1/2} \quad \textbf{8}$$

The coefficient is a direct consequence of the shape numerically derived in Figure 1.5. The equation applies to simple diffusion controlled reactions on flat electrode surfaces. There are experimental situations where diffusion is irrelevant such as thin layer voltammetry: the electrolyte comprises a layer much thinner than the diffusion layer thickness; or highly porous electrodes where the electrode effectively surrounds the electrolyte with pores smaller than the diffusion layer thickness. With the Nernstian condition in these situations, the shape of the voltammetric peak should be like Figure 1.2.

1.8.5 Electrode Kinetics

One further physical factor is necessary to consider is kinetics. If the O/R reaction at the electrode surface is slow the Nernst equation will not be satisfied and thermodynamic equilibrium will not be achieved. So if the the O/R reaction proceeds with O to R conversion with rate constant k_f and R to O with rate constant k_b the reacton is thought to occur simultaneously in both directions at the electrode surface such that:

Net flux (O to R) = $k_fC_o - k_bC_r$ **9**

The two rate constants are described by the electrochemical absolute rate equation, using activated complex theory, in terms of a single constant, k_s,

$$k_f = k_s \exp\{\frac{-\alpha nF}{RT}(E-E_0)\}$$
$$k_b = k_s \exp\{\frac{(1-\alpha)nF}{RT}(E-E_0)\} \quad \textbf{10}$$

The rate of reaction increases as overpotential, $E-E_0$, is applied. But k_s is an intrinsic parameter describing the rate of reaction. Another parameter, α, is used to account for asymmetry and varies between 0 and 1. Due to the kinetic effect, the peaks for the reaction (as in Figure 1.5) will shift apart. Slow kinetics are caused by hindrance close to the electrode so that the number of particles allowed to react is drastically reduced, possibly by rotation and stereo chemical hindrances. In activated complex theory the slow kinetics are accounted by a transitionary state (or activated complex) during the reaction from O to R, acting as an energetic barrier. The overpotential is needed, specifically, to overcome this barrier. Some electrochemical reactions cannot occur or are impaired from occurring at an electrode surface without the presence of a bridging ligand. This is thought to be the case with As(0)/As(III) and Cl^- ions (Arnold and Johnson, 1967). Reactions where kinetic effects dominate the reaction are thermodynamically irreversible, whereas those where the Nernst condition holds are reversible. The transitionary region is referred to as quasi-reversible.

Cyclic voltammetry is considered a diagnostic technique for electrochemical reactions since the peak shape and positions can be described with a number of equations and related to physical variables. However, there is a limit to the low concentration of analyte in solution able to produce a measurable peak above background capacitance and oxidation/reduction reactions. Several techniques, developed for chemical analysis, make use of a preconcentration (deposition) phase. Metal ions are present principally as soluble positive ions in solution. If the working electrode is held at sufficiently low potentials a metal ion near the electrode will reduce to its native state, thereby becoming insoluble. The metal will deposit on the working electrode surface. The longer the electrode is held at the negative potential the more ions will be deposited. Although carbon graphite makes a good inert electrode, a mercury film (either pre- or co-deposited) generally improves deposition of Cd, Cu, Pb and Zn. Some metals such as Ca and Li cannot be deposited so easily due to the extreme negative potentials needed for reduction. The evolution of hydrogen from hydrolysis of water occurs before these metals are reduced.

When the potential is raised, the metal ions strip from the surface. 'Strip' refers to the process of forming soluble cations as the electrode takes electrons from the ions. There are a number of ways to strip the surface with a potentiostat, a linear scan being one of the most common. This technique is called anodic stripping voltammetry (ASV). Since the source of metal ions is surface bound the peaks generally do not show the diffusion tail of Figure 1.5. Alternatively, instead of a linear scan a pulsed scan can be used. Sharp pulses help to elevate the currents associated with stripping. Differential pulse measures the difference between pulse attack and return currents thereby selecting quick reactions, and cancelling slow reactions, leading to signal to noise ratio improvements. The technique is called differential pulse anodic stripping voltammetry (DPASV). For squarewave anodic stripping voltammetry (SWASV), the waveform is specified by the frequency, scan rate and modulation height; square wave waveform is like a specific kind of DPASV where the pulse period is half the step period (Kissinger and Heineman, 1996). The current is sampled at the end of the pulse as shown in Figure 1.6 (D) since this optimises the current contributions from diffusion redox processes over capcitive currents.

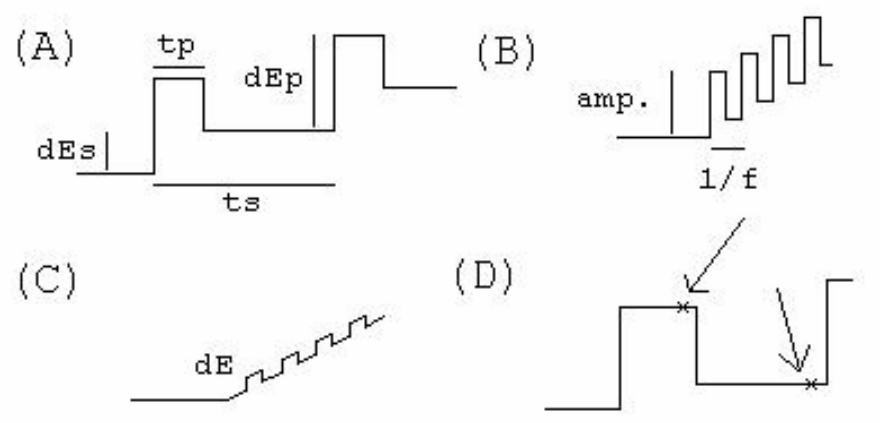

Figure 1.6 The potential-time shapes for differential pulse and square wave voltammetry. (A) Differential pulse with step time tp and height dEs, pulse time tp and pulse height dEp. (B) Square wave voltammetry with frequency, f and amplitude. (C) Analogure form of differential pulse superimposing pulse with height dE on a linear slope. (D) Current sampling (shown with cross)

Another technique is potentiometric stripping analysis (PSA), also known as constant current anodic stripping (CCAS). After the deposition phase, instead of controlling the potential, either a current is set by the circuit or the reoxidation is induced chemically and the change in potential is measured (Jagner, 1982). Technically the circuit used for this procedure is not a potentiostat. By taking the differential of potential with time analogous peaks are obtained to ASV. Some researchers have reported favourable characteristics of peak resolution and background currents (Jagner, 1982, Munoz and Palmero, 2005).

Metal electrodes have good affinity for deposition of metal ions in solution due to the formation of intermetallic surface layers. For analytical applications one metal, mercury, has been preeminent since it is the only liquid metal at room temperature. Therefore, the mercury surface is smooth and can be replaced easily. The hanging mercury drop electrode (HDME) is a popular choice since the electrode produces a new drop of mercury for each experiment. The drop is smooth and reproducible not suffering from past history, as solid electrodes do: formation of oxidation layers, passivating films, roughening or corrosion.

Mercury electrodes have also been made using deposited films on solid electrode surfaces. A solution of mercury salt with the electrode held at the reducing potential will form a film. At low concentrations, the film is made up of discrete drops across the electrode surface each with several microns diameter (Stulikova, 1973).

Many mechanisms exist for modifying electrodes and electrochemical schemes. Catalytic layers and adsorptive polymers can be deposited or applied to electrode surfaces increasing affinity or electrode reactions. Some electrochemical procedures use complexation with ligands to modify reaction rates and values of formal potentials. Alternatively, the use of micro electrode wires and arrays make use of the inherent convergent diffusion profile to increase analyte currents over the capacitive background, thereby increasing sensitivity (Wang, 2000). Other peripheral procedures include increased temperatures, stirring and sonication to increase reaction rates.

Some of these modified procedures use cathodic depositions if anions are to be concentrated onto an electrode surface.

For example, Turyan and Mandler (1997) used a gold electrode with a self assembled monolayer of 4-(mercaptoethyl) pyridinium as a working electrode sensor for Cr(VI) with sensitivity reported down to 0.001 ppb. The advantage is due to the high chemical affinity between the pyridinium and chromium. The same authors (Turyan and Mandler, 1994) also developed a sensor for Cd(II) using omega-mercaptocarboxylic acid self assembled monolayer with sensitivity down to 0.00045 ppb. The sensor was used to determine Cd(II) in seawater.

Cathodic stripping voltammetry (CSV) can be used to determine a variety of metals on mercury electrodes. For example, van den Berg (1986) used differential pulse cathodic stripping voltammetry (DPCSV) with a HDME to determine Pb, Cd and Cu using complexation with 8-hydroxyquinoline. The metal–quinoline complex could be concentrated on the mercury surface by deposition at cathodic potentials. After 1 min deposition with stirring, a sub nM concentration sensitivity was obtained. The authors also review the determination of other metals such as Al, Ni, V, Fe, U, Cr and Zn by similar methods, such as complexation with catechol. A greater sensitivity in comparison with ASV was reported and in some cases, such as copper, simpler peak shapes were observed.

Sadana (1983) used intermetallic formation of arsenic and copper with DPCSV at a HDME. Arsenic is not amenable to direct determination at a mercury electrode by ASV, thought to be because the arsenic does not dissolve in the mercury. Also difficult is the close proximity of oxidation of Hg to As when attempting CSV (Holak, 1980). However, codeposited with copper, arsenic will solubilise. A detection limit of 1 ppb was reported (Sadana, 1983) after a 2 min deposition time.

The use of mercury electrodes is discouraged due to the perceived dangers of the mercury (Wang *et al.,* 2001). The inclusion of extra electrode layers and procedures inevitably increases procedural complexity when developing an analytical technique,

particularly for *use in the field*. Any new kind of electrode preparation will, ultimately need to be scaled up for manufacture taking more development time and money, so with an eye to commercialisation, there is an inherent advantage to staying with simpler analytical methods.

1.9 Electrochemistry of Arsenic

1.9.1 Electrochemistry of Arsenic Pre 1970

The analytical electrochemistry of arsenic was reviewed in 1969 by Arnold and Johnson. The review concerns polarography with mercury electrodes involving reduction of arsenic compounds in solution. In general, the sequential reduction of arsenic from arsenate to arsenite, to native As, and to AsH_3 is possible in acidic solutions. But the reduction waves are normally complex, having more than one peak. It was possible, however, to use surfactants to suppress one of the peaks, such as gelatine, peptone, glucose, thymolphthalein, sodium Methyl Red, Fuchsine, Methylene Blue and Triton X. Also complexing agents, such as carboxylic acids, were found to simplify the peak in some cases. The pH exerts an unexpected influence, considering that As(V) to As(III) and As(III) to As do not require hydrogen ions in the mass balance equations.

The double wave in general does not vary between mineral acids. The extra maximum was thought to be catalysation of hydrogen evolution by the arsenic, possibly related to arsenic adsorption (Arnold and Johnson, 1969, Cavicchioli *et al.*, 2004).

The reduction of arsenate was possible in 11.5 M HCl (Meites, 1954) with two waves, or 100 % phosphoric acid, with a single wave. Some advantages could be found including complexing agents: the most promising electrolyte reviewed contained 2 M $HClO_4$ and 0.5 M pyrogallol (White and Bard, 1966). As(V) was easily reducible with three peaks attributed to As(V) - As(III) – As – AsH_3 at -0.11, -0.46 and -0.72 V (vs SCE) respectively (Arnold and Johnson, 1969).

Reduction in neutral or alkaline media was comparatively uncommon. In general, the reduction wave becomes more negative as the pH is raised to neutral. A range of alkaline solutions with complexing agents give reduction peaks between -0.85 and -1.75 V.

For example in a lithium electrolyte (0.1 M LiCl/0.01 M LiOH) a peak could be observed at -1.88 V (vs Ag/AgCl), attributed to As(III) reduction to arsine. Arsenate could not be reduced in alkaline media (Arnold and Johnson, 1969, Cavicchioli *et al.*, 2004).

This early work, measuring the reduction of solubilised arsenic and not using a deposition protocol, was not as sensitive for trace level arsenic applications compared with more recent stripping type techniques.

1.9.2 Determination of Arsenic using Stripping Voltammetry

The first reported attempt at using ASV for As(III) determination was on platinum electrodes, conducted by Trushina and Kaplin in 1970 (as cited as Forsberg *et al.*, 1975). Forsberg *et al.,* (1975) studied the arsenic reaction on mercury, gold and platinum electrodes reaction using ASV and DPASV. The ASV reaction was poor on mercury electrodes attributed to low solubility of arsenic in mercury.

As(III) in solution was deposited (on metallic electrodes) between 0.1 and -1.7 V (vs Ag/AgCl) with maximum oxidation peak found around -0.5 to – 0.7 V (in 0.01 to 1 M $HClO_4$). Although the formation of arsine at lower potentials could account for the reduction in signal, the sharp drop in sensitivity beyond the optimum potential was thought to be caused by a thin hydrogenated film in which the arsenic would not be soluble.

Low pH was found to be necessary for a reasonable signal. Out of the mineral acids tested the As oxidation peak in 0.1 – 1 M concentration was largely similar. However,

the decrease in peak could be explained by the shifting of the As reduction potential as the pH increases (Arnold and Johnson, 1969).

For example, a marked reduction in peak area was observed as acid was diluted (6 – 0.001 M $HClO_4$ and HCl). The optimum potential was found for pH 4 and pH 10, at -0.7 ± 0.1 V to -1.0 ± 0.3 V. A similar pattern was seen in 1, 0.1 and 0.01 M $HClO_4$ where optimum deposition potential varied from -0.15 ± 0.05 V, -0.25 ± 0.05 V, to -0.55 ± 0.10 V respectively Forsberg *et al.,* (1975).

The gold was thought to be better than platinum due to the higher hydrogen over potential, allowing lower potentials to be used. For ASV, the limit was determined as 0.02 ppb on gold in a 1 M $HClO_4$ electrolyte with a 20 min deposition time at -0.2 V (vs Ag/AgCl). The same detection limit was obtained for DPASV after a 10 min deposition time. Mercury and copper were serious interferents in this procedure. Forsberg *et al.,* (1975) confirmed the effect noted by Trushina and Kaplan (1970), that adding gold salt to the analysis of arsenic on a platinum electrode greatly increases the sensitivity. This was explained as an increase of surface area as the gold salts deposits during the deposition phase. The enhanced sensitivity was not seen with the gold working electrode, however. In a review by Munoz and Palmero (2005) many researchers have added gold salt for arsenic determination on gold electrodes to improve active surface area and reversibility.

The number of papers concerning the voltammetry of arsenic has escalated in recent years, as shown in Figure 1.7. An escalation of research regarding arsenic analysis by voltammetry has really taken place during the last ten years. Since 1992/1993 the scale of arsenic contamination has become apparent (Smith *et al.,* 2000) with the resulting need for good detection kits. Even the last few years has seen a large effort, perhaps due to the establishment of the US EPA limit of 10 ppb down from 50 ppb in 2002 (Smith *et al.,* 2002).

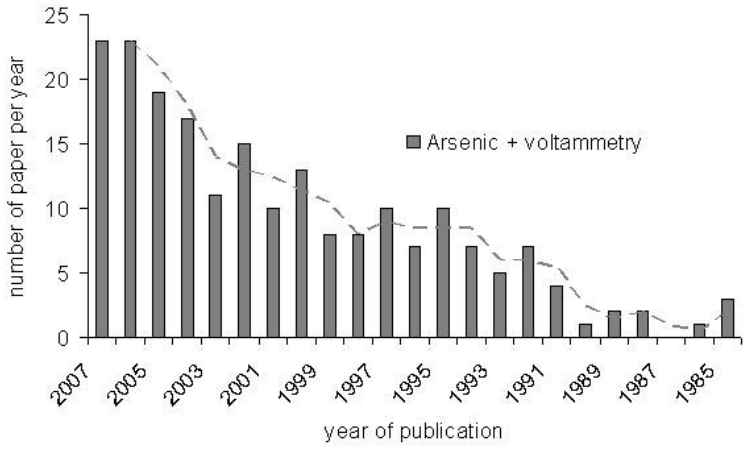

Figure 1.7 Papers published concerning arsenic and voltammetry on an online academic search engine, Web of Science (WOS, 2008)

More recent reviews reveal that much of the work regarding the analysis of arsenic has been split into two categories: those methods using CSV codepositing As(III) with Cu, Se, Pd, Pt or Au onto a mercury electrode and measuring the reduction current (Cavicchioli *et al.*, 2004); and those utilising gold electrodes with ASV, DPASV or PSA. Concern for the latter methods surrounds the maintenance of the electrode surface and the need to incorporate conditioning procedures.

Cathodic stripping voltammetry methods typically contain mercury or copper-mercury amalgam (Piech *et al.,* 2007) electrodes. Whilst this discourages *in situ* use, it is considered practical by some (He *et al.*, 2007). However, much research has been conducted in recent years to replace mercury with the relatively environmentally benign bismuth (Wang, 2005). Analogous behaviour for anodic stripping of Cd, Pb and Zn has been observed for mercury and bismuth films. Bismuth oxidises at a slightly negative potential compared to mercury: Cu is not so easily determined.

A CSV 'mercury free' method for As(III) determination used *in situ* plated bismuth and codeposition with selenium. The catalytic hydrogen wave was used to determine the quantity of As present at -1.15 V (vs Ag/AgCl). The technique was sensitive to a range 0.01 to 1 ppb As after a 30 s deposition time. But several metals including Cu, Hg, Pb and Cd interfered and could not be tolerated above 1 ppb when determining 1

ppb As(III). However, sub pptr levels could easily be obtained with longer deposition times (Jiajie and Nagaosa, 2007).

1.9.3 Types of Gold Electrode

Besides solid gold polycrystalline and monocrystalline electrodes there are a variety of methods for producing a gold electrode surface.

Gold electrodes can be prepared by deposition of gold salt onto carbon (Sun *et al.,* 1997, Dai, *et al.,* 2004), platinum (Huang and Dasgupta, 1999), boron doped diamond (Song and Swain, 2007), or indium tin oxide (Dai and Compton, 2006a). It is also the basis of a method published by the US EPA for ASV determination of arsenic (US EPA Method 7063, 1996), as well as mercury. Sun *et al.,* (1997) used a gold film electrodeposited on a carbon graphite electrode. After polishing with 0.5 µm alumina powder and rinsing in nitric acid and distilled water, the carbon electrode was submerged in 40 ppm Au(III) solution and left for 5 min with an open circuit, whilst the solution was purged with N_2. Then the gold was deposited for 4 min at a -0.2 V. Between each test, the electrode was held at 0.5 V for 10 s and rinsed. Svancara *et al.,* (2002) deposited gold salt on to a polished carbon paste electrode, by holding the potential at 1.5 V for 60 s then -1.0 V for 15 s (vs SCE). Dai *et al.* (2004) achieved a particularly low detection limit in 1 M HCl by choosing the conditions of gold film deposition carefully; 9.6 pptr limit was achieved. With the right conditions, the gold nucleates on the surface conferring nano array type characteristics with the advantage of convergent diffusion. The gold salt deposition method probably carries most favour at the present time (for example, the US EPA approved method). However, there is some disagreement concerning the electrode maintenance between tests needed to ensure analytical reproducibility.

Gold surfaces have also been produced by electron beam evaporation (Feeney and Kounaves, 2002), chemical synthesis of nanoparticles (Song *et al.,* 2006), gold powder composite electrodes with polymer resins such as polymethylmethacrylate (PMMA) (Navratil, *et al.,* 2003) or with carbon based inks and pastes (Simm *et al.,*

2005). Although no papers have been published for gold screen-printed electrodes, these electrodes have been assessed by Cooper (2004), Noh (2005), Cauchi (2005) and Bolbot *et al.,* (2007). Composite materials are of concern when stability of materials in the desired electrolyte conditions becomes compromised (for example Navratil *et al.,* 2003).

Gold preparation procedures also allow for various electrode designs. Different morphologies of gold electrode have been utilized such as disk (Forsberg *et al.*, 1975), fibre (Huang *et al.,* 1988, Salaun, *et al.,* 2007), microarray (Feeney and Kounaves, 2002) and nano array (Dai *et al.,* 2004). Relative advantages of preparation, complexity, time and cost as well as inherent reproducibility must be considered in light of the analytical advantages obtained with different configurations.

1.9.4 Working Electrodes other than Gold or Mercury

More recently researchers have reassessed the use of gold electrodes. Simm *et al.,* (2005), showed that by carefully selecting the electrolyte (0.1 M HNO_3) the oxidation wave of the silver could be positive enough to allow the arsenic peak to be evaluated, with a detection limit in the low ppb range. Silver is less expensive than gold; however, the technique is highly susceptible to Cl^- ion contamination, as well as Cu interference.

The technique of electrocatalytic oxidation of As(III) to As(V) using electrodes other than gold or mercury, has been pursued in recent years. For example, Dai and Compton, (2006b) used platinum nanoparticles electrodeposited on glassy carbon. Iridium, electrodeposited onto boron doped diamond has been used for arsenite determination in a pH range 2-8. A detection limit 0.15 ppb was obtained. Since this technique does not involve a deposition phase (As(III) is soluble) amperometry was used with a stirred solution to increase transport rates (Salimi *et al.,* 2004).

Although this oxidation technique is competitive with typical stripping techniques, it does not appear to address the fundamental problem affecting non mercury electrodes:

of electrode past history; and the onus on the analyst to carefully polish and rinse the electrode surfaces, even with film/nanoparticle deposition procedures. However, screen-printed electrodes offer the disposability route. Iridium catalysed carbon powders may offer a future development for screen-printed detection of As via the oxidation route.

1.9.5 The electrolyte

The electrolyte used in the majority of the literature, concerning both mercury and gold surfaces, is HCl (Cavicchioli *et al.,* 2004, Munoz and Palmero, 2005). Whilst at low concentrations the mineral acids have a largely similar effect on the arsenic peak (Arnold and Johnson, 1969, Forsberg *et al.*, 1975), HCl at higher concentrations has usually facilitated improved peak reversibility and, in some cases, improved peak magnitude. However, lower concentrations of HCl improve safety. Researchers with various experimental setups have drawn different conclusions about the optimum concentration between 0.1 M and 7 M HCl (Munoz and Palmero, 2005). The effect of interfering ions must also be considered Cu, Hg are among the common interferents with stripping peaks close to the arsenic. Pb and Fe can form intermetallic compounds also.

1.9.6 The Speciation of Arsenic and the mechanism of reaction

Arnold and Johnson (1969) tried to explain the HCl effect using the then available data for the speciation of As(III) in high concentration electrolytes, as shown in Figure 1.8 (Arcand, 1957).

Arcand (1957) studied the extraction of As from high concentration HCl electrolytes into an organic solvent. The Cl species are non polar and are presumed extractable. The As and Cl present in the organic phase could be measured by titration. Arsenic extracted appreciably above 1 M HCl, and was almost entirely extracted by 11.5 M. The ratio of As:Cl in the organic phase at 11.5 was 1:3, dropping to 2:1 as HCl concentration dropped. This was strong evidence for the presence of Cl groups substituting for hydroxy groups sequentially. By using a best fit model Arcand

derived both the partition constants between the organic-aqueous phase and the formation constants for each species. The assumption was made that only $As(OH)_3$, $As(OH)_2^+$, $As(OH)_2Cl$, $As(OH)Cl_2$ and $AsCl_3$ were present. Particularly $AsCl_4^-$ was omitted, even though as a charged species it would not be expected in the organic phase. One particular problem with the quantitative derivation is the assignment of individual ion activities in the concentrated electrolytes; Arcand (1957) assumed equal activity to H_3O^+ and Cl^-.

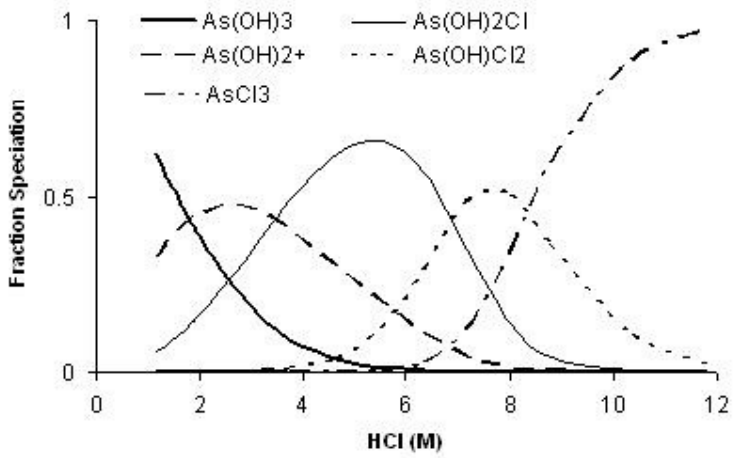

Figure 1.8 Speciation of Arsenic in concentrated HCl electrolytes according to Arcand (1957)

More recently Sella *et al.,* (1991) used the Zdanovskii-Stokes-Robinson relation to derive single ion activities, based on the degree of hydration (the number of water molecules bound to the H^+ and Cl^- ions). Sella and Bauer, (1990) measured the individual ion activities electrochemically using the H/H_2 and Cl/Cl_2 redox couples. The possibly questionable part of the experiment utilized an insoluble metallocene couple to keep track of the solution potential independently of either Cl^- or H_3O^+. It had to be assumed that the metallocene kept a consistent potential with the changing electrolyte, and appeared to work. Sella *et al.* (1991) assumed the same speciation options as Arcand (1957) and produced extractions for arsenic in both HCl and $CaCl_2$ solutions and using the single ion data. This produced a, possibly, more accurate map of arsenic speciation with HCl concentration, as shown in Figure 1.9. The positively charged $As(OH)_2^+$ is more prevalent in this scheme than for the work of Arcand (1957).

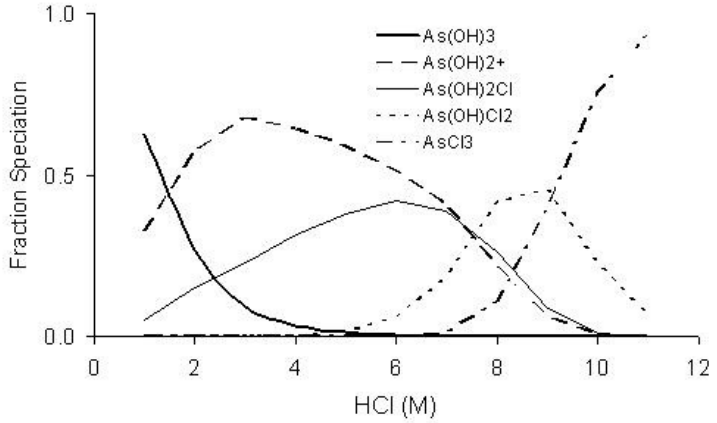

Figure 1.9 Speciation of arsenic in concentrated HCl solutions with single ion activity correction according to data reported by Sella *et al.,* (1991)

The Zdanovskii-Stokes-Robinson relation is controversial: whilst it explains the ionic activities of many electrolytes at high concentrations, there are many it does not explain. The degree of hydration of some ions has been questioned, also, altering the interpretation of the theory (Hamann *et al.,* 2007).

The speciation of inorganic and organic species was calculated by Hasegawa *et al.,* (2002). Extracting into organic solvent and using a more accurate atomic adsorption technique, principle components analysis was used to fit the data. Methylated forms of arsenic formed chlorinated species at much lower HCl concentrations. In deriving the inorganic species $As(OH)_2^+$ was omitted without explanation. Also for the high HCl concentrations the expected decrease in water activity was also omitted. Also the single ion activity correction was not used. Despite these differences the speciation was broadly similar to that of Arcand (1957).

These studies show that obtained precise speciation data is difficult in these electrolytes. But the broad picture is consistent: it is thought that $As(OH)_3$ goes to $As(Cl)_3$ in successive steps of Cl^- ion substitution, which is not complete until > 10 M HCl. The first Cl^- is not substituted until about 2 M HCl. The presence of $As(OH)_2^+$ could account for the pH dependence of the As(III) reduction in mineral acids.

Arnold and Johnson, (1969) considered in detail the available polarographic data of arsenic reduction HCl solutions. The mechanism is complicated due to the fact that the number of electrons exchanged is not clear cut (3 would be expected for As(III) to As). There may be a single or multi step reaction. However, the authors preferred a multistep reaction dependent of a 'chloride bridging mechanism' since it could explain the HCl dependence in part. They believed that intermediate formation of As(I) was likely due to the calculated number electrons exchanged. As of 2005, Munoz and Palmero note that little has been advanced in the understanding of this reaction. The change in speciation and chloride bridging effect could explain the slight positive shift in the oxidation peak cathodically, improved reversibility and increasing signal at high concentrations.

1.9.7 Metal Interferences

In addition to the arsenic stripping peak, the possibility of interfering metals must be considered. Sb(III), Bi(III), Hg(II), Pb(II) and Cu(II) can in some circumstances cause problems. Copper forms a compound with arsenic as does selenium and iron which can reduce the observed peak (Munoz and Palmero, 2005).

The stripping peaks for As, Hg and Cu could be separated by an appropriated choice of electrolyte according to Huang *et al.*, (1988) and Huang and Dasgupta, (1999) who use 4 M HCl + 2.5 M $CaCl_2$ and 4.5 M HCl respectively for metal stripping. In these examples excess copper could be tolerated (20 fold excess to As(III) for Huang and Dasgupta, 1999).

In experiments with screen-printed gold electrodes Noh (2005) used 1 M HCl but found that 1:1 presence of Cu:As caused significant interference with As determination. However, Cooper (2004) found that in 4 M HCl a 20 fold excess of copper was tollerable. Munoz and Palmero, (2004) were able to use 1.2 M HCl with 160 ppm Au(III) as chemical reoxidant and *in situ* plating in the presence of over 10 fold copper when a PSA procedure was employed. Although copper was not problematic, Bi and Sb would strip at the same potential forming a coalesced peak at

1:1 concentrations with As. Dai *et al.,* (2004) based their highly sensitive nanoparticle array technique using 1 M HCl but admitted that ion exchange would be necessary to remove copper interference, limiting direct use on drinking water. For drinking water applications environmentally prevalent Cu is likely to be the main interference; the US EPA limit for this metal is 1300 ppb.

1.9.8 Speciation of Copper, Mercury and Gold

The change in potential of copper and mercury peaks can be attributed to Cl^- speciation, as shown in Figure 1.10. Copper has two oxidation states. While Cu(I) is unstable in the absence of ligands, Cl^- ions stabilise this oxidation state (Wang, *et al.,* 1997, Sherman, 2007). It can be seen in Table 1.8 (page 35) that complexed metal ions (such as Ag and Cu) strip at lower potentials than the uncomplexed metal. The mercury moves the most with increasing HCl concentration (Huang and Dasgupta, 1999): mercury is the most highly coordinated of As, Cu and Hg. It is also possible that complexation with Cl^- discourages intermetallic formation.

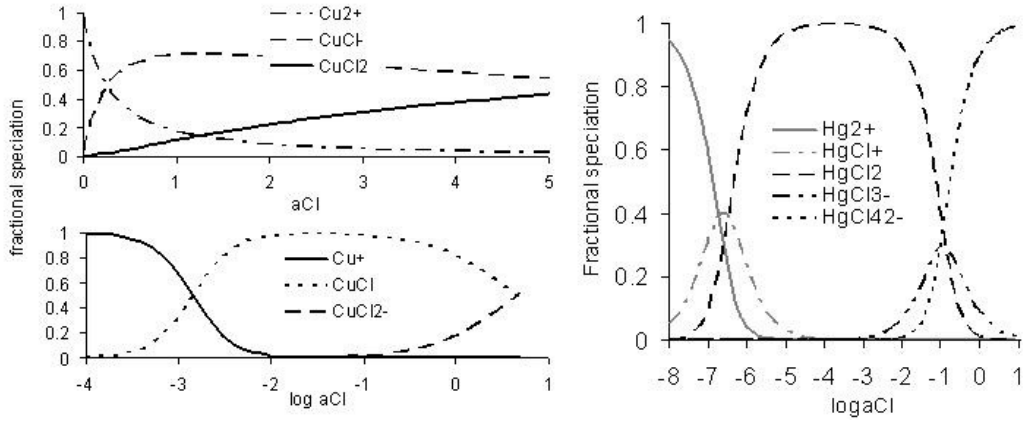

Figure 1.10 Speciation of copper and mercury in concentrated Cl^- ion solutions (data from Sekine and Ishii, 1970, Wang *et al.,* 1997c and Sherman, 2007)

Also, it must be noted that the stripping of As, Cu and Hg from the gold surface may have significant alloying effects when the metals deposit at sub monolayer quantities. The alloy effect generally increases the stability of the reduced metal causing the

potential of stripping to increase. This effect is underpotential deposition (Herzog and Arrigan, 2005).

Gold surfaces may become complexed with Cl^- ions if the potential of the electrode is positive enough. Li *et al.,* (2004) studied the gold speciation in 2 M HCl with Raman Spectroscopy as the electrode potential was varied. $AuCl^-$ was detected at potentials above about 0.8 V (vs Ag/AgCl) up to 1.2 V. $AuCl_4^-$ peaks were seen simultaneously with $AuCl^-$. Above 1.2 V gold oxide layers were formed, and the Au-Cl peaks disappeared. The $AuCl_4^-$ could be detected diffusing into solution. The boundary between Au-Cl layers and gold oxide layers can allow the propagation of spontaneous oscillations. Theses oscillations and the dissolution of the gold lead to surface roughening. The gold surface appeared to have approximately 10 µm pits on the surface after the electrochemical procedures.

1.9.9 Determination of As(III) and As(V)

Few papers have considered the determination of organic arsenic compounds directly. Hasegawa *et al.,* (2002) showed that methylated arsenics used in the study did not decompose even in concentrated HCl. It is also known that arsenobetaine can only be decomposed with strong oxidising conditions as it is highly recalcitrant (Cavicchioli, *et al.* 2004).

Also, few papers consider the electrochemical reduction of As(V): on mercury electrodes, as already noted, As(V) can be reduced either in extreme situations such as 11.5 M HCl or 100 % phosphoric acid at negative potentials or with some chosen complexing agents such as manitol or pyrogallol (Arnold and Johnson, 1969).

Some work has shown that the conditions under which arsenate can be reduced can be extended. Huang and Dasgupta, (1999) used a gold film deposited on a platinum wire (250 µm diameter) in 4.5 M HCl stripping solution. 1 M HCl was used for deposition (flow cell setup) with -0.2 and -1.6 V potentials used for As(III) and As(V) respectively. Although the -1.6 V deposition produces hydrogen evolution and

associated high background currents, the small surface area minimises the effect. Huang, *et al.,* (1988) also used gold deposited on a 10 µm diameter platinum wire with a flow cell setup, depositing As(V) in 1 M HCl at -1.8 V, and stripping in 4 M HCl + 2.5 M $CaCl_2$. A smooth wire helped to detach the large bubbles formed by percolation, more efficiently than flat surfaces (Salaun *et al.,* 2007).

Salaun *et al.,* (2007) used a 5 µm gold fibre to reduce As(III) and As(V) in a variety of HCl concentrations, when the deposition potential was altered accordingly. In pH 8, seawater samples a -1.2 V deposition potential for As(III) stripping at - 0.35 V (vs Ag/AgCl) was used. For As(V) the sample is acidified to pH 1 with HCl, 30 s at -1.0 V deposits both As(III) and As(V). It is thought that the As(III) is oxidised initially by Cl_2 generated at the counter electrode. The stripping peak was seen at -0.05 V. The optimisation of deposition potential showed that at pH 1, the As(III) response would decrease with deposition lower than -0.8 V. Response to As(V) in this medium started at -0.7. The response to As(III) and As(V) was equal at -1.0 V and lower. The reduction in arsenite could be due to the formation of AsH_3. Monomethylarsenate was found to deposit and strip as inorganic As(V). Dimethylarsenate would also strip but at a slightly modified potential, indicating some kind or complex even in the reduced state (Salaun *et al.,* 2007)

It has been common for a chemical reduction of As(V) to As(III) to be used, prior to electrochemical determination. Reducing agents have included hydrazine with a strong acid, ascorbic acid with iodide, iodide alone, sodium sulfite, cysteine, gaseous sulphur dioxide and manitol (Arnold and Johnson, 1967, Cavicchioli, *et al.* 2004, Munoz and Palmero, 2005). Difficulties (for *in situ* application) are found since many of the procedures need heating to complete the reduction for 10 -30 min. Sulphur dioxide method requires apparatus for gas flow. The use of cysteine has been shown to cause a broader arsenic stripping peak at slightly positive potentials (Svancara *et al.,* 2002, Cooper, 2004). Also cysteine is not stable in concentrated HCl solutions.

1.9.10 Sample Pretreatments

Cavicchioli *et al.,* (2004) reviewed the necessary steps for sample pretreatment before the determination of arsenic. With natural water no sample digestion was needed. With polluted waters and wastes mild digestion possibly clean up were needed such as filtering. For solid specimens, significant sample digestion or at least analyte extraction was required. Food and seafood samples in particular require oxidative digestion to decompose methylated and the recalcitrant species of arsenic; UV digestion was common for breaking down organics.

A novel technique was investigated by Cepria, *et al.,* (2005) using physical (abrasive) immobilisation of contaminated soil particles on to a glassy carbon electrode surface. Peaks were visible for Pb, Cu and As (III and V). The peak for arsenic (in 0.1 M oxalic acid solution) could be obtained when As was present in more than 10 ppm (based on calibration with As_2O_3 additions and suitable for soil screening), but the sensitivity was severely affected by the presence of iron.

1.10 Screen-Printed Sensors

Typically for analytical applications, the objective is to make low-cost, reproducible technique. If a large number of sensors is required, a scalable manufacturing technique is needed, which can preferably be automated.

To produce a sensor a controlled structure or pattern of materials, a template is needed. Materials can be deposited by processes including chemical precipitation or adsorption, electrochemical deposition, cold vapour deposition or sputtering. The sensor design can be produced by methods including photo patterning, motorised deposition or selective etching.

The printing process enables material to be deposited using a template into specified patterns. Although there are many printing processes there are only a few basic principles (Gilleo, 1996). The intaglio or gravure where ink is held in the recessed

areas of a template; relief or letter press, where ink is held on the raised sections of the template; lithographic processes use regions of hydrophobic and hydrophilic (differing surface tensions) on the printing plate; screen-printing (or 'transil') where ink is forced through a stencil. Additional specialised methods include ink jet, electrostatic and lasermarking (Gilleo, 1996). Screen-printing is the only printing method suitable for 'thick film' deposition. Most printing methods print layers 2-3 µm thick. Also many techniques require low viscosity, thus solids contents. Thick film deposition (10-20 µm) and high solid contents are generally required for printing conductors (Gilleo, 1996, Hobby, 1997).

Screen-printing is seen as a black art tending toward an exact science by some (Hobby, 1997). Screens are made using a polymer or steel mesh, with thin wires woven like cloth. There maybe 60 to 500 counts (wires) per inch. In general, the spacing must be at least three times the particle diameter. For precision applications, the mesh is fixed to a steel or aluminium frame with high tension (frames bearing as much as 800 N), precluding the wooden frames used for textile patterning. On top of the mesh a mask is used to provide the template pattern. Historically, photosensitive gelatine and dichromate were used before being replaced by diazo materials. However, photosensitive polymers are now used. The entire screen is covered in emulsion on the reverse side. The emulsion is then pushed through to the front surface, allowed to dry and exposed to a light pattern. The light induces a reaction immobilising desired areas of the polymer. The remaining emulsion is washed out with water. The thickness of the emulsion affects the thickness of the print deposit (Gilleo, 1996, Hobby, 1997).

Whilst printing is possible from a cylindrical roll, flatbed printing is more common. During operation, the ink is spread out evenly across the screen with a stainless steel flood bar (no downward pressure). To print, a squeegee is drawn across the screen with a controlled downward pressure. Some screen-printing systems use the squeegee for both flood bar and printing.

Upon the application of pressure, the screen is pushed momentarily down on to the printing substrate. Control of the off contact distance, and squeegee pressure determine the quality of ink deposition. Since squeegees are normally made from polyurethane, the wear is significant for maintaining equal pressure. A motorised apparatus controls the squeegee position, height and pressure. The screen is in held in place using a clamping system and substrates are aligned with x, y and angle fine control positioning. Precise positioning is needed when alignment between substrate and deposited ink is required. Alignment can be achieved either optically or manually by eye (Gilleo, 1996, Hobby, 1997).

Upon being pushed through the mesh the inks reforms as a single layer. A schematic of the printing process for the flood bar and squeegee action is shown in Figure 1.11.

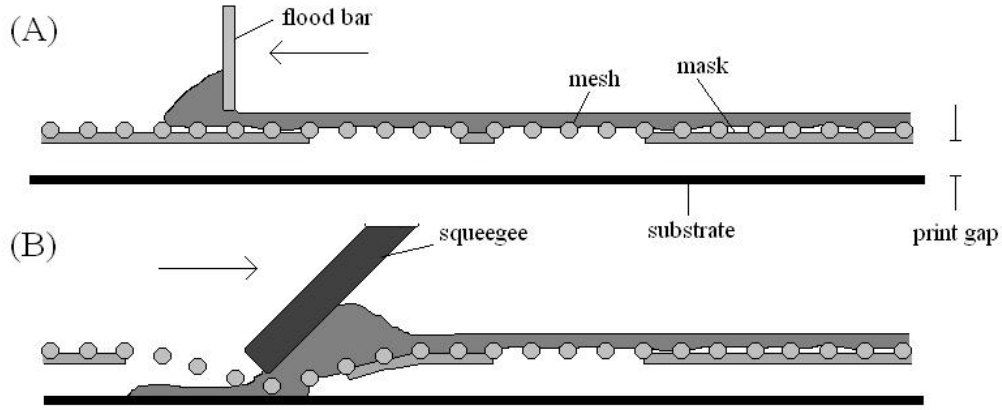

Figure 1.11 Screen-printing schematic: (A) action of flood bar from right to left, providing a smooth layer of ink, (B) action of squeegee from left to right with downward pressure to deposit the ink

Thick film, inks are prepared by mixing a solvent, polymer, and powder solids in proportions to provide adhesion and flow viscosity. Mixing is performed initially in a plenary mixer. Most reproducible results are obtained using a three roll mixer over time period of about 24 hr. Three rollers rotate at differing speeds sequentially, with a narrow distance between the surfaces. If the distance is too narrow, ductile particles become flake shaped and/or aggregated (Prudenziati, 1994, Gilleo, 1996). The ink is removed from the mill using a take off blade with care to avoid scraping the roller material.

Screen-printed inks are used for industrial applications including biosensors, automotive, fuel cells, surface mount technology electronics, semiconductor manufacturing, display and membrane switch applications (DEK, 2008). These applications have grown significantly in the last 20 years: for example Figure 1.12 shows the number of publications on screen-printing from 1985 to 2005 from a handful of publications per year to over 300.

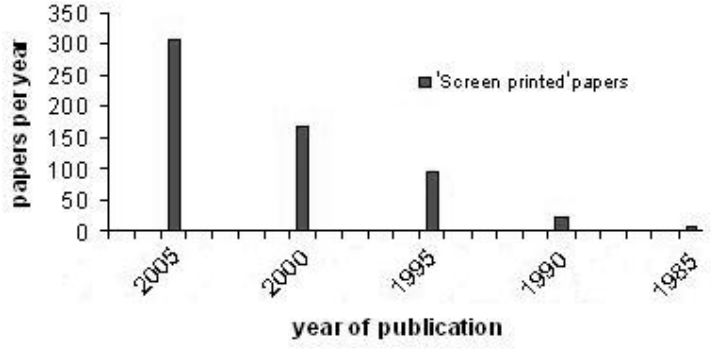

Figure 1.12 Growth of publications on screen-printing and applications from 1985 to 2005 according to the Web of Science (WOS, 2008)

Screen-printing inks for conductors can be put into two categories: those that print with ceramic adhesive component (such as glass particles which melt at high temperature) on a metallic or ceramic substrate (Nascimento and Lucio, 1998); and those which incorporate a polymeric resin dissolved in a solvent which can be evaporated at lower (< 200 °C) temperatures compatible with paper and flexible plastic substrates (Newman and Turner, 2005). The ceramic inks generally still contain polymer-solvent component to provide the flow characteristics for printing. The latter inks are relatively inexpensive due to the lower processing temperatures and inexpensive substrate materials (Nascimento and Lucio, 1998).

The largest application in the field of biosensors for screen-printed electrodes is, undoubtedly, the measurement of blood glucose (Newman and Turner, 2005). In 2000, an estimated 135 million people were suffering from diabetes. Those being treated are advised to check their blood glucose measurements twice a day. Although the older reflectance based technology is still preferred by some, the vast majority of strips use screen-printed electrochemical strips. The leading manufacturers (with UK

addresses) include Roche Diagnostics Ltd (West Sussex, UK), Lifescan (Inverness, UK), Abbott (Maidenhead, UK) and Bayer (Newbury, UK) contributing to a global multibillion dollar market (Turner *et al.,* 2006). These strips incorporate an enzyme, glucoseoxidase, with a redox mediator such as potassium ferrocene according to a scheme developed by Cass *et al.,* (1984). Glucoseoxidase as the name suggests facilitates changes in redox state of glucose; however, the reaction needs an electron donor. Electron transfer direct to the electrode is difficult due to the size of the biomolecules. A facile redox reaction can be used to 'shuttle' charge from the site of the glucose reaction to the electrode surface. According to Cass *et al.,* (1984), a linear response on a graphite electrode for 1 - 30 µM glucose in blood suitable for diabetics was found to be stable in the presence of expected levels of oxygen, pH and temperature.

Of the electrochemical test strips 95 % weight is made up of polymers. The polymers may contain the additives associated with plastics. Uniformity and mix of the polymers is important and in excess of 100 polymers have been tested for application to electrochemical response of glucose (Usmani, 1994). However, screening of polymers and additives was necessary to avoid interferences. Viscosity, solid content, particle size, surfactants, residual initiators, glass transition temperature, tough film and low tack were all considered for the final preparation. A copolymer of styrene and acrylate with addition of mica to reduce tack was found to be the best choice (Usmani, 1994).

Many sensor designs have since been modelled on the successful glucose sensor (Hart *et al.,* 2004). Much of the work has been to show *proof of principle* for the determination of a wide variety pharmaceutical, environmental and food toxin applications. The list includes: organophosphates, nitrates, pesticides, phenols, poly aromatic hydrocarbons and tri-nitro toluene (TNT); anti depressants such as Triclosan, Codeine and methamphetamine. Hart *et al.,* (2004) predict that many of these applications will become commercialised.

1.10.1 Screen-printed Sensors and Metal Ions

Wang and Tian (1992 and 1993b) used screen-printed carbon with mercury and gold coating to determine lead for various applications such as blood, urine and drinking water. A patent was filed to cover the application of mercury film to carbon screen-printed electrodes for Cd, Cu and Pb (Wang, 1994). The mercury, gold and bismuth films (Wang, 2004) are electrochemically pre-deposited or codeposited with the sample. Mercury has also been pre loaded in the electrodes as solid mercury oxide (Honeychurch and Hart, 2003).

The use of screen-printed electrodes for determination of metal pollutants was reviewed by Honeychurch and Hart (2003). The common metal ions included Cu, Pb, Cd and Zn, usually with a Hg film; more recently uranium, aluminium, nickel, silver (Dilleen *et al.,* 1998) and chromium(VI) (Turyan and Mandler, 1997) have been detected with specialised techniques. Carbon screen-printed electrodes with mercury (Kadara *et al.*, 2003, Cooper, 2004, Noh *et al.,* 2005) and bismuth (Kadara and Tothill, 2004, Kadara and Tothill, 2005) films have been used for extracted soil samples. In addition to the formation of amalgam with a film such as mercury, methods exist for chemical modified screen-printed electrodes such as chelating agents to concentrate target ions. Few studies have used bare screen-printed surfaces. The number and size of peaks is thought to be dependent on the heterogeneous electrode surface. Also a patent by Lane *et al.,* (2000) shows the use of the Ercon polymeric gold ink showing the possibility of interference free determination of cadmium, copper and lead. Noh and Tothill (2005) used unmodified gold screen-printed electrodes to determine Pb in water samples. No work on arsenic was reported in the review (Honeychurch and Hart, 2003).

Both Cooper (2004) and Noh (2005) have looked at As(III) on screen-printed gold electrodes, but both encountered problems with unidentified interference. Song, *et al.,* (2006) immobilised (electrochemically deposited) poly(L-lactide) stabilised 10 nm gold particles on carbon screen-printed electrodes. In natural water samples arsenite was determined down to 0.1 ppb, in a 1 M HCl medium. Zen *et al.,* (2003) used

Prussian blue-modified carbon screen-printed electrodes as mediator for the oxidation of As(III) to As(V) using a flow injection system with a limit of detection of about 1.5 ppb.

1.10.2 Screen-Printing Inks

According to Wang *et al.,* (1998), Forrow and Bayliff (2005) and Morrin *et al.,* (2003) the formulation of screen-printed inks, in general is proprietary, but has a profound effect on the electrochemical performance. Carbon inks were tested from four suppliers Gwent Electronic Materials, Ltd (Pontypool, UK), DuPont (DuPont Microcircuit Materials, Bristol, UK), Acheson Colloids Company (Plymouth, UK) and Ercon, Inc (Wareham, MA, US). Some inks demonstrated better thermodynamic reversibility such as the Gwent ink (C10903D14) whereas other inks demonstrated greater stability with wider potential ranges in common electrolytes. When subjected to SEM the inks have differing compactness of upper layers composed of carbon powder and polymer. The DuPont gold ink BQ331 according to Cooper (2005) demonstrates excellent reversibility akin to the atypical Gwent carbon ink.

Various methods for improving the thermodynamic reversibility have been developed for screen-printed electrodes, including laser (Osbourne *et al.,* 1996), electrochemical (Cui *et al.,* 2001, Morrin *et al.,* 2003, Wei *et al.,* 2007), chemical (Fogg *et al.,* 1995, Wei *et al.,* 2007) and polishing (Cui *et al.,* 2001) pretreatment. Many of these traeatments are consistent with the removal of top layers of inert polymer from the electrode surface exposing the particulate surface resulting in better thermodynamic reversibility (Osbourne *et al.,* 1996, Wang *et al.,* 1998, Cui *et al.,* 2001, Wei *et al.,* 2007). However studies, such as Fogg *et al.,* (1995), show that addition of polymeric surface layers with electron transfer characteristics can also improve the reversibility. The effect of heat pretreatment has been found to affect some inks and can be attributed to morphological changes in the electrode surfaces (Morrin *et al.,* 2003).

In a few publications, home-made inks have been compared with commercial inks for performance (Osbourne *et al.,* 1996, Wang and Musameh, 2004, Rao *et al.,* 2006),

using polystyrene (PS), PMMA and polyvinylchloride (PVC) dissolved in appropriate solvents. Carbon inks typically show slow kinetics. Newman *et al.,* (1995) fabricated a number of catalytic inks using a water soluble hydroxyl ethyl cellulose polymer. Although the catalytic materials such as Pt, Rd and Pd have sensing advantages, water, as the ink solvent, is problematic due to its relatively low boiling temperature and tendency to evaporate prematurely from the printing screen. Also, the polymer disintegrates in aqueous test solutions.

Also, there is research focusing on carbon powder added to render plastics conductive which shows the effect of powder-polymer affinity. If the powder and polymer have high affinity, the polymer tends to cover the powder reducing conductive pathways. However, if the affinity is low the particles are partially exposed. If the affinity is too low, then powder aggregation dominates over dispersion (Jurado *et al.* 1991, Lux, 1993, Cheah *et al.* 2001). In addition, the use of polymer blends can cause the formation or polymer microstructures. Low entropy of polymer mixing, Morgado *et al.* (2001) can cause structure on the nano to micro scales.

1.11 Conclusion

Due to the circumstances of the project, it is difficult to provide a simply defined perspective. The shift in initial objectives within the first 6 months was dramatic and a single coherent point of view will not be visible throughout the work. Certain general points may be noted, that are relevant since much work has already been conducted on biosensors, screen-printed strips and metal ion sensing: research in many areas has accelerated in recent years, whether it is arsenic contamination, screen-printed technology or biosensors. Thus, it is difficult to enter any of these fields without considerable reference to past research, before providing something ‘new’.

One of the problems affecting screen-printed sensors is the tension between the need to fabricate, possibly customised, sensors based in a climate where the formulations are proprietary (Wang *et al.*, 1998). Improper formulations can manifest interferences

(Usmani, 1994) or inefficient electron transfer characteristics (Wang *et al.*, 1998, Morrin *et al.*, 2003).

Despite some efforts (Zen *et al.,* 2003, Cooper, 2004, Noh, 2005 and Song, *et al.,* 2006) a simple method for determination for arsenic using screen-printed electrodes is not forthcoming, as yet. Yet, screen-printed electrodes are unique in their ability to tackle the issue of electrode reproducibility and maintenance which acts as a hindrance to electrochemical methods used *in the field*.

It has been the author's *intent* to provide a useful system for real-world application in the complex practical climate, whereby any number of preexisting systems are in place and the prepared product must provide a performance advantage (if only slight). Without this there is no financial justification. Thus, the focus of much of the work is highly specific (i.e. looking at sensor based interferences). It has been the author's perception, whether rightly of wrongly, that one of the significant hurdles to sensor readiness is the gulf between purely academic and commercially viable work. The persistence to continue with the particular gold screen-printed electrodes is due to the ostensible fact that they should work, and intuition is that there is no satisfactory reason (as yet) why they do not. Out of this came a significant amount of reiteration in experimental methods returning to the same problems with slightly changed permutations and combinations of hypotheses and equipment. Since the author has attempted to setup the rational for the work, acknowledging that not all questions could be resolved, the project inherently lacks the clarity that many thesis's would have (where the framework would have been established by supervisers with experience).

The reader may ask why this project was initiated. The project was devised by Dr S.J. Setford and Professor S. Saini (previously of Cranfield University). The gold screen-printed electrodes evaluated (Cooper, 2004) were promising both for sensor research and as commercial opportunity. The idea was to combine carbon based and gold based screen-printed electrodes with a portable potentiostat (built *in house* by P. Knight, D. Pitts and Dr C. Walton of Cranfield University) to be used for metal ion

assessment for contaminated land assessment (and any other applications forthcoming). For the carbon (with mercury film) both electrochemical protocols and soil extraction procedures had been considered (for example, Cooper, 2004), for As and Hg on gold sensors only the electrochemical procedure had been devised. Thus, this PhD project was setup to assess the As and Hg sensors when used for *in situ* soil extraction. Real and synthetic soil samples were to be prepared and spiked with concentrations of As and the extraction effeciencies of various procedures compared. Assuming good results a procedure would be developed for combined use of carbon and gold sensors assess soil extracts under real conditions (with multiple complexing and interfering ions and large possible concentration ranges possible on contaminated land sites). The results would be verified by comparison with an established heavy metal detection technique, such as ICP-MS. The author had had previous experience with the preparation of synthetic soils spiked with contamination (Schifano *et al.,* 2007).

However, the reader will find no work on soil extracts in this thesis. The reader may ask why the the multi ion sensor for contaminated land samples was sidelined in favour of single ion detection. This was because commercial contacts advised that a single ion sensor is more marketable and highly desirable in the case of arsenic in drinking water. Also the detection of metal ions in drinking water is considerably simpler than contaminated land samples.

1.11.1 Objectives

The objectives of this research project have shifted significantly during the course of this investigation. The project started by aiming to achieve the objectives listed in set 1. However, these were modified to cover the objectives listed in Set 2 and 3.

Objectives Set 1, Initial Objectives

The initial objective here would be to repeat the electrochemical procedure reported by Cooper (2004) for the determination of As and Hg on gold screen-printed electrodes and to include:

Characterisation of the sensors in more detail, if necessary, and optimisation of the conditions.

Finding an alternative method for As(V) determination (preferably without lengthy heating pretreatment of the sample)

Develop, characterise and optimise the practical single phase extraction of As(III) and As(V) and Hg from soils.

Spike synthetic and real soils with As and Hg, assess extraction efficiency and electrochemical performance. Verify with ICP-MS or equivalent.

Develop method combining carbon (mercury film) and gold sensors for a contaminated soil screening.

Test portable potentiostat and multi sensors on site

Objectives Set 2, Understanding Sensor Performance

Focus on developing single metal ion sensor for As (and Hg).

Electrochemical assessment of problems with sensor stability and characterisation of interference.

Characterisation of sensor interference with *in house* fabricated sensors.

Characterisation of ink qualities by microscopy, FTIR, Raman Spectroscopy, GCMS, XPS and NMR.

Attempt to link physical and chemical properties to electrochemical performance (particularly for the Nicholson Method).

For new model of electrode behaviour, design a suitable experiment to test the predictions clearly, or test the model with explicit simulation.

Objective Set 3 Development of Sensor for Determination of Arsenic

Investigate mitigation of interference by sensor design modifications and evaluate effectiveness.

Characterise and optimise electrode modifications, such that electrode may substitute for gold electrodes in established analysis procedures

Develop method for As(III) determination below drinking water limit,

Optimise electrochemical parameters with conditions facilitating analysis with minimal interference.

Develop method for As(V) chemical or electrochemical reduction of suitable practicality for *in situ* use.

Test method with real drinking water samples, both in the UK and from contaminated hotspots.

Chapter 2 Materials and Methods

2.1 Introduction

This chapter contains the general methods used in this thesis. Many methods were developed during the course of the work, so there is some discussion included with the descriptions. In general, the methods involved electrochemical and spectroscopic investigations. Electrochemical experiments focused on DuPont sensors using a polymeric gold working electrode. However, a number of other electrode systems were also used both separately and combined in a number of permutations to help isolate certain behaviours. These other electrodes included non DuPont commercial electrode inks printed *in house*, *in house* formulated inks painted or printed *in house*, as well as standard metal electrodes. The spectroscopic techniques were intended to study reaction products occurring on the electrodes elucidating behaviours, but were also useful for informing *in house* ink formulations. In some places, data acquisition and analysis has been refined using software such as Matlab and some explanation is given for these methods.

2.2 Materials

2.2.1 Electrochemical

An Autolab PGstat20 or PGstat10 with PGstat modules 1, 2, 3 for multielectrode experiments (Windsor Scientific, Slough, UK) was used with GPES v4.9 software (installed on a Windows PC). Also used was a BAS Electrochemical Analyser 100 W/B (Bioanalytical Systems Inc., US) was used with BAS software 2.0 (installed on a Windows PC). The different systems had advantages according to the demands of the experimental protocol.

All reagents, unless other wise stated were obtained from SigmaAldrich (Poole, UK) and were of analytical grade. HPLC water was used for aqueous samples as standard. Disposable polypropylene sample tubes of 50 and 10 ml capacities were used for

prepared solutions. Any glassware used was stored and washed in a 5 % Nitric Acid bath and rinsed before use with HPLC water and acetone. Electrolyte preparations usually include mineral acids and salt solutions, prepared by dissolving the appropriate amount of salt into HPLC water.

2.2.2 Software

Mathematical software was used for both numerical modelling of voltammetric experiments and data handling from real experiments. Microsoft Excel (2003, Microsoft, California, US) various versions were used, Matlab v6 or v7 (The MathWorks, Inc., Cambridge, UK) and Pascal (Free Pascal IDE for Win32, v 1.08). Standard PC workstations were used for computation. The majority of mathematical processing was conducted in Matlab due to the in built mathematical functions and display facilities. Pascal was used in one instance of voltammetric modelling to compare with the equivalent program in Matlab for processing speed. Pascal was, for some processes, significantly faster allowing for greater accuracy in simulation. Generally Microsoft Word was used for simple voltammetric analysis and display.

2.2.3 Microscope and Image processing

To make measurements an Olympus BX40 microscope (Olympus UK, Ltd., Watford, UK) was used with computer controllable staging and automatic digital camera allowing extended ranges to be imaged at high resolution. The microscope was fitted in parallel to a Labram 300 Raman microscope (Horiba Jobin Yvon Ltd., Middlesex, UK) so Raman spectroscopy Labspec software v5.21 (Horiba Jobin Yvon Ltd., Middlesex, UK) was used to acquire images. The images were then processed with ImageJ software (National Institute of Health, Maryland, US), and Matlab v7 for additional procedures. The microscope had inbuilt scale with a setting for each of the 4 lenses, (10x, 50x, 50xLWD and 100x). The overall magnification of the 100x lens was enough to show 1 µm details.

2.2.4 Ink Formulations

UCAR VAGH and Elvacite 4028 (polymethylmethacrylate-co-butylmethacrylate) were obtained from Union Carbide, (Yorkshire, UK) and Lucite International, Ltd (Southampton, UK) respectively, as advised by Towlson (1997). According to formulations from the patent literature (Chan, 1997, 1998, Chan and Kuty, 2000, Williams *et al.,* 2001, Dorfman, 2005, Tierney, 2006), polymers including polystyrene-co-acrylonitrile (PSAN), polyvinylidenechloride-co-acrylonitrile (PVDC-co-PAN), polyvinylidenefluoride-co-hexafluoropropylene (PVDF-co-HFP), polydimethylsiloxane (PDMS), and polymethylmethacrylate (PMMA) were obtained, in powder or pellet form, from SigmaAldrich (Poole, UK). For Polymer X (associated directly with BQ331, see Section 5.3.3) the supplier will remain undisclosed.

Gold spherical powder, 99.96 % (3.0 - 5.5 µm), graphite flake 99 % (7-10 µm), carbon powder, synthetic conducting grade -325 mesh and silver powder 99.9 % (4-7 µm) were obtained from Alfa Aesar (Lancashire, UK). Palladium 5 % on carbon, platinum 5 % on carbon and Rhodium 5 % on carbon were obtained from Avocado Research Chemicals (Lancaster, UK). Solvents including γ-butyrolactone, diethyl oxalate, diethyl glycol monoethyl ether and diethyl glycol monoethyl ether acetate were obtained from SigmaAldrich (Poole, UK). Screw-top glass vials (of 25 ml capacity) with plastic lids, disposable polypropylene pipette tips (of 200 and 1000 µl capacities), polypropylene centrifuge tubes (2 ml capacity) were used for transfer and mixing of solutions. Powders were weighed out with stainless steel spatula and aluminium foil on a weighing balance (Sartorius R160P Semi-Micro Balance, Epsom, UK).

2.3 Electrochemical Experiments

2.3.1 General Screen-Printed Design and Connection

The focus of this project was on screen-printed electrodes, particularly those produced by DuPont Microcircuit Materials (Bristol, UK). These were typically used as

received. The plastic strip functioned both as support for the sensor surface and support for 50-200 µl of sample. The sensor was a three track design on 125 µm thick polyethyleneterephthalate (PET). The carbon ink tracks were printed first onto the PET sheeting. A 1 cm × 1.5 mm gold track overlaid the centre track at one end, with an Ag/AgCl aligned on the left hand track. The third surface was composed bare. A partially transparent/blue insulating ink protected the majority of the sensor with a circular aperture exposing the sensor end. The design is shown in Figure 2.1, which matches the design used previously at Cranfield for example: Cooper (2004), Kadara (2005), Noh (2005) and Cauchi (2005). Unlike the *in house* design, the electrodes were printed eight at a time using a smaller screen.

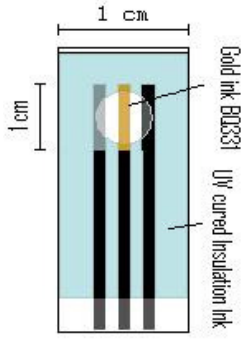

Figure 2.1 DuPont Gold Screen-printed Electrode Design

The other end of the sensor included three carbon track contacts. A plastic chip component with internal steel pins provided electrical connection to the potentiostat, as shown in Figure 2.2. The chipsets were not normally electrically shielded. The steel pins scratched the carbon contact pads so that a good electrical connection could be assumed. However, repeated use could result in the build up of carbon material causing short circuit in the chip. Also, care was needed not to allow the electrolyte to enter the chip, since the steel pins could act as electrodes. It was possible, with poor alignment, that the one electrode track would straddle two pins in the chip. To verify the measured signal, a second chip could be used for a substitute.

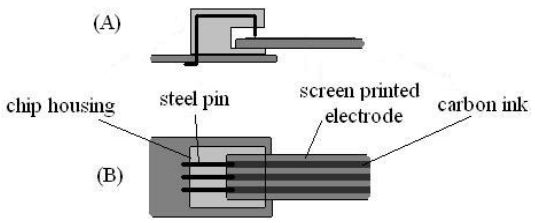

Figure 2.2 Screen-printed electrode circuit connection: (A) side cross section (B) Top down view with cut away

A multimeter such as a TEK DMM870, (TEK, Bracknell, UK) was used to measure resistance; two probes were used between the chip contact and the sensor end of the working, counter and reference electrode track (example shown in Figure 2.3). Since the track was usually scratched by the probe, measurement was preferred after electrochemical experimentation.

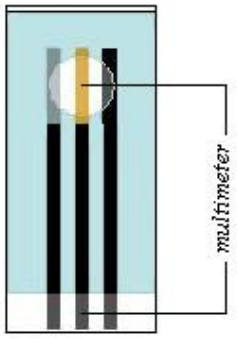

Figure 2.3 Resistance measurement of electrode with multimeter

2.3.2 DuPont Sensors Compositions

Collaboration between Cranfield and DuPont Microcircuit Materials (Bristol, UK) started in 2001/2002 looking for applications for a novel gold polymeric ink, in development at that time. The ink was developed in the US, and since this time no changes have been made to the formulation, so far as information has been made available. Cooper (2004) and Cauchi (2005) have since worked with BQ331. The online literature (DuPont Microcircuit Materials, 2001) teaches that BQ331, is designed for biosensors and cures within 10 minutes at 130 °C to a typical thickness of 10-20 μm.

The variable ink compositions compounded by rebranding, made the task of following the sensor compositions complicated. According to discussions with representatives of DuPont Microcircuit Materials (Bristol, UK), redesign of screen layout or redevelopment of the gold ink would be a costly enterprise. Changing the carbon, silver or insulation inks or changing curing conditions, however, was convenient. Typically, when problems were encountered the parameters, such as increased curing time (for example Table 2.1, group B) or change in encapsulant ink (Table 2.1, group C) were changed first. Therefore, over the course of the project a number of different sensor compositions were used. The gold ink BQ331 has been consistent throughout.

Table 2.1 Sensor compositions assessed by Cauchi (2005) prior to this project

Group	Gold Ink	Carbon Ink	Reference Ink	Insulation ink
A	BQ331	7105	5874[e]	5036
B	BQ331	7105	5874	5036[c]
C	BQ331	7105[f]	5874	5018[b]
D*	BQ331	E100735-155[a,d]	5874	E017257-1[a]

[a]formulations in development; [b]UV cured; [c]cured for 30 min at 130 °C rather than standard 15 min; [d]later identified as BQ221; [e]also identified as BQ164; [f]also identified as BQ225; *Selected for further trials

The first set of sensors for this project was of the composition D as shown in Table 2.1. Further batches' compositions are given as they appear during the text.

2.3.3 In House printed Sensors

In house sensors were printed with the same three track design as given in Figure 2.1. Some other designs were considered in Section 3.3.1. The standard inks used were Electrodag Carbon 423 SS and Electrodag Ag/AgCl 6038 SS (Acheson Colloids, Reading, UK). The usual insulation ink was Epoxy thermoset resin SB 242 (ESL Europe, Reading, UK). The electrodes were printed *in house* on a DEK 248 semi automatic printer (DEK, Weymouth, UK). The base plastic was 250 µm PET sheeting (Cadillac Plastics, Ltd, Swindon, UK). Custom DEK 325 steel meshes were the same as those used for previous projects at Cranfield such as Cooper (2004), Kadara (2005) and Noh (2005).

For other commercial inks samples of printed Ercon gold, R 464 DPM 78 (Ercon, Inc., Redwood City, USA) and Gwent Gold, C2041206D2 (Gwent Electronic Materials, Ltd, Pontypool, UK), kindly donated by M.F.M. Noh and M. Huerich (ex-Cranfield students). These inks were not purchased separately, due to the high cost, but a thorough comparison of the available polymeric inks would have been advantageous.

Residuals of both inks were obtained for spectroscopic experiments (Section 5.3.2). The Gwent gold could not be used electrochemically due to over diluted with solvent, the printed electrodes demonstrating phase separation between powder and resin. Printed Ercon samples were available from the project of Noh (2005). These electrodes probably had reduced activity due to age (> 2 years). A reasonable electrochemical comparison with the DuPont ink was possible, by comparing with results presented in the thesis of Noh (2005), as described in Section 4.3.7.

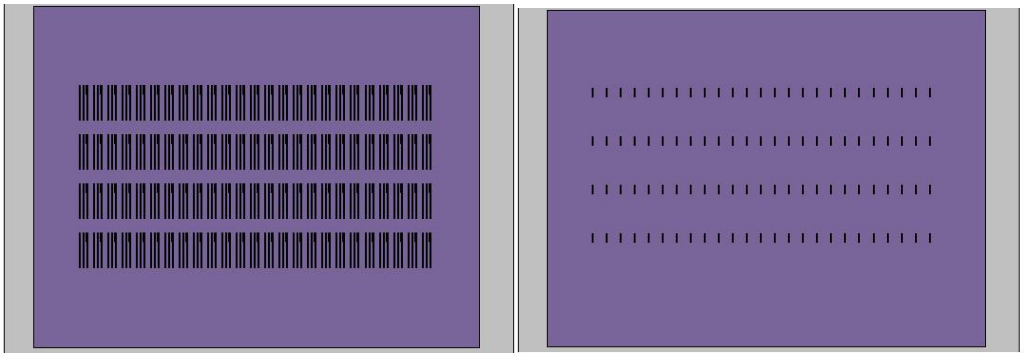

Figure 2.4 Screen design for *in house* printed electrodes with 1×1 m aluminium frames, steel mesh (not visible), purple polymeric mask, printing patterns in black. Left is the design for tracks and right is the design for working electrode overlay.

Screens (325 mesh) were obtained from DEK (Southampton, UK) with custom design as shown in Figure 2.4.

2.3.4 Standard Electrodes

For other electrochemical experiments standard platinum (1.6 mm diameter), gold (1.6 mm diameter) and glassy carbon (3.0 mm diameter) disk electrodes were used, obtained from Bioanalytical Systems, Inc., (BAS, West Lafayette, USA). The electrodes come housed in 6 mm diameter cylindrical housing 7.5 cm long of poly(chlorotrifluoroethylene) (CTFE); a metal pin extends through the length of the housing providing electrical connection and protrudes 0.75 cm from the far end of the housing.

The electrode surfaces come highly polished and were maintained with the suitable electrode polishing kit (BAS, West Lafayette, USA). Typically 0.05 µm alumina powder was added to a brown textmet/alumina pads with HPLC water. Having been rinsed in water and acetone the electrode was first used to spread the alumina and water evenly over a patch of the Texmet pad. Then, a *figure of eight* was described with the electrode applied with a medium downward pressure to polish the surface. After polishing 50 – 80 times the electrodes were rinsed in water and acetone, sonicated in water (to remove traces of alumina) and rinsed again before being used for voltammetric experiments. A description of electrode maintenance is given by

Bott (1996) and Cooper (2004). The electrodes were aligned for experiments using polypropylene blocks with 6.5 mm holes drilled. Rubber O rings, supplied with the electrodes held them in place. Typically crocodile clips were used to provide connection to the potentiostat.

Reference electrodes used were supplied by Bioanalytical systems, Inc. A silver wire coated in chloride was mounted into a 7.5 cm glass capillary tube sealed with an epoxy composite at the connection end. At the other end, the glass tube tappers to a small orifice. Heat shrunk Teflon affixes a ceramic Vycor frit protecting the end. The electrode was stored typically as recommended (Bott, 1995), in saturated NaCl or KCl and kept in a darkened pot (to avoid photosensitive reaction of silver). The Vycor Frit permits slow ion diffusion; otherwise the Ag/AgCl reference electrode is isolated from the experimental electrolyte. In some experiments a platinum foil piece was used (AlfaAesar, Lancashire, UK), since the cylindrical design of the standard electrodes was not convenient for some electrode tests. The foil was about 0.25 mm thick and approximately 1×1 cm^2. The foil was not easily polished, but was washed and rinsed in organic solvents such as acetone and methanol and acid such as HCl and HNO_3 between experiments. Standard electrode connected in a standard cell utilised a glass beaker (25 ml) or shot glass to hold the electrolyte, as shown in (Figure 1.3A).

2.3.5 Screen-printed-Standard Electrode Combination

The screen-printed electrode as mentioned already, needed only 50 - 200 µl drop on the strip surface. For some experiments standard electrode were combined with printed strips: standard electrodes held in polypropylene blocks were suspended above the printed strip so that the disk (gold, platinum or carbon) touched the electrolyte solution. In this design one or more active standard electrodes could be used with the screen-printed tracks either passive or active.

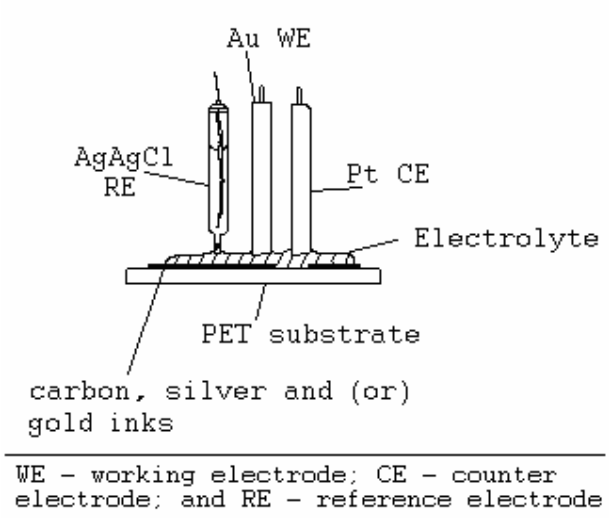

Figure 2.5 Schematic combination of standard and screen-printed inks

2.3.6 Microband Electrodes

The preparation for microband electrodes is discussed in Section 6.3.4. This design required that the screen-printed electrode be submerged into a beaker of electrolyte. According to private discussions with representatives of MTI Diagnostics (Cambridge, UK) and Lab21 Diagnostics (Cambridge, UK), immersion of screen-printed electrodes into a pot of electrolyte is preferable to a small spot surface with either planar or microband design.

2.3.7 Standard Electrochemical Procedures

Standard procedures for DPASV experiments (Cooper, 2004) for determination of As(III) and Hg(II) in 4 M HCl.

Table 2.2 DPASV standard parameters as used by Cooper (2004) and Cauchi (2006)

Parameter	Standard value
deposition potential, E_{dep}	0 (V)
deposition time, E_{time}	30 (s)
initial potential	0 (V)
finish potential	0.5 (V)
scan rate	10 (mV/s)
step time	0.5 (s)
pulse duration	0.05 (s)
pulse height	50 (mV)

For interference experiments a multi scan cyclic voltammetry was used. Standard parameters are shown in Table 2.3. The scan range was appropriate for gold electrode in acidic solutions avoiding hydrogen and oxidation processes. 40 scans lasted approximately 20 min a suitable length of time before the solution evaporates and long enough to allow fast to medium kinetic chemical and electrochemical reactions to proceed. The repeated acquisition of voltammograms allows persistent and incidental interferences on the voltammogram to be distinguished.

Table 2.3 Cyclic voltammetry standard parameters

Pre treatment	none unless otherwise stated
Number of scans	40
Standby potential (V)[a]	0
Start potential (V)	-0.2
1st vertex potential (V)	0.5
2nd vertex potential (V)	-0.2
Step potential (V)	0.00442
Scan rate (V/s)[b]	0.05

[a]vs screen-printed Ag/AgCl – the ratio of Ag:AgCl in BQ164 (5874) is 65:35, high enough to maintain stable potential in the absence of solution Cl^-, on time scales < 20 min at least.

2.3.8 Data Analysis for Cyclic Voltammetric Procedures

The data obtained from experiments of 40 consecutive scans were saved using GPES software automatically. The filename root is chosen by the user and suffixed by a set five digit counter (‘00001’ for scan one, ‘00002’ for scan 2 and so on), ending with ‘.ocw’. Matlab is used to upload these files automatically. Initially the appropriate folder is chosen. The function ‘dir’ displays all the files; ‘dir(‘*.ocw’)’ displays all the ‘.ocw’ files where * allows for any text in the filename before ‘.ocw’; ‘n =

dir('root*.ocw')' selects all the file names identified by the filename root and puts them into a structured array, n. The length of this array is equal to the number of files, which should be 40 by the parameters given in Table 2.3. In Matlab syntax:

For i = 1:length(n), a = importdata(n(i).name)

For all the files in the array n, the data is imported using 'importdata' function into a temporary number array 'a', one by one. A has between 2 and 6 columns of tab separated data depending on the number of current channels recorded. The first column is the potential of the scan (V). The current channels values are given in amps. The potential data is put into an array 'v' and the current is placed sequentially into a large matrix 'X' multiplied by 10^6 (scale in μA).

v = a(:,1); X(:,i) = (:,2)*10e6;

or for four channel data:

v = a(:,1); X(:,4*i-3:4*i) = (:,2:5)*10e6;

As the counter, 'i', toggles through the files in array 'n', the data is added to the array X column by column. The data can be plotted easily. The 'plot' function gives the voltammograms simultaneously (for an example see Figure 4.9C):

plot(v,X);

For a three dimensional plot the 'mesh' function can be used. But some groundwork is needed to prepare the data. The 'meshgrid' function is used to prepared an x-y grid points, the data in matrix 'X' is then used as the height of the surface on each point of surface. Critically, having v in the meshgrid function allows the display of the voltammetric surface folded over for the return cycles (for example Figure 4.10B).

[A B] = meshgrid(v, 1:40); mesh(A',B',X);

The meshgrid also prepares the data for 'surface' plots.

Title and labels can be added with 'title', 'xlabel', 'ylabel' and 'zlabel'. If many related matrices are loaded they can be combined into a structured array holding both the numerical data and text data for description and parameters. Then the plotting mechanism can be automated to include information for each diagram automatically. For example Figure 5.16 and Figure 5.17 used this procedure.

2.4 Preparation of *in house* Inks

Several methods to produce gold surface were considered including the melting of gold nano particles via the method of Huang *et al.,* (2003) (experiment shown in Appendix A4), the use of aqueous binders such as hydroxyl ethyl cellulose (Ehrreich, 1982, Newman *et al.,* 1995), and 'printable' sol-gel methods (for example Wang, 1997a, 1999a, Guo and Guadalupe, 1998, Kalleder *et al.,* 2005). However, the standard within industry for screen-printable inks involves either meltable glass frit component (high temperature) or an organic binder in a suitable solvent (low temperature) (Prudenziati, 1994, Gilleo, 1996, Hobby, 1997, Towlson, 1997, Kalleder *et al.,* 2005).

The nano particle method would need significant futher ink development (Appendix A4); the aqueous polymers would be soluble in aqueous, particularly acidic electrolytes, printability of sol-gels is tenuous without a viscosity modifier such as an organic polymer; and high temperature inks would be more expensive to prepare than low temperature formulations (also many glass frit formulations contain redox active metals). Also, the existing DuPont sensors are based entirely on these low temperature formulations.Therefore *in house* inks here are based on low temperature (< 200 °C) polymeric inks.

2.4.1 Carbon Painted Formulations

Resins as listed in Section 2.2.4 were dissolved in suitable solvents. Elvacite and the polymethylmethacrylate were dissolved in diethyl oxalate at approximately 25 % wt polymer in solvent and mixed approximately 2:1 by weight polymer solution to carbon powder. Polymer X was dissolved in a suitable solvent at 25 % wt and mixed 2:1 with carbon powder. The fluoro-polymer dissolved only with difficulty: acetone could dissolve the polymer but drying occurred too quickly for mixing and printing to be feasible even at 4 °C. It was found that γ-butyrolactone would also dissolve the polymer above about 90 °C and would gel at lower temperatures. Hand painting was achieved using a hotplate for both the polymer solution, mixing cap for powder, and electrode substrate. Either γ-Butyrolactone or diethylene glycol monoethyl ether (DEGEE) was suitable for polystyrene-co-acrylonitrile and polyvinylidenechloride-co-acrylonitrile. Electrodes were heated at about 120 °C (until dry) to evaporate solvents; the effect of heating regimes was not investigated. The synthetic conducting grade graphite carbon powder was used for the above. The formulations were painted onto screen-printed substrates with Electrodag Carbon and Silver in the standard design and no insulation ink.

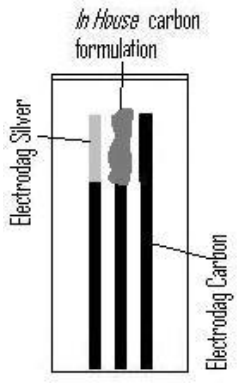

Figure 2.6 Schematic of hand painted electrodes using screen-printed base with standard design

2.4.2 Gold Painted Formulations

For the quantities produced conventional screen-printing was not an option. For example, polymeric gold inks produced by Gwent Electronic Materials

(C2041206D2) and Ercon (R 464 DPM 78), are supplied in minimum 25 g portions (gold and organic vehicle), because preparation and printing is not feasible for smaller amounts. To tackle the objective of producing screen-printable gold electrodes a greater investment in gold powder would be needed. The formulations presented in Table 2.4 were based on the successful carbon formulations in Section 2.4.3.

Table 2.4 Three gold ink formulations for hand painting

Polymer	Gold Powder*
PMMA[a]	100 mg Gold powder; 2.5 mg PMMA; 7.5 mg diethyl oxalate
PSAN[b]	100 mg Gold powder; ~4 mg PSAN; ~12 mg; γ-butyrolactone
Polymer X[c]	100 mg Gold powder; ~3.75 mg polymer X; ~11.25 mg; γ-butyrolactone

*Spherical gold powder 3-5 µm; [a]Poly (methyl methacrylate) M_w 120,000; [b]Poly (styrene -co-acrylonitrile), M_w 165,000; [c]As found in BQ331 - identity withheld, see Chapter 3 and 4; [d]7-10 µm graphite flake;

2.4.3 Carbon Printed Formulations

To study the reproducibility and realistic properties of a screen-printed ink formulations were prepared. It was soon found that the synthetic carbon used previously, when used in polymer X, PMMA or PSAN formulations, was incompatible with the bare steel mesh on the screen. The ink would not spread, but rather recoiled from the mesh. However, this problem was avoided by using the 7-10 µm carbon flake. The poly(vinylidenechloride-co-acrylonitrile) was incompatible with the carbon flake in either γ-butyrolactone or DEGEE forming a rubbery solid. However the PMMA, PSAN and polymer X/ carbon flake formulations could be printed. The Rh and Pd carbon powder were also tested with these polymers. Neither was compatible with the PSAN or polymer X. The Rh carbon was compatible with the PMMA. The formulations given in Table 2.5 were developed to have as much powder content whilst still maintaining a wet viscosity suitable for printing and providing a good coverage.

Table 2.5 *In house* ink formulations for manual screen-printing

Polymer	Carbon flake[d]	Rh Carbon powder[f,g]
PMMA[a]	0.34 g Carbon flake; 0.17 g PMMA; 0.51 g diethyl oxalate	0.5 g Rh Carbon powder; 0.25 g PMMA; 0.75 g diethyl oxalate
PSAN[b]	0.5 g Carbon flake; 0.25 g PSAN; 0.75 g DEGEE[e] or γ-butyrolactone	*
Polymer X[c]	0.5 g Carbon flake; 0.25 g Polymer X; 0.75 g DEGEE[e] or γ-butyrolactone	*

[a]Poly (methyl methacrylate) M_w 120,000; [b]Poly (styrene -co- acrylonitrile), M_w 165,000; [c]As found in BQ331 - identity withheld, see Chapter 5; [d]7-10 µm graphite flake; [e]diethylene glycol ethyl ether; [f]Rhodinised (5 %) carbon powder as catalyst; *Rh Carbon powder with these polymers formed non-fluid aggregates which were unprintable

The finalised carbon formulations were printed by hand through the DEK screens. Four stainless steel nuts (as in nut and bolt head), approximately 3 mm thick were taped, one to each corner of the aluminium frame to provide a highly parallel print gap on a stable flat bench surface. The substrate was then elevated with layers of the PET sheeting. A suitable number of sheets was selected by trial and error to fine tune the print gap: 3 – 4 sheets was subsequently chosen.

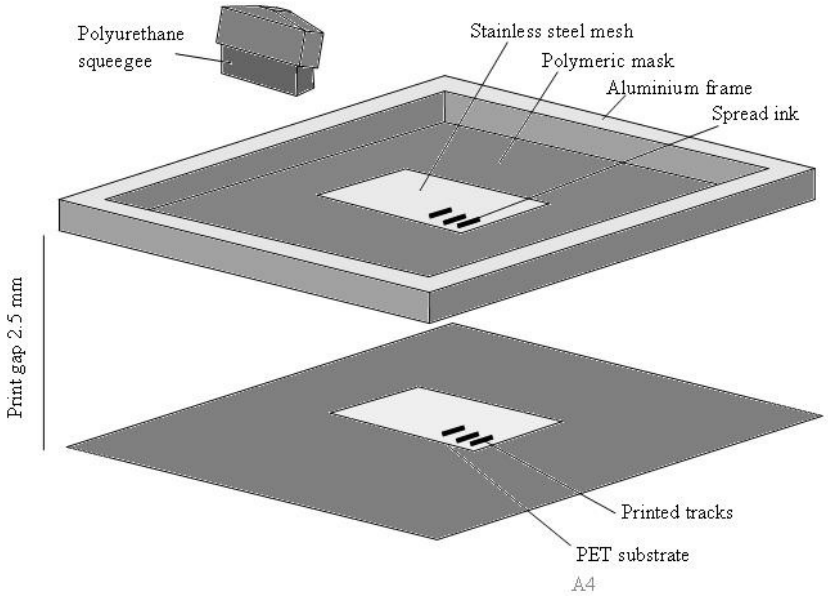

Figure 2.7 Hand printing apparatus using squeegee, stainless steel mesh at high tension in aluminium frame with (purple) photo cured polymeric mask printing onto PET sheet (drawing not to scale)

The carbon formulations were printed both as track lengths of the same design as Figure 2.1. The formulations were also printed overlaying the screen-printed *in house* electrodes. Alignment of the screen was achieved by eye. Either the pipette tip or the squeegee was used to spread the ink across the mesh to mimic the flood bar action (see Figure 1.11). Within a 30 minute session, about 150 electrodes could be printed. However due to the hand-eye coordination and hand printing method with some blockages forming in the screen, only 100 electrodes were usually viable.

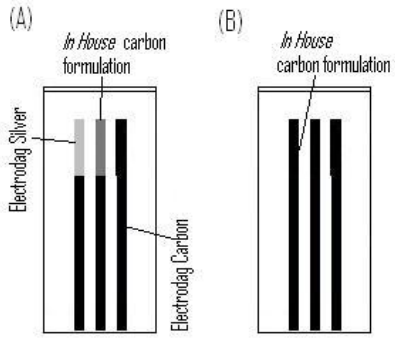

Figure 2.8 *In house* printed design. (A) Standard design with Electrodag carbon tracks and Electrodag Silver reference onto which is printed an *in house* carbon for the working electrode; (B) Three tracks printed directly onto PET of an *in house* carbon ink.

2.5 Spectroscopic Methods

A number of analytical approaches were used to probe the electrode system including FTIR, NMR, GCMS and XPS. FTIR and NMR approaches used an extraction procedure whereas XPS and GCMS were used directly on sensor strips.

2.5.1 Analytical Equipment

For Infrared measurements Equinox 55 bench top unit, with IR Scope II microscope were controlled using OPUS software (Bruker, Coventry, UK). The attenuated total reflectance (ATR) accessory fitted into the Equinox 55 bench top unit Gateway ATR accessory kit, (Graseby Specac Ltd., Kent, UK). An Electronic library of Infrared and Raman Spectra for Inorganic compounds and Organic Salts was used for spectral

comparisons (Academic Press, Kent, UK). The FTIR was fitted with standard DTGS and MCT detectors. Liquid nitrogen was used to cool the MCT detectors in both the microscope and the bench top unit. Raman spectra were taken with a Labram 300 controlled with LabSpec v5 software (Horiba Jobin Yvon Ltd. Middlesex, UK). An Olympus BX40 optical microscope was also built into the same system. Calibration was performed as standard before use with a sample of silicon.

NMR was performed with the guidance of Dr M. Whitcombe (Cranfield Health, Cranfield University) on a 400 MHz, JNM-ECX series FT NMR system (Joel Ltd., Hertfordshire, UK). One-dimensional H^1 proton spectra were acquired; spectra with natural C^{13} levels were likely to be too weak to be useful. XPS was performed by Dr M. Kershaw (School of Applied Sciences, Cranfield University) using a VG Scientific ESCAlab 200D Surface Analysis Equipment for AES and XPS. GCMS was performed with assistance of Dr C. Walton (Cranfield Health, Cranfield University) with a Perkin Elmer, TurboMass Spectrometer, Autosystem XL GC and Automatic thermal desorption system ATD 400 (Perkin Elmer, Buckinghamshire, UK). A Zebron Capillary GC column was used, 60 m by 250 µm (inner dimension), and coated with cyanopropylphenyl-methyl polysiloxane as the stationary phase (Phenomenex, Cheshire, UK). Pure helium gas was used as the mobile phase.

2.5.2 Ink Extraction Procedure

As might be expected screen-printing type solvents, such as γ-butyrolactone and DEGEE would dissolve many inks (except where heavy crosslinking had been employed). The PET substrates were generally unaffected (at least for short term exposure < 2 hr). Low boiling point solvents such as acetone, chloroform, methanol and ethyl acetate were useful since no heating regime was needed to encourage evaporation.

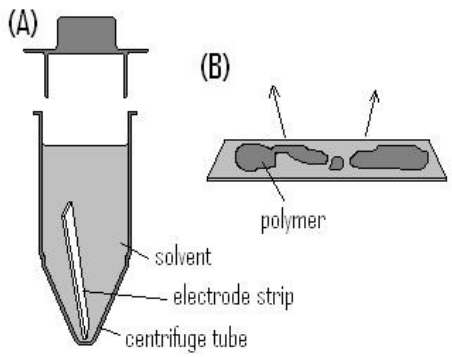

Figure 2.9 (A) Extraction of screen-printed ink in polypropylene centrifuge tube into a low boiling point solvent, (B) Evaporation of solvent onto a clean surface leaving polymer residue

Electrode strips were prepared by removal of target ink from strip (using scissors). To obtain a reasonable quantity of material, 8 strips (area 1.5 mm × 1 cm) were added to 2 ml (polypropylene) centrifuge tubes with about 1 ml of solvent, as shown in Figure 2.9A. Shaking/stirring was needed to disperse the inks. Between 5 min and 2 hr stirring (Vortex Genie II, Scientific Laboratory Supplies, Yorkshire, UK) was required depending on the ink. The dispersion was visible by the formation of a suspension of the ink powder. The powder would generally settle, attributable to the higher density of carbon (about 2.20 g/cm^3), silver (10.5 g/cm^3) or gold (19.3 g/cm^3) in comparison to most organic solvents. Extractions were also possible for individual strips (area 1.5 mm × 1 cm) in a 200 µl centrifuge tube with about 150 µl of acetone.

BQ331 is cured (DuPont Microcircuit Materials, 2001) but the integrity of the printed ink was easily attacked by solvents. Polymeric residuals were visible as thin transparent, cloudy or oily layers if the extraction solvent was allowed to evaporate on a flat surface (solvent-only controls did not show these residues).

The insulation ink(s), reference, carbon(s), Ercon gold and Gwent gold were also subject to study. DuPont Gold BQ331, Gwent Gold, DuPont Ag/AgCl BQ164, Insulation ink BQ411 Electrodag Carbon 423 SS and DuPont Carbon R471 extracted within 5 min into acetone. The other inks tested extracted with difficulty taking 1 – 2 hrs before the sensor PET substrate was clear. This was advantageous for separating the DuPont gold from the under layer of Carbon ink (except when R471 was used).

This procedure could be used to obtain the powders also which could be weighed (Section 5.3.1).

Chapter 3 Concerning Theory and Practice for Characterisation of Screen-Printed Electrode Surfaces

3.1 Introduction

This chapter is somewhat separate from Chapters 4 to 6 which form a continuous body of research. Therefore most of the content of this chapter is not necessary for understanding the later chapters. In this chapter the (apparent) anomalous redox behaviour of some screen-printed sensors is considered particularly with regard to calculation of the electron transfer constant by the method of Nicholson.

Anecdotally, the implementation of the Nicholson method has been found to be troublesome by some researchers within Cranfield Health (C. parker, M.F.M. Noh, R.O. Kadara, for example) since the method touches upon a dense mathematical procedure. Also, sensors with BQ331 working electrode evaluated by Cooper (2004) showed some curious behaviour not expected within the Nicholson scheme.

The model is developed based on the work of previous researchers (Nicholson, 1965a, 1965b, Pajkossy and Nyikos, 1988 and Strømme *et al.,* 1995) to extend the method of Nicholson for rough surfaces. Although this method has been found unnecessary for characterising screen-printed electrodes with typical physical conditions, it may have inherent theoretical interest if the theory could be experimentally validated.

In general, the performance of screen-printed electrodes depends upon the physical and chemical properties of the sensor. To characterise the sensor, resistance, sensor-electrolyte capacitance, electrochemical active area, and the electron transfer rate constant may be measured. These properties can be linked to structural properties such as ink thickness, particle packing, and polymer coverage; and to physiochemical properties such as particle-particle, particle-polymer and polymer-polymer affinity, as well as surface chemistry of the particles (Lux, 1993, Jurado *et al.,* 1991, Cheah *et al.* 2001) and direct chemical reactivity of polymer matrices (Usmani, 1994). Whilst considered proprietary, the ink formulation can have a profound effect upon sensor

performance and a suitable attempt is needed to link the measurable properties to sensor performance if optimal performance is to be obtained.

3.1.1 Electrode and Solution Resistance

The resistance, R, of a track is related to the intrinsic resistivity, ρ, by the length, l, and the cross sectional area, A in Equation 11.

$$R = \rho \frac{l}{A} \qquad \textbf{11}$$

Thick film deposition technique normally has thickness between 1 and 50 µm (Gilleo, 1996) which results in small cross sectional areas. By Equation 11 this causes high resistances. The resistivity of the material depends upon both particulate type (gold, silver and platinum have higher conductivities than carbon or other semi conductor) and on particulate loading. The length and width of track depend on the chosen printed design.

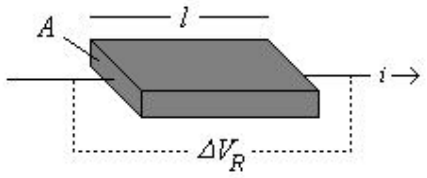

Figure 3.1 Schematic resistor of length, l, area, A with a current, i passing through

At any time the potential drop, ΔV_R, across the working electrode track with resistance, R, as a current, i, passes through, is given by Equation 12

$$\Delta V_R = iR \qquad \textbf{12}$$

When a potentiostat is connected to screen-printed electrodes, the potential set (or measured for a current controlled experiment) by the potentiostat is different from the electrochemical cell by an amount ΔV_R according to the current flowing through the

working electrode (i.e. the measured current). For 1 μA through 1 kΩ of resistance there will be 1 mV of potential correction.

Uncompensated resistance has two effects (i) in voltammetric measurements the potential of the working electrode and the potential set by the potentiostat working electrode connection differ by a correction of iR where i is the current through the working electrode and R is the resistance. (ii) The current associated with capacitance decays with time constant RC where C is the capacitance of the electrode surface, for larger track resistance the capacitive current takes longer to decay (He & Faulkner, 1986). The second effect is on the potentiostat rise-time. Particularly high resistances slow the speed at which the potentiostat can set the conditions resulting in distorted current-voltage waveforms. The problem associated with iR correction can be corrected after voltammograms have been acquired if the track resistance is known.

The electrolyte has resistance also; Table 3.1 shows the conductivity of some electrolytes as listed in the literature. The resistance of a screen-printed strip has been calculated from this data using expected electrode and electrolyte solution dimensions. The co-planar design and limited drop size complicate predicting the exact resistance. Electrolytes at higher concentrations (> 1 M) give resistances less than 100 Ω. More dilute electrolytes (< 0.01 M) produce resistances greater than 1 kΩ thus producing impedances in excess of carbon tracks.

Table 3.1 Conductivities for selected electrolytes and metallic copper (Lide, D.R., *et al.* 2003) and calculated solution resistance for a typical cell

Electrolyte	Conductivity ($\Omega^{-1}m^{-1}$)	Solution resistance[d] (Ω)
Benzene (pure)[a]	5×10^{-12}	6.7×10^{13}
Distilled water[b]	1×10^{-3} to 1×10^{-4}	6.7×10^{5}[c]
AgCl (saturated)	1.73×10^{-4}	1.9×10^{6}
0.1 M NaCl	1.05	320
1 M NaCl	7.44	45
NaCl (saturated)	21.4	16
4 M HCl	~ 70	4.8
copper	6.5×10^{7}	5.1×10^{-6}

[a]due to trace water, [b]due to dissolved CO_2, [c]for conductivity of 5×10^{-4} $\Omega^{-1}m^{-1}$, [d]based on parallel electrodes of 5 mm separation and 0.1 cm^2 area and no edge effect

In terms of electrochemically useful units the potential correction is equivalent to 1 mV offset per µA current per kΩ resistance. Since most peaks have significant width in cyclic voltammetry, a 10 mV offset is tolerable, equivalent to 10 µA through 1 kΩ or 1 µA through 10 kΩ. The allowed tolerance changes depending on application, with factors such as analyte potential, reversibility and peak shape, incidence of interferences and concentration, and on the intelligence of interpretation built into software. To a first approximation the resistance of the counter and reference electrodes is not as important as the working electrode resistance. However, particularly high impedances can affect the stability of the reference electrode seen as oscillations in the voltammogram, saturated currents or low/zero currents according to the design specifications of the potentiostat. The effect of resistance can be compensated if the impedance value is known. This can be achieved, either electronically with the potentiostat or within the software stage. With appropriate, relatively complex, hardware the resistance of an electrochemical system can be measured.

A simple and concise method used by the Bioanalytical Systems Electrochemical Analyser 100 W/B, developed by He and Faulkner (1986), uses a pulse method to extract the resistance from the current decay profile (Bioanalytical Systems, 1996). The potential is set to avoid extreme potentials or redox couples. A set percentage of all of the resistance can then be compensated. However, oscillations can occur close to 100 % compensation particularly if the capacitance of the electrode changes during

the experiment or if the electrode surface is not stable (He and Faulkner, 1986). Care must be taken to avoid subsequent changes in the resistance due to electrolyte evaporation or electrode movement.

Polymer thick film electrodes require that both the electrode and electrolyte resistance be considered. Standard metal and carbon electrodes usually have negligible resistance compared with the solution values in Table 3.1 as the value for metallic copper shows.

3.1.2 Nicholson Method

The Nicholson method (Nicholson, 1965a) allows the calculation of the heterogeneous rate constant of an electrode surface with an easily implemented electrochemical procedure. A facile redox couple, commonly a ferrocyanide or ferrocene is present at mill molar level in a weak electrolyte. A triangular potential waveform is applied to a suitable electrochemical cell containing the electrolyte, and the current is recorded. For a good redox couple a forward and reverse peak is expected with measurable peak position, height and area.

Data is acquired for the peak position and scan rate. This is compared to the result of the mathematical result of Nicholson (1965a) which takes the form a tabulated series of numbers (available, for example in Bard and Faulkner, 2001). A fit is obtained between the mathematical description and the experimental data with a parameter rate of electron transfer. Although the procedure is independent of common parameters such as electrode area and analyte concentration, care is needed for different electrode geometries and unaccounted solution resistance (Nicholson 1965a).

The process by which the analyte in solution interacts with the electrode is outlined in Section 1.8. In brief, three phenomena act to shape the current-voltage relationship: (i) the analyte in solution has an energy distribution due to thermal motion, (ii) diffusion of analyte in solution due to thermal motion and (iii) kinetic rate of interaction at the electrode surface.

Generally speaking, diffusion is a second order differential equation in solution and the reaction at the electrode is treated as boundary condition. With a cyclic voltammetric waveform and a build up of analyte product at the surface due to slow kinetics, the boundary condition is too complex for an analytical solution. However the second order equation can be reduced to a first order equation using Laplace Transform theory (Smith, 1966).

In general kinetics across a macro scale electrode surface will be heterogeneous. That is, nano and possibly micro scale regions on the electrode surface will exhibit variable conditions affecting the rate of electron transfer. For the Nicholson type of treatment, homogeneous kinetics, across the electrode on the macro scale, is assumed.

By macro scale it is meant that the dimensions are greater than the effective diffusion layer thickness. The diffusion layer refers to the region of solution affected by the change in analyte concentration due to the reaction at the electrode surface.

On the nano and micro scale, the electrode surface is thought to comprise of a variety of active and inactive sites, and so referred to as heterogeneous. Any complexities resulting from potential or time dependence of these activated sites are assumed to be not present. Electrochemical cycling, or even resting in an electrolyte, of a freshly polished electrode can cause the surface rate constant to change with time, due to slow dynamic processes such as oxidation. Often a prepared electrode will be electrochemically cycled until the voltammetric profile appears stable, before the Nicholson method is applied.

Despite the assumed simplicity of reaction kinetics it is known that some surface adsorbed contaminants, such as surfactants cause complex behaviour, depending on the ability and potential dependence of the adsorbed layers ability to transfer charge to the underlying electrode.

The Nicholson method was developed at a time (pre 1965) when numerical processing of numbers was conducted longhand. Thus, dimensionless parameters

were used so that the numerical results obtained had the widest possible application. The use of dimensionless parameters, grouping several physical parameters, also allows the equations to be written concisely helping to avoid mistakes made during copying. However, these dimensionless parameters coupled with the involved mathematics and electrochemical properties can be hard to visualise for the non-mathematical analytical scientist so mistakes are easily made.

A parameter, ψ, is used for the kinetic properties including the rate constant, k_s, and the scan rate, v.

$$\psi \propto k_s / \sqrt{v} \qquad \textbf{13}$$

The constant of proportionality which includes physical terms such as the molar gas constant, temperature, Faraday constant, diffusion coefficient and electron transfer constant has not been included here for conciseness. For a planar electrode, the relationship between the peak to peak separation, ΔE_p, and the ψ can be described concisely (as will be seen in Figure 3.22 on page 142). The data tabulated for ψ and ΔE_p is given in Bard and Faulkner for ΔE_p up to 212 mV.

For large ψ (> 100), ΔE_p is independent of ψ; this is the Nernstian or the thermodynamically reversible limit. The peak shape is diffusion controlled. For small ψ (< 0.1) the peak separation is proportional to the logarithm of ψ. This range applies to kinetically controlled peak shapes in the thermodynamically irreversible limits. In between these limits is the quasi-reversible limit where peak behaviour shifts from reversible to irreversible ($0.1 < \psi < 100$).

The relationship between ψ, ΔE_p and scan rate, v, is such that, in the irreversible region, the linear relation between ΔE_p and ψ translates to a linear relationship between ψ and v. ΔE_p increases by about 116 (±3) mV per decade increase in v or by about 232 mV per decade change in ψ. The value of 116 mV can change by several mV according to the overall scan range chosen and the precision of the simulation. Thus, any data acquired from planar electrodes with a standard redox couple such as

ferrocyanide is expected to fit this relationship. The kinetic rate constant is derived from the intercept of the linear fit.

The relationship does not hold for micro spherical electrodes, thin fibres, porous electrodes, thin layer electrolytes or surface confined redox species. In all these incidences the diffusion profile is non-linear. However, where the diffusion profiles are geometrically simple, equivalent relationships have also been derived.

3.2 Theory

3.2.1 Background Rough Electrodes

Many screen-printed electrodes exhibit a degree of roughness and many exhibit some anomalies when conducting cyclic voltammetry. Thus the aim of this section is to link surface roughness to cyclic voltammetry. Screen-printing inks are typically composed of 0.1 – 10 µm powders dispersed in soluble resins, printing thickness is usually within 10 – 50 µm (Gilleo, 1996). The particle dispersion in the resin is dependent on the polymer-polymer, polymer-particle and particle-particle affinities (Jurado *et al.* 1991, Lux, 1993, Cheah *et al.* 2001). When the polymer and particulate component are poorly compatible, the particles tend toward forming aggregates, minimising the particle polymer contact area.

It is well known that many rough surfaces exhibit self similar characteristics, that may be approximated by fractal geometries. In electrochemistry the study of rough surfaces has been conducted with Faradaic currents as potential step, sinusoidal and cyclic voltammetry and also with measurements of capacitance. A review of work in this field was recently published by Go and Pyun (2007). This type of research has included both capacitive based measurements (using impedance spectroscopy) and Faradaic diffusion based measurement probing different physical processes. Pajkossy (1991) concluded from a review of work on capacitive measurements that no general model describing the effect of fractal surfaces could be obtained attributed to the thin nature of the capacitive layer and subsequent sensitivity to surface crystallinity. Faradaic measurements, applied to voltammetry or potential steps were more reliable since the diffusion layer is several orders of magnitude larger.

Pajkossy and Nyikos (1988, 1989a, 1989b), Pajkossy *et al.*, (1994) and Strømme *et al.* (1995) have shown that surfaces exhibiting roughness on a scale comparable to the diffusion layer thickness fundamentally affects a cyclic voltammetric profile both theoretically and experimentally. Vasconcellos *et al.* (2006) have given a statistical-thermodynamic approach to i_p behaviour in reversible systems and provide

experimental verification with AFM derived roughness values. These authors have shown that it is possible to find quantitative agreement between fractal values of surfaces between electrochemical and other techniques such as AFM.

Fractal electrodes have been created by micro patterning, (Pajkossy and Nyikos, 1989b), and by aggregated growth mechanisms (Pajkossy, 1991) on metallic electrodes. Approximately fractal, rough electrodes have been made, for example, by using unpolished and etched electrodes (Go *et al.* 2003), or graphite-resin binder mixtures (Lee and Pyun, 2003)

Le Mehaute and Crepy (1983) first considered the "fractal geometry of kinetics" where kinetics in this sense refers to the kinetics of particle diffusion as opposed to the kinetics of electron transfer at the electrode surface. A number of formulations were hypothesized and a time fractional differential equation was suggested to describe the flux of particles to the electrode surface. The apparent fractal dimension coming from the model description did not match the optically derived values. Deriving a single expression is difficult since many different structures necessarily having unique diffusion profiles, can have the same fractal parameters. Thus, a single equation, describing the concentration profile, could not be applicable generally.

The link between geometric and fractal diffusion profiles provides a means by which to visualise the physical process of diffusion in different scenarios. These geometric examples are distinct from fractals in that many surfaces can share the same fractility Hausdorff Dimension, whilst the detailed structures lead to a plethora of diffusion profiles. Therefore, a single diffusion equation could not be expected for the fractal case.

Finding an expression for diffusion to a surface, without the inherent symmetry of a sphere, flat plane or wire, is complicated in terms of the diffusion profile and associated mathematics. Thus treating the problem from first principles is unpromising. However, a link between the basic physical process and the voltammetry can be made by considering geometrical simple situations. Oldham

(1973) considered a general mathematical expression for spherical, cylindrical, planar, concave cylindrical, and hollow spherical. The general diffusion equation for an analyte at concentration, C, is represented by Equation 14:

$$\frac{\partial C}{\partial t} = D\nabla^2 C \qquad \textbf{14}$$

where t is time and D is the diffusion constant. For a variety of physical situations Oldham (1973) gave the following expression in terms of a single spatial coordinate r. The value R corresponded to the radius of sphere or cylinder whether convex or concave. The value of g takes the value 1, 1/2, 0, -1/2 and 1 for spherical, cylindrical, planar, concave cylindrical and concave sphere respectively.

$$\frac{\partial C}{\partial t} = D\frac{\partial^2 C}{\partial r^2} + \frac{2gD}{R \pm r}\frac{\partial C}{\partial r} \qquad \textbf{15}$$

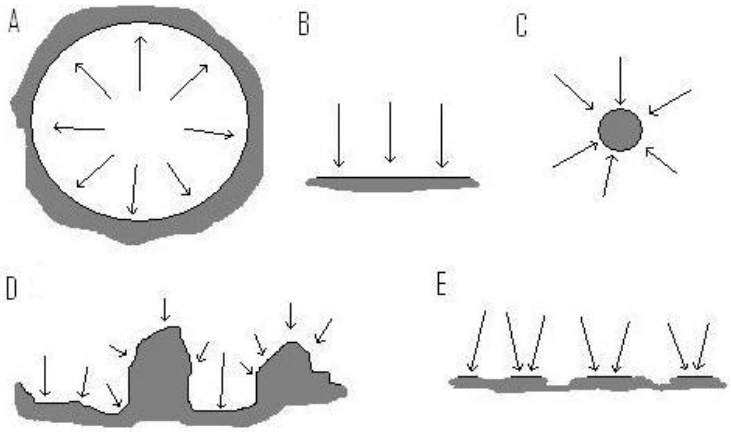

Figure 3.2 Schematic diffusion profiles: (A) concave spherical or cylindrical, (B) planar, (C) convex spherical or cylindrical, (D) rough, and (E) partially active

Figure 3.2 shows the schematic diffusion profiles for geometrical and rough surfaces. The concave sphere (or cylinder) has a divergent concentration profile meaning that the solution has less ability to supply the electrode surface with reactants. The long tail associated with diffusion is shorter than for the standard planar geometry (B). The convex spherical (or cylindrical) electrode features convergent diffusion. The convergent diffusion means that the replenishment of redox active species from

solution is stronger – there by providing a supply of the species longer than would be the case for linear diffusion. Thus the expected cyclic voltammetric peak has longer tailing. In the extreme, where the radius of the sphere (or cylinder) is much less than the diffusion layer thickness, the voltammogram is sigmoidal. A rough surface, (D) is physically analogous to the convex sphere in that the reactants diverge to the surface shortening the diffusion tail; in the extreme the rough electrode is effectively a porous electrode and the diffusion process is minimalised; the partially active surface (E) is physically similar to the convex sphere because the reactants converge to the surface lengthening the tail.

In the theory, a unit cell of the diffusion phase is considered. The shape of the cell is constructed suitable to the symmetry of the diffusion process on a macro scale. A flux density, J, passes through the unit cell so that J enters on one face of the cell only and leaves at the opposite face. The build up of diffusing particles in the cell is related to the net influx. Consider a small spherical electrode; the lines of flux to the surface are radial so the continuity equation for concentration, C, at a distance, r from the surface is:

$$\lim \Delta t \to 0; \lim \Delta r \to 0; \frac{\Delta C}{\Delta t} = \frac{\Phi(r + \Delta r/2) - \Phi(r - \Delta r/2)}{\Delta r * A(r)} \quad \textbf{16}$$

Where Φ is the sum of the flux density J over the area of the unit cell, A.

$$\Phi(r \pm \Delta r/2) = A(r \pm \Delta r/2) * J(r \pm \Delta r/2) \quad \textbf{17}$$

The ratios of the area across depend on the area scaling with r; in spherical symmetry A scales with r^2. Then,

$$\frac{A(r \pm \Delta r/2)}{A(r)} = \frac{k(r \pm \Delta r/2)^2}{kr^2} \approx 1 \pm \Delta r/r \quad \textbf{18}$$

Alternatively for a cylindrical symmetry, two-dimensional radial symmetry causes the area to scale with r. The area scaling term is then given by;

$$\frac{A(r \pm \Delta r/2)}{A(r)} = \frac{k(r \pm \Delta r/2)}{kr} \approx 1 \pm \Delta r/2r \qquad \textbf{19}$$

This treatment can be extended to include planar, hollow cylindrical and hollow spherical symmetries with the area scaling r power 0, -1 and -2 respectively. This translates to

$$\frac{A(r \pm \Delta r/2)}{A(r)} = \frac{k(r \pm \Delta r/2)^g}{kr^g} \approx 1 \pm g * \Delta r/2r \qquad \textbf{20}$$

Where g = -2, -1, 0, 1, 2 according to the scaling factor of the area, defined at a value twice that used by Oldham (1973). Assuming Fick's first law holds with a diffusion coefficient D and r defined as zero at the centre of symmetry opposed to the electrode surface.

$$\frac{\partial C}{\partial t} = D\left\{\frac{\partial^2 C}{\partial r^2} + \frac{g}{r}\frac{\partial C}{\partial r}\right\} \qquad \textbf{21}$$

Explicit numerical solutions for a fully reversible electrode, with cyclic voltammetry reveal the range of voltammogram shapes, shown in Figure 3.3. It is possible to consider the hypothetical situation where the area scales as a non integer value. There is probably no geometrical shape that fulfils this generalised criterion whilst maintaining homogenous diffusion profile across an entire surface. However, non integer scaling is a type of fractional extension and provides a continuous range of voltammetric shapes between those shapes shown in Figure 3.3.

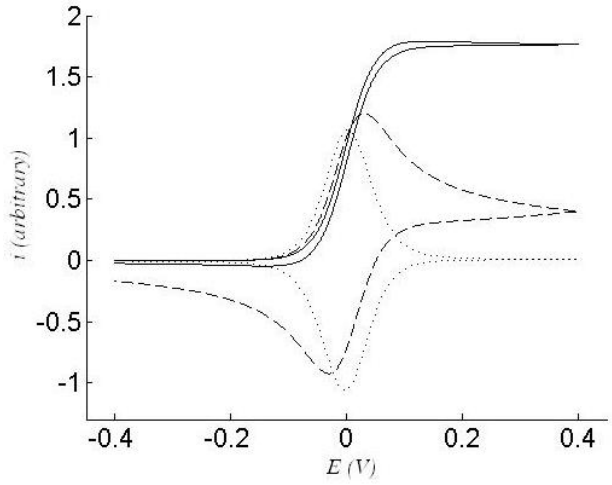

Figure 3.3 Voltammograms for spherical micro electrode (-), for standard planar electrode (--) and concave spherical electrode (..) (g = 2, 0, -2 respectively). Calculated by explicit simulation: see Section 3.3.5.

Because the physical process at a rough electrode is similar to a concave spherical electrode, and partially active electrode is similar to a convex spherical electrode, a similar range of voltammetric shapes would be expected. The parameter g is connected to the surface dimension and diffusion process.

The simplest way to consider the diffusion equation is to consider a unit length, λ and unit time, τ. Any event in a diffusive phase is liable to propagate in space and time. The diffusion equation is a second order differential in space and first order in time. In local regions the differentials can be considered as finite differences of unit time and length:

$$D = \frac{\lambda^2}{\tau} \qquad \textbf{22}$$

For example, after time, τ the diffusion process moves length $(D\tau)^{0.5}$. When an electrode boundary is introduced to a diffusive phase with electrode active species a simple approach is adopted to avoid the complex diffusion profile. As time increases during diffusion, the characteristic length increases. The electrode area 'seen' by the diffusion process is effectively reduced. The effective area will scale with the

characteristic length with exponent 2 on a planar electrode. However, on the fractal electrode, the scaling changes as surface details are lost or gained.

Nyikos & Pajkossy (1988) showed that this electrode area scaling consideration could be used to derive a new form for the Cottrell equation, and that the exponent, β, on rough or partially active electrodes could be related to the surface dimension, D_f (the Hausdorff dimension with subscript f to denote 'fractal'). The methodology was particularly effective since consideration of highly specific and complex diffusion profiles was avoided.

$$i \propto t^{-\beta} \qquad \textbf{23}$$

$$\beta = (D_f - 1)/2 \qquad \textbf{24}$$

In a second paper, Pajkossy & Nyikos (1989a) verified the fractal Cottrell expression with both explicit simulation and direct experiments with well defined fractal electrodes. The expression derived could be applied generally to different potential schemes. An expression for cyclic voltammetry in terms of a Laplace transform was obtained which could be compared with explicit simulation of results.

Using the Laplace transform the mass transfer and electrode process can effectively be separated. The mass transfer can be derived independently of the potential regime so that the result derived from a Cottrell experiment can be applied to cyclic voltammetry (or any other regime such as differential pulse). The bulk concentration is given by C*, the surface concentration by C^s, Γ denotes the gamma function, j is the current density and τ is a time variable used in the integral. The plus-minus sign is chosen depending on whether the analyte is destroyed or created at the electrode surface. The integral expression is a convolution expression and simulations using this term as referred to a convolution models herein. This process constitutes partial analytical solution to the diffusion equation. σ is the coefficient as defined by Pajkossy & Nyikos (1989a).

$$C^s(t) = C^* \pm \frac{\Gamma(1/2)}{\Gamma(\beta)\Gamma(1-\beta)\sigma} \int_0^t \frac{j(t)\partial\tau}{(t-\tau)^{1-\beta}} \qquad \textbf{25}$$

By contrast, explicit simulation does not analytically solve the diffusion equation. In principle, it involves representation of a continuous diffusive phase by a discrete number of spatial and temporal points, representing the diffusion equation by finite differences. As long as the number of points is small enough, the concentration and flux, at every point can be calculated at a time, t from the values at a small time, Δt before. At the electrode surface the Nernst equation is satisfied. Irreversible kinetics can also be modelled.

Besides being limited by the number of discrete points, numerical solutions can suffer from instability if provocative quick processes are included. With the simulated diffusion process, physical quantities can oscillate or become unrealistically large. Modelling kinetics at electrode surfaces becomes a problem when the kinetics are quick. If Nernst equilibrium is assumed, the kinetic calculations are avoided.

The diffusion process describes the macro scale limit for the random walk of many small particles. Another way explicit models have been handled is to consider individual particles moving in a random walk with a probability of reacting at the surface. The length of the random walk step must be smaller than the surface structure detail. In this way authors could reliably simulate cyclic voltammetry at rough surfaces considered as fractals with number of particles of the order of 40000 and number of steps of the order of 10000 (Nyikos & Pajkossy, 1986), (Pajkossy & Nyikos, 1989a, 1989b). The stochastic nature of the model was clearly visible in the cyclic waveforms produced. This kind of stochastic behaviour is not visible under normal circumstances with electrochemical experiments since the practicable numbers are many orders of magnitude greater than 10000.

The advantage of using individual particles to model diffusion is that the conservation of particles is inherent in the process, so model instabilities are less likely to appear. However, the modelling of individual particles requires a much greater level of information than models based on the diffusion equation. Many particles are needed to generate enough data to approximate the overall diffusion process. Where a 2

dimensional model is feasible for explicit diffusion models, realistic 3 dimensional models take excessive computation without resorting to specialised resources.

The surface dimension can be measured in several ways. The most common is the Hausdorff dimension. As with the topological dimension, the Hausdorff dimension describes the minimum number of discrete directions needed to cover a fractal space. For a plane two directions, commonly denoted x and y, are needed; for a line, one direction; or for a volume three. The Hausdorff dimension can often be given for a generated fractal where the pattern of formation is known. Other measures include the correlation and information dimensions (Procaccia and Grassberger, 1983). In many cases the Hausdorff information and correlation dimensions are the same; otherwise the correlation dimension is less than the information dimension which is less than the Hausdorff dimension.

It is necessary to make a distinction between non standard diffusion problems. Some physical situations cause the diffusion profile to be non Fickian. Compte and Metzler (1997) and Bisquert and Compte (2001) derived a time fractional diffusion equation by consideration of non standard particle diffusion such as those satisfying Levy distributions. It is doubtful whether a time fractional diffusion equation derived from non-Fickian diffusion is an accurate physical description for this application since diffusion in the aqueous solution is expected to be normal. Metzler and Klafter (2000) give a detailed account. However the non-Fickian time-fractional diffusion equation can be used to derive a description the same as that derived by Pajkossy and Nyikos (1989b), except for some constant coefficients. The diffusion equation for species denoted i, with concentration C_i could be written:

$$\frac{\partial C_i}{\partial t} = D_i \frac{\partial^{\varepsilon-1}}{\partial t^{\varepsilon-1}} \frac{\partial^2 C_i}{\partial x^2} \qquad \textbf{26}$$

The alternate fractal parameter is related by $\varepsilon/2 = \beta$. And using the Laplace transform the following could be derived:

$$C_i(0,t) - C_i^* = \pm \frac{1}{\sqrt{D_i}\,\Gamma(\varepsilon/2)} \int_0^t \frac{J(\tau)d\tau}{(t-\tau)^{1-\varepsilon/2}} \qquad \textbf{27}$$

So a similar result can be obtained (Equations 25 and 27) using different physical conditions: either particles diffusing abnormally to a flat surface or particles diffusing normally to a fractal surface.

Strømme *et al.* (1995) used the convolution expression of Pajkossy and Nyikos (1989b) and derived the fractal form of the Randles-Sevcik equation (shown in Equation 28), applicable to reversible electrode surfaces. Two methods for predicting the surface dimension were derived (i) the reversible peak to peak separation of redox couple in the absence of solution resistance and (ii) the increase in peak current with scan rate.

$$i_{peak} = \left\{ A_{macro} (\gamma \lambda_i^2)^{(\beta - 0.5)} \right\} \frac{\Gamma(1-\beta)\Gamma(\beta)}{\Gamma(1/2)} \left(\frac{nFv}{RTD} \right)^{\beta} nFDC_O^* \chi_{\max}(\beta) \qquad \textbf{28}$$

χ is the well known dimensionless current constant as used by Bard and Faulkner (2001) which can be replaced by an appropriate numerical constant when β is known. The maximum χ depends on β and is given by Strømme *et al.* (1995) graphically. The area, A, term is given in curly brackets: γ is the root of the ratio of diffusion coefficients (for the oxidised and reduced species) and λ_i is the length corresponding to the inner cut off where the transition between smooth and fractal surface characteristics occurs. The term is needed because the active area depends on the characteristic diffusion length and thus can be expected to vary during the experiment. The gamma functions are as before. F, n, R, T, D and C have their usual electrochemical meanings. The current peak, i_{peak}, depends upon the scan rate v^{β}. The result applies to reversible electrode surfaces.

Extension of fractal electrochemical models to slow surface kinetics has been limited. The effect of slow kinetics on the effect on hydrogen diffusion within metal hydrides has been studied using potential step functions (Pyun and Go, 2007). However there is little apparent applicability to cyclic voltammetry. Cyclic voltammetry on a fractal

electrode has not yet been extended to include heterogeneous kinetics, as would be necessary for most screen-printed electrodes.

3.2.2 Application of Nicholson Method to Heterogeneous Electron Kinetics on a Rough Surface

At the electrode, boundary conditions are imposed. A reaction causes either the reduction of an oxidised species, O or an oxidation of a reduced species, R as shown in Equation 29. Each reaction causes n electrons to be transferred; in this context n is usually 1.

$$O + ne \Leftrightarrow R \qquad \textbf{29}$$

The transfer of electrons over time causes an electron flux, J which can be related to a measured current, i in terms the Faraday constant, F and active electrode area A, as shown in Equation 30. The net flux of oxidised species 'into' the electrode must equal the net flux of reduced species exiting the electrode, as shown in Equation 31.

$$J = \frac{i}{nFA} \qquad \textbf{30}$$

$$J = D_O \frac{\partial C_O}{\partial x} = -D_R \frac{\partial C_R}{\partial x} \qquad \textbf{31}$$

Initially all the diffusive phase is considered to be uniform with concentrations denoted with '*'. The concentration of analyte far from the electrode remains at this initial concentration. For t = 0:

$$C_O = C_O^*; C_R = C_R^* \qquad \textbf{32}$$

And for t > 0:

$$C_O(x \to \infty) = C_O^*; C_R(x \to \infty) = C_R^* \qquad \textbf{33}$$

At the electrode surface with kinetic influence the electron flux J is given by Equation 34.

$$J = k_f C_O(0,t) - k_b C_R(0,t) \qquad \textbf{34}$$

where k_f and k_b describe the rate constants for oxidation and reduction respectively (f refers to forward, and, b, backwards). Standard electrochemical theory (Bard and Faulkner, 2001) relates k_f and k_b to a single standard rate constant k_s. Activated complex theory is used to describe the kinetic factor relationship with energy and temperature.

$$J = k_s \left\{ e^{-\frac{\alpha nF}{RT}(E-E^0)} C_O(0,t) - e^{(1-\alpha)\frac{nF}{RT}(E-E^0)} C_R(0,t) \right\} \qquad \textbf{35}$$

α here is used in its standard electrochemical context as the electron transfer constant used to describe asymmetry in the rate constants for the forward and backward reactions. For a symmetrical reaction α = 0.5 and this approximation is normally used here after. For very fast kinetics, where k_s is large, the J/k_s ratio tends to zero and the Nernst equation can be redeemed. Thus the electrochemical absolute rate equation, devoid of any fractal consideration, represents the kinetics. To this it is possible to combine the fractal mass transfer expression of Pajkossy and Nyikos (1989a). In keeping with the planar derivation of Nicholson (1965), dimensionless parameters were introduced, serving two purposes: (i) equations expressed more concisely and (ii) the result is more widely applicable. The disadvantage is the output is harder to understand.

For cyclic voltammetry, the potential E at time t, can be related to the initial potential E_i, length of scan, λ, half-scan number n_s and scan rate,v.

For n_s odd (negative going scan):

$$E = E_i + \lambda * (n_s - 1) - vt \qquad \textbf{36}$$

For n_s even (positive going scan):

$$E = E_i - \lambda * n_s + vt \qquad \textbf{37}$$

Parameter 'a' is introduced which contains the scan rate, v.

$$a = \frac{nFv}{RT} \qquad \textbf{38}$$

Secondly if the electrochemical system is assumed to be at equilibrium, then the Nernst condition gives the following represented by θ:

$$\theta = \frac{C_O^*}{C_R^*} = e^{\frac{nF^*(Ei - E^0)}{RT}} \qquad \textbf{39}$$

Thirdly a parameter S_λ is introduced to account for the exponential form of the cyclic sweep concisely shown for the forward and reverse sweep:

$$S_\lambda = e^{-at + \lambda^*(n_S - 1)}; S_\lambda = e^{at - \lambda^* n_S} \qquad \textbf{40}$$

for odd and even half-scans respectively. So J, now with consideration for the cyclic potential sweep procedure, is given by:

$$J = k_s(\theta * S_\lambda)^{-\alpha} * \{C_O(0,t) - \theta * S_\lambda C_R(0,t)\} \qquad \textbf{41}$$

Dimensionless time parameters are introduced:

$$y = at; z = a\tau \qquad \textbf{42}$$

This gives the complicated expression for J, where J is present of the left hand side and in the convolution expressions on the right hand side.

$$J = k_S(\theta * S_\lambda)^{-\alpha} \left\{ \begin{array}{l} C_O^* - \dfrac{\xi}{\sqrt{D_O}\Gamma(\beta)a^\beta} \int_0^y \dfrac{J(z)dz}{(y-z)^{1-\beta}} - \\ (\theta * S_\lambda) * \left\{ C_R^* + \dfrac{\xi}{\sqrt{D_R}\Gamma(\beta)a^\beta} \int_0^y \dfrac{J(z)dz}{(y-z)^{1-\beta}} \right\} \end{array} \right\} \qquad \textbf{43}$$

and,

$$\xi = \frac{\Gamma(1/2)}{\Gamma(1-\beta)} \qquad \textbf{44}$$

Further dimensionless parameters are introduced, (i) the dimensionless current function χ for the fractal case:

$$\chi(y) = \frac{1}{C_O^*} \frac{\xi * J(z)}{\sqrt{D_O}\Gamma(\beta)a^{\beta}} \quad \textbf{45}$$

And (ii) ψ the dimensionless kinetic factor:

$$\psi = \frac{\xi * \gamma^{\alpha} k_s}{\sqrt{D_O}\Gamma(\beta)a^{\beta}} \quad \textbf{46}$$

The simplified version of the final convolution expression:

$$\frac{\chi(y)(S_\lambda \gamma\theta)^{\alpha}}{\psi} = 1 - S_\lambda - \left\{1 + S_\lambda \gamma\theta\right\} * \int_0^y \frac{\chi(z)dz}{(y-z)^{(1-\beta)}} \quad \textbf{47}$$

This expression is equivalent to Nicholson's (1965a) for heterogeneous electron transfer kinetics at an electrode surface but extended using the fractal parameter as derived by Nyikos and Pajkossy (1988). To see the result of this equation a numerical solution is required, as given in Section 3.3.6, because χ (the current function) appears both inside and outside of an integral sign.

3.3 Materials and Methods

3.3.1 Electrode Materials and Design

Several designs were considered in this chapter. Figure 3.4 shows three designs for sensors. (A) and (C) have been used for immunosensors; the circular aperture aids surface preparation when pipetting drops of reagent.

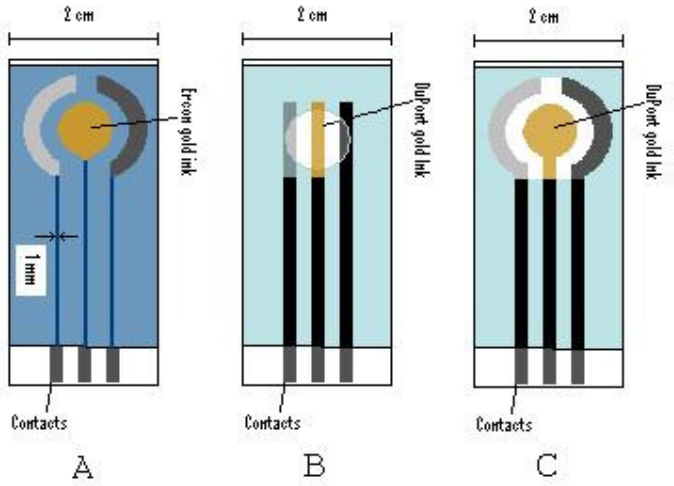

Figure 3.4 Electrode tracks for three systems, all *in house* designs: (A) immunosensor design using Ercon gold ink with thin carbon tracks, (B) DuPont printed metal ion sensor design using DuPont gold ink, and (C) DuPont printed, modified immunosensor design using DuPont gold ink

The earlier design (A) shows particularly thin tracks; with carbon tracks of resistance above 10 kΩ typically, and up to 50 kΩ occasionally. The thicker track design of the metal ion sensor (B) was applied to the immunosensor design so that the track resistances are about 1 kΩ. However, even with the thicker width resistances have been measured above 40 kΩ when diluted high conductivity or otherwise low conductivity carbon inks are used.

Ceramic electrodes were provided by DuPont (DuPont Microcircuit Materials, Bristol, UK) to investigate the use of these inks in biosensors (otherwise used in the printed circuit board industry). The platinum and gold inks were designated high temperature firing inks, cured at 850 °C on alumina substrate (DuPont Microcircuit Materials, Bristol, UK). Standard low temperature polymeric inks provided reference and insulation inks the counter. The design was the same as the standard metal ion sensor shown in Figure 3.4B with complementary inks as shown in Table 3.2.

Table 3.2 Materials for gold and platinum ceramic electrodes

Working electrode	Platinum[b] (Product 9141)	Gold LF141[b]
Counter electrode/tracks	Carbon BQ225	Carbon BQ225
Reference electrode	Ag/AgCl 5874 (BQ164)[d]	Ag/AgCl 5874
Insulation layer	E107257-1[c]	E107257-1[c]
Substrate	Alumina[a]	Alumina[a]

[a]635 μm alumina 'snap-strate'; [b]fired at 850 °C; [c]experimental UV cure formulation no particulate filler; [d]Ag/AgCl product 5874 rebranded as BQ164

The polymeric gold Dupont Sensors used in this Chapter were of Batch AO (with composition as will be described Table 4.2 on page 169). Electrodes of immunosensor design were kindly donated by C. Parker and M. Huerich. Generally these electrodes were printed *in house* on a DEK 248 semi automatic screen-printer (DEK, Weymouth, UK) with Electrode Carbon Silver for track and reference electrodes (given in Section 2.3.3); Epoxy thermoset resin SB 242 onto PET sheets using custom DEK screens. Samples of similarly *in house* printed electrodes of metal ion sensor design using Ercon gold ink were passed down (via M. Huerich) from M.F.M Noh. *In house* ink formulations were prepared as described in Section 2.4. Equipment and software is as described in Sections 2.2.1 and 2.2.2.

3.3.2 Nicholson Method Procedure

Typically the fit was implemented by using a model template in the form of a Microsoft Excel file. In brief, the model data (ψ vs ΔE_p) was tabulated along with values for temperature, Faraday constant, electron number, diffusion constants and so on. By using the relationship in Equation 48, a model fit for peak separation against logarithm of scan rate was generated (ΔE_p vs logv). The parameter for the rate constant, ks, could then be changed to best fit experimental data. The electron transfer constant, α, was taken as 0.5 generally; the derivation of the electron transfer rate, k_s, is relatively independent of α (Nicholson 1965a). Values of the diffusion coefficient used were 7.26×10^{-6} cm^2/s and 6.67×10^{-6} cm^2/s for the oxidised and reduced forms of ferrocyanide respectively. The temperature was taken as 297 K.

$$\log(v) = 2\log(\gamma^{\alpha} k_x) + \log\left\{\frac{RT}{\pi D_o nF}\right\} - 2\log(\psi) \qquad \textbf{48}$$

Table 3.3 Kinetic parameter, ψ, vs peak separation, ΔE_p. Extension to existing published data obtained by solving Equation of Nicholson in Matlab

ΔE_p (V)	ψ
0.2	1.18×10^{-1}
0.25	7.27×10^{-2}
0.3	4.46×10^{-2}
0.35	2.74×10^{-2}
0.4	1.68×10^{-2}
0.45	1.03×10^{-2}
0.5	6.32×10^{-3}
0.55	3.88×10^{-3}
0.6	2.38×10^{-3}
0.65	1.46×10^{-3}
0.7	8.97×10^{-4}
0.75	5.50×10^{-4}
0.8	3.38×10^{-4}
0.85	2.07×10^{-4}
0.9	1.27×10^{-4}
0.95	7.8×10^{-5}
1	4.79×10^{-5}

In general, experiments used potassium ferrocyanide redox couple dissolved at concentration between 0.1 and 5 mM in a 0.1 M KCl electrolyte. Scan rates between 1 and 500 mV/s were used. Each experiment recorded 3 to 5 scans; the second scan was used for further analysis. As standard a new sensor was used for each measurement. Equipment and software is as described in Sections 2.2.1 and 2.2.2.

3.3.3 Ink Thickness and Roughness Measurements

Screen-printed inks were observed using a microscope (equipment and software described in Section 2.2.3). Particulate size and dispersion was observed using 10, 50 and 100 x lens.

The 50 x LWD object was used to observe the electrode fixed to a glass slide. The ink surface was brought into focus first then the substrate by altering the staging height. The difference in staging height was read from the microscope setting.

To account for surface roughness, another method used images acquired over a range of staging heights. Images were taken at 1- 5 µm intervals. A Sobel edge correction (using ImageJ software) was used for edge detection. The degree of edge detection was taken as an indication of focus. The height with the most focus was used as the average height for the surface. Extended surface ranges in the x-y plane were used to provide reproducible statistics; typically the range is greater than 100 × 100 µm. A 50 x LWD lens was used for this procedure.

3.3.4 Surface Reconstruction Image Processing

The change in staging height showed very clearly the change in focus on the inks surface demonstrating the capability to measure quantitatively the height variation. One method to find the ink thickness used an average of surface height measurements. Images were taken at successive 1 or 2 µm heights over a suitable range of (< 30 µm). The 50xLWD lens was best for this procedure. The images could be a single exposure, or automated extended image composites, over the x-y plane, to get more representative measurements. The saved images were transferred to ImageJ software and stacked; 'stacked' refers to the process of layering the images so that the points in the x-y plane are aligned and surface height is represented by the z axis; the images are contained and stored as a single file. The images could be replayed as an animation showing the change in focus at a rate of about 1 µm/s. The *in focus* regions typically show well defined edges particularly at particulate-polymer boundaries; whereas non focussed regions are typically blurred.

ImageJ features an edge detection and edge enhancement facility, based on a Sobel edge detection algorithm. The algorithm produces whiter pixels where sharper edges occur in the original image, which it evaluates from the comparative hue and tone with a local set of pixels (the pixel window). Darker pixels result from the absence of edges. The window is moved across the image to evaluate the whole surface. Since the output is directly related to the difference in pixel values the process is a (two dimensional) form of differentiation. The edge detection algorithm determines how the local set of pixels is chosen and relative weightings are applied to produce the

differential. The output images are effectively greyscale with whiter shades depicting edges and blacker shades the absence of edges. An intensity measurement facility, based on the pixel whiteness was then used to evaluate quantitatively the effective measurement of the surface focus, over the selected region in the image.

For the reconstruction of the surface of BQ331 ink surface, images were taken every 1 µm over a 30 µm range. A 3 by 3 composite area was chosen using the 50xLWD lens. The images were uploaded to ImageJ where they were stacked and edge detection was applied. The images were then converted to 8-bit greyscale and thresholding was used to reduce the images to binary information. The choice of threshold limits is set manually and contributes a subjective element to the image process. The aim is to select the surface or focused pixels whilst eliminating all other visual information. An example of the thresholded images is given in Figure 3.20.

Each point on the thresholded images represents a surface point in the x-y plane, and the image number from 1 to 30 represents the height, z, of that surface point. Therefore it should be possible to reconstruct the surface. However the somewhat arbitrary nature of the thresholding process and distortion of marginally focussed images contributes to significant noise. Some points in the x-y plane are represented on more than one slide, whilst other locations on the x-y plane have no representative surface points.

The image stacks were uploaded into Matlab which were stored as a structured array. The images were manipulated so that the binary information was represented by 1s and 0s in a rank 2 matrix representing the x-y plane. The 1s represented surface points. The matrices were then scaled according to height, for example the ones in image 2 were replaced by 2, in image 3 by 3 and so on. The matrices then had to be combined into a single rank 2 matrix. A selection process was necessary for incidences of multiple points: initially the point selected was the point associated with the highest image, however this was superseded by selection of the average data point height resulting in some non integer values (not a problem).

Some points in the final matrix were missing (represented by 0); these were of sufficiently low density that the values could be interpolated from neighbouring squares. Therefore for each point the 24 nearest neighbours were chosen and an average value was used.

The program, given in Appendix A3, was run from Matlab script editor. Due to the large number of data points some processes took several minutes to compute.

The resulting surface was noisy with spike like features. A 5 by 5 point smoothing algorithm was applied across the surface to eliminate this noise. The resolution of the smoothed surface was equivalent to about 4 μm. The surface is shown in Figure 3.21. A value for the Hausdorff dimension was estimated using the numerical procedure of Vasconsellos *et al.,* (2006). Also the surface map could be used to put together a single *in focus* colour image of the surface. Appendix A3 shows the calculations for these processes.

3.3.5 General Voltammetric Modelling

Most of the voltammetric modelling conducted would be considered trivial and could be easily reproduced with reference to Bard and Faulkner (2001) and a suitable mathematical package; the application to rough surfaces with slow electron kinetics is not.

Models were split into two groups: (i) those that used explicit simulation (Bard and Faulkner, 2001) of the analyte concentration in solution reacting at an electrode using the Nernst and diffusion equations; and (ii) those that use a Laplace transform (Smith, 1966) to provide a mathematically simpler alternative which involves summing a convolution (such as Nicholson, 1965b). The first approach requires that the solution phase is conceived as a grid with a value at each point for concentration; the diffusion equation (Equation 7) is descretised as given in Equation 51.

$$C(n_t+1,n_x)=C(n_t,n_x)+\frac{D\Delta t}{\Delta x^2}\{C(n_t,n_x+1)-2C(n_t,n_x)+C(n_t,n_x-1)\} \quad \textbf{49}$$

$C(n_t, n_x)$ is the concentration at time t, grid reference n_t, at position x, grid reference n_x; D is the diffusion coefficient; and Δx and Δt are the lengths in spatial and temporal dimensions between neighbouring points. All models used had uniform point spacing. $D\Delta t/\Delta x^2$ was necessarily less than a value of 0.5 to maintain numerical stability (Bard and Faulkner, 2001)

This type of approach was conducted in one or two spatial dimensions (using the method of lines). Computing resources precluded the simulation of 3 dimensional diffusion profiles. The advantage of the explicit 2 dimensional approach is the ability to handle complicated electrode shapes, but limited by the resolution of data points (set by Δx, Δy and Δt) compared with computing resources.

This approach was used to demonstrate the diffusion profile in Figure 3.32 with Nerstian conditions at the electrode surface during cyclic voltammetry. The diffusion coefficient was 1×10^{-5} cm^2/s; spatial step size 3.2 µm; temporal step size, 5 ms; scan rate, 50 mV/s; scan range -0.25 to 0.25 V; number of scans 3, C ox initial 0 for all x; and C red initial 1 for all x.

A similar approach was used in Figure 3.3 to evaluate Equation 21 with Nernstian conditions and cyclic voltammetry at an electrode boundary. Parameters were: time step 5 ms, total time 32 s, spatial step 3.2 µm, spatial range 500 µm, scan range -0.4 V to 0.4 V, scan rate, 50 mV/s, C ox initial 0 for all x; and C red initial 1 for all x. The value for $D\Delta t/\Delta x^2$ was 0.488 just below the 0.5 threshold for stability.

The convolution approach generally results in an expression like that shown in Equation 21. When applied, with suitable electrode boundary conditions, gave an expression like that shown in Equations 45 to 47. For usual planar conditions β would be equal to a value of 0.5. The diffusion profile was not given explicitly in these

cases. The convolution was evaluated via the method shown in Section 3.3.6, derived by Nicholson (1965b). A Matlab script is given in Appendix A2. These examples show the full model for rough surfaces but are backward compatible for the standard planar case as derived by (Nicholson, 1965a). A convolution model was used to determine the relationship between ψ and ΔE_p in Table 3.3 (page 116) using a script run in Matlab. Parameters include diffusion coefficient of 10^{-9} m^2/s, potential step dE, 2 mV, scan range altered according to expected peak separation. Electron exchange number 1, electron transfer coefficient, α, 0.5

3.3.6 Numerical Implementation of Heterogeneous Kinetics

The method of Nicholson (1965b) is modified to numerically solve the convolution expression. The continuous integral is approximated to a discrete summation. For a time y, the convolution must sum for all values, z, from the start up to z = y. For example, schematically for the tenth point 10 calculations are needed, for the eleventh point 11 calculations, for the twelfth, 12 and so on. To find all current values up to point twelve the number of calculations must be 1 + 2 + … + 11 + 12 for the 1st, 2nd, 11th and 12th points respectively, which is an approximation integration of the point number. Therefore the total number of calculations needed to evaluate the convolution up to y in N steps is proportional to N^2. The range of integration M is split into N steps and δ = M/N. The time is discretised: (i) the n^{th} step is given by at/δ and (ii) the variable of integration $\upsilon = z/\delta$.

$$\int_0^y \frac{\chi(z)dz}{(y-z)^{1-\beta}} \rightarrow \delta^{\beta} \int_0^n \frac{\chi(\delta\upsilon)d\upsilon}{(n-\upsilon)^{1-\beta}} \qquad \textbf{50}$$

The integral is split into n parts numbered from υ = 0,1…i...n There is a singularity when n = υ which is avoided when integration by parts is applied:

$$\int_0^n \frac{\chi(\delta\upsilon)d\upsilon}{(n-\upsilon)^{1-\beta}} = \frac{1}{\beta} * \left[\chi(1) * n^{\beta} + \sum_{i=1}^{n-1} (n-i)^{\beta} \left[\chi(i+1) - \chi(i) \right] \right] \qquad \textbf{51}$$

Thus an expression is obtained from which results can be computed:

$$\frac{\chi(n)(S_\lambda(n)\gamma\theta)^\alpha}{\psi} = 1 - S_\lambda(n) - \left\{1 + S_\lambda(n)\gamma\theta\right\} * \frac{\delta^\beta}{\beta} * \left[\chi(1) * n^\beta + \sum_{i=1}^{n-1}(n-i)^\beta\left[\chi(i+1) - \chi(i)\right]\right] \quad \textbf{52}$$

It is necessary to consider three cases, for n = 1, n = 2 and, n = k (for k > 2):

For n = 1:

$$\chi(1) = \frac{1 - S_\lambda}{\frac{(S_\lambda\gamma\theta)^\alpha}{\psi} + \frac{\delta}{\beta} * (1 + S_\lambda\gamma\theta)} \quad \textbf{53}$$

For n = 2:

$$\chi(2) = \frac{1 - S_\lambda - \frac{\delta}{\beta} * (1 + S_\lambda\gamma\theta) * \left[(2^\beta - 1)\chi(1)\right]}{\frac{(S_\lambda\gamma\theta)^\alpha}{\psi} + \frac{\delta}{\beta} * (1 + S_\lambda\gamma\theta)} \quad \textbf{54}$$

For n = k; k>2:

$$\chi(k) = \frac{1 - S_\lambda - \frac{\delta}{\beta} * (1 + S_\lambda\gamma\theta) * \left[k^\beta\chi(1) - \chi(k-1) + \sum_{i=1}^{k-2}\left[\chi(i+1) - \chi(i)\right] * (k-i)^\beta\right]}{\frac{(S_\lambda\gamma\theta)^\alpha}{\psi} + \frac{\delta}{\beta} * (1 + S_\lambda\gamma\theta)} \quad \textbf{55}$$

An example script in Matlab using this numerical formulation is given in Appendix A2. The results of the script are given in Sections 3.4.7 and 3.4.8.

3.4 Results

3.4.1 Electrode resistance

For ceramic platinum electrodes, the resistance of the tracks varied according to position on the ceramic sheet as shown in Figure 3.5. Approximately five out of eight

electrodes had a lower (< 2 kΩ) resistance. The electrodes on the left hand side measured up to 6 kΩ. Such skewed distributions are well known (Gilleo, 1996), and result either (both) from uneven printing, such as printing pressure, print gap or ink thickness, or (and) from uneven firing due to uneven oven temperature, ventilation, or exposure time.

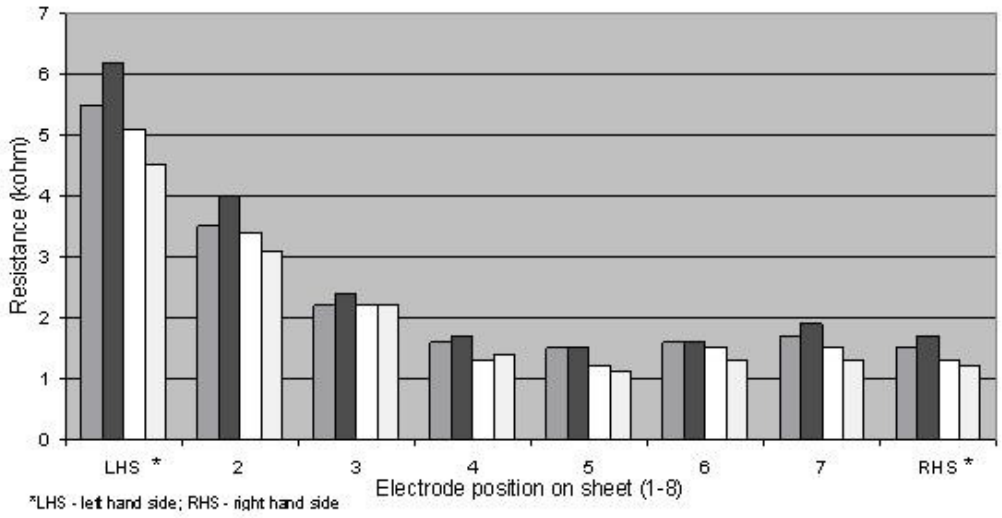

Figure 3.5 The resistance of platinum ceramic electrodes on 4 sheets with composition given in Table 3.2.

Electrodes tested based on the immunosensor design (Figure 3.4A) generally had resistances above 10 kΩ and as high as 50 kΩ were observed. The Dupont sensor electrodes generally had resistance of 1 ± 0.5 kΩ with the differing carbon inks. The Dupont sensors used for Section 3.4.3 (Batch AO) had track impedance 980 ± 50 Ω. Some sensors of the metal ion design (Figure 3.4B) printed *in house*, such as those coming from the work of Noh (2005) also had resistances from 10 kΩ to 40 kΩ. Why this should be is not clear: possibly an aged or diluted carbon ink was used.

Although there are methods for estimating the resistance (such as the method described by He and Faulkner, (1986) in the absence of Faradaic reagents and suitable hardware, using a multimeter post experiment, or studying the voltammograms with wide potential ranges (>1.5 V) for non polarised behaviour, the maximum slope giving an estimate of resistance) and applying corrections, particularly high

resistances can mean that there is a potential drop across the working electrode itself. Noble metal inks have high conductivity so that this drop would be negligible. However, with carbon inks the drop across the working electrode, for example has been found with in excess of 100 Ω per 5 mm length of track with the metal ion design. A numerical prediction via explicit modelling is feasible but highly impractical for analysing redox behaviour.

3.4.2 The Nicholson Method Applied to Screen-Printed electrodes

Previously, the Nicholson method was applied to carbon screen-printed electrodes. The (unpublished) data for Figure 3.6 was kindly donated by C. Parker. The sensor composition used inks given in Section 2.3.3. The design was of immunosensor type, shown in Figure 3.4(A) on page 114 where it is further discussed. The solution was 0.5 mM potassium ferrocyanide in 0.1 M KCl. The electrodes were scanned at 10 – 100 mV/s over a range between -0.6 and 1 V. The electrodes received no pretreatment.

The result shows a steep increase in the peak separation with scan rate, of nearly 400 mV per decade increase in scan rate, and a reasonably linear relationship. It is not possible to fit the simulation to this data; the Nicholson model expects no greater than about 116 mV per decade increase in scan rate.

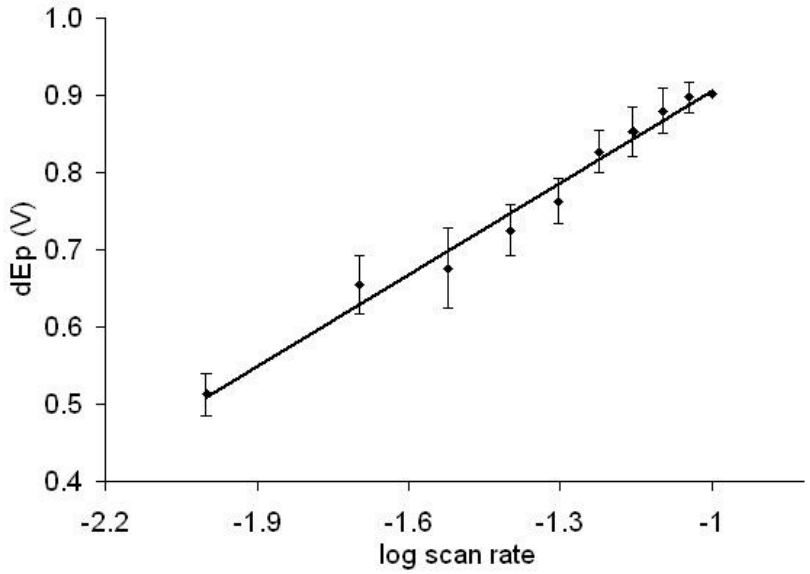

Figure 3.6 The peak separation of a ferrocyanide redox couple at scan rates from 10 to 100 mV/s on unpretreated carbon screen-printed electrodes

The data shown in Figure 3.6 can be explained with the effect of resistance. Figure 3.7 shows the same data with a 40 kΩ resistance correction applied. The linearity is poor, but a tentative value of 1.7×10^{-4} cm/s can be applied to the electrode surface. Since the original electrodes had been disposed, electrodes taken from the same batch were tested for (working electrode) track resistances: values ranged 20 – 40 kΩ. These values were much higher than expected for the design, probably attributed to dilute carbon ink or low-grade carbon powder. Calculating the rate constant with such high resistances cannot give reliable results.

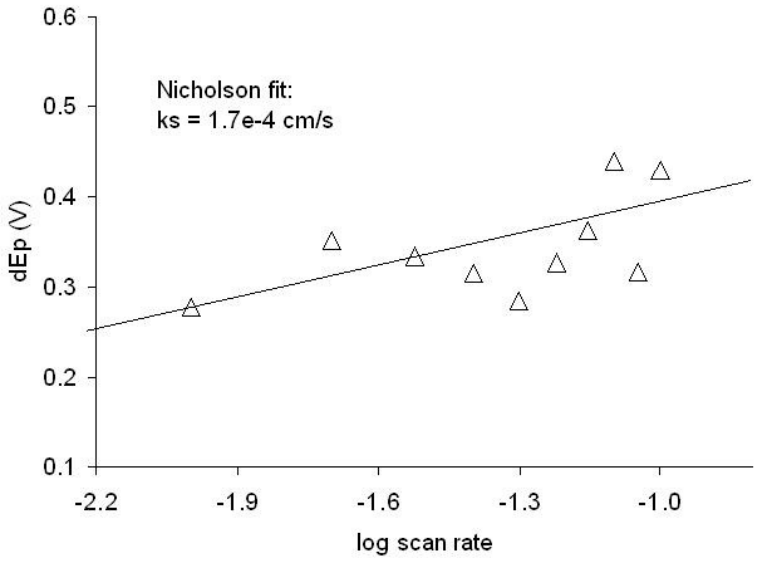

Figure 3.7 Data acquired from Figure 3.6 applied with 40 kΩ resistance correction and Nicholson model fit

The Nicholson method was applied to the ceramic electrodes. Figure 3.8 shows the application of the Nicholson method to the iR-corrected data: a rate constant of 4.2×10^{-3} cm/s is found indicating quasi-reversible behaviour at low scan rates. The non-iR corrected data is also shown (units kΩ) with high resistances (> 2 kΩ) indicated for individual measurements. The results clearly demonstrate the effect of high track resistance when trying to measure the rate constant.

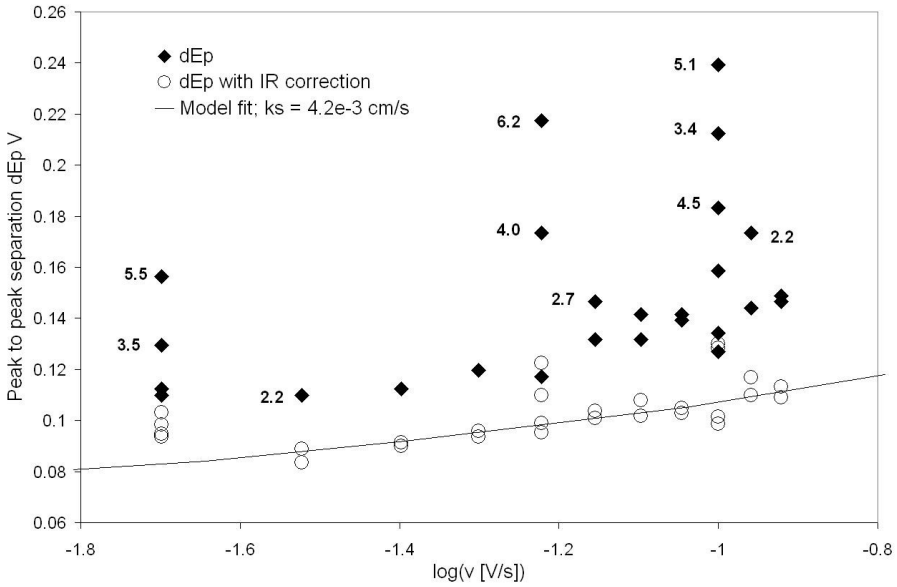

Figure 3.8 Plot of peak separation and logarithm of scan rate: Nicholson method applied to screen-printed electrodes with high temperature platinum working electrode.

Due to the high dependence on the resistance, the necessity of making large corrections needs to be avoided when applying the method. This has not always been the case in the laboratories here, for example the calculation of rate constant for Ercon gold ink (R 464 DPM 78) by Noh (2005). Noh's thesis shows cyclic voltammograms for 0.5 mM ferrocyanide in 0.1 M KCl at scan rates of 10, 25, 50 and 75 mV/s. The peak separation increased by about 250 mV over less than a decade increase in scan rate, too much for the Nicholson method. No record of the track or solution resistance was presented.

However, a prediction of the resistance can be made from a cyclic voltammogram (in Noh's thesis) in 0.05 M HCl from -1.5 to 1.5 V comparing a gold disk electrode with the screen-printed Ercon gold. Gold has a low hydrogen overpotential so the figure displays a large range of non polarised behaviour. In the non-polarised limit, the voltammogram becomes a linear slope set by the working electrode and solution impedance. Over the range -1500 to - 700 mV the current is linear and increases from -91 to about -14 μA, equivalent to resistance of about (800/77)10 kΩ. Now the peak current for the redox couple shows values of 2 – 6 μA, so the maximum peak potential

correction is approximately 60 mV for the forward peak and -40 mV for the reverse peak, totalling 100 mV. This would considerably reduce the peak separation excess.

For the gold ceramic electrodes a similar kinetic result was found: 1×10^{-3} cm/s. The resistances were lower so the correction needed was marginal. The results are shown in Figure 3.9.

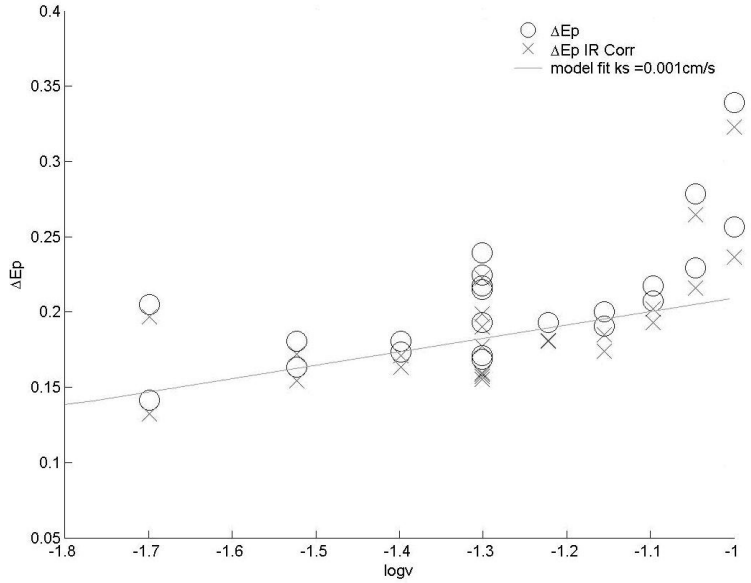

Figure 3.9 Plot of peak separation and logarithm of scan rate for gold ceramic electrodes with composition given in Table 3.2. Peak to peak separation is given with and without iR correction.

The sensors were found to be useful for analysis in non-aggressive electrolytes, showing good voltammetric shapes, shown in Figure 3.10.

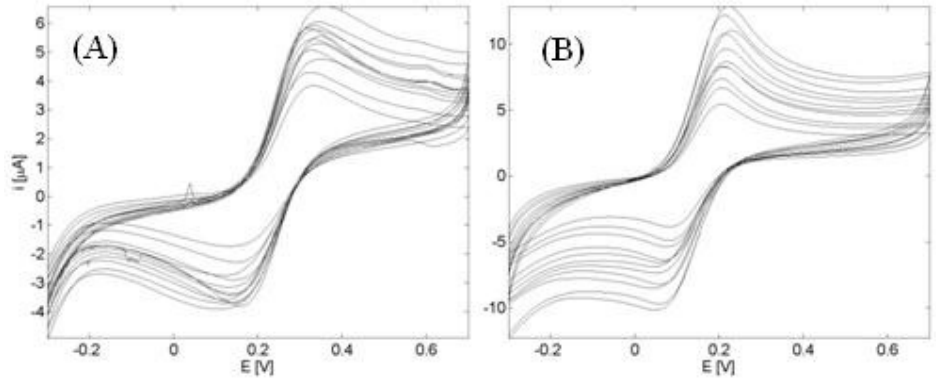

Figure 3.10 Voltammograms for (A) gold and (B) platinum high temperature screen-printed electrodes using 0.5 mM ferrocyanide and 0.1 M NaCl electrolyte at scan rates between 10 and 100 mV/s

The factors in the formulation of the Nicholson method the were expected to affect the slope between ΔE_p and v were considered. For example the number of electrons in the reaction affects both the slope and peak width; however, the ferrocyanide is known to be a one electron transfer reaction and the peak shape is compatible with single electron transfer. A value of 0.5 for planar electrodes comes from the fact that the diffusion differential equation is second order in space and first order in time. The Nicholson treatment does not account for solution resistance (Nicholson, 1965a).

Tested with 0.5 mM ferrocyanide and 0.1 M NaCl, the PMMA/carbon formulation did not produce well defined peaks and the background currents were low indicating slow kinetics. The PSAN and polymer X combined with carbon powders produced good peaks, although the reverse peak was typically not as strong as the forward peak. As assumed planar configurations, the kinetic rate constants were measured as 1.5×10^{-6} and 2.5×10^{-5} cm/s respectively for the PSAN and polymer X formulations.

The hand painted gold formulations did not provide reasonable ferrocyanide peaks with any of the polymer formulations. Several efforts to improve the reversibility were tried. The gold-polymer surface was polished on an alumina pad. Another method involved etching the polymer back with sodium hydroxide (Wei *et al.,* 2007) which resulted in a measurable but poorly shaped voltammogram with ferrocyanide.

3.4.3 DuPont Gold Ink BQ331

The electrodes were characterised by Cooper (2004) with a suitable redox agent in buffer and found to be reversible to quasi reversible. The peak to peak separation was observed at about 100 ± 15 mV; but this value did not increase as expected with scan rate. BQ331 shows behaviour inconsistent with Nicholson model, since reversible behaviour expects 57 - 60 mV peak separations which are independent of scan rate. Although the batches tested by Cooper (2004) and the many batches supplied since have contained various carbon inks the resistances measured have been consistently about 1.0 ± 0.5 kΩ and always less than 2 kΩ. These values applied to the carbon inks printed onto the PET substrate as opposed to the ceramic substrate as discussed elsewhere (Figure 3.5).

An example of the results is shown in Figure 3.11. The spike occurring close to 0 V is interference, unrelated to the redox couple. Many of the results show a reduction in the redox peaks in the first few scans with some consequent peak to peak separation increases. This phenomenon does not show any apparent trend with scan rate, ferrocyanide concentration or interference peak and probably indicates the limiting factor in reproducibility afforded by these sensors without electrochemical pretreatments. The current range for the lower concentrations, 0.3 – 3 μA for 0.1 mM ferrocyanide, 2 – 7 μA for 0.5 mM, shows that the track resistance is not significant in the peak separation. For the higher concentrations the ranges are 4 - 14 μA for 1 mM and 12 – 45 μA for 5 mM. Therefore the peak position due to resistive effects surpasses the 10 mV tolerance corresponding to about 10 μA current (1 mV correction per μA per kΩ). Individual resistances were not recorded. Also note that the cathodic peak is generally smaller than the anodic peak.

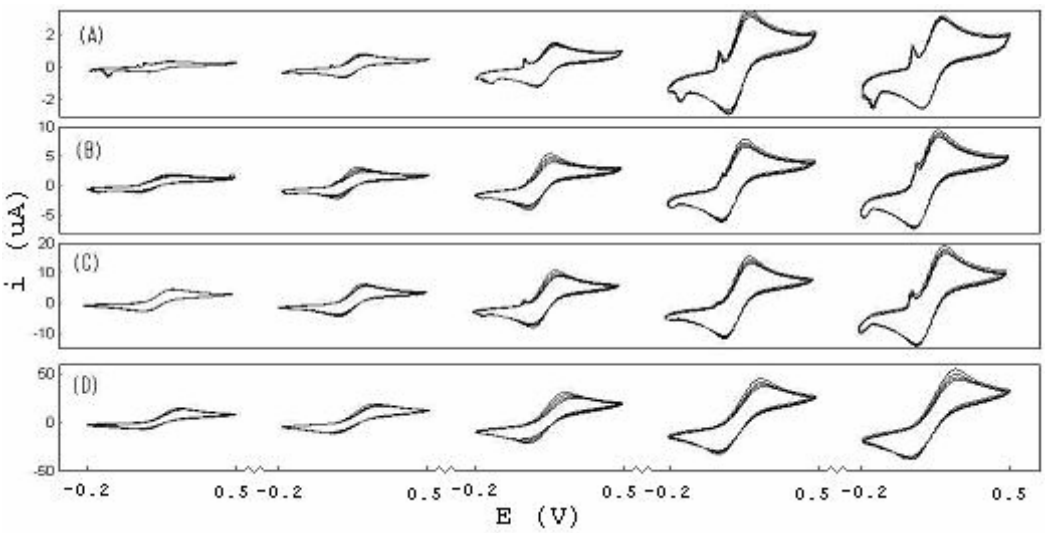

Figure 3.11 DuPont metal ion sensors with BQ331 working electrode cycled with ferrocyanide redox couple at concentrations 0.1 mM (A), 0.5 mM (B), 1 mM (C) and 5 mM (D) in 0.1 M NaCl with scan rates 10, 20, 50, 100 and 150 mV/s from left to right respectively shown. Scan range -0.2 to 0.5 V (vs Ag/AgCl).

A plot of the peak current with scan rate is shown in Figure 3.12B; the exponents calculated (slope of log-log plot) were 0.52, 0.53, 0.68, 0.84 (2.d.p) for 5, 1, 0.5 and 0.1 mM respectively. The lower concentrations have exponent values > 0.5 where 0.5 is expected for Faradaic current at planar electrodes (Bard and Faulkner, 2001) and a value of 1 is expected for highly rough or porous (diffusionless) electrodes. The higher values for lower concentrations could be attributed to background capacitive currents. However, the background currents were measured in a separate experiment with a 0.1 M NaCl electrolyte at 0.01, 0.02, 0.05, 0.1 and 0.15 V/s. A potential of 0.2 V was chosen as relevant value 0.1, 0.1, 0.2, 0.35 and 0.45 µA were measured respectively. The effective correction to the current was very small affecting only the measurements at the lowest concentration.

The poor stability of many of the electrodes in the first five scans inevitably reflects in both the peak separation and the peak current calculations. Further attempts were made to compare conclusions drawn if the first or third scan was used for analysis (not shown). It is difficult to reach any definite conclusions. The peak separation is roughly 100 – 200 mV, but not necessarily increasing with scan rate but does in many cases increase with scan number. This instability is probably attributed to the fresh

gold surfaces which have not yet settled. It will be necessary to show that, when used with an analyte such as arsenic, the screen-printed gold demonstrates sufficient reproducibility.

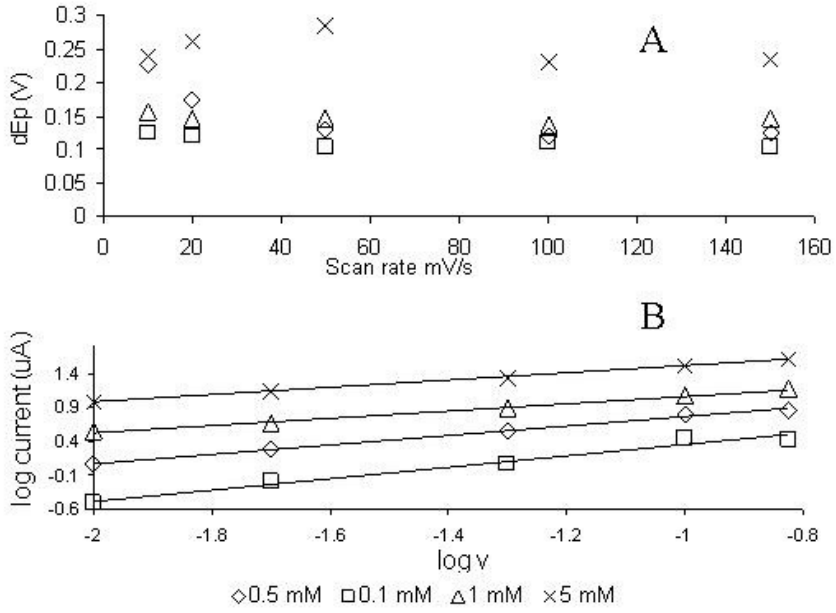

Figure 3.12 For ferrocyanide at four concentrations, as indicated, on DuPont sensors. (A) Plot of peak separation against scan rate and (B) plot of the logarithm of current against logarithm of scan rate

There are two principle limitations when using a redox couple to analyse an electrode surface. At high concentrations or fast scan rates a large current results in iR losses causing changes in peak to peak separation. At low concentrations , the electrode capacitance can influence the currents strongly and peak positions can be difficult to measure. Slow scan rates lower than 1 mV/s suffers from long experiment times and capability of the instrumentation. Generally, with an appropriate concentration, such as 0.5 mM ferrocyanide for the DuPont sensors, an experimental window is defined by capacitance and resistance. For planar electrodes, the scan rate is effectively limited between 1 mVs and 500 mV/s, and preferably 10 – 100 mV/s. As mentioned, 0.5 mM ferrocyanide was chosen and a scan range from 1 to 150 mV/s was used to investigate the electrode surface.

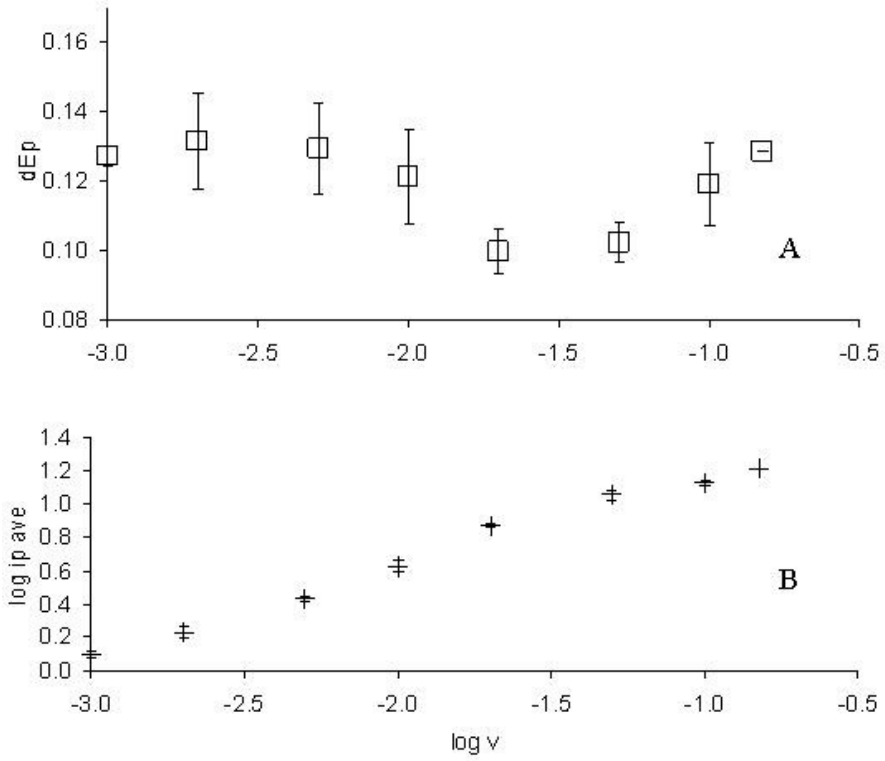

Figure 3.13 (A) plot of peak separation with the logarithm of scan rate, (B) log-log plot of current against scan rate for DuPont sensors with 0.5 mM ferrocyanide and 0.1 M NaCl.

In Figure 3.13B, the exponent measured for the current was calculated to be 0.53, close to that expected of a planar electrode. A distinctive hump or deviation from the linear exponent, occurred around 20 – 50 mV/s (-1.3 to -1.7 logarithm values) which coincided with a dip in the values of peak separation shown in Figure 3.13A. As before, the peak separation did not show a steady increase with scan rate.

3.4.4 Microscopic Investigation of Thickness and Surface Roughness

Various inks were studied microscopically, the details for which are given in the Materials and Methods, Section 3.3.4. Despite a degree of roughness, the commercial inks showed no gaps in surface coverage (whereas homemade inks showed partial coverages). Finding the intrinsic resistivity from the measured resistance and physical dimensions could not be done simply because the strip shape was not geometrically simple. Using this technique, no surface roughness could be measured for the PET substrate, although blemishes were visible attributed to scratches and dust particles.

One method to find a representative ink thickness, despite surface roughness, was to take an average of the surface height, although the procedure was lengthier. Images were taken at successive 1 or 2 µm heights over a suitable range of approximately 30 µm. The successive images were subjected to edge detection and intensity measurement algorithms; a measurement of surface roughness and thickness could be acquired.

The process was applied to platinum ceramic electrodes. Extended images were taken at the platinum ink edge with approximately half the image as platinum ink and the other half as ceramic substrate. The dimensions of the scanned area were 340 by 600 µm with the 50x LWD lens using the automatic staging and 15 images were taken 1 µm apart. Figure 3.14 shows an example image with applied edge detection. The reflective platinum particles in the top half image show clearly showing the power of this technique when applied to noble metal inks. The ceramic substrate was also found to have significant roughness (unlike the PET substrate). In Figure 3.14, it is necessary to note that the image is a composite with 5 across and four down; there is some banding in image brightness at the joins which could be mistaken for surface morphology.

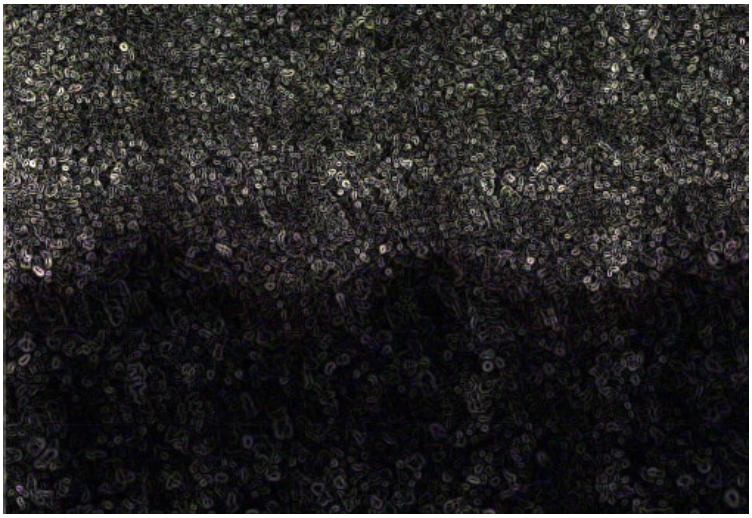

Figure 3.14 Image of ceramic platinum ink (top half) and ceramic substrate (bottom half) after application of the Sobel edge detection algorithm in ImageJ

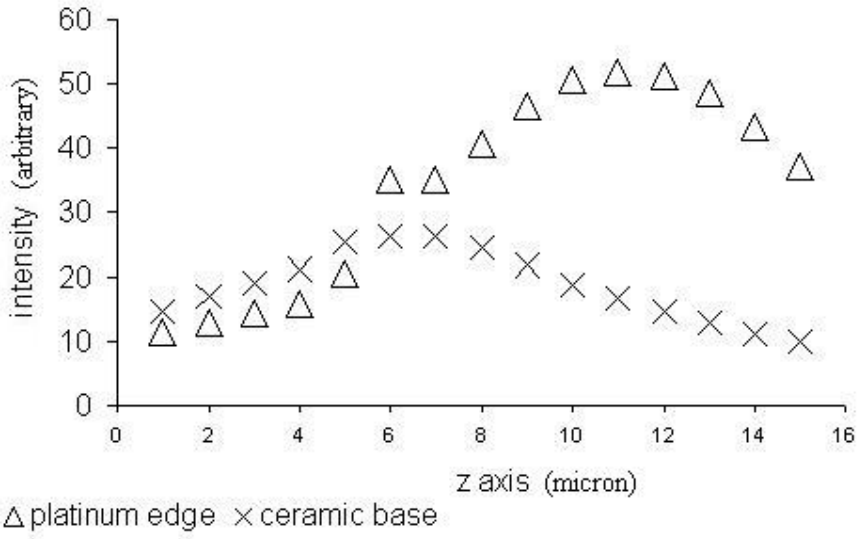

Figure 3.15 Ink thickness and roughness measurements for platinum ceramic electrodes based on edge detected images

The intensity measurement for ceramic and platinum inks is shown in Figure 3.15. Intensity measurements were applied to the ceramic substrate and platinum ink separately. Clear peaks in the ceramic and platinum surfaces were visible with smooth bell curves for intensity drop off. The difference in ceramic and platinum peak is about 6 µm; the roughness of the platinum, measured as the peak width at half height is as high as 9 µm; roughness of about 5 µm for the ceramic. The platinum ink edge is slightly graded so the ink thickness is likely to be over estimated. So in a separate experiment the roughness was measured on the platinum alone. The ink roughness was again measured as 9 µm. Beyond the simpler measurement of ink roughness and thickness by the method described, there is also the possibility to reconstruct the surface with clear surface variation data.

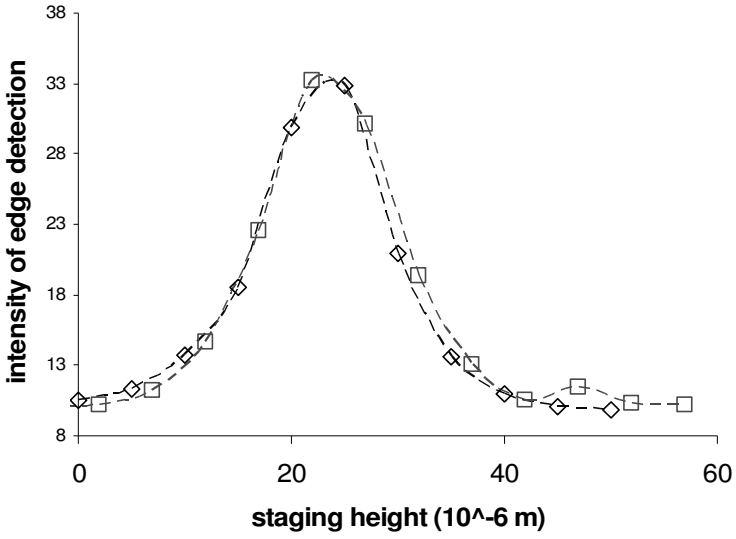

Figure 3.16 Roughness of polymer X/carbon powder formulation printed onto PET for two independent samples

Various carbon formulations were printed and checked for roughness. Polymer X/carbon powder, as shown in Figure 3.16, gave a bell shaped peak for edge detected intensity with peak width at half full height of approximately 15 µm. The PMMA/rhodinised carbon ink, printed through a mesh with 118 µm spacings (145 thread counts per inch), with a larger powder size, gave a larger variation of surface height; an approximate bell shaped curve with peak width at half full height of 35 µm was found. To compare screen effect the PMMA/ carbon powder formulation was printed through both 325 and 145 meshes and had approximate 20 µm roughness in both cases. The Ercon gold ink (R 464 DPM 78) was printed through a 325 mesh and the surface roughness was found to be approximately 15 µm.

The number of tested inks was limited by the time needed (1-2 hrs) to acquire and process the images. The evidence collated suggests that the particle distribution sets a minimum limit on roughness and the mesh spacings need to be large enough to allow passage of the particles.

Using larger increases the roughness, as seen with the PMMA/ rhodinised carbon powder formulation, when the screen acts as a filter to larger particles. A selection of

commercial inks was tested for full range thickness by hand-eye comparison *in situ*, avoiding the long time needed for image acquisition. All inks tested including, DuPont carbons, BQ221, 7105, BQ242, R430, R471 and Acheson Electrodag 423 SS were similar with thickness range under 25 µm.

Hand painted inks did not have well defined measurable roughness due to the general sloping surfaces. The thickness was generally much greater than the printed inks and could be > 500 µm.

3.4.5 Comparison of Ercon and DuPont Gold Ink

Figure 3.17 shows the Ercon gold ink (R 464 DPM 78) surface from electrodes printed *in house*. The surface shows aggregates of gold 10 – 20 µm amongst a dispersion of smaller particles. It cannot be concluded from this example that the Ercon surface is typical of the ink, since the ink storage and printing process may also play a role in particle dispersion. Further examples of the printing with various screens, squeegees and substrates would be needed, at considerable expense to provide this certainty. By contrast the DuPont surface, Figure 3.18A, is highly uniform. According to private discussion with DuPont, BQ331 is filtered to remove larger gold particles. Whilst the subtle effects of particle powder affinity probably affect the dispersion, the differences in particle dispersion between inks are not necessarily to do with particle-polymer compatibility.

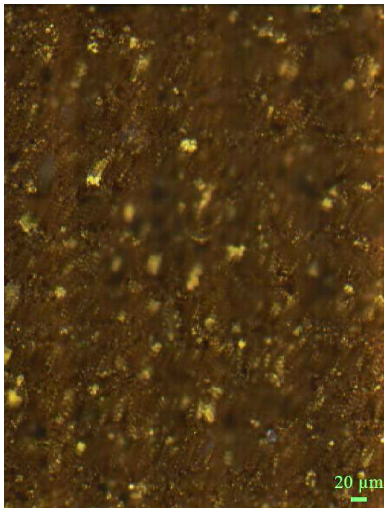

Figure 3.17 Extended surface image of screen-printed Ercon gold ink (R 464 DPM 78) with enhanced contrast

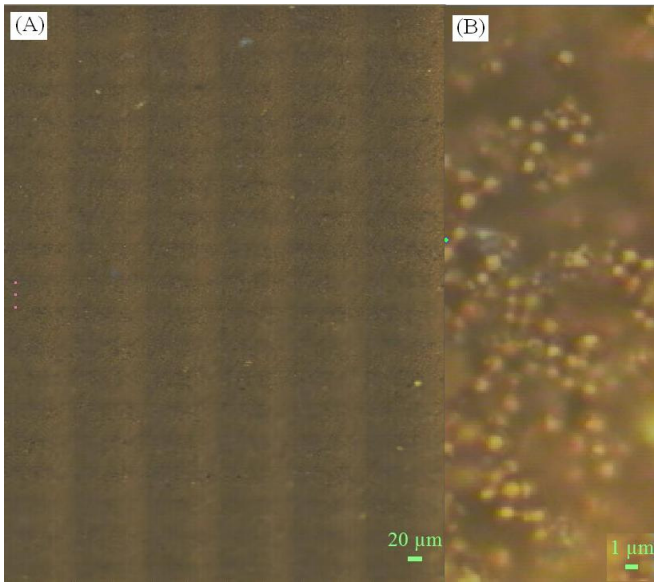

Figure 3.18 DuPont BQ331 gold ink surface (A) under 50xLWD lens. Scale chosen to be comparable with Figure 3.17 (B) Individual gold particles shown with 100x lens scale. Blurred areas due to focus

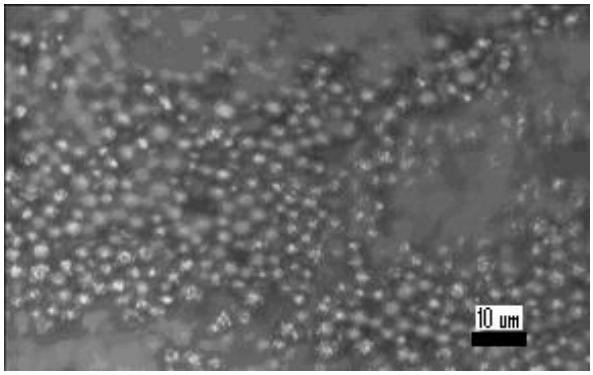

Figure 3.19 Image using 50 xLWD lens for, PSAN/gold powder hand painted formulation

As an aside, inks comprising PSAN, PMMA or polymer X mixed with gold particle formulations (the formulations for which are given in Section 2.4.) all showed well distributed particles similar to BQ331. This shows that such a distribution does not depend upon a surfactant additive.

3.4.6 Surface Reconstruction of BQ331 Surface

The BQ331 surface showed qualities making feasible a reconstruction of the surface as a three dimensional map. The gold-polymer boundaries, unlike carbon inks, gave sharp edges when in focus (Figure 3.18B), but, unlike the Ercon gold ink (R 464 DPM 78) did not show edges when much out of focus.

After processing (as explained in Section 3.3.4) thresholding was used to reduce the images to binary information. The choice of threshold limits is set manually and contributes a subjective element to the image process. The aim is to select the surface or focused pixels whilst eliminating all other visual information. Figure 3.20 shows a selection of the thresholded images. The main part of the roughness occurs over 10 slides indicating an approximate 10 µm roughness. Although edge detection shows clearly individual particles, thresholding loses this information.

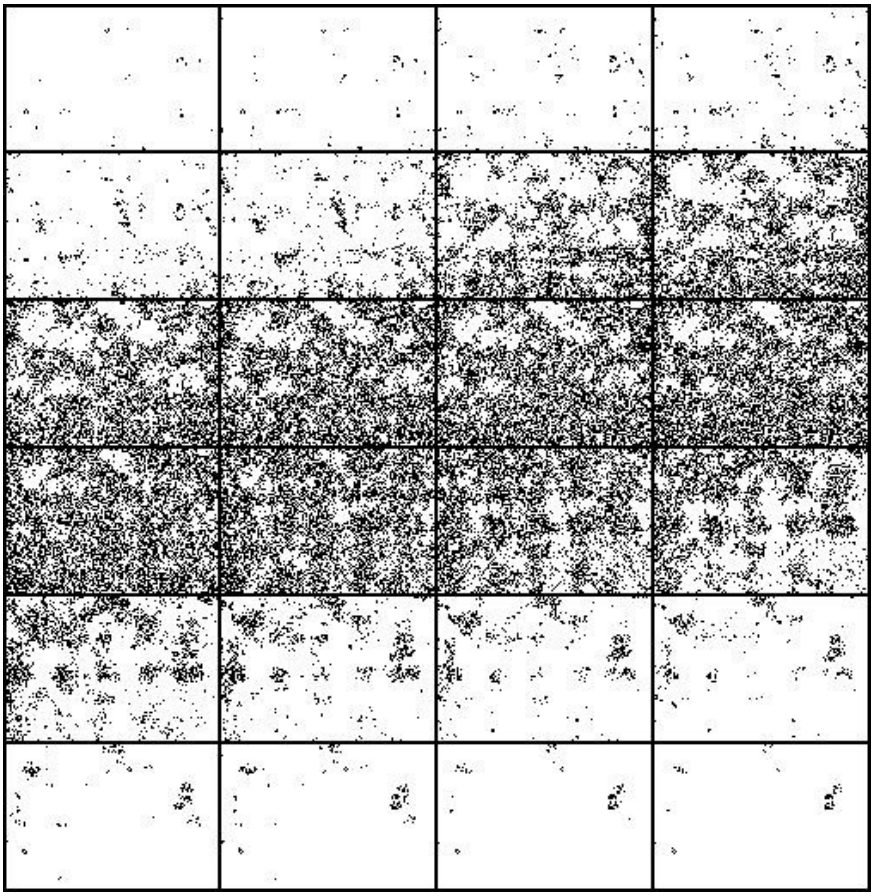

Figure 3.20 Micrographs of BQ331 surface, after edge detection and thresholding. 24 images shown each 1 µm apart

Each point on the thresholded images represents a surface point in the x-y plane, and the image number from 1 to 30 represents the height, z, of that surface point. Therefore it should be possible to reconstruct the surface. Noise results from the somewhat arbitrary nature of the thresholding process which reduces the greyscale image to binary. Some points in the x-y plane end up without any representative height, which then need to be interpolated. More detail is available in Section 3.3.4.

Figure 3.21 shows the surface map of BQ331, the z axis gives the µm height, the units of x-y planes relate to data point rather than µm. An artificial greyscale has been used for clarity. However low values are probably over represented in this image since the interpolation mechanism of missing points did not allow for the fact that neighbouring points may also be missing. This fact was realised sometime after the original work.

An approximate estimate of the distortion due to missing points would be needed (evaluated from the composite thresholded data). The interpolation scheme could be improved by only calculating from non missing (zero) neighbouring points.

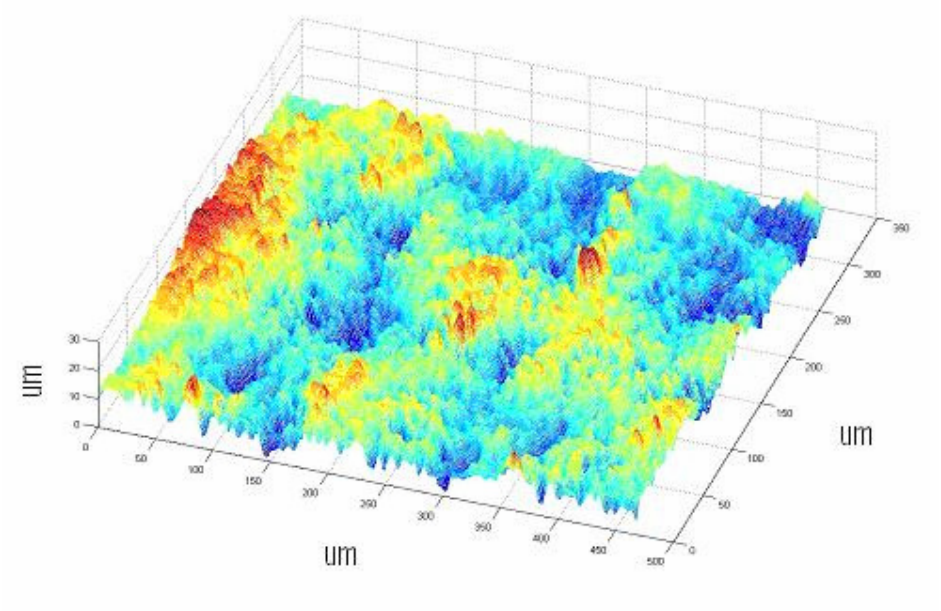

Figure 3.21 Surface map of BQ331 surface from reconstructed microscope images

3.4.7 Theoretical Model: Model Verification

Modelling was implemented in Matlab v7 and separately with Pascal. On the one hand Matlab, contained inbuilt functions such as the gamma function simplifying the script, on the other hand, Pascal executed the demanding convolution integral in a substantially shorter timeframe. The time for the program to run was found to be proportional to N^2 where N is the number of integration steps. Matlab contained the necessary functions to plot voltammograms, and calculate the peak potentials and currents. Using Pascal the voltammetric data were analysed in Microsoft Excel since it lacked the range of mathematical functions.

Since the model is a generalisation of two existing models (i) Nicholson's model (1965a) for heterogeneous kinetics at a planar electrode and (ii) reversible kinetics

with rough electrodes Strømme *et al* (1995) in the appropriate limits, it should reproduce the previously published results.

For the planar case, Variation of ΔEp with kinetic factor ψ. Matlab was used with potential step of integration (dE) of 1 mV. The values of ΔEp and ψ were calculated in the program. The result was plotted against Nicholson's own data and good agreement was found. The result is shown in Figure 3.22.

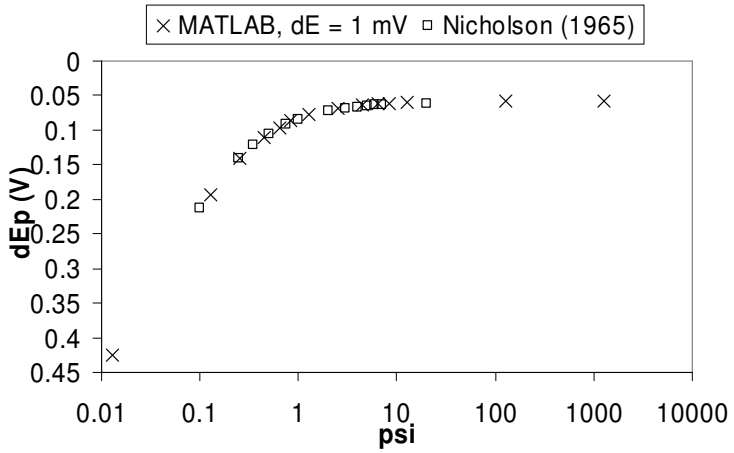

Figure 3.22 Heterogeneous kinetics on a planar electrode: comparison with data of Nicholson for the relationship of ΔE with ψ.

Under some circumstances the simpler Pascal program performed calculations more rapidly than Matlab. For a reversible voltammogram on a planar electrode the precise peak separation depends on both the scan range and the potential step, dE, used so that the peak to peak separation, ΔE_p can vary from 57-59 mV. Comparison of the peak to peak separation in the Pascal program with text book results (Bard and Faulkner, 2001) is shown in Table 3.4.

Table 3.4 Peak to peak separation as a function of switching potential for reversible planar electrode

$E_\lambda - E_p$ (mV)	Bard and Faulkner (2001) ΔEp (mV)[c]	Pascal program ΔEp (mV)
71.5	60.5	60.1[a]
121.5	59.2	58.6[a]
171.5	58.3	58.0[a]
271.5	57.8	57.6[b]

[a]dE = 0.05 mV, [b]dE = 0.2 mV, [c]estimated dE = 0.26 mV; E_λ is the switching potential

For the fractal case with reversible kinetics, the variation of voltammogram shape is shown in Figure 3.23:

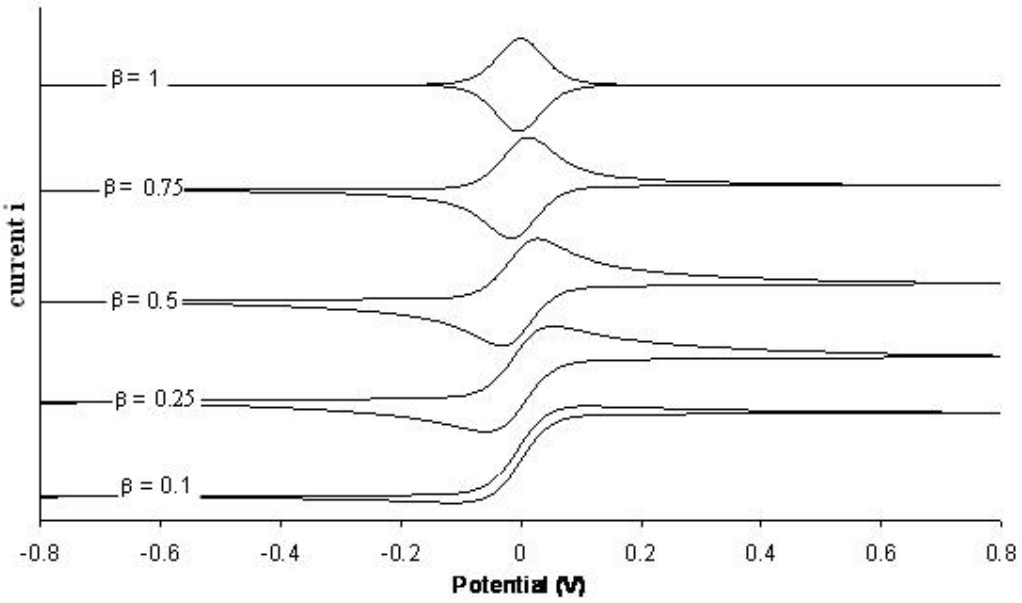

Figure 3.23 Voltammetric profile for different values of fractal parameter β with reversible kinetics

The peak separation and peak current function, ψ are shown against β in Figure 3.24 and Figure 3.25. These results match up well to the published results by Strømme *et al.* (1995).

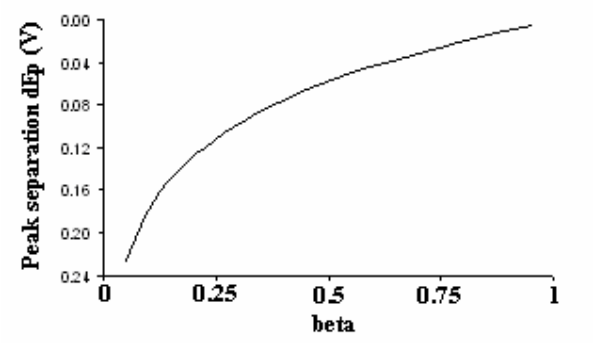

Figure 3.24 Peak separation for reversible kinetics as a function of fractal parameter β

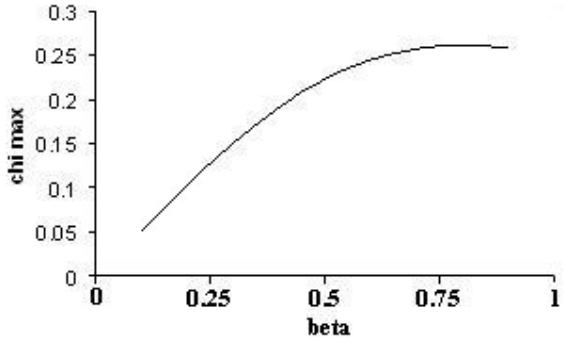

Figure 3.25 Peak current function χ (chi) for reversible kinetics as a function of fractal parameter β

3.4.8 Theoretical Model: Predictions

Next the model was applied to heterogeneous kinetics. Parameters were chosen for a variety of roughness and kinetic values such that an outline impression of the behaviour could be assessed. At this stage the surface correction term as used by Strømme *et al.* (1995) was not included so that the current scaling was relative. Figure 3.26 shows simulated voltammograms for a rough and kinetically slow surface between 1 and 100 mV/s. In comparison to a planar, the peak separation is narrower at slow scan rates but widens at a greater rate per increase in scan rate.

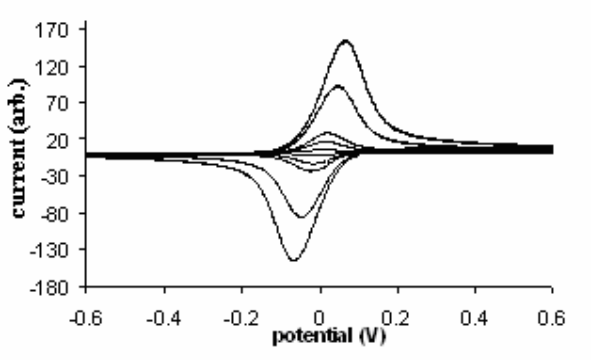

Figure 3.26 Voltammograms for various scan rates, 1 – 100 mV/s, with β = 0.875 and k_s = 0.01 cm/s

For a partially active surface the peak separation is wider but increases more slowly with scan rate or in the case of Figure 3.27 increases slowly as the kinetic rate constant is decreased.

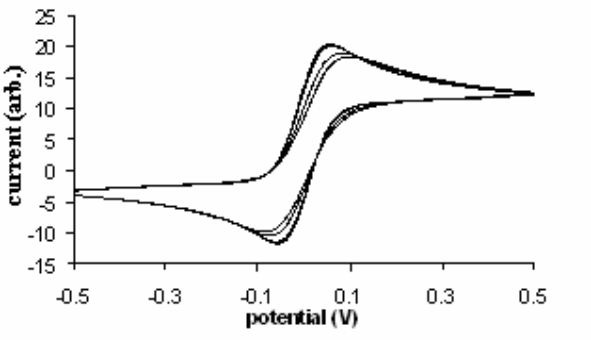

Figure 3.27 Voltammograms for various values of k_s: 0.35 to 3.5×10^{-3} cm/s, with β = 0.25 and scan rate, v = 50 mV/s

The Nicholson plot of Figure 3.22 was extended to include various fractal values in Figure 3.28. In the reversible limit, the peak separation, ΔEp varies accordingly with β as shown in Figure 3.24. In the irreversible limit, the relationship between logψ and ΔEp is similar in that it is linear with approximately the same slope and slightly differing offset. There is an approximate 232 mV change in ΔEp per decade change in log ψ.

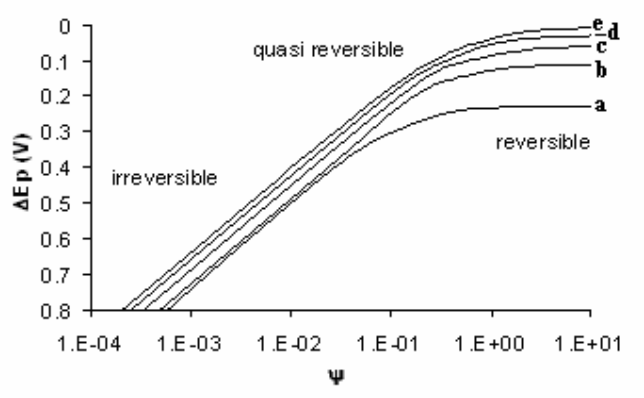

Figure 3.28 Nicholson plot for extended to various values of β: (a) 0.05 (b) 0.25, (c) 0.5, (d) 0.75 and (e) 0.95

ψ is proportional to the rate constant k_s and the scan rate with exponent – β; and so log ψ is proportional to β×logv or logk_s. Therefore ΔEp is proportional to β×logv or logk_s. Under standard planar conditions β = 0.5 and ΔEp is proportional to 0.5×232 mV = 116 mV; so there is 116 mV increase in ΔEp per decade increase in scan rate. Extension shows that the increase of ΔEp with scan rate varies from near zero when beta is close to 0 (in the limit there are no peaks since the voltammogram is sigmoidal), to approximately 232 mV when the electrode is highly rough or porous.

In the planar case it is well known that the current peak, i_p increases with the square root of the scan rate. This relation holds for the reversible limit and the irreversible limit. However, the peak current in the quasi reversible limits does not satisfy this relation, because the currents due to the forward and reverse peaks change from being coupled (superimposed) in the voltammetric peak shape to being uncoupled (independent of each other) as the scan rate increases. Therefore, it would be expected that the relation developed by Strømme *et al.* (1995) for the reversible relation where i_p is proportional to v^{β}, would hold also in the irreversible case, but not in the quasi reversible case. Figure 3.29 shows the peak current scan rate relation for a simulated electrode of fractal parameter 0.75 (rough). In the reversible limit (k_s = 0.1 cm/s) the exponent is equal to 0.75 (3 d. p.); in the irreversible limit the ($k_s = 1\times10^{-5}$ cm/s) the exponent is 0.74 (nearly 0.75). However the offset of these two limits of reversibility is pronounced and at intermediate values of k_s such as 1×10^{-3} cm/s the peak current

behaviour shifts between the two limits, with a resulting smaller measured exponent of 0.692. Figure 3.29 demonstrates the equivalent relationship already familiar in standard texts (Bard and Faulkner, 2001) for planar electrodes, which holds for fractal electrodes

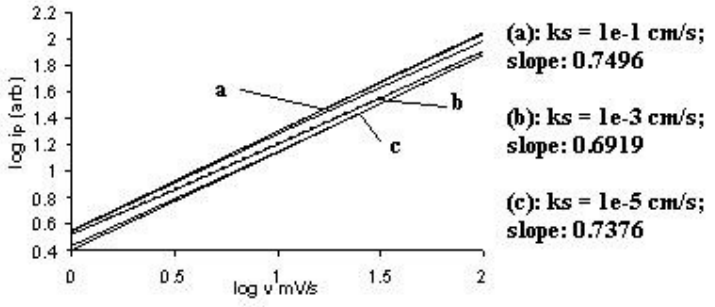

Figure 3.29 Plot of peak current with log scan rate for simulated voltammograms with β = 0.75 and various rate constants with values as indicated

Thus, as has been noted by Strømme *et al.* (1995), the fractal geometry of an electrode can be, in principle, analysed by two methods (i) the peak separation behaviour and (ii) the peak current behaviour as they change with scan rate and it should be possible to elucidate the fractal geometry of the electrode surface.

Pajkossy and Nyikos (1989b), in their third paper on diffusion to fractal surfaces, mentioned explicitly that their method could be applied to voltammetry with heterogeneous kinetics. The reasons, in hindsight, for not doing so arise in the practical difficulties involved with finding a surface with reasonably consistent kinetics and suitably rough surface, particularly if the engineered electrode is to have a precise fractal structure as opposed to being rough only, and so constitute a difficult theory to verify experimentally. Furthermore, problems associated with capacitance and potential corrections much reduce the effective range of scan rates that can be probed.

3.4.9 Application to Gold Screen-Printed Electrodes: Theory and Surface Roughness comparison

Application to DuPont gold working electrodes (BQ331), was intended to explain: (i) the relatively wide peak separation with little apparent change with scan rate (ii) the dip in peak separation as shown in Figure 3.13B and (iii) the peak current and peak separation behaviour. These three aims place progressively exacting demands.

If the electrodes are assumed to be reversible then, by varying the fractal parameter, the peak separation could be altered. According to Figure 3.24, the about 100 mV peak separation could easily be accounted for with an altered fractal parameter with approximate value $\beta = 0.3$. This suggests a low dimension, partially active surface ($D_f < 2$). If the microscope image of BQ331 is referred to in Figure 3.18 it is possible to see a general gold surface with some instances of brighter spots spaced 100 – 500 μm apart. The brightness of the gold indicates the degree of polymer coverage because polymer layers dull the surface. Secondly the polymer coverage has a direct relation to the apparent kinetic rate of electrochemically active sites (Buess-Herman, 1994), for example with carbon screen-printed electrodes Cui *et al.* (2001), Osbourne *et al.* (1996), and Wei *et al.* (2007). Thus, especially bright spots could have reversible kinetics, and the relative spacing causes a micro array effect. However these sites acting alone would constitute a very small active area. The most effective way to test this is to compare, the peak current behaviour, also shown in Figure 3.13A. However, the exponent on the peak current is slightly in excess of a planar electrode and in no way indicating a partially active surface.

If another approach is taken, and a slightly partially active surface with good reversibility is said to co exist with a rough but relatively slow kinetic surface, then, noting that the low dimensional surface has a low peak current exponent and the high dimensional surface has high peak current exponent, a transition in behaviour could be expected due to the increase in scan rate. The wide peak low dimensional surface provides more current at lower scan rates; then as the scan rate increases the current contribution from the rougher bulk surface increases more quickly predominating at

higher scan rates. This case cannot be modelled very well because the diffusion gradients surrounding the surfaces are not well separated and diffusional overlap is bound to occur. It was found that combining low and high dimension surfaces could effectively moderate the peak current exponent. The model could also explain the 'dip' in peak separation as the current changed predominance of one surface to another. A suitable dip could be obtained with low dimension, $\beta = 0.3$, and high dimension, $\beta = 0.8$ shown in Figure 3.30. A similar dip could be maintained if the two β converged toward 0.5. With β further separated the current increase showed as more pronunciation in the change in slope as the scan rate increased – not seen in the experimental data. As the β values converged, the peak current data more closely fitted the experimental data but the necessary kinetic values to attribute to the low and high dimensional surfaces also converge if the potential fit data was also to be maintained. If the kinetic values are not sufficiently different, then the two surfaces could not be recognised as electrochemically distinguished. It was not possible to explain the 'hump' seen in the peak current data by combining surfaces of differing dimensions, shown in Figure 3.31.

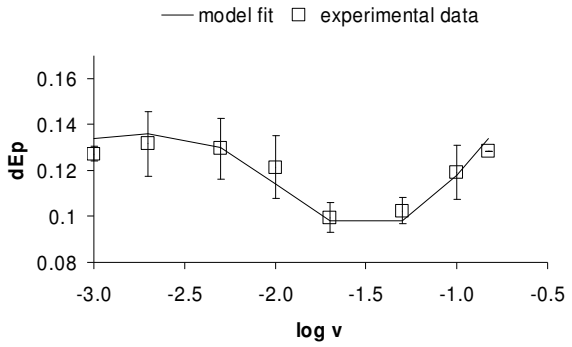

Figure 3.30 Peak separation data of Figure 3.13A with best model fit

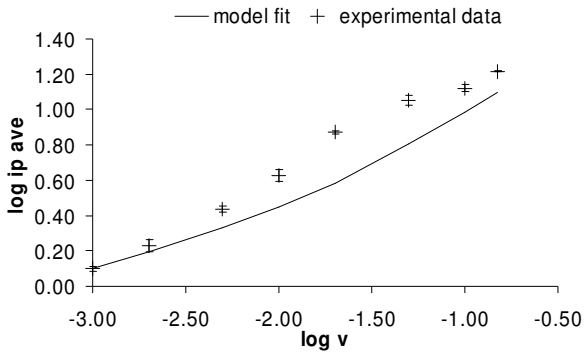

Figure 3.31 Peak current based on data of Figure 3.13B with best model fit

In hindsight (after private communication with T. Pajkossy), the kinetic behaviour of gold itself had been neglected since there is no guarantee that before geometrical considerations, the kinetic behaviour is standard. A straightforward polishing metal surface such as gold or platinum, according to basic electrochemical theory should show reversible kinetics manifested as a peak to peak separation of about 59 mV independent of scan rate. However in practice this is very hard to realise with polishing, acidic chemical treatment and electrochemical cycling. Flame annealing is recognised as a good way to reduce atomic scale imperfections on the electrode surface. A gold disk electrode was tested after polishing and electrochemical pretreatment in the same electrolyte and the same range of scan rates. A similar range of peak separation was seen, which did not conform to the simple models of textbook electrochemistry. Polished gold disk electrodes, that have not been abused, do not have the micro scale roughness; thus the behaviour cannot be attributed to geometry but rather to the underlying activation and passivation mechanisms. The available gold disk electrodes cannot be flame annealed (>400 °C) as they are house in poly(chloro triflouroethylene) casing. The quality of gold on the screen-printed electrodes cannot be tackled without testing directly the gold powder during the production phase.

The production of gold powder is reviewed by Kodas *et al.* (2004). Two methods are available: either precipitation of gold salt from solution and reduction of the precipitate or by spray pyrolysis. The powder needs to be washed to remove the reducing agent and there is the possibility that the reducing agent residual remains a

contaminant. Spray pyrolysis involves nebulisation of an aqueous gold salt (gold chloride for example) which is heated quickly to between 500 – 1000 °C to decompose the salt (Glicksman, 1997). The fine spray helps to form spherical powders. The particular advantage lies in the fact that powders produced this way are 'densified' which means the aggregates are well packed. This is probably an electrochemical advantage if a more uniform surface can be assumed.

Further to this it is known that the DuPont gold ink used a surface active agent in the formulation to aid metal polymer compatibility. The identity of the reagent has not been disclosed. According to similar examples, the powder is covered in monolayer of surfactant which maybe selected from a variety of reagents such as oleic acid, metal stearate or Triton X (Gilleo, 1996, Chan, 1998, Chan *et al.* 1999 and Osman *et al.* 2004). Therefore, this surfactant is expected to cover the gold active surface during voltammetry. Although most organic molecules lack facile electron transfer mechanisms, some are known to promote transfer (Buess-Herman, 1994). It is probable that any such surface active agent affects the voltammetric behaviour and even the gold alone is kinetically complex without careful treatment.

3.5 Discussion

3.5.1 Electrode Design

The issue of finding the heterogeneous rate constant for screen-printed electrodes is complicated by the resistance associated with the electrode track since generally only solution resistance is mentioned (Nicholson, 1965a). However, it is clear from the way a potentiostat-electrode system works that solution and track resistance are equivalent. This was clearly demonstrated in Figure 3.8. Since the current is generated by setting a potential between the working and reference (in voltammetry), and because the current through the referene electrode is negligible the only potential drop through the working electrode track is of concern. There is also a drop through the counter electrode track, but the potential of the counter electrode is usually ignored (except if it becomes exteme, generating reaction products poisoning the solution).

Particularly high resistances (> 10 kΩ for current 10 µA), will affect normal amperometric or voltammetric experiments. Where a potential has been set at x by the potentiostat, the potential of the working electrode varies significantly with the current passing through; and results are also susceptible to sheet resistance distributions as are common in screen-printing (Gilleo, 1996). If the resistance is low (< 1 kΩ for a carbon track) the sheet distribution is is a negligible problem. The issue could be circumvented by the use of gold ink (or silver, if contamination is not an issue) but such an approach increases material costs greatly. As a result of this the immunosensor design was changed (as shown in Figure 3.4 on page 114) from design A to design C. Resistance could also be further decreased by adding several carbon layers.

Also, the size of the electrode can be considered. Screen-printed sensors provide a self-contained system; the tracks provide a link from the electrochemical cell to the potentiostat. If the sensor is miniaturised handling becomes an issue, if the sensor is increased in size the costs become greater. The tracks also provide protection to the potentiostat connection from electrolyte contamination. If conducting steel pins are used in the connector, these may act as electrodes when submerged. Also, the pins may corrode in the electrolyte (such as HCl). A design 5 – 10 cm long has remained popular in commercial applications such as the blood glucose strip (Newman and Turner, 2005). The strips are long enough to handle without touching the active sensor area whilst pushing the contact end into the connector. Thus the tracks need to carry current over a 5 – 10 cm length which can offer considerable resistance if carbon is used.

Another factor to consider is ink thickness, which is typically between 10 – 30 µm. Although increasing the ink thickness will decrease resistance, alternate print settings with larger particle and mesh sizes are needed to make this practical, and brittleness will increase with thickness making the sensors more fragile. Track width can decrease the resistance. However, either a two or three track system needs to be fitted onto a single, low-cost strip; the spacing between needs to be large enough (for example > 500 µm) to keep incidence of short-circuits low. The intrinsic conductivity

of the ink can be improved by increasing the particulate loading, to a point; however beyond that point the printing ink will lack the viscosity and possibly adhesion characteristics necessary to form complete prints. The choice of polymer can also affect the intrinsic viscosity, via the polymer-powder affinity affecting the inter-particulate contact, or due to the densification on curing. Some printed inks are known to have porous and so less dense surface layers (for example, Forrow and Bayliff, 2005).

The best cost effective measure (for the immuno and metal ion sensors, at least) is to use carbon with reasonable dimensions (such as > 1 mm width tracks, ~ 20 µm thick and less than 10 cm long) and to check the printed ink to confirm resistance is low enough. Check the potential drop (using $\Delta V_R = iR$) during experiments to estimate whether this has a bearing on the results. If high resistance must be tolerated then use electrodes with the same working electrode resistance as much as possible. However, professional screen-printing is limited to about 5 % accuracy (Gilleo, 1996).

3.5.2 Electrode Thickness and Roughness

In estimating the ink thickness two problems were encountered: (i) sloping substrate: the electrode substrate (PET) secured to a glass slide surface, still manifested a slight slope contributing uncertainty to comparisons; a time consuming procedure of estimating the substrate slope in the vicinity and making a suitable correction could be used. (ii) The variation in surface height was as great, or in some cases equivalent to the thickness of the ink; despite the large roughness, commercial inks showed no gaps in surface coverage (printed homemade inks showed partial coverages).

Various carbon and gold inks were produced *in house*. Selections of polymers were tested with a variety of powders. The selection of materials is given in Section 2.4. Most of the development work was conducted with the carbon formulations due to the low cost. The gold powder was expensive for two reasons: (i) the gold is expensive and (ii) high density requires greater weight per surface coverage. For the quantities produced conventional screen-printing was not an option. For example, Gwent

Electronic Materials (C2041206D2) and Ercon, Inc. (R 464 DPM 78), supply in minimum 25 g portions of gold ink (gold + organic vehicle), because preparation and printing is not feasible for smaller amounts. The finalised carbon formulations were printed by hand through a standard screen-printing design.

Microscopy revealed the particulate composition of the surface. Initially differences in carbon track resistances were tested for difference in ink thickness; but two problems were encountered: (i) sloping substrate and (ii) the variation in surface height.

The change in staging height showed very clearly the change in focus on the inks surface demonstrating clearly the capability to measure quantitatively the height variation.

Therefore it is possible to get a measure of ink thickness but the process takes in excess of 1 hr. With the variation in thickness being so large it may be difficult to relate the extrinsic resistance to intrinsic resistivity.

With the Ercon gold ink (R 464 DPM 78) there were visible aggregated gold particles massed in regions of approximately 10 – 20 µm. The resulting sharp edges were clearly visible even when out of focus. Some of the edges for carbon-polymer boundaries were not easily identifiable since the carbon is not as reflective as the noble metals and the polymer is generally transparent or partially transparent.

3.5.3 Surface Roughness and Cyclic Voltammetry

The DuPont sensors, with working electrode ink BQ331, show behaviour (for example, Figure 3.13) which is difficult to explain according to the theory of Nicholson. An attempt was made to explain this behaviour by considering the rough and/or the possible partial activity of the surface leading to a mixture of convergent and divergent diffusion. With the more generalised model a greater flexibility for reproducing experimental results was possible (Figure 3.31). However, several points make this explanation doubtful: the surface roughness of the ink lies within an

approximate 20 µm range, needing probably more than 500 mV/s scan rates (as will be seen in Section 3.5.4) before the roughness is relevant. Secondly, the behaviour of a standard gold surface alone is often non standard when using a Faradaic agent like potassium ferrocyanide unless extensive attention is paid to the gold surface. Among the possibilities of polishing, acidic treatment and electrochemical pretreatment, flame annealing is one of the few ways to generate ideal behaviour (personal communication Professor T. Pajkossy, Budapest University of Technology and Economics, Hungary). Also it is known that BQ331 includes an (undisclosed) surface active agent on the gold. Thus, it is very difficult to draw conclusions about the gold ink behaviour.

In general the Nicholson method has been successfully applied to inks (for example, Wang *et al.,* 1998) and several inks here including DuPont platinum ceramic formulation 9141, *in house* carbon formulations PSAN/carbon flake and polymer X/ carbon flake. The measured roughness values of screen-printed inks appear to be similar in general 10-20 µm. So roughness in general is expected to affect cyclic voltammograms only for higher scan rates.

Despite this set back, the theoretical model that has been developed could have applications elsewhere. Some authors have used the fractal Randles-Sevcik Equation of Strømme *et al.* (1995) to predict the fractal coefficient without clearly showing that the electron transfer is quick (for example, Lee and Pyun, 2003, Vasconcellos *et al.,* 2006) relying on the coincidence of AFM derived fractality with electrochemical. The model here, generalising slow and fast electron kinetics, predicts that with quasi-reversible kinetics an underestimate of the fractal parameter would be a danger as the forward and reverse peaks decouple (Figure 3.29). However, the technique should still be valid for the fractal parameter with fully irreversible electron transfer although the Randles-Sevcik equation would need to be modified to predict the correct current magnitude. The difficulty is that resistive widening of the peak separation will obscure electron transfer effects. These are basically the same issues as those occurring on planar electrodes $i_p < v^{0.5}$ in the quasi reversible limit (Bard and

Faulkner, 2001) and resistive distortion prevents measurement of k_s (Nicholson, 1965a).

The main advantage of using this heterogenous kinetic rough surface model derived here would be the robust supporting evidence of both peak current and peak separation behaviour that could be obtained if the physical conditions are sufficiently controlled. Prediction of both parameters would give good confidence for the electrochemically derived fractal parameter and for the physical basis of the model.

There remain difficulties in providing a quantitative test for the model since screen-printed resins can exhibit both roughened and partially active surface characteristics acting simultaneously, where the resin/particle mix causes blocking and the printing deposition causes roughening. One of two approaches is needed, either to find a commercial ink which happens to have small particle size in comparison to roughness, or to produce such an ink *in house*. For example carbon black powders for use in screen-printing inks can be obtain with size distributions much less than 100 nm (Forrow and Bayliff, 2005). With suitable dispersion in an ink the surface would be uniform on the microscale, and assuming the the printing process still conveys 10 – 20 µm roughness the opportunity to measure the fractility, independent of surface blocking characteristics, would be possible.

3.5.4 Effect of Diffusion Length

Due to the number of electrochemical techniques designed for the use of fractal investigation and apparent incomplete understanding of the process, the validity of some published work has been questioned (Eftekhari, 2006), particularly when investigating nano structures. Since, as noted already, the values derived by capacitive measurements have limited applicability when surfaces are inhomogeneous. The diffusion layer has a characteristic thickness but this thickness is not discrete.

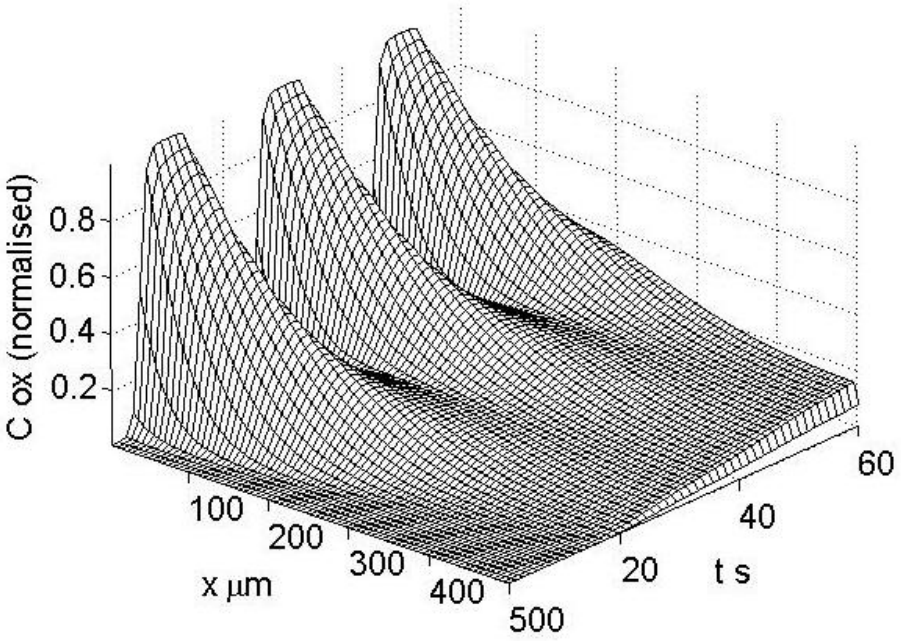

Figure 3.32 Explicit simulation of 1 dimensional concentration profile during cyclic voltammetry with Nernst boundary condition.

Figure 3.32 shows the concentration profile, for oxidised species C ox, of a simple redox couple at a planar electrode surface (at x = 0). The main region for each cycle lies within 100 µm of the electrode surface. The concentration is affected out beyond 500 µm. Therefore, the diffusion length is not easily described, and the process is most likely influenced by the electrode geometry over an order of magnitude.

Eftekhari, A. *et al.* (2005) noted that inference of electrode fractility is only relevant on a scale equivalent to the diffusion layer. They gave a relation for the diffusion layer thickness, δ for scan rate, v, and diffusion constant, D, as shown in Equation 56.

$$\delta = 0.36\sqrt{D/v} \qquad \textbf{56}$$

Table 3.5 Diffusion layer thickness as a function of scan rate for a standard aqueous one electron redox reaction, using Equation 56 (Eftekhari *et al.*, 2005)

Scan rate[a]	Diffusion layer thickness[b] (μm)
1	360
2	254
5	160
10	114
20	80
50	51
100	36
200	25
500	16
1 (V/s)	11
10 (V/s)	3.6

[a]units of mV/s unless otherwise stated; [b]based on single reversible electron transfer and diffusion coefficient of 1×10^{-5} cm/s

Table 3.5 shows explicitly the length of the diffusion layer as a function of scan rate in aqueous solutions. The influence of concentration diffusion from the electrode surface appears significantly larger than the 51 μm (for scan rate of 50 mV/s) predicted in Table 3.5. However, when considering the voltammetric peak only the initial change in concentration is relevant. The diffusion after this peak affects only the tail currents. Figure 3.33 shows a comparison of the current with concentration profile both at the surface and 50 μm.

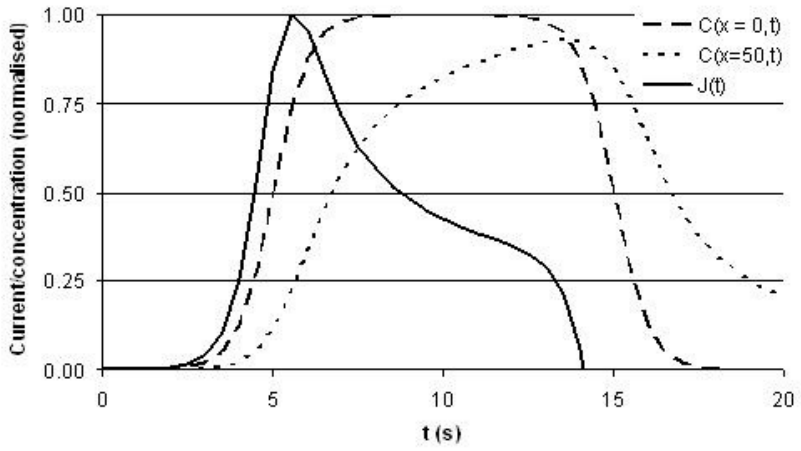

Figure 3.33 Simulation of Figure 3.32 showing current, surface concentration and concentration at 50 μm from the electrode surface for 1 scan

The current peak occurs shortly before the concentration at the surface reaches maximum. The concentration at 50 μm reaches 50 % of maximum shortly after the

current peak. Therefore, the bulk of the concentration profile in Figure 3.32 is occurring after the current peak maximum affecting only the tail; and the 50 μm would appear a reasonable measure of the diffusion at the peak maximum being near 50 % of maximum. (note ΔEp was about 60 mV indicating adequate spatial and temporal step size in the simulation).

The obvious way to probe smaller details is to use faster scan rates. However, using scan rates in excess of 100 mV/s causes practical difficulties when using non-micro scale electrodes: (i) the background capacitance current increases faster than the peak current (ii) larger currents causes larger iR drop losses in both the electrolyte (and electrode tracks for screen-printed substrates). Another way to reduce the diffusion length was reported by Eftekhari *et al.* (2006) with the use of viscous electrolytes and lower temperatures. In practice, with the use of glycerol-water mixtures combined with a temperature of about 4 °C, the diffusion layer thickness was reduced to the low nanometre range.

3.5.5 Future Direction

The Nicholson method was investigated and an extension was made to the technique to account for rough surfaces. However, little progress was made interpreting the voltammograms obtained from practical printed strips. A number of factors confound analysis such as the gold itself, roughness, and multiplicity of reversible states. There is no need to consider the electrode roughness in typical experiments in aqueous solutions unless high scan rates (> 1 V/s) or short timescales for general voltammetric procedures are required since the electrodes are, in effect planar. Where high scan rates are used the effects of non Faradaic currents and ink impedance is likely to obscure measurements of peak separations used by the Nicholson method. Measurement of peak current is more tolerant of the impedance and thus may find a use at high scan rates where roughness becomes an issue. The exponential scaling law should be applicable to the Randles-Sevkic equation if the electrode surface is either entirely reversible or irreversible but not for the quasi-reversible case. The modified Randles-Sevkic does not estimate the heterogeneous rate constant, however. The

design of an arsenic or mercury sensor is unlikely to need any modifications due to roughness so continuation of this theory is of a low priority. However the work has some intrinsic theoretical value, as specially prepared screen-printed surfaces, where particle aggregation and ink roughness generate fractal like surfaces could be used to test the more complex model of heterogeneous kinetics. The model here developed describes behaviour more completely than is presently found in the literature taking into account, heterogeneous kinetics and diffusion for general rough surface subjected to cyclic voltammetry in a single expression. Since the modified method closely parallels the existing methods of Nicholson, the requirement for additional description is minimised. As with most electrochemical equations the benefits of the equations are limited by confounding factors such as electrode preparation and impedance – more so for the need to prepare the fractal surface at the correct scale without causing complexities associated with surface defects.

To pursue the theoretical study there are several ways forward. One method that has been explored is to print an ink on top of a conducting substrate (such as gold sputtered electrodes) which reduces the electrode resistance to less than an ohm. However, care is needed to avoid the gold contacting the electrolyte directly. Also this method still needs to account for solution resistance for higher scan rates.

Besides increasing the scan rate, the diffusion constant can also be reduced to lower the diffusion length (Equation 56). According to the Einstein-Stokes equation (not shown) the diffusion constant is inversely proportional to the viscosity of the solvent. For probing smaller roughness scales Eftekhari *et al.,* (2006) used glycerol-water mixtures. It was shown that nanoscale roughness effects could be studied with a Faradaic agent during cyclic voltammetry. The viscosity relation for glycerol-water mixtures is shown in Table 3.6.

Table 3.6 Viscosity of Water-glycerol mixtures at 25 °C Shankar and Kumar (1994)

Glycerol fraction	Viscosity (mPaS)
0	0.90
0.1	1.1
0.2	1.5
0.3	2.0
0.4	2.8
0.5	4.3
0.6	7.3
0.7	15
0.8	37
0.9	120
0.95	280
1.0	710

The accessible diffusion lengths are given in Table 4.2. This technique would be highly effective for studying the screen-printed surfaces provided that the polymers are not dissolved in the glycerol. This fact was tested with DuPont gold sensors. After 10 minute exposure to glycerol, the ink was found to be intact even with abrasive treatment.

Table 3.7 Diffusion lengths calculated[d] from diffusion coefficients reported by Eftekhari *et al.* (2006)

Scan rate, v (V/s)	Diffusion length, δ (m)[b]		
	A[c]	B	C
0.001	1.2e-5	1.2e-4	3.7e-4
0.005	5.2e-6	5.2e-5	1.7e-4
0.01	3.7e-6	3.7e-5	1.2e-4
0.05	1.7e-6	1.7e-5	5.2e-5
0.1	1.2e-6	1.2e-5	3.7e-5
0.5	5.2e-7	5.2e-6	1.7e-5
1	3.7e-7	3.7e-6	1.2e-5

[b]two significant figures, [c]at 20 °C otherwise at 25 °C, [d]using $\delta = \sigma\sqrt{\frac{D}{v}}$, (A) 100-0 Glycerol-water with D = 1e-12 (m^2/s), (B) 50-50 Glycerol-water with D = 1e-10 (m^2/s), and (C) 0-100 Glycerol-water with D = 1e-9 (m^2/s)

However, controlling the viscosity is hampered by temperature and salt concentration. Shankar and Kumar (1994) determined the viscosity of water-glycerol mixtures at temperatures from 10 to 50 °C. The variation with temperature is large for glycerol alone: at 20, 25 and 30 °C with values of 1.160, 0.714 and 0.475 PaS respectively, where as water alone varies 1.01e-3, 0.897e-3 and 0.803e-3 PaS. The viscosity of

water changes very slightly upon addition of NaCl: at 0.1 mol/kg the viscosity is 0.89 mPaS and near the solubility limit at 4.2 mol/kg the viscosity is 1.39 mPaS (Zhang and Han, 1996). In glycerol the viscosity changes by about 5 % with 0.1 M or 25 % with 0.5 M NaCl addition (Hammadi, 2004).

Probably the largest issue associated with using screen-printed inks to test the theory is the requirement to separate the effects of particle size and ink roughness which have opposing effects in terms of surface dimension.

3.6 Conclusions

Some of the problems encountered by previous researchers when applying the Nicholson Method can be explained by the electrode resistance. To a degree the problem can be corrected if the resistance is measured allowing the electron transfer rate constant to be obtained. This high resistance is an issue for electrode design since sheets of electrodes often exhibit variable resistance distributions, affecting measured potentials during analytical experiments when producing calibration curves.

However, the behaviour of the DuPont gold sensors is not affected unduly by resistance and displayed 'anomalous' behaviour. An attempt to explain this behaviour by the consideration of surface roughness was unsuccessful due to complication of gold surface behaviour alone, and the unknown effect of a surface active agent included in BQ331. For BQ331, the kinetic reversibility is very good for a screen-printed ink presumably allowing for good peak resolution.

The Randles-Sevcik equation had already been extended to rough reversible surfaces in the literature (Strømme *et al.*, 1995). Here with the same considerations the method of Nicholson has been extended to rough surfaces for the first time. However, it has not been possible to experimentally verify the predictions, yet.

The most promising way forward, in terms of testing the theory, appears to be the use of glycerol/water mixtures to lower the diffusion constant thereby reducing the diffusion profile to a range equivalent to the screen-printed roughness. The viscous electrolyte should make this possible at reasonable scan rates where the current is still small enough to avoid high resistive effects. Secondly it maybe necessary to produce an ink where the particle size is much smaller than the rough extent to allow the effect of rough on diffusion to be probed independently of the heterogeneous effect of particle-polymer boundaries.

Chapter 4 Detection of Arsenic and Mercury using DuPont Screen-printed Strips

4.1 Introduction

This is the first of the main experimental chapters (Chapters 4 to 6) which form the main theme for this thesis. The work picks up from previous research within Cranfield University: the thesis of Cooper (2004) and patent of Bolbot *et al.,* (2007), with a passing reference to the thesis of Cauchi (2005) and later to the thesis of Noh (2005). This chapter is loosely split into three: (i) the determination of As(III) and Hg(II) with the method used by Cooper (2004), Cauchi (2005) and Bolbot *et al.,* (2007) with DuPont gold electrodes; (ii) the study of presumed sensor interference in pure electrolytes with extended temporal behaviour; and (iii) determination of As(III) via the alternate method of Noh (2005). Whilst persistence with the first method may seem foolhardy in light of the problems, prevailing literature evidently supports this approach (Sections 1.9.2 and 1.9.7).

4.1.1 Background

DuPont Sensors

Given the relatively long history surrounding screen-printed electrochemical sensors, it is surprising that low temperature gold electrodes have been investigated only in the last few years (Section 1.10). At least in part, this is due to the high cost and density of gold materials and associated development costs. The Cranfield collaboration with the gold ink from DuPont Microcircuit Materials (Bristol, UK) concerning gold ink extends back to 2001-2002. According to discussion with representatives from DuPont, the product, now called BQ331, was developed in the USA for a client, specifically for biosensor applications in the years preceding 2001. Several gold formulations were compared for the client, and the optimal ink was to become BQ331.

As discussed in Section 1.10. The market for biosensors is estimated at $7 billion most of which (87 %) is taken up by Glucose measurement (Turner *et al.,* 2006). The majority of the glucose market is dominated by screen-printed strips featuring a three track design much like the metal ion sensor in this project. One significant difference is the inclusion of an enzyme, principally glucose oxidase limiting the curing and handling conditions. However biosensor fabrication is a small part of a wider industry, in context of screen-printed conductors in microelectronics, having applications such as automotive industry, photovoltaics, surface mount electronics, and touch membrane switches for keyboards and calculators, (DEK, 2007). The principle of the technology comes under the umbrella of plastic and composite coatings. Therefore, the technologies and availability of information in patents, textbooks and journal papers reflects a balance of commercial interests and cross-fertilisation of ideas between disciplines.

The 'BQ' in BQ331 and other DuPont screen-printed inks, stands for Biomedical Quality. Evidently, the gold ink was designed for medical type applications, although, at the outset, the degree of engineering in the formulation was unknown (to the author). Whether there are substantial differences in an ink designed for biochemical (including immobilised whole cell sensors) and those for inorganic chemistry only such as metal ions, is unknown because the ink formulations are proprietary. It is possible that the branding of the ink reflects the largest market and gives confidence to customers in that market that the formulation suits their needs, not necessarily indicating specific design parameters. In general, an ink for biomedical applications works in an aqueous controlled pH, dissolved ion range and temperature (particularly when enzymes are used), whereas inorganic based sensors may work at extreme pH, ion content and temperature. However, even when inorganic methods are used, mild conditions are preferable due to safety to user, disposal of consumables and simplicity of procedure.

DuPont Ceramic Gold Electrodes

DuPont introduced a new selection of 'Lead Free' (LF) ceramic inks as a range of environmentally friendly alternatives to traditional ceramic inks. Gold LF141 is also cadmium and nickel oxide free according to the literature (www2.dupont.com/MCM/en_US/PDF/datasheets/, accessed 2006). As of the time of writing (2008) LF141 gold conductor is no longer advertised on the DuPont Microcircuit materials website, but similar gold conductors LF143 and LF144 are.

With the ceramic gold ink LF141, the fact that it was advertised as Pb (mp 327 °C), Cd (mp 321 °C) and NiO (mp 600 °C) free suggests that these components are usually present in ceramic based inks. Even so, other metals and/or metal oxides are probably present. They probably aid adhesion; having melting temperatures below gold (mp 1064 °C) allowing firing temperatures lower than 1000 °C. Also, this view is backed up by Lane *et al.,* (2000) who found copper oxide, cadmium oxide and bismuth oxide in gold conductor formulations.

With the removal of these components, representatives at DuPont contacted Cranfield as to the possibility of using this type of ink for metal ion sensing applications. The electrodes were screen-printed to the same design as the polymeric electrodes, onto alumina sheets. The gold conductor was fired at 850 °C for at least 10 min. Then the other components including carbon, Ag/AgCl and insulation were provided with the usual polymeric inks, as shown in Table 3.2. Evidently the presence of heavy metals in the gold formulation could present critical problems with sensititve metal ion sensing. There is no reason to believe that other metals or metal oxides whether environmentally benign or not, would have also been removed. Therefore, some scepticism would be expected.

Lane *et al.,* (2000) described the use of ceramic screen-printed inks for the anodic stripping voltammetric determination of silver and cadmium. The ceramic inks contained bismuth oxide, cadmium oxide and copper oxide, measured using Energy Dispersive X-ray Spectroscopy, for which peaks could be seen when voltammograms

were acquired. The identification for copper and bismuth peaks was confirmed by standard addition of these metal ions. The high temperature ceramic inks were irreproducible for use as electrochemical sensors.

Evaluation of Gold Screen-Printed Sensors for As and Hg in Cranfield University

Although good reproducibility for As and Hg determination was found by Cooper (2004), considerable noise and some background redox peaks were visible in many of the voltammograms shown. The origin of these peaks was not identified, but the influence of the Cl^- ion was noted, because the peaks were less often seen in the absence of Cl^-.

In a private communication (14/06/2005), J. Cooper expressed some concern about the need to keep the work area clean in the vicinity of testing and certain processes occurring due to the interaction of the gold surface and chloride ions. However, there was no indication that repeating the results would not be possible.

Since the work of J. Cooper, Cauchi (2006) evaluated some batches of DuPont sensors using the electrochemical procedure of Cooper. The work of M.Cauchi focussed on computational techniques such as neural networks and principal component analysis and so did not seek to adjust the electrochemistry. In a report (unpublished) for DuPont in 2004, Cauchi showed feasible calibration from single electrode per concentration data for As(III) between 100 and 800 ppb. A finite shelf life was noted for older electrodes where sensitivity had decreased. Also a test had been made for a possible interaction between residual solvent and the UV curing of the insulation ink. However, no statistical difference could be seen between the batches, which would not be possible to justify on the basis of single electrode data. In his thesis, the electrochemical behaviour of the DuPont sensor was studied with triplicate measurements. With the more detailed investigation it was concluded that further study was needed to understand the cause of the irreproducibility.

Although no further work detailing the detection of arsenic on screen-printed electrodes was found, in a private communication Professor Brian Birch (Luton University, UK) noted that the detection of arsenic on either ceramic based or on low-temperature screen-printed gold sensors was irreproducible (work unpublished). It could be speculated that for this work, due to the links with Gwent Electronic Materials (publications list, GEM, 2000), Professor Birch had evaluated the Gwent gold ink C2041206D2.

The authors of the patent, Bolbot *et al.,* (2007) were not, at the time of writing, aware of the Ercon and Gwent gold inks, so the patent only covers the use of DuPont gold ink. The fact that metal ions such as arsenic and mercury have been investigated on these other inks does compromise the patent, but does not invalidate it, if a substantial advantage with the DuPont ink can be shown. Also, the priority date would have to be considered.

Therefore, the aim of this section was to reproduce the calibration plots found in Bolbot *et al.,* (2007) and Cooper (2004), finding ways to improve the stability and reproducibility.

4.2 Materials and Methods

4.2.1 DuPont Sensor compositions

These sensors are essentially the same as those used by Cooper (2004), Cauchi (2005) and Bolbot *et al.,* (2007). The DuPont included batches D^{+}, (compositon as batch D), a small number of C and A with compositions shown in Table 2.1 on page 77 and design shown in Figure 2.1 on page 75. Subsequent batches include groups 1- 4 with compositons shown in Table 4.1.

Table 4.1 DuPont Sensors received July 2005

Group	Gold Ink	Carbon Ink	Reference Ink	Insulation ink
1	BQ331	BQ225	5874[e]	BQ425[b]
2	BQ331	BQ225	5874	BQ425[c]
3	BQ331	BQ221	5874	BQ425
4	BQ331	BQ225	5874	BQ411

[b]UV cured; [c]cured for at 130 °C and with infrared heating; [e] identified as BQ164;

Unless otherwise stated, the study for the electrolyte effect was conducted with batch BI sensors: composition shown in Table 4.2.

Table 4.2 DuPont Sensors received November 2005

Batch	Working electrode	Counter Electrode	Reference Electrode	Insulation ink
AO	BQ331	BQ225	BQ164	BQ425[a]
AI	BQ331	BQ225	BQ164	BQ425
BO	BQ331	BQ242	BQ164	BQ425
BI	BQ331	BQ242	BQ164	BQ411

AO (BO) – Batch A (B) oven cured at 130 °C, AI (BI) – Batch A (B) cured by infrared treatment; [a]UV cured

Ceramic based gold sensors using DuPont gold ink LF141 (cured at 850 °C) were of composition given in Table 3.2 on page 115 and design shown in Figure 2.1 on page 75. These electrodes were used in the same way as the polymeric based electrodes.

Evaluation of sensor samples included visual inspection of print alignment, inspection of ink colour, ink coverage, and scratch resistance. The conductivity of ink tracks was measured with a multimeter such as the TEK DMM870, (TEK, Bracknell, UK).

4.2.2 Stripping Voltammetry of As and Hg

The preparation of As and Hg samples procedures followed the methods of Cooper (2004), Cauchi (2005) and Bolbot *et al.,* (2007). The electrochemical equipment is described in Chapter 2.

General chemicals, such as acids and solvents were of analytic grade unless otherwise stated. For metal ions 1000 ppm aqueous spectroscopic standards Cu(II), Hg(II),

Cd(II), As(V), Pb(II) were obtained from SigmaAldrich (Poole, UK). Samples were prepared by dilution with HPLC water. Arsenite was prepared from arsenic (III) oxide powder (SigmaAldrich). For example, 0.1320 g of As_2O_3 was dissolved into 1 ml 25 % wt NaOH subsequently acidified with 2 ml of concentrated HCl and diluted to 100 ml HPLC water resulting in an acidic 1000 ppm stock solution. Stock solutions were stored at 4 °C. Solutions of arsenic(III) were prepared by dilution in hydrochloric acid electrolytes. In some cases, 1 mM of hydrazinium chloride was added to guard against oxidation of the arsenic following the recommendation of (Svancara *et al.,* 2002). Sample solutions were not deaerated or stirred.

The DPASV parameters, described in Table 2.2 on page 82, were used for arsenic and mercury determination. Cyclic voltammetric parameters varied according to application, with the scan range generally within -0.3 to 0.6 V according to the capacitive range of a gold surface. Scan rate was within the range 1 – 1000 mV/s, with step height set as small as possible < 1 to 4 mV, depending on the values allowed by the potentiostat.

In a separate study using a method described by Noh (2005), a deposition phase at -0.3 V for 30 s was used with a 200 mV/s scan rate for oxidative stripping. As(III) solutions with concentrations between 10 and 1000 ppb were prepared in 1 M HCl without hydrazinium chloride and stored for no longer than 1 day. Since the oxidation of As(III) to As(V) could be unpredictable, the method method of Noh (2005) was subsequently used to assess As(III) solutions. By comparing the peak for 100 ppb As(III) in 1 M HCl with a voltammogram obtained when the solution was prepared fresh the oxidation state of the arsenic could be inferred.

Matlab v7 (The Maths Works, Cambridge, UK) and Microsoft Excel were used to analyse the results needed to separate the arsenite peak from the interference.

4.2.3 Interference Study

Electrolytes were prepared by dissolving suitable salt or dilution of concentrated acid with HPLC water. A few such as HCl and HNO_3 were of highest purity, most, however were standard laboratory grade due to cost, obtained from SigmaAldrich (Poole, UK), Across Organics or BDH (Poole, UK). Where possible, depending on solubility, electrolytes were prepared to 4, 2, 1 and 0.5 M strength in HPLC water. An Autolab multistat (PGstat 10 with PGstat 2, 3, and 4 modules) with four channels was used for analysis to keep overall experiment time down. A short Matlab script was written to automatically load and sort the data allowing various 2 and 3 dimensional plots to be made, explained further in Section 2.3.8. For cyclic voltammetry, parameters are given in Table 2.3 on page 82.

A comparison was made for some electrolytes between screen-printed and standard electrochemical cells. For this, standard gold disk electrode with platinum disk counter electrode and glass capillary Ag/AgCl reference electrode (BAS, West Lafayette, USA) were inserted into a 25 ml beaker of 4 M HCl, without removal of oxygen. The setup is shown in Figure 1.3A on page 37.

Nafion solution (5 % in a mixture of alcohols, from SigmaAldrich) was used to prepare membranes over the working electrode surface. About 3 µl was pipetted and carefully spread over the sensor and allowed to air dry for at least 10 min.

Solubility of contamination experiments used standard gold, platinum and carbon disk electrodes (BAS, West Lafayette, USA), polished and cleaned as described in Chapter 2.

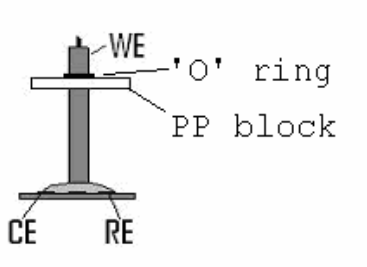

Figure 4.1 Schematic for measurement of interference on standard electrodes with screen-printed electrode substrates, side view. WE – working electrode, CE – counter electrode, RE – reference electrode and PP – Polypropylene.

The standard electrodes were held with an o-ring supported in a drilled (6.5 mm hole) polypropylene block, in a clamp stand. The electrode was positioned above a screen-printed electrode as shown in Figure 4.1. The reference and counter electrodes were used from the screen-printed strip.

Standard cyclic voltammetry parameters with 40 scans were acquired. The scan range was extended to include the whole interference peak.

4.3 Results

4.3.1 Inspection of Sensors

Good alignment and complete print coverage of gold, silver and carbon inks on the DuPont sensors was visible. The provided sensors were consistently smudge and spatter free. Gold and silver compositions gave sub ohm resistances with multimeter probes set about 1 cm apart; for a carbon track the typical resistance was about 1 kΩ. Variation was seen between ink batches, however the upper limit measured was less than 2.5 kΩ and the lower limit greater than 600 Ω. The ceramic gold and platinum sensors showed a higher degree of variation in resistance, shown in Figure 3.5 on page 123 despite using similar carbon inks and print conditions. Some batches of the DuPont sensors, such as batch D, include insulation inks, where as other omit the pigment, such as D^{+}.

The insulation layer of batch D^+ showed visible signs of cracking along the length of the underlying carbon tracks, as shown in Figure 4.2.

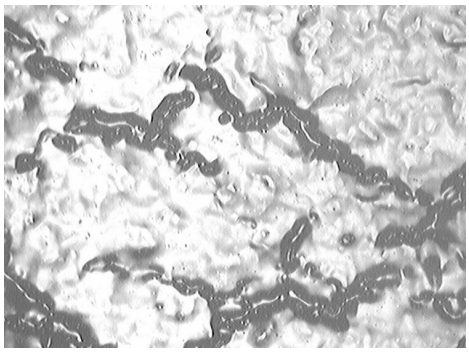

Figure 4.2 Microscope image of Batch D^+ insulation layer (white) on carbon tracks (black). The 10x lens was used

4.3.2 Arsenic and Mercury Determination in 4 M HCl

The Batch D^+ electrodes were compared with a few remaining older electrodes from Cooper (dated 2002-2003, group A) and Cauchi (dated 2004, group C), having sensor compositions as shown in Table 2.1 on page 77. The electrodes were tested with standard redox couple, 0.1 mM ferrocyanide in 0.1 M KCl. Figure 4.3 shows the electrochemical response using CV at 50, 100 and 150 mV/s with scan range as indicated.

The older batches A and C showed the expected waveform for the ferrocyanide peak with formal potential E^0 of about 180 mV (vs Ag/AgCl in 0.1 M KCl). Also the current was as expected for 0.1 mM ferrocyanide. The older batch, A, showed a smaller/ weaker response indicating an ageing effect after 2-3 years. In addition spike peaks could be seen at +0.05 V and -0.15 V on the forward and reverse scan respectively. Batch D^+, as shown in Figure 4.3A, showed a large peak, > 50 μA and about 100 mV with no apparent relationship to the ferrocyanide. Further electrodes from the same batch D^+, but in storage at DuPont (Bristol, UK) since printing were

also evaluated: the response was the same as shown in Figure 4.3A. No electrodes from any other batch showed this behaviour. The Batch D^+ electrodes were also scanned in 4 M HCl, and later in a variety of acids and neutral electrolytes and buffers. The large peak seen Figure 4.3A was typical irrespective of either H^+ concentration or anion type.

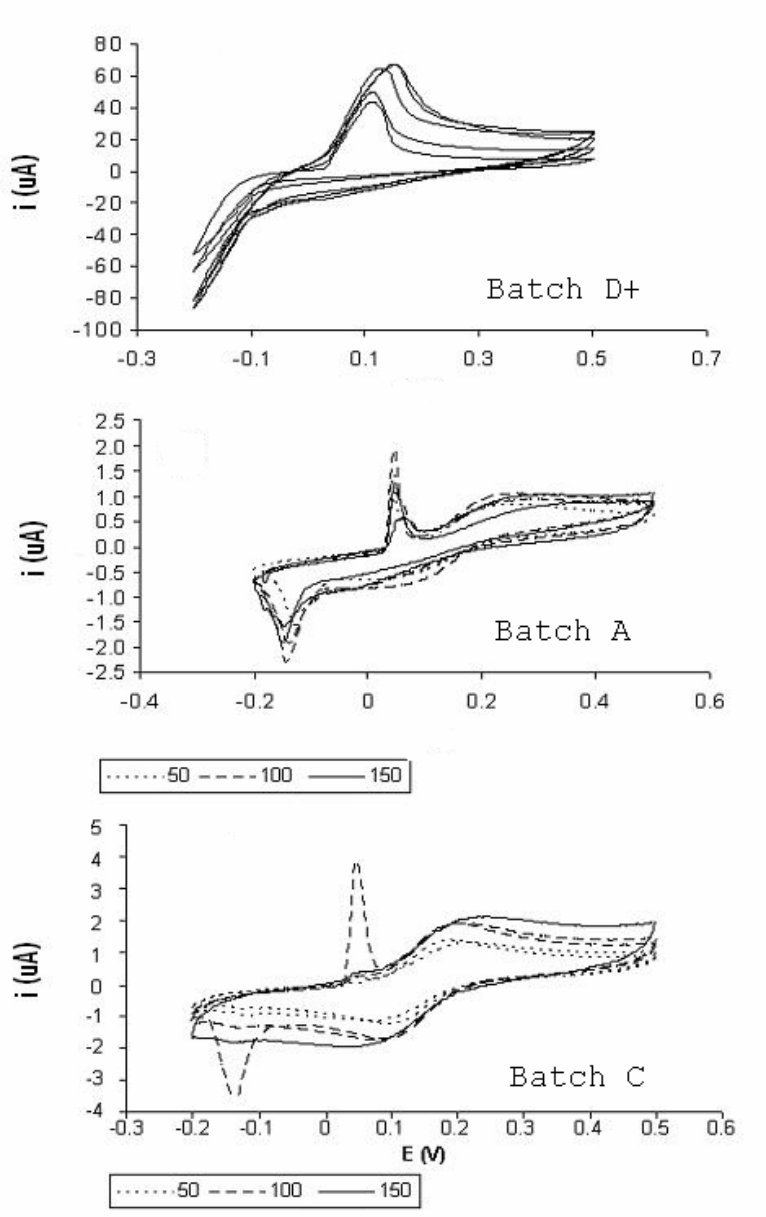

Figure 4.3 Cyclic voltammetry of 0.1 mM ferrocyanide and 0.1 M KCl at 50, 100 and 150 mV/s, as indicated, on (A) Batch D^+ DuPont sensors, (B) Batch A sensors, and (C) Batch C sensors.

Various efforts were tried to eliminate the problem such as heating (up to 150 °C for 1 hour), solvent washing (drops of acetone, methanol and HPLC water) and vacuum chamber with bench-top pump. None improved the performance of D^+. Also, replacement of counter and reference electrodes was tried with standard carbon and glass capillary reference electrode. However no method succeeded in eliminating or reducing the interference.

Another four groups of sensors were provided with varied carbon, insulation ink and the inclusion of an infrared heating procedure as given in Table 4.1. The objective of testing was now to repeat the work of Cooper (2004).

All four groups were tested in ferrocyanide solutions (not shown) and with As and Hg solutions prepared in HCl. Figure 4.4A shows the response of group 1 with DPASV procedure in 4 M HCl (multiple repeats), the current was less than 5 μA: the large peak of batch D^+ was not seen. Groups 2, 3 and 4 also did not display the peak. Many repeats are shown in Figure 4.4 highlighting that many processes influence the reproducibility. Figure 4.4B shows a response for As and Hg at 250 ppb at the potentials reported by Cooper (2004) and Cauchi (2006).

However, there are two visible interference peaks at 0.1 V and 0.4 V (vs Ag/AgCl in 4 M HCl). The 0.1 V peak is close enough to overlap the As(III) peak and the 0.4 V peak overlaps the Hg(II) peak. Also there is a process affecting the baseline.

In addition to the solvent, temperature and vacuum treatments (as with batch D^+), electrochemical procedures such as preanodisation (up to 1.5 V for 30 min), pre cathodisation (down to -0.8 V for 30 min) or cycling (for example -1 to 1 V at 1 V/s for 50 scans) were used to try to improve the stability of these sensors (results not shown). Some procedures degraded stability (solvent washing) and increased background (electrochemical pretreaments) currents whereas others made no difference (oven curing, vacuum treatment).

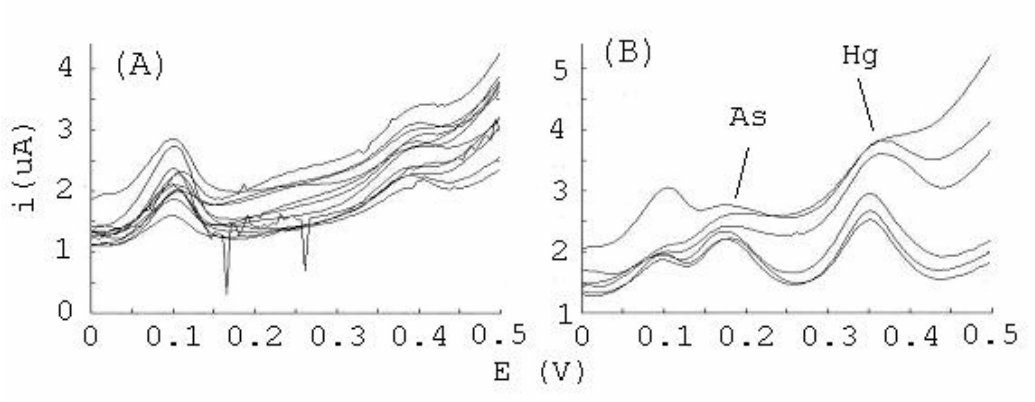

Figure 4.4 DPASV on DuPont sensors (batch 1) in, (A), 4 M HCl (10 repeats, new sensor for each repeat) and, (B), 4 M HCl with 250 ppb of As(III) and Hg(II) (6 repeats, new sensor for each repeat). Includes 1 mM Hydrazinium chloride.

The reproducibility was an issue at higher concentrations as seen in Figure 4.5 where 6 repeats of 750 ppb As and Hg are shown. One of the six in particular shows flattened peaks but simultaneously with an increased background. Therefore, it is not clear whether peak height or peak area estimation would be more suitable for calibration purposes.

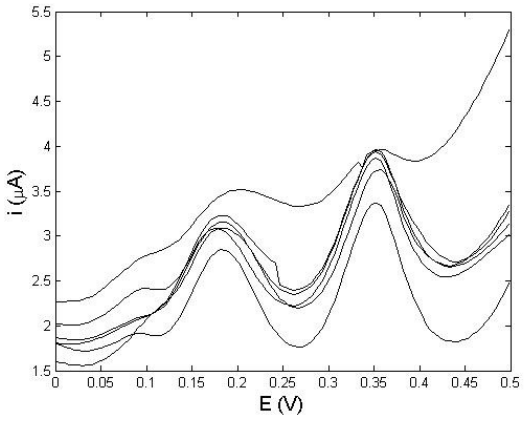

Figure 4.5 DPASV on batch 1 sensors for 750 ppb As(III) and Hg(II) in 4 M HCl (6 repeats on different electrodes). Includes 1 mM Hydrazinium chloride.

The electrochemical response of the sensors was analysed for levels of As(III) and Hg(II) from 100 to 800 ppb. A calibration for both peak area and peak height is shown in Figure 4.6. The peak height and peak area are in reasonable agreement. However

the height measurements have a greater variability. Neither measurement scheme leads to effective metal ion quantification in the range shown. The results from batches 2 and 4 were marginally better than batch 1. However, it is clear the same background processes are also occurring.

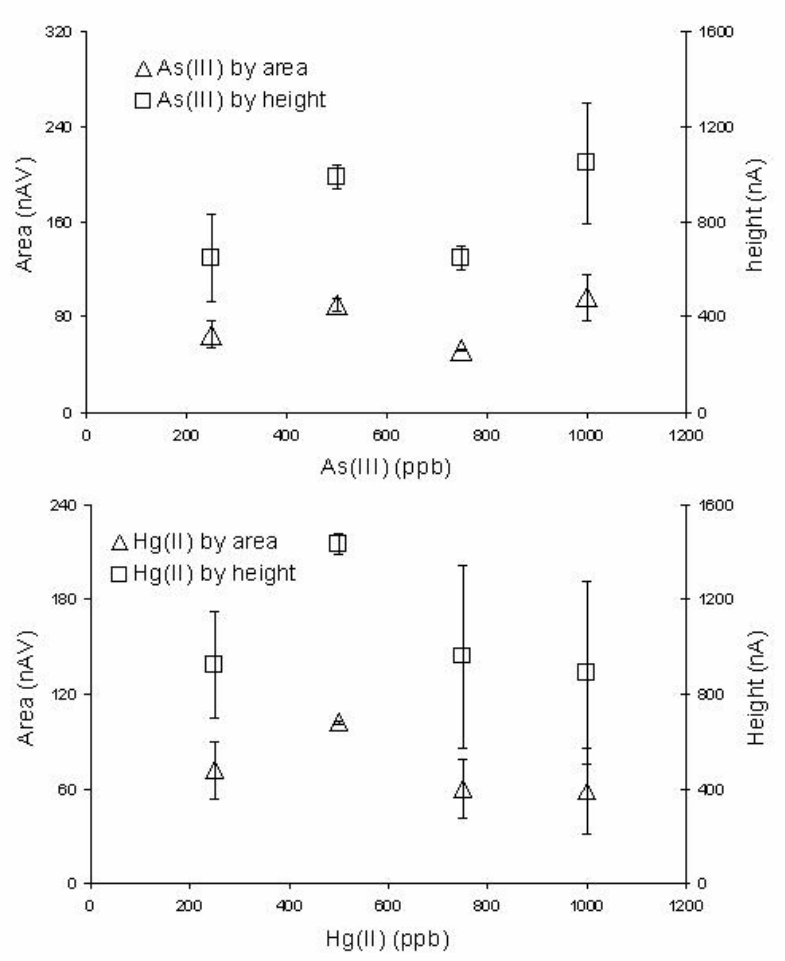

Figure 4.6 Calibration of As and Hg in 4 M HCl (with 1 mM hydrazinium chloride) with a DPASV procedure using both peak height and peak area measurements.

Because the cause of irreproducibility in baseline and background redox compounds could not be ascertained, the experiments were repeated in a different laboratory with different pipettes, and sample solutions by a co-worker. The use of a multi potentiostat enabled a greater degree of automation. All samples were tested in triplicate.

The same underlying irreproducibility was seen, with batches 2 and 4 being marginally better than batches 1 and 3. The calibration data for group 2 is shown in Figure 4.7.

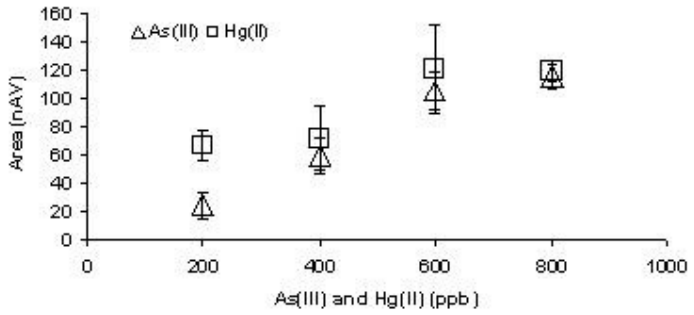

Figure 4.7 Calibration of As(III) and Hg(II) in 4 M HCl (with 1 mM hydrazinium chloride) by DPASV performed by M. Cauchi

At this point it was clear that the sensors could show a number of interferences which are of primary concern in the possible production of viable sensors.

Using a further set of batches AO, BO, AI and BI the same tests in 4 M HCl with and without As(III) also showed interference similar to batches 1-4, as shown in, Figure 4.8.

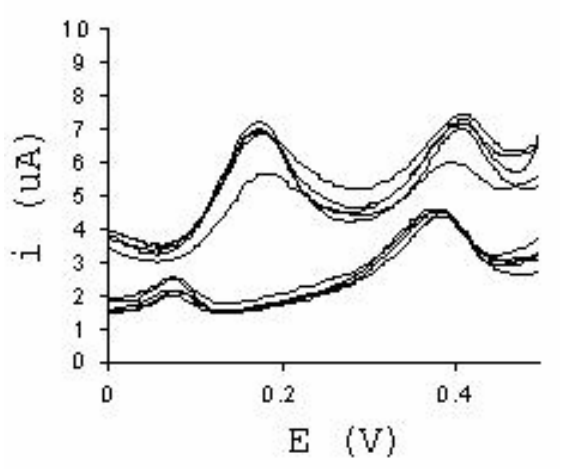

Figure 4.8 DPASV in 4 M HCl electrolyte using standard procedure with (above) and without (below) 5 ppm As(III) for (five repeats, new electrode per repeat).

4.3.3 Electrolyte effect with DuPont Sensors

To maintain consistent comparison between experiments standard parameters were set for cyclic voltamettry, as shown in Table 2.3. The potential range was suitable for low currents to be obtained at the gold surface. The number of scans lasted about 20 min a reasonable length of time compared to sample drop evaporation.

A number of electrolytes were prepared varying both cation and anion. Where possible electrolytes were selected for maximum solubility, since the target electrolyte as optimised by Cooper (2004) was highly concentrated 4 M HCl. Electrolytes included sodium chloride, nitrate, iodide, perchlorate and sulphate, potassium bromide, sulphuric, perchloric, nitric, acetic and formic acid. In addition LiCl was prepared in methanol and dimethylsulfoxide (DMSO) to assess the effect of water itself.

A standard electrochemical cell was used first with a beaker (25 ml) of 4 M HCl. The experiment was repeated six times (with polishing of the working electrode between each run). Two plots are shown; Figure 4.9A shows a three dimensional mesh plot, with sample number being the third axis; and Figure 4.9B shows for one of the six repeats usual voltammogram format. With the standard cell there is no visible interference, apart from a small redox peak close to 0.4 V which decreases with scanning.

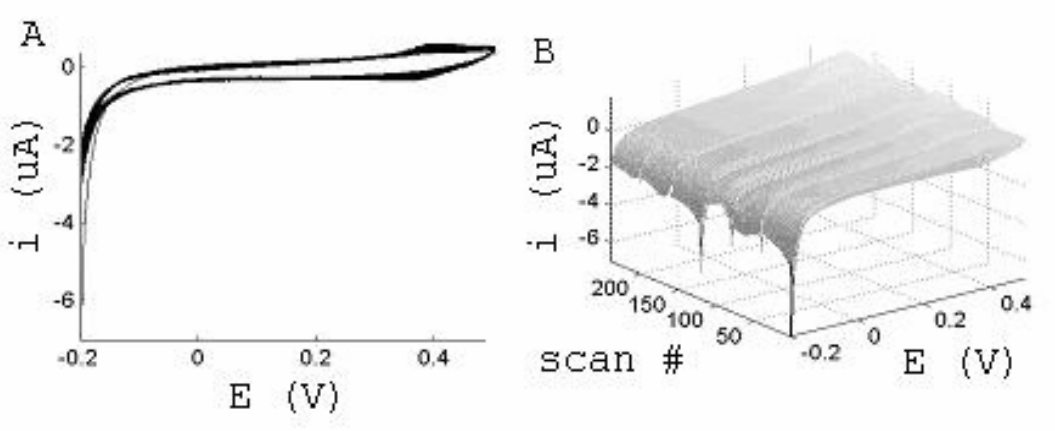

Figure 4.9 Mesh and voltammogram view of 6 experiments with standard electrodes in 4 M HCl.

By contrast a DuPont sensor scanned in 4 M HCl reveals three redox type peaks and a widening of the baseline probably attributed to increasing electrode capacitance, as shown in Figure 4.10. These peaks are those seen directly interfering with As(III) determination. The spike peak around 0 V is small and tends to stay the same or decrease with scanning in this experiment. The larger (primary) peak around 0 V, builds up swiftly. Figure 4.10B shows 6 examples of the procedure. The redox peak around 0.2 V (secondary peak) increases but apparently reaches a maximum. In some cases the build up is slow reaching only few µA after 40 scans, but with other electrodes such as batch 3 (see Table 4.1 for composition, voltammograms not shown) gave peaks up to 30 µA for the same conditions. The peak rarely shows signs of stabilising or decreasing with scanning. In light of this 0 V large peak, it is difficult to envisage any kind of electrochemical pretreatment, as is often used on carbon screen-printed electrodes, stabilising or improving the sensor signal. Since the primary and secondary peaks build up from low values after the initial scan, the interference for single use sensors may be less problematic. However, when deposition phases were included, the peaks were invariably swifter and more severe (not shown).

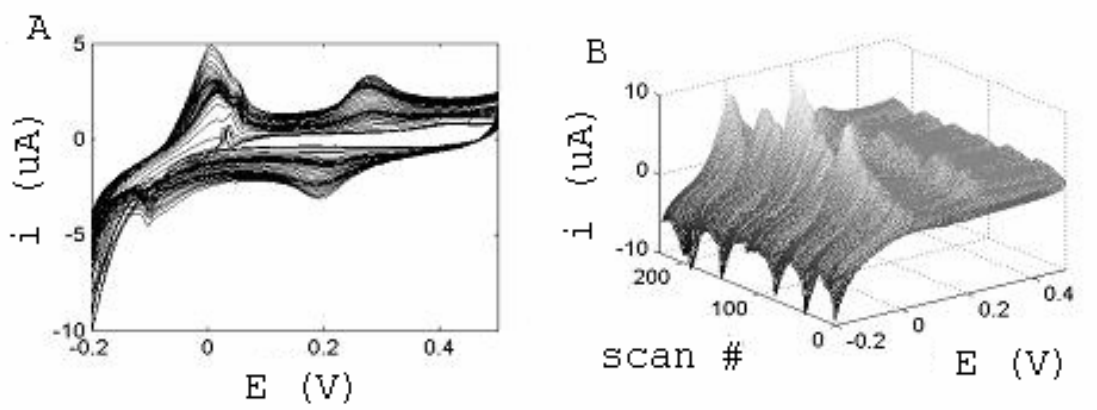

Figure 4.10 Mesh and voltammogram view of six DuPont electrodes (Batch BI) tested in 4 M HCl.

Other chloride containing electrolytes showed the same pattern. Figure 4.11A, B, D and E show the interference at 4, 2, 1 and 0.5 M for sodium and calcium chloride. Electrolytes with 0.5 and 1 M concentrations show little primary but reasonable secondary interference. The spike is visible on some electrodes for all concentrations,

but incidence is 'intermittent' with respect to individual electrodes. The primary peak interference in 4 M NaCl and 4 M $CaCl_2$ appears more aggressive than in 4 M HCl, and so acidity is apparently not a factor.

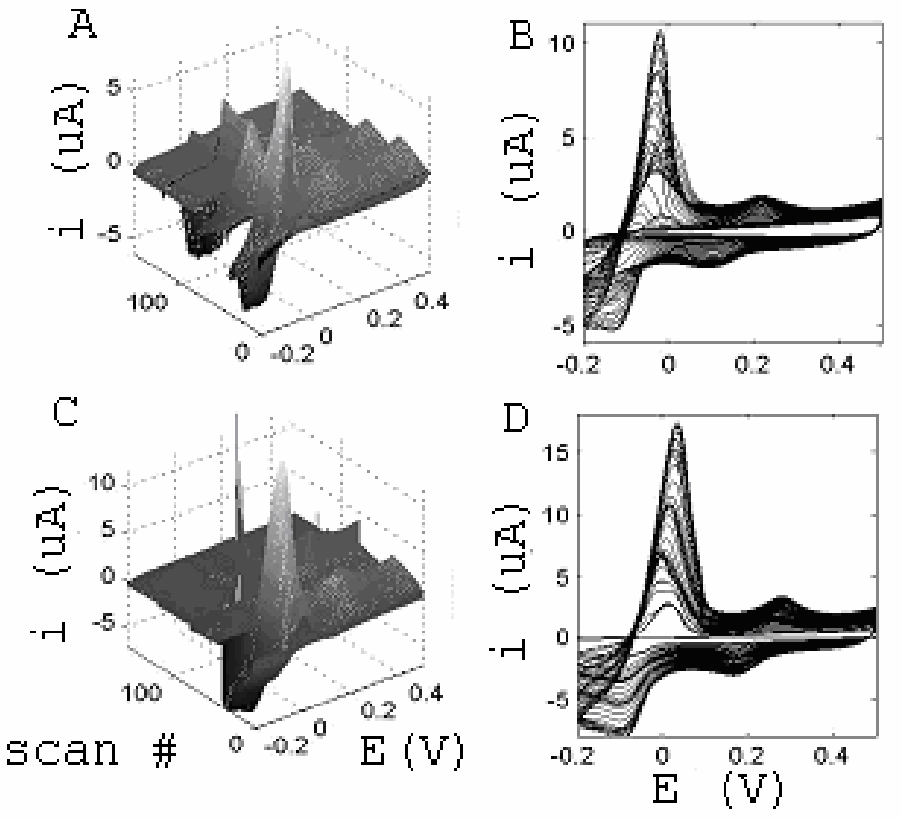

Figure 4.11 Electrode interference in chloride containing electrolytes, sodium chloride and calcium chloride.

The potassium bromide also exhibited the same pattern of behaviour, although the severity of the effect was more apparent at lower concentrations, as shown in Figure 4.12. Also, a similar large primary peak was seen (Figure 4.13 bottom left) with sodium iodide even in 0.1 M concentrations; the experiment was terminated after several scans.

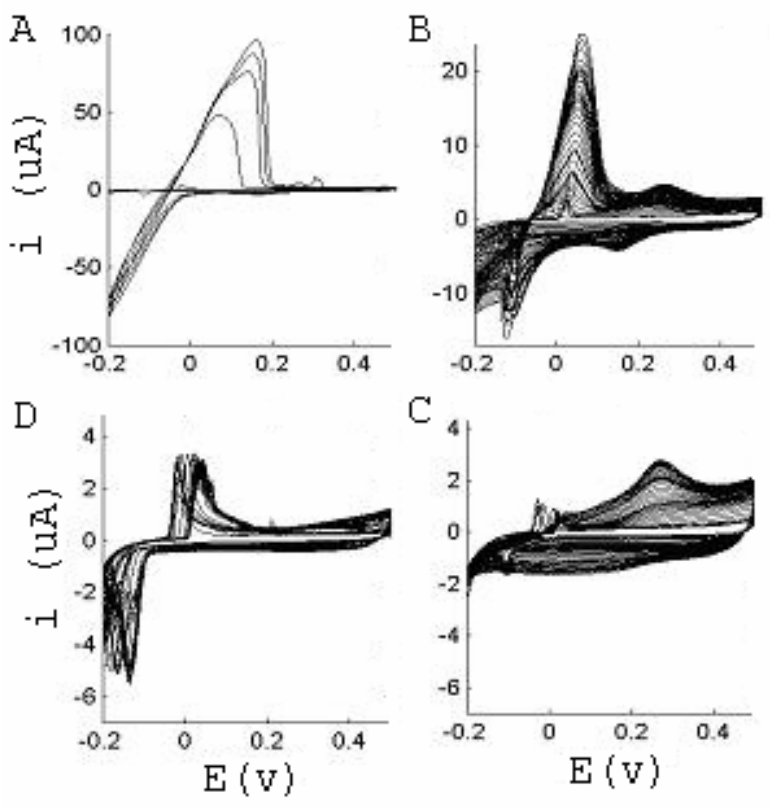

Figure 4.12 Voltammograms for potassium bromide electrolyte with batch BI electrodes. Electrolyte concentration (A) 4 M, (B) 2 M, (C) 1 M, and (D) 0.5 M

Of other electrolytes, the nitrate, perchlorate and sulphate salts whether neutral or acidic kept good currents (< 1 μA) over the 40 scan experiment. Some oxidation was apparent above about 0.2 V in the strong nitric and sulfuric acids. Neither the primary, secondary or spike peaks seen in the chloride electrolyte were visible. However, another characteristic peak for these electrolytes is apparent, whose potential and shape tends to be erratic. This peak occurred during the initial scans, visible for sodium perchlorate and nitrate in Figure 4.13. In general, this peak was seen with nitrate, perchlorate, sulphate, acetate buffer (pH 4.5) and phosphate electrolytes both as acids and neutral salts. The peak was equally seen in Ultra Trace nitric acid (Fluka) as in technical grade nitric acid (SigmaAldrich).

Since acid reagents can contain levels of metals, efforts were made to obtain the highest purity. However the cost becomes prohibitive for a large number of

chemicals. Highest purity nitric acid was compared with standard reagent grade electrolytes and showed no observable difference in electrochemical response for cyclic voltammetry or ASV. It was concluded that the highest purity was not necessary for the studies of electrode interference, but may need to be reassessed for successful ultra trace element analysis. It is possible that the ink formulations have a residual contamination level dependent on the polymer source chemicals and production processes.

For some other electrolytes, formic acid showed a particularly large background current rendering the sensor unusable at all tested concentrations (0.5 to 4 M). Acetic acid showed a redox peak with the first scan then subsequent settled scans with mild background increases. These results are also in Figure 4.13.

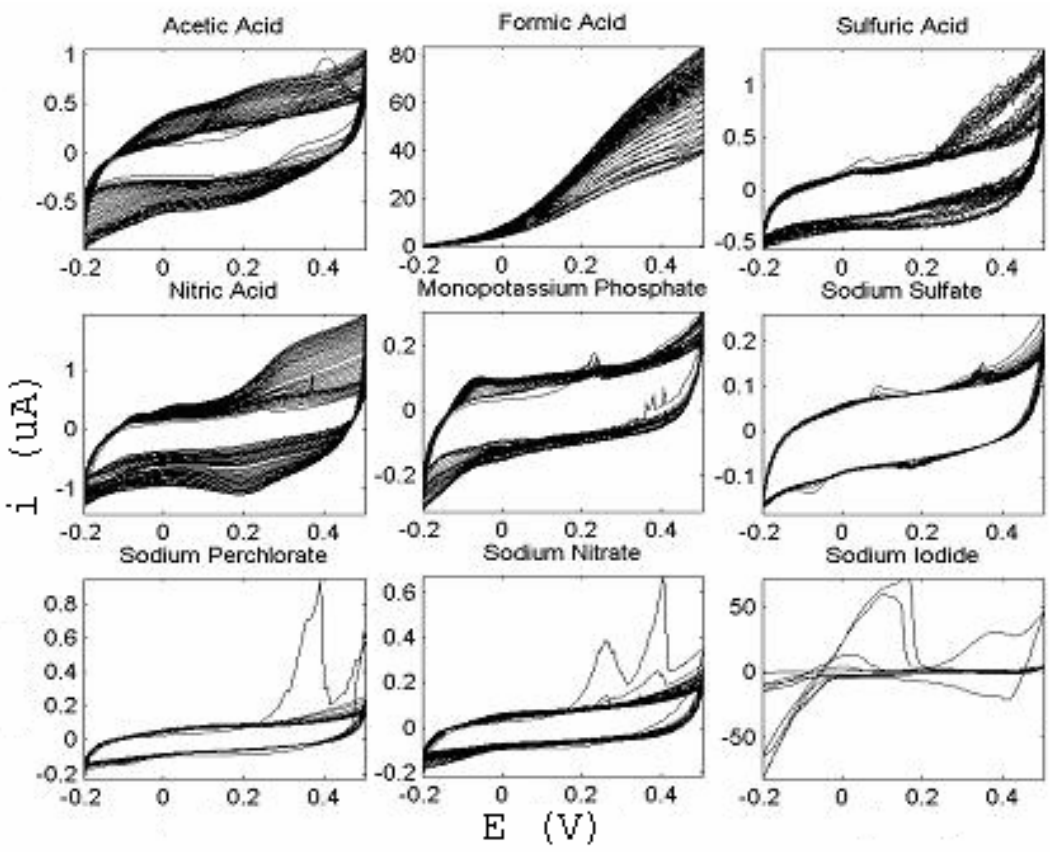

Figure 4.13 Voltammograms for nine electrolytes at 4 M concnetration, except monopotassium phosphate (1 M). Batch BI sensors were used; 40 scans for each experiment using standard CV parameters.

Lithium chloride was dissolved 2 M in methanol and 4 M in dimethyl sulfoxide (DMSO). As shown in Figure 4.14 and Figure 4.15, cyclic voltammetry reveals the same pattern of peaks for high Cl^- ion content. Therefore the water is not implicated in the peak unless only trace level is required. The large background changes in Figure 4.15 are probably due to dissolution of working electrode polymer in the solvent.

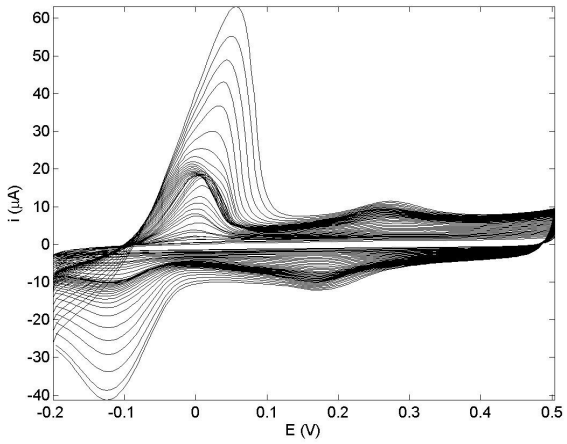

Figure 4.14 DuPont sensor cycled in 4 M LiCl in methanol cycled using standard CV parameters

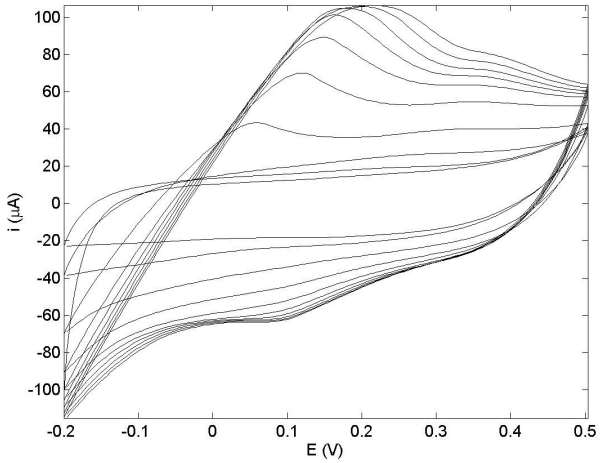

Figure 4.15 DuPont Sensor cycled in 2 M LiCl in DMSO using standard CV parameters

The peak shape is indicative of solubilised contaminant so a membrane was tried. Nafion 5 % in alcohol was pipetted to the working electrode surface area of a DuPont sensor. Cycled in 4 M HCl the Nafion protected surface is shown in Figure 4.16. A Nafion film is impermeable to anions, thus prevention of the phenomenon indicates that the interference, or component thereof, is negatively charged. However application of the Nafion film increased the background currents (5 – 10 μA) and attempts to use such prepared sensors for As(III) detection was found to be difficult.

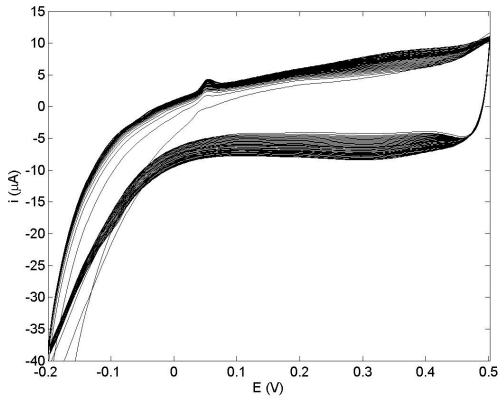

Figure 4.16 Nafion film protected DuPont sensor cycled in 4 M HCl using standard CV parameters

4.3.4 Electrolyte effect with Ceramic Gold LF141

The prepared gold ceramic electrodes were subjected to cyclic voltammetry with parameters of Table 2.3 to various electrolytes to investigate the effective working ranges.

Figure 4.17 shows the voltammograms for a variety of electrolytes. The result in 4 M NaCl is recognisable from the polymer gold sensors (Figure 4.11). However the acidic electrolytes cause a redox couple close to 0 V not seen with the polymeric electrodes. The 4 M HCl electrolytes appears to have a multitude of redox processes suggesting a combination of the peaks associated with Cl^- ions and those particular to the other acids plus another redox couple at 0.4 V. The large background currents would be incompatible with arsenic or mercury determination.

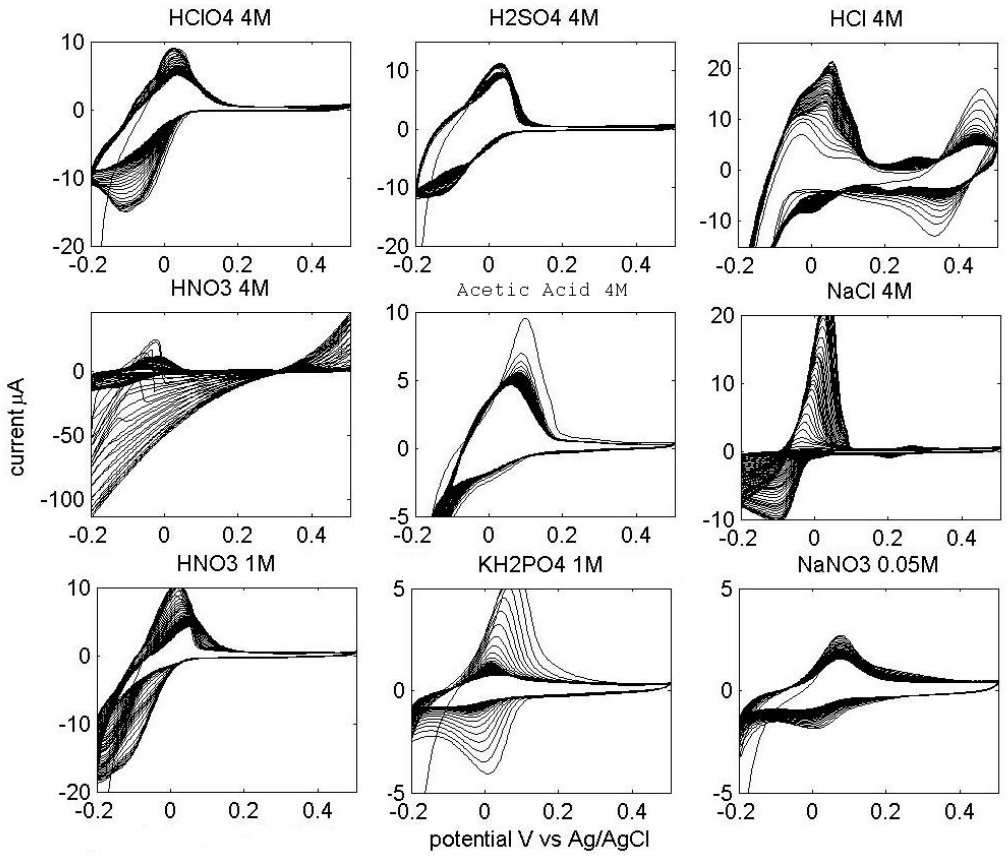

Figure 4.17 Voltammograms in various electrolytes using ceramic gold electrodes (LF141) using standard cyclic voltammetric parameters

4.3.5 Effect of Trace Cl^- ion

Electrolytes without Cl^- ion typically showed an absence of the primary secondary and spike interference. Whilst an erratic peak is visible in non Cl^- ion electrolytes dissipation within a few scans would be expected. Perchloric acid was studied with low levels of chloride to ascertain performance of the sensors with these conditions.

Perchloric acid (1 M) was prepared with 0, 1, 10 and 100 mM Cl^- added as HCl. Electrolytes of 1, 10 and 100 mM HCl were also prepared. The DuPont Sensors (Batch BI) were scanned with standard CV parameters (shown Table 2.3).

Perchloric acid (1 M) alone shows very stable CV over 40 scans. A small peak is visible in the first 1 to 2 scans, as shown in Figure 4.18.

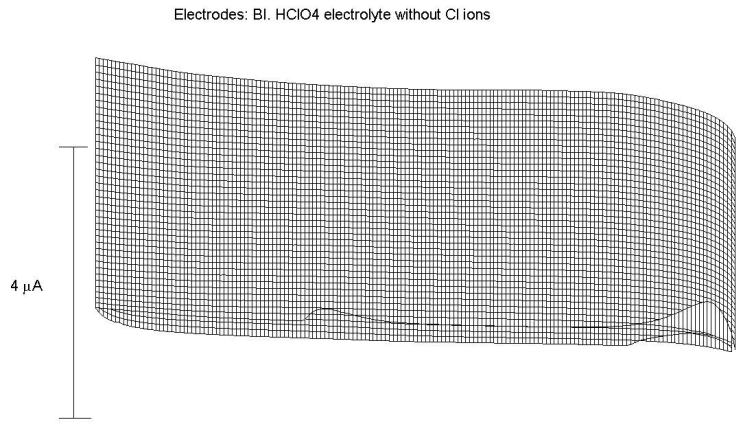

Figure 4.18 DuPont electrode in perchloric acid electrolyte, 40 scans. X axis -0.2 to 0.5 V, the scan number axis recedes into the page and the vertical is as marked, the current axis.

Chloride was added at 1, 10 and 100 mM levels to the perchloric acid and also to pure water samples. Figure 4.19 shows that the transient first scan peak is gone and both the spike and secondary peak are present. The 3-dimensional mesh plot shows a vivid account of the spike peak in particular. The secondary peak shifts with Cl^- concentration (repeat over four repeats) suggesting direct complexation or bonding of Cl^- during this reaction. The spike peak shows little sign of changing peak position with Cl^-, some peak shifting is visible and the factors governing the incidence, or stability are not clear. On the basis of four sets of experiments (not shown) the perchloric acid apparently serves to elevate the spike at 1 and 10 mM Cl^- concentrations, whilst tending to decrease the secondary peak. The spike peak shape is clearly non-standard for electrochemistry and does not exhibit diffusion tailing so could be due to a surface sorbed compound. By comparing the similarity of the non Cl^- strong acids - whichever electrolyte is chosen, the spike and secondary peak cannot be avoided since most natural samples will contain some chloride. As(III) would be expected to strip directly between the spike and secondary peak.

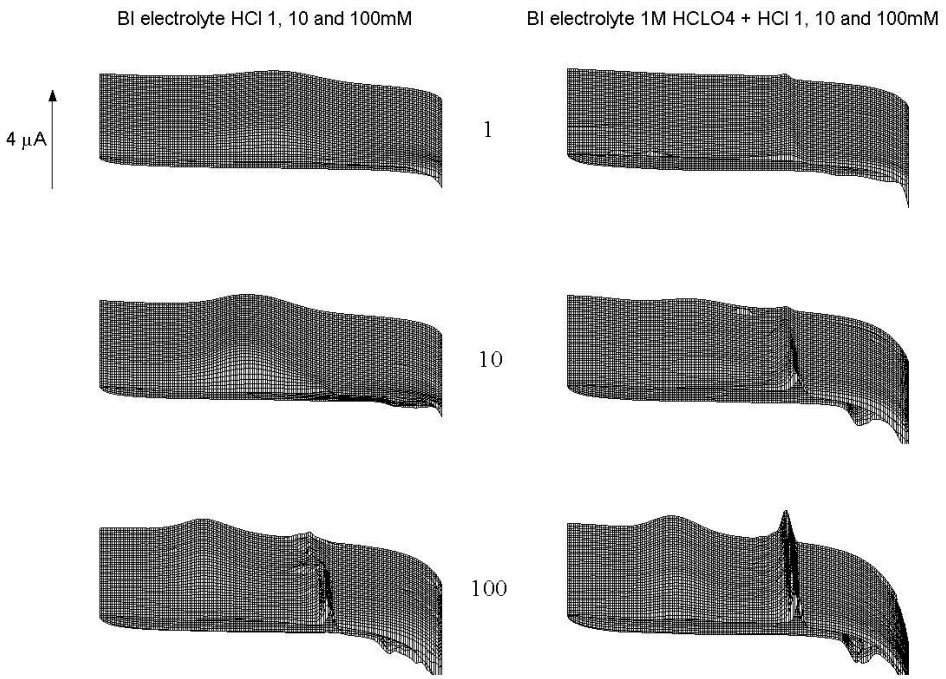

Figure 4.19 The effect of trace chloride, with and without perchloric acid, on voltammogram. Scan from -0.2 to 0.5 V, the scan number axis recedes into the page and the vertical is as marked, the current axis.

4.3.6 Solubility of Interference

Non-screen-printed electrodes including a gold disk, carbon disk, and platinum foil were used as working electrodes suspended above DuPont sensors using the screen-printed counter and reference; the scematic is shown in Figure 4.1 (page 172). Electrodes were polished and rinsed before each experiment. In particular, 4 M KBr was used as electrolyte, to generate large, immediate interference. An example cyclic voltammogram for gold, platinum and carbon working electrode is shown in Figure 4.20. The same pattern of interference for the primary and secondary peaks (for example Figure 4.11 on page 181) could be detected on the gold, and the primary peak could be detected on the carbon and platinum, confirming that the interference is soluble and irrespective of working electrode composition. However, the spike peak was not detected using the standard parameters of Table 2.3.

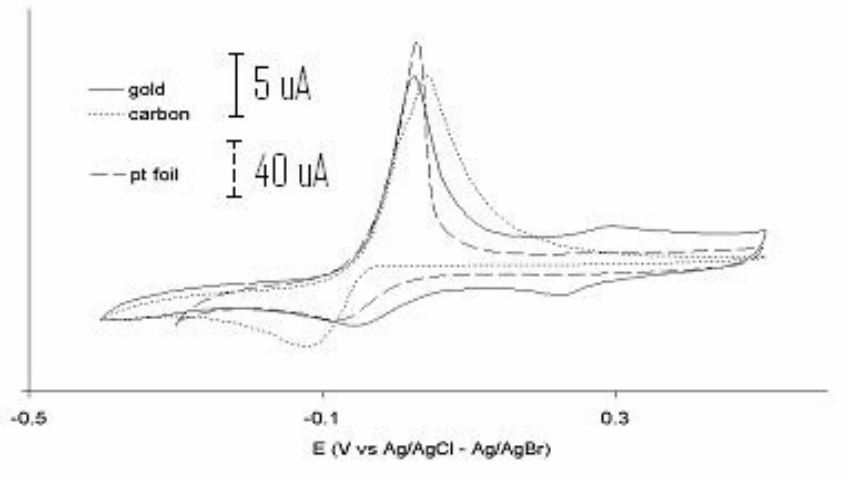

Figure 4.20 Example scan of working electrode probe cycled above DuPont sensors in 4 M KBr electrolyte – current has been scaled to fit

4.3.7 Arsenic determination in 1 M HCl

Noh (2005) developed a method for As(III) analysis effectively avoiding interference. Using 1 M HCl and -0.3 V deposition for 60 s followed a 100 mV/s scan from -0.3 up to 0.8 V, As(III) concentrations as low as 10 ppb were successfully analysed. The spike peak occurred at about 0.08 V and the As(III) at 0.230 – 0.280 V. The As peak

is broad: as much as 0.3 V at the base and about 0.15 V wide at half peak height. A 200 ppb concentration resulted in only a 1 µA peak, however a 10 ppb concentration still recorded a viable peak. Unfortunately the baseline also recorded a slight upward hump which might be mistaken for a false positive at low concentrations. The calculated limit of detection was 0.7 ppb, as required for the analysis of drinking water. The voltammograms shown are very stable (unlike the DuPont sensors) allowing good confidence. The effect on 100 ppb As(III) of Zn, Pb, Fe, Cr, Cd and Ca was tolerable. However the effect of copper was detrimental considering the likely occurrence of this metal. 100 ppb Cu(II) copper was found to shift the 100 ppb As peak by more than 0.1 V, at 200 ppb Cu(II) the arsenic was a shallow shoulder and at 1000 ppb Cu(II) the As(III) was not visible. Hg(II) is also troublesome, but high levels of Hg, > 100 ppb, in natural samples is less likely.

The method of Noh (2005) was modified and reproduced on the DuPont sensors. A -0.3 V, 30 s deposition phase preceded a 200 mV/s scan from -0.3 to 0.5 V scan, the reverse scan was also recorded. At least three measurements were taken for each measurement.

Figure 4.21 shows the As(III) response at 0, 50, 200 and 800 ppb. The peak is clear at 50 ppb with about 0.1 V base width, much narrower than the equivalent on the Ercon sensor (about 0.3 V). However, the peak width at 800 ppb is similar to the Ercon ink, about 0.3 V. The secondary interference is visible and becomes part of the As peak at higher concentrations, contributing to uncertainty in As area determination. The spike peak occurs similarly on both gold inks, at about 0.05 to 0.1 V. However, the baseline at 0.1 V is significantly less stable on the DuPont than with the Ercon ink. Both height and area estimations of arsenic are thus subject to uncertainty. As(III) determination below 25 ppb was difficult, despite evidence of sensitivity down to 10 ppb.

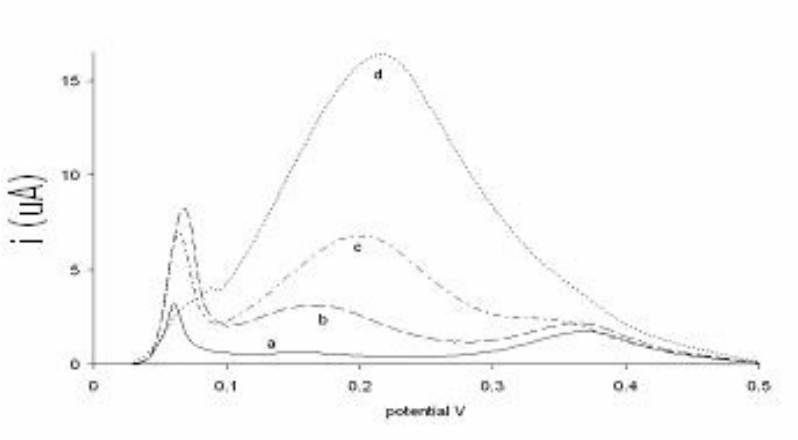

Figure 4.21 As(III) stripping using -0.3 V, 30 s deposition and 200 mV/s scan from -0.3 to 0.5 V: 1 M HCl (no hydrazinium chloride) (a) 0 ppb, (b) 50 ppb, (c) 200 ppb and (d) 800 ppb As(III).

To look more closely at the arsenic peak alone and to consider how the peaks could be deconvoluted, the voltammograms were loaded into Matlab. Two end points were chosen where the baseline avoided redox reactions, being most stable, and a linear background was calculated and subtracted from the original voltammograms (as seen in Figure 4.21). A quadractic baseline matching both end points in slope and position was also tried, but some of the backgrounds were found to intersect the experimental voltammogram causing strange shapes in the subtracted voltammograms. Other methods such as cubic spline fit required a substantial number of fitted points whilst minimising irreproducible processes and was found less efficient than a simple linear fit. The linear subtracted peaks were loaded into Microsoft Excel and a manual peak fit was tried.

A simple derivative logistic curve was used for fitting; i.e. a model peak without diffusion tailing or heterogeneous kinetic effects. With the form where y is current, x is potential, A, B and C are the fitted constants:

$$y = A\frac{\exp\{-Bx\}}{(\exp\{-Bx\}+C)^2} \qquad \textbf{57}$$

'A' relates to the fitted peak height, and B and C give the peak position and width. Three peaks were needed to model the spike, secondary and As(III) peaks. A spreadsheet (Microsoft Excel) was used to enter these values for each peak

minimising. The total model voltammogram (the sum of the three model peaks) was evaluated against the experimental signal minimising the sum of squares difference between the two. Some examples gave excellent fits but this trend did not extend to all samples. An example for 100 ppb As(III) is shown in Figure 4.22. Due to the particularly large spike peak in this example the arsenic peak is almost entirely lost, but the deconvolution appears to be effective.

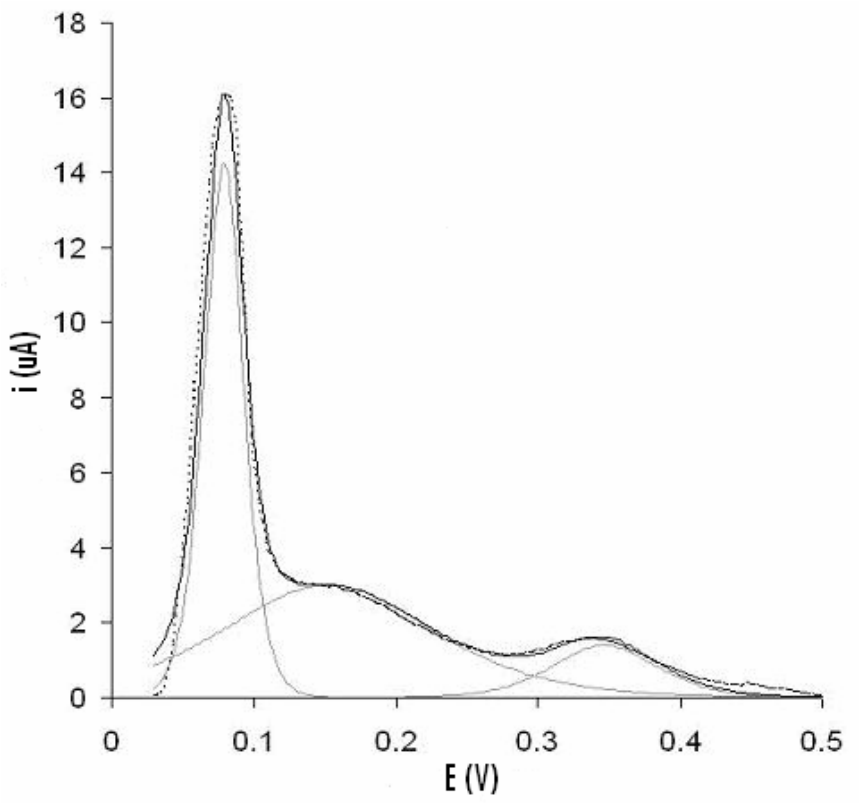

Figure 4.22 Peak fit for 100 ppb As(III) stripped in 1 M HCl (no hydrazinium chloride). Grey - individual simulated peaks, black - composite of fitted peaks, and dotted - the experimental voltammogram

By comparing the calibration plots from direct peak height, area and deconvoluted method, the deconvoluted method clear gave the most reproducible results. Figure 4.23 shows the full calibration from 10 to 1100 ppb. There is an apparent linear fit from 10 up to 100 ppb, which can be attributed to saturation of the reversible active sites. Also the peak shape for As(III) shifts and broadens around 100 ppb as is implied in Figure 4.21.

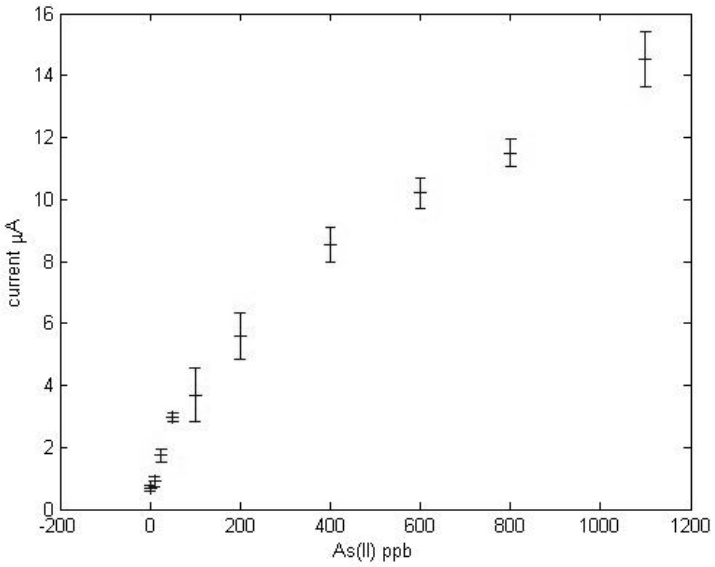

Figure 4.23 Derivative logistic curve fitted As(III) stripping calibration curve for 10 to 1100 ppb As(III) in 1 M HCl

The lower range was used to estimate an effective limit of detection, as shown in Figure 4.24. Considering that the blank is not at zero (caused by a slight upward curve in the baseline), and taking the baseline height plus three times the standard deviation at 50 ppb a value of about 10 ppb was found. With the elimination of the interference, the detection limit would be lower.

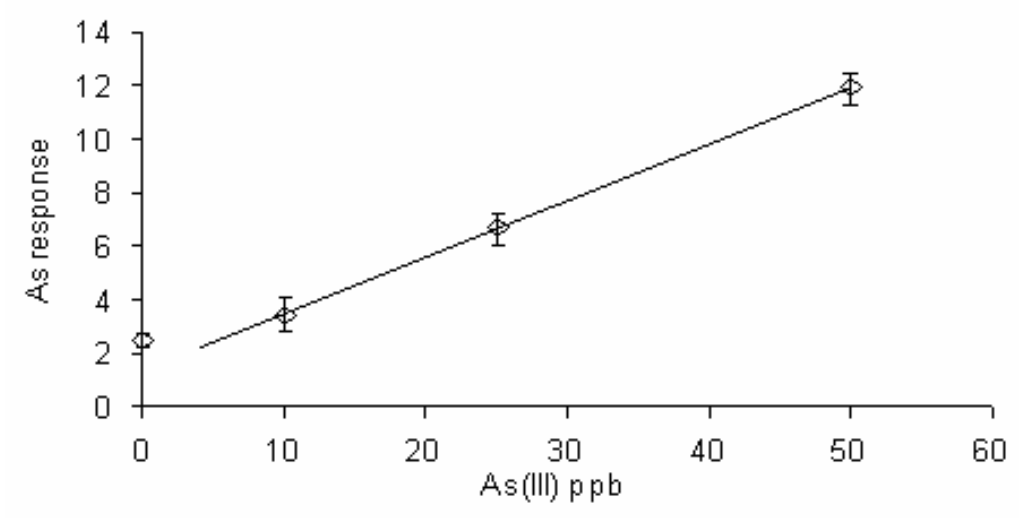

Figure 4.24 Calibration curve for 0 to 50 ppb As(III) in 1 M HCl (no hydrazinium chloride) measured by the height of the fitted As(III) peak

It is difficult to envisage an analysis technique that would better assess the As(III) concentrations. Voltammograms do not provide the rich complementary information which statistical techniques, such as principal components analysis or neural networks, could take advantage of. The limiting factor for software based analysis must be the quality of information received by the potentiostat. Therefore the critical factor is the function of the analytical transducer.

4.4 Discussion

4.4.1 Electrochemical performance of Sensors

No useful electrochemical response for potassium ferrocyanide or metal ions could be found, on the electrodes of batch D^+, due to the presence of a large background peak. On inspection, the only difference compared with Batch A or C, was cracking in the insulation layer, as shown in Figure 4.2. Although the cause of the cracking is uncertain, it may be associated with the large interference peak. For example, cracking may indicate gas or solvent generated by the carbon underneath during curing, either physically or chemically damaging the coherence of the insulation polymer. It is possible that an electrochemically active compound was present in one

or more of the sensor inks, remaining as the result of incomplete polymerisation or polymer crosslinking. None of the pretreatment procedures tried mitigated the problem. Therefore, without a suitable method to probe further the electrode surface, it was necessary to shelve the batch D^+ electrodes. (The batch was later used for spectroscopic experiments in Chapter 5.)

DuPont provided further batches (Batches 1-4 and batches AO, BO, AI and BI). These batches did not demonstrate the large background peak of D^+ and responses were obtained for arsenic and mercury (between 100 and 800 ppb) in 4 M HCl. However, the incidence of background peaks at 0.1 and 0.4 V (AgAgCl in 4 M HCl) caused problems with reproducibility, overlapping the arsenic and mercury peaks. Also, the shift in background current from test to test was noticeable. As a result, calibration curves were poor. Again a number of pretreatments were attempted to improve the stability including electrochemical pretreatment none were found to give significant improvements.

High HCl (sometimes with Cl^- salt) is typical for stripping determination of arsenic on gold electrodes (Huang *et al.,* 1988, Sun *et al.,* 1997, Huang and Dasgupta, 1999) because of improved electron kinetics and peak magnitude (Caviccioli *et al.,* 2004 and Munoz and Palmero, 2005). Irreproducibility has been blamed on film dissolution on gold film electrodes Sun *et al.,* (1997) due to $AuCl_4$ formation; on As(III) oxidation by Cl_2 or HClO generated at the counter electrode during deposition (Saluan *et al.,* 2007); and more generally on oxygen in non deaerated solutions. But peaks due to interference in laboratory prepared solutions are not mentioned in these papers. Obviously interfering metals can be introduced with real samples and care is taken to deal with these by choice of sample treatment, ion exchange, electrolyte or deposition potential. High HCl solutions 2 – 7 M have been chosen to avoid Cu(II) interference (for example Huang *et al.,* 1988). Kopanica *et al.* (1998) noted an interference coming form the electrode cell for Cl^- concentrations much above 0.2 M. The interference, sharp spike at 85 mV and broad peak around 0.4 V, was not identified.

It is difficult to reconcile the results of Cooper (2004) and Bolbot *et al.,* (2007) using these same DuPont sensors. Within Cooper's thesis, background phenomena are acknowledged present in the voltammograms with Cl^- electrolytes with or without deposition phases and not explained beyond their link with Cl^-. But these peaks are not present for As and Hg voltammograms shown from which calibration curves were drawn. As a result calibration curves are much more precise.

It was for this reason that the calibration curves using batches 1-4 were repeated by a colleague using independently prepared solutions, consumables, in a separate laboratory and with different Autolab equipment, to rule out, for sure, any introduced interference. The results were shown in Figure 4.6 and Figure 4.7. Whilst there was some improvement in the calibration in Figure 4.7 the same background processes were visible.

A number of trivial and non-trivial issues can occur whilst acquiring data: sometimes insertion into chip alignment is poor and carbon contact shorts the chip pins; occasionally one or more tracks fails to contact the pin; sometimes abrased carbon ink powder accumulates in the chip eventually short circuiting. Poor reference electrode contact or electrolyte in the chip itself can cause particular problems since the effect on the voltammogram is not immediately obvious. Unknown effects, such as solvent adsorption from the ventilation systems may change the reactivity of the gold surface. Operator error may incorporate the wrong sample. Inevitably, the output data is screened for outlying results, the criteria for which is subjective.

Disguarding data when the voltammogram shows resistive behaviour or electrical noise is unambiguous. But, when one or more electrodes fails to pickup an analyte whilst keeping reasonable background currents is harder to justify. The criteria used by Cooper (2004), Cauchi (2005), or Bolbot *et al.* (2007) are not clarified. It should be conceded that such criteria when proving the principle or a technique (appropriate to Cooper (2004)) would be less stringent than when attempting to commercialise a technique (appropriate to this thesis).

Thus it is not clear why the results of Cooper were so much more reproducible than the results here, but voltammogram selection criteria may be a part of the answer. However looking at the data in this thesis it is difficult to envisage removing only a small number of voltammograms from the calibration set and obtaining results equivalent to Cooper (2005). There must have been a smaller level of interference before.

Now, even if an interference-free batch of DuPont sensors were to be obtained, without knowing the cause and possibility of inference recurrence, commercialising the sensors could not be justified.

Also for commercialisation by application to drinking water the sensor needs to function below 10 ppb As. A substantial improvement in reproducibility and removal of interference would be needed with this design.

4.4.2 Electrolyte effect

Rather than pursue calibration plots for As and Hg again, the interference was studied itself. With multiple scan cyclic voltammetry, the distinction between transient blips and persistent interferences would be seen. In addition the temporal behaviour of peaks would be observed and the peak shape would be used to distinguish surface adsorbed or soluble species. Alternative electrolytes and cleaning procedures would give further indications as to the chemistry.

The data clearly indicated that a serious interference appeared with screen-printed electrodes in high Cl^- solutions (Figure 4.10, Figure 4.11, Figure 4.14 and Figure 4.15), whilst being absent from a standard cell with gold working electrode (Figure 4.9). It appears that a similar reaction is occurring with the bromide ion (Figure 4.12) and there is evidence for the iodide ion also (Figure 4.15 bottom left). The Cl^- ion interference was present in non aqueous solvents containing LiCl (Figure 4.14 and Figure 4.15). There were three distinguishable peaks. The largest 0 V (primary) peak was only present for high Cl^- concentrations (> 2 M), the peak generally increases

with scanning. The spike peak was seen at conentrations as low as 1 mM Cl^- (Figure 4.19). The secondary peak was also visible appeared to shift with Cl^- ion concentration between 1 and 100 mM (Figure 4.19). The spike peak tends toward stable peak height with scanning, sometimes decaying, but rarely becoming large. The secondary peak does appear to increase with scanning for higher Cl^- ion concentrations ($Cl^- > 1$ M). Similar characteristics seem to be present with the Br^- ion electrolyte

This interference was not observed with non halide anion electrolytes. Whilst highly concentrated oxidise acids such as HNO_3 could digest the electrode materials scanning in 1 – 4 M HNO_3 (also $HClO_4$, H_2SO_4) was generally stable with currents generally below 1 µA during the whole 40 scans. A different interference peak was seen with nitrate, perchlorate, phosphate and sulphate type electrolytes (Figure 4.13). This erratic peak would dissipate after 2 – 3 scans. These electrode sensors can withstand strong acids, maintaining a stable and low background current.

With a heterogeneous mixture of materials comprising the sensor it is difficult to ascertain the cause of these peaks. However, it was shown that the interference was soluble (Figure 4.20), which provides the possibility to accumulate the interfering material on a cleaner surface such as a platinum foil piece (see Section 5.2.7). The interference could be mitigated with a Nafion membrane on the working electrode (Figure 4.16). Since Nafion excludes negative ions, the interference is probably negatively charged. Thus it can be hypothesised that the interference contains one or more Cl^- ions, in a negatively charged soluble complex.

DuPont electrodes of the same design but with ceramic gold ink (LF141) and alumina substrate, also demonstrated a number of interferences (Figure 4.17). In Cl^- solutions certain peaks were characteristic of the polymeric electrodes. Extra sustained peaks were seen in acidic solutions. These kinds of formulations are known (for example Lane *et al.,* 2000) to contain metals and metal oxides helping to adhese the gold powder. There is a high proabability of one or more electrochemical interactions of these components. The tentative conclusion is to extrapolate the results from LF141 to most ceramic gold inks (sol-gel based compositions would not generally contain these components: e.g. Wang *et al.,* 1997a). With the stability in strong acid solutions the polymer formulation (BQ331) looks more promising than the ceramic formulation (LF141), assuming the interference can be identified.

4.4.3 Arsenic determination in 1 M HCl

Inclusion of Hydrazinium Chloride

Although Cooper (2004) and Cauchi (2005) included hydrazium chloride with As(III) to prevent oxidation according to (Sadana, 1983, Jurica *et al.,*1999, Svancara *et al.,* 2002, Sun *et al.,* 1998), the effectiveness of this is questioned in the literature (Saluan *et al*., 2007) since traces of strong oxidants oxidise As(III) regardless of hydrazinium chloride many authors do not use a stabilisation agent (Huang *et al,* 1988, Huang and Dasgupta, 1999, Feeney and Kounaves, 2002). Salaun *et al.,* (2007) list a number of causes, such as oxidation caused by dissolved O_2, or Cl_2 and HOCl, generated at the counter electrode; in general, the As oxidation state is controlled by kinetic factors and is not in thermodynamic equilibrium (Cullen and Reimar, 1989). Therefore, it is not clear whether hydrazinium chloride is sufficient.

Ercon and DuPont Gold Ink

Having observed sensor performance up to 6 M HCl Noh (2005) chose a 1 M HCl electrolyte. Clearly, the same kind of interference had been encountered with recognisable spike peak between 0.05 and 0.1 V (vs Ag/AgCl) and primary peak for

high HCl concentrations. The secondary peak visible on the DuPont sensors does not appear to be visible with the Ercon gold ink. In general, the Ercon gold ink suffers the same interference but appears to exhibit a more stable baseline response than the DuPont sensors.

Noh's calibration curve was effectively repeated in this work (Figure 4.23). However, a deconvolution process was needed to extract peak information (for example Figure 4.22) for lower concentrations. An approximate 10 ppb limit was found (Figure 4.24). Whilst this technique is sensitive and reliable interference to Cu(II) is problematic. A method like ion exchange would be needed for sample preparation (Cavicchioli *et al.,* 2004 and Munoz and Palmero, 2005). The Cl^- interference is still a severe limitation.

4.5 Conclusion

A clear persistent interference has been identified causing difficulty with arsenic and mercury determination using gold screen-printed electrodes. This interference has been seen with both DuPont and Ercon gold inks. The problem varies with Cl^- ion concentration; it was not possible to achieve a meaningful calibration plot in 4 M HCl using the method of Cooper (2004) and Bolbot *et al.,* (2007).

Unfortunately, by consensus in the literature (Arnold and Johnson, 1967, Munoz and Palmero, 2005), Cl^- ions are necessary for good As(III) stripping characteristics. The use of a 1 M HCl electrolyte provided a reliable calibration for As(III) down to 10 ppb (limited by the interference), but this electrolyte is less convenient when measuring arsenic in the presence of copper (Noh, 2005, Song *et al.,* 2006, Huang and Dasgupta, 1999, Huang *et al.,*1988, Jagner *et al.,*1981).

The emphasis with this work is to create a commercially viable sensor. To do this it is necessary to identify and remove the interference. More than one approach can be used to this effect. One: attempt to make a gold (or carbon) ink with controlled components to identify which are reactive. Two: study the electrodes directly with a

number of spectroscopic techniques with the intention of identifing the problem directly.

Chapter 5 Spectroscopic Investigation of Screen-printed Inks

5.1 Introduction

This Chapter continues from Chapter 4 where a serious interference had been observed preventing the acquisition of calibration plots for As(III) and As(V). To understand the interference, the problem required breaking down. The analytical approach is not easy since the ink formulations are proprietary. Clearly, something in the ink or sensor design causes irreproducibility which could be either avoidable or inherent.

A 'two pincer' approach was adopted to tackle the lack of understanding of the electrode behaviour. On the one hand, ideally produced electrode compositions with a minimum of components could be used as standards for adding further chemicals suspected of inducing interference. On the other hand, analytical methods could be used to probe the electrode surface to identify reaction products, directly.

Analysis of the electrode material properties has the side effect of revealing ink properties – which in turn informs electrode ink formulations which can be used to test theories of interference.

5.1.1 Hypothesis of Voltammetric Induced Polymer Breakdown

Few studies could be found examining the electrochemically induced breakdown of polymer materials. Although, for example Usmani (1994) noted that the choice of polymer for glucose sensors had to be screened to avoid reactive groups.

Simple organic molecules (such as methanol or formic acid) can electrochemically react at low overpotentials (less than 1 V vs NHE) on highly catalytic surfaces when in acidic conditions (Hamann, 2007). Some of these processes lead to the formation of passivation layers.

Polymers containing redox active groups have been studied for the effect on voltammetric profiles. For example, Flanagan *et al.* (1978) looked at polyvinylferrocene, which had essentially the same voltammetric characteristics as ferrocene. Interactions between adjacent ferrocenes in the chain can affect peak shape.

Some polymers, including methylmethacrylates can be polymerised by anions generated electrochemically (Hamann *et al,.* 2007). Polyaniline and polypyrrole can also be polymerised using cyclic voltammetry (for example Borole *et al.* 2002) giving large progressive peaks.

Pud (1990) noted that solid phase polymer dielectrics may be electrochemically reduced or oxidised along a thin surface layer that lies within the electrochemical double layer along the polymer-electrode-electrolyte three phase interface. However, for a conducting polymer the reaction is not confined only to the polymer-electrolyte interface.

Barker, *et al.* (1978) showed that polytetrafluoroethene was reduced when in contact with a platinum wire at – 2 V. Reduction occurred forming a conductive carbon material spreading out from the area of contact. However the reduction was limited as the potential at the horizon of reduction rose above -1.7 V. The electrolyte was tetrabutylammonium fluoride in dimethylformamide (DMF).

Navratil *et al.* (2003) used a composite gold powder/ polymethylmethacrylate electrode. Unidentified interference was found when Cl^- exceeded about 0.15 M.

Another issue to consider is the possibility of polymer additives. Pfaendner (2006) reviews the plastics industry and the essential role of additives such as antioxidants, heat stabilisers and, light stabilisers. Polymerisation and depolymerisation processes often involve the propagation of free radicals which can be initiated, for example, by heat, UV or chemical treatment. The addition of scavengers to stabilise the free radicals can prevent propagation and progressive polymer chain scission.

Hindered amines and phenols are phenols and amines with steric hinderance to the primary functional groups. These groups scavenge free radicals in danger of damaging polymer integrity. Polypropylene (used in pipette tips and sample tubes) needs stabilisers when subjected to heat treatment during manufacturing.

Liquid phase compounds are often added to brittle plastics such as PVC to impart flexibility, such as long chain hydrocarbons. Concern has been raised over the ability of some additives to leach from PVC products.

The production of some plastics includes low level use of metal catalysts such as antimony oxide in PET or otherwise Cu, Fe or Pt. Metallic and carbon fillers (such as powders used in screen-printing inks) tend to adsorb mobile additives to surfaces preventing the functions of those additives. Due to the typical toxicity of monomer compounds such as the vinyl types commercial production of plastics is required to avoid the presence of these materials (Pfaendner, 2006).

Clearly, many compounds might be found in prepared polymer electrochemically active. Ni *et al.* (2000) studied the electrochemical activity of anti-oxidants including butylatedhydroxyltoluene (BHT) in perchloric acid mixed with methanol. Peaks were measured between 300 and 1100 mV (vs Ag/AgCl).

Chemical degradation may lead to electrochemically active products. Ravens (1960) showed that PET fibres were hydrolysed by HCl acid solutions by attack of hydrogen ions on the ester groups. The rate of decomposition of the fibres was found to be proportional to the partial pressure of the hydrochloric acid. Molecules of HCl entered to the polymer fibres and disassociated according to the dielectric properties of the fibre. Once ionised the H^+ and Cl^- could attack the ester groups. The breakdown was thought to include multiple pathways, which would include carbon radicals and other groups, potentially electrochemically active.

The review of literature here appears unsatisfactory or incomplete; if polymer degradation occurred this easily by electrochemical means then it would have been the subject of much research, with review articles and descriptions of mechanisms.

The possible mechanism for polymer breakdown was based on several points: that the main difference between the screen-printed electrode and standard gold electrode is the presence of the polymer with a high area surface contact with the powder; that the interference of the primary and second peaks in high Cl^- electrolytes is accumulative; and that screen-printed electrodes, in the literature are rarely used with such aggressive electrolytes as 4 M HCl.

On the other hand, organic compounds tend to be less aqueous soluble and non-conducting if adsorbed to the electrode surface. For the hypothesis of polymer breakdown to be feasible the electrolyte anion effect would be needed to facilitate the reaction. Having seen that the DuPont sensors show interference with neutral or acidic chloride, bromide but not either neutral or strong acids of nitrate, perchlorate or sulphate anions, a polymeric reaction that explains the interference would be needed, including the halide ion.

It should be noted that the standard electrodes (BAS, West Lafayette, USA) used in this project were housed in polychlorotrifluoroethylene casing. Presumably if the route of attack during polymer degradation was on carbon chains these electrodes should also be affected. However this design has a much lower degree of contact area between polymer, electrode and electrolyte than does a screen-printed electrode. Also, the chloro and fluoro groups could act to protect the carbon chain backbone.

5.1.2 Techniques for Studying Electrode Surfaces

Many techniques have been used either to study electrode reactions *in situ* or to study the change in state (Hamann *et al.,* 2007). In principle any reaction product or sample of electrode itself could be isolated and subject to an array of analytical tests. With the exception of proprietary systems such as screen-printed electrodes, for electrode

surfaces (such as monocrystalline or polycrystalline, metallic or carbon surfaces) the identity of the compositional materials, at least, is understood. Surface structure, ordering, active sites, surface functional groups, and contamination can be less certain. Electrode inks are unusual in this context since the identity of the components is often unknown.

XPS has been used with screen-printed inks both to study the film (for example, Gilmartin *et al.,* 1995b, Amador-Fernandez *et al.,* 2001, Gao *et al.,* 2003) and electrochemical reaction mechanisms (for example, Song *et al.,*2006a,). For example, Gilmartin *et al.* (1995b) checked the oxidation state of Co(II) added to a screen-printed ink which was initially in the + 2 valence state and then in the + 3 valence state after oxidation. Raman Spectroscopy has also commonly been used (for example, Prasad *et al.* 2007, Song *et al.* 2006a) to determine reaction mechanisms, and phase transitions in bulk film materials (for example Zhang *et al.,* 1994)). Electron Spin Resonance is effective for measuring transient radicals generated during a reaction (Hamann *et al.* 2007). GC-MS and HPLC having been used to confirm the nature of analyte reactions occurring at a sensor surface (Honeychurch *et al.* 2004).

Laser induced breakdown of (high temperature) screen-printed electrodes coupled with spectroscopy (a type of atomic emission spectroscopy) has been used to identify the elemental composition, made by comparison with standard materials (Amador-Fernandez *et al.,* 2001).

Scanning electron microscopy (SEM) has often been used with the development of screen-printed electrodes to look at the surface integrity and compactness (Gilmartin *et al.* 1995a, Cui *et al.,* 2001, Gao *et al.,*2003). SEM was used to study the structure of Ercon gold ink (R-464 DPM-78) by Noh and Tothill (2006). The image showed gold powder aggregates 1 – 10 µm across. Also the SEM EDX showed the expected presence of Au, C and O. The polymer used in this ink is a polyester according to the information provided with the ink (Ercon, Inc., Redwood City, USA).

5.1.3 Nuclear Magentic Resonance (NMR)

NMR is based on the excitation and time-resolved relaxation of nucleic spins via the application of radio frequency electromagnetic radiation in very strong (> 1 Tesla) magnetic fields (using low temperature super conducting magnets). The first target would be hydrogen spectra since hydrogen has a simple spin moment and is found in most materials. The usual isotope of C (98.9 % natural abundance) has no spin, so that analysis of this element requires measurements of either residual (1.1 %) or doped C^{13}. Other elements are less common, but possible. As with FTIR, Fourier transform NMR can be used to produce 1 dimensional spectra indicating the presence and quantity of various organic groups made possible by the coupling of the nuclear spins within the molecular structures. With NMR, 2 dimensional experiments using time resolved observation of peak relaxation provides further information about the proximity of the functional groups seen in the 1 dimensional spectra (Horst, 2005). However, like FTIR, NMR is not associated with trace level sensitivity. Also, although the analysis of solids is possible via the technique of magic angle spinning, measurement in solution phase is more common. This is because the liquid phase allows unhindered excitation and relaxation of the analytes in solution. As the viscosity increases the peak widths increase losing the fine detail. Thus even the analysis of polymers in solvents can be difficult, as the viscosity tends to increase (Horst, 2005).

5.1.4 Fourier Transform Infrared Spectroscopy Attenuated Total Internal Reflectance (FTIR ATR)

Infrared spectroscopy is a powerful technique for studying compositional and structural features of organic and inorganic materials. Also it is simple to implement, but sensitivity of trace compounds is limited (Gunzler and Gremlich, 2002). Infrared spectroscopy is based on the interaction between infrared light and materials. The light has suitable energetic properties to induce excited vibrational states in molecular bonds. Some organic groups can be identified by the energy spectra of absorption, for which there exist tabulated lists of examples with which to compare unknown materials (Guinzler and Gremlich, 2002). Many simple materials can be identified by

the spectra in the mid IR region (400 to 4000 cm^{-1}) via comparison with known standards (Guinzler and Gremlich, 2002). The simplest methods (schematically) include measuring the infrared passing through a material not absorbed (transmission spectroscopy), or the IR light reflected from a material (diffuse reflectance).

5.1.5 X-ray Photoelectron Spectroscopy (XPS)

X-ray photoelectron spectroscopy (XPS) measures the electrons emitted after the sample is irradiated with X-rays. The energy of the emitted electron is related to the X-ray energy minus the binding energy of the electron in the atomic shell. The advantages of this technique are the thin surface penetration (1 – 10 nm), effective sensitivity of about 0.1 % and ability to do a wide elemental analysis (Seah, 1984). Modern XPS is usually synonymous with Auger Electron Spectroscopy (AES) because the same equipment stimulates both effects.

XPS can perform some polymer analysis, for example Tan *et al.* (1993) used XPS to look at the oxidation states of C, O and F due to the surface treatment of Teflon. But the technique is more effective for general inorganic characterisation, for all elements with mass greater than lithium.

5.1.6 Screen-Printed Formulation Basics

In principle the electrode inks are prepared with a polymer, powder and solvent. However, before this fact was appreciated, one experiment conducted for this thesis (included in Appendix A4) explored a different approach. A method by Huang *et al.* (2003) took advantage of the low melting temperature of size-controlled gold nano particles using a preparation described by Hostetler *et al.* (1998). Following the method a melted layer of gold was achieved on top of carbon screen-printed electrodes (as described in Appendix A4). The prepared electrodes did not show a response to As. Comparison using a microscope clearly revealed the particulate nature of the BQ331 surface, indicating that the melted gold approach was not the method used.

Although novel, such a method had several problems including the need to add a reagent for viscosity and/or adhesion to the ink to allow screen-printability, or at least chemical modification to stabilise the particles in solution (to provide uniform dispersion). A considerable cost (in terms of gold salt) would be incurred before consistent results could be achieved, the end result probably being novel and not commercial. On the other hand Gwent Electronic Materials, Ltd (Pontypool, UK) advertise (www.g-e-m.com, accessed 2008) 'organo-metallic' inks. The description of stabilised nano particles melting and coalescing at low temperature matches the method here. The only explicit formulation is silver based, but other noble metal inks could be made with custom orders. This would be a better approach to explore this option.

In principle the electrode inks are prepared with a polymer, powder and solvent. A review of carbon composite electrodes by Alegret (1996) shows that equivalent powder-polymer electrodes including the use of poly epichlorohydrin-co-bisphenol (epoxy), polytetrafluoroethylene (Teflon), polyols crosslinked with isocyanates (polyurethane) and polyester are commonly used. The methods of sensor production can include melt and solvent processing; high pressure and sintering; or *in situ* polymerisation around electrode powders. Often biomaterials such as enzymes are included which preclude the use of the electrode in non neutral buffered conditions.

Whilst hydrophilic polymers have been used for screen-printed electrodes (for example, Newman *et al.*, 1995) these are problematic since they disintegrate in aqueous solution. A systematic way of obtaining screen-printing formulations was not found. However, a number of, possibilities were obtained incidentally in the literature. Screen-printed formulations using organic based solvents are described such as poly vinyl, methacrylate resins (Towlson, 1997), solvent processable fluoro resins (Dorfman, 2005), general array of possible polymers (Chan, 1997, Chan, 1998, Williams *et al.,* 2001, Chan and Kuty, 2000, Tierney, 2006).

Screen-printed compositions used for making non biosensor applications such as touch membrane switches show the typical polymers having the most suitable

qualities for facile screen-printing (Dorfman, 2005), including polyester, polyvinyls and polymethylmethacrylates stating the allowable range of viscosity and recommended proportions of polymer solution and carbon and or silver fillers. Chan and Kuty (2000) describe formulations for screen-printable electrodes and include a range of further specific polymers with beneficial characteristics. Silver and graphite (Chan, 1997 and Chan, 1998), noble metal coated graphite (Williams *et al.,* 2001), platinised and rhodinised carbons (Chan and Kuty, 2000, Tierney, 2006) for medical and iontophoretic electrodes have been described.

5.2 Materials and Methods

5.2.1 Materials

General descriptions of DuPont sensors, *in hous*e printed electrodes and *in house* ink formulations are given in Sections 2.3 and 2.4. Amongst the batches tested, were 4 batches provided June 2006, testing two new carbon inks R430 and R471, and a new silver ink E107255-45B, the composition of these batches is given in Table 5.1.

Table 5.1 DuPont Sensors Received June 2006

Batch	Insulation	Carbon	Reference
JA	E1077257-1	BQ225	5874
JB	E1077257-1	BQ225	E107255-45B
JC	E1077257-1	R430	E107255-45B
JD	E1077257-1	R471	E107255-45B

5.2.2 Extraction of Inks

Methods for the extraction of inks are given in Section 4.3.2. Since there remained large numbers of sensors from DuPont batch D^+ which showed no electrochemical usefulness (as described), these sensors were deemed useful for spectroscopic method development.

To measure the approximate weight of gold powder, 8 gold strips with area coverage 1×0.15 cm^2 of BQ331 from batch D^+ were added with about 1.5 ml of acetone to a 2

ml centrifuge tube. A 5 min extraction with stirrer/shaker, periodically checking for detachment, shifted all the gold from the strips. After settling the acetone was carefully adsorbed off, the last portion was allowed to evaporate. The strips were removed with tweezers. The gold powder formed a coalesced lump which was removed with a stainless steel spatular tip onto a pre weighed aluminium foil piece (approx. 2×2 cm^2). The gold powder plus foil piece was then weighed on a R160P Semi-Micro Balance (Sartorius, Epsom, UK).

5.2.3 FTIR Study of Extracts

Failing the use of direct transmission spectroscopy or diffuse reflection, attenuated total reflectance spectroscopy (ATR) can be used. This method has several advantages (Fahrenfort, 1961). Since transmission and reflectance based methods are highly dependent on sample thickness or dispersion affecting the amount of incident IR light adsorbed and transmitted.

For this technique, the polymer solution was cast onto a crystal surface (typically ZnSe). As with simple transmission spectroscopy the absorbance of infrared is measured but with the ATR technique a single beam of light is reflected off the sample surface many times whilst contained within the ZnSe crystal, as shown in Figure 5.1. According to the polymer film-crystal boundary penetration of the light is of order about 1 µm with each reflection, according to the optical properties of the boundary and the angle of incidence of the light through the crystal. Thus, the transmission to absorbance balance is well controlled by the experimental design (Fahrenfort, 1961). Also the ZnSe is stable and water tolerant (unlike KBr) so there is less chance of problems occurring in the method. The ZnSe is susceptible to acidic attack. Other ATR crystal surfaces exist including Si and Ge although they were not used in this study.

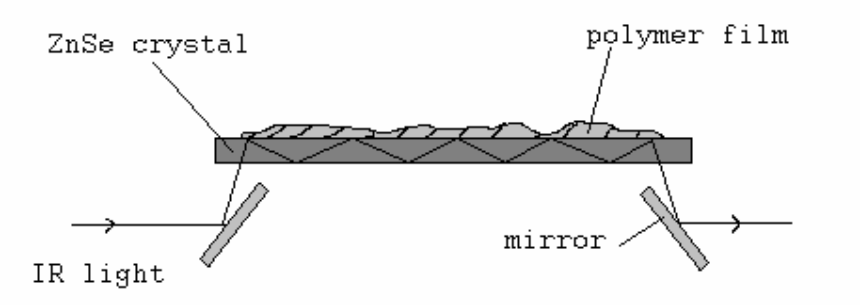

Figure 5.1 The infrared light path with the FTIR-ATR technique with an ink extract polymer sample

CO_2 and H_2O affect the basic infrared signal. H_2O affects the signal both as vapour and liquid on the surface. Although the sample chamber can be purged with N_2 it has been sufficient to use background corrections (as is standard with the FTIR operating procedure) to eliminate most of the interference. Peaks caused by the changing levels of CO_2 and H_2O even with background corrections, are common as positive or negative peaks due to ventilation and people in the vicinity. Acetone itself causes strong peaks in the spectrum (CH_3 and C=O), so sufficient time is needed for evaporation.

The FTIR was set to take 32 scans, with approximately 1 second exposure per scan for a range from 700 to 4000 cm^{-1} (typical for mid IR range). The output from the infrared source is typical shape of black body radiation: the signal is strongest in the mid-infrared region and falls off at the extremities of wavelength. The range detected is limited depending on detector sensitivity and possible absorption of light by the crystal The ATR plate is first cleaned with acetone and tissue (lint free), allowed to dry briefly (1-2 min) then a background spectrum is taken. Then the prospect sample is added to the plate and the sample measurement is conducted with the result shown as a ratio of the sample measurement to the previous background measurement. Therefore for a sample blank the IR spectrum is at ratio of about 1 across the wavelength range. With high adsorption, the ratio will drop with a limit at zero when no light transmits – not usually a problem for ATR technique as with transmission spectroscopy (Fahrenfort, 1961). 50 µl of sample solution was found to be sufficient to cover the crystal plate with the sample.

Spectra were acquired for controls (using batch D^+) with acetone alone, acetone and PET, acetone, PET and carbon (BQ221), acetone, PET, carbon and gold ink sequentially. Generally two repeat measurements were taken for each solution (cleaning the crystal in between with acetone/paper towling). Controls were used only to establish validity of the technique. Otherwise the technique was repeated as standard for all further tests.

A comparison was made of BQ331 spectra from different batches. In addition, one demonstration sample (sample of BQ331 printed onto PET sheet by DuPont to demonstrate the product adhesion abrasion resistance and conductivity to new customers) was used, the significance being the absence of carbon under the substrate. Similarly, carbon ink spectra from multiple batches were compared using longer 1 – 2 hr extraction times, where needed.

Spectra for the Ercon and Gwent gold polymeric inks were acquired by selecting opportune pieces where the gold ink had been smeared directly on the PET substrate from samples printed by M. Heurich for an unrelated biosensor project on immunosensors.

For study of polymer powders such as polymer X, a small quantity of powder (several mg) was added to 1.5 ml acetone in a 2 ml centrifuge tube and shaken/stirred for 5 min.

For interference analysis tests, individual electrode strips (with surface area 0.15 cm^2) of DuPont sensors were added to a 200 µl centrifuge tube with about 150 µl of acetone. The tubes were subjected to 5 min stirring/shaking. Spectra were acquired after 50 µl of extract sample had been applied to the FTIR ATR trough. For the interference tests, spectra for the gold working electrode could be compared for sensors unused and sensors electrochemically cycled prior to extraction.

5.2.4 NMR study of Extracts

For the measurement of proton spectra the solvent used must contain no H realised by the used of pure deuterated solvents. Deuterated chloroform was used since only one H per molecule needs to be replaced (acetone has six hydrogens) which is reflected in the low cost compared with other dueterated solvents.

For NMR analysis, samples were prepared from 8 pre-electrochemically cycled strips (CV parameters Table 2.3, in 4 M KBr) and 8 fresh strips of batch AO sensors. The 8 cycled strips were extracted into about 1.5 ml dueterated chloroform in a 2 ml centrifuge tube for about 5 min. The 8 non cycled strips were extracted similarly. Also, for comparison, about 2 mg of polymer X was dissolved in 2 ml deuterated chloroform in a poly propylene tube. Extraction used automatic stirring/shaking. The sample tubes for the NMR consist of about 3 mm diameter glass tubes, to which the extract was added.

5.2.5 FTIR reflectance Spectroscopy

The ATR method is not always convenient. The ZnSe crystal is not stable in strong acids. To attempt to test for the BQ331 product (or degradation product thereof), the aqueous extract was used. But a salt such as NaCl will leave a large quantity of deposit after evaporation. HCl will evaporate but interact with the ATR trough. Another method was to attempt reflectance spectroscopy. Aluminium foil could be used but also reacts with HCl. A piece of platinum foil was found to overcome these difficulties. Having been exposed to the DuPont sensors, various concentrations of HCl (and other aqueous electrolytes) were added dropwise (approx 10 µl) to the platinum foil on top of a hot plate (about 100 °C). The temperature accelerated evaporation leaving a residue on the platinum. The schematic for the measurement process is shown in Figure 5.2. The system is measuring absorption due to surface residue. The same range of wavelengths and measurement settings were used as with FTIR ATR. However, the detector was a N_2 cooled MCT detector.

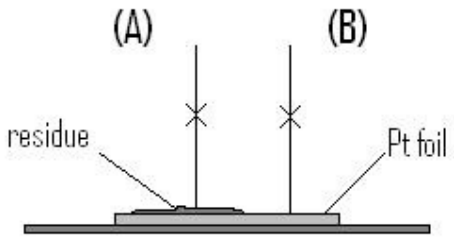

Figure 5.2 Schematic for reflectance spectroscopy using Pt foil. Absorption due to residue (A) is compared with background measurement from foil alone (B).

5.2.6 Preparation of *In House* Inks

The materials are listed in Section 2.2.4. Polymers were prepared to about 25 % in solvents. Typically, 12 g of solvent was added to 4 g of polymer. Usually the solvent had to be mixed manually (a 1 ml polypropylene pipette tip was used) since the solution would become too viscous to use a magnetic stirrer. The solution would have to be left to dissolve for several hours and then mixed again for several days until a clear solution was achieved. Bubbles formed during stirring would disperse after several hours at rest. Elvacite 2048 and PMMA were dissolved in diethyl oxalate. UCAR VAGH was dissolved in γ-butyrolactone. Either γ-butyrolactone or diethylene glycol monoethyl ether was suitable for PSAN and PVDC-co-PAN polymers. PVDF-co-HFP was dissolved either in acetone or γ-Butyrolactone. PVDF-co-HFP in γ-Butyrolactone gelled below 90 °C so had to be kept on a hotplate whilst mixing and used.

About 0.1 g of solvent/polymer mixture was added to a small polypropylene cap and mixed with about 0.1 g of carbon powder (conducting grade 325 mesh, 99.9995 % pure), and mixed with a pipette tip, as shown in Figure 5.16. It was not possible to prepare precise quantities due to viscous nature of the dissolved polymer.

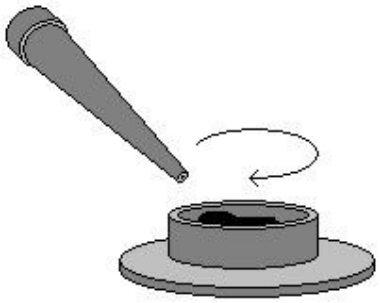

Figure 5.3 Pipette tip (200 µl) and polypropylene cap (from 2 ml centrifuge tube) to mix small quantities of ink

For the fluoro polymer the cap was kept on a hot plate at 90 °C.

The substrates were prepared with design in Figure 2.1 using PET substrate, Electrodag carbon and silver inks. No insulation ink was printed. The same pipette tip was used to apply the mixed ink on top of screen-printed carbon tracks. The electrodes were then fired at 120 °C for about 20 min. For the fluoro polymer the electrodes were placed on the hotplate at 90 °C to apply the ink and then fired in the oven at 150 °C.

5.2.7 XPS direct electrode analysis

Choices for sample preparation included dissolution of the polymer in acetone and collection of the deposited gold particles. The powder would need immobilisation for which imodium foil could be used (being soft). The other option was to test the sample surface directly. However direct analysis involves a contributing signal for many components such as the polymer, flow agent, curing agent, gold itself and the surface modifier on the gold particles. Direct analysis had the advantage of simplicity and was thus preferred.

For XPS preparation 4 DuPont electrodes (batch AO) were electrochemically cycled in 4 M KBr (CV parameters Table 2.3) for 40 scans generating large interference. Another four uncycled electrodes were also selected. In addition a piece of platinum foil, first cleaned in acetone and 4 M HCl was electrochemically cycled (CV

parameters Table 2.3) in proximity to a DuPont sensor, as shown in Figure 5.4. It was necessary to use foil since the standard electrodes used in this project, with a long cylindrical design could not fit in the XPS sample chamber.

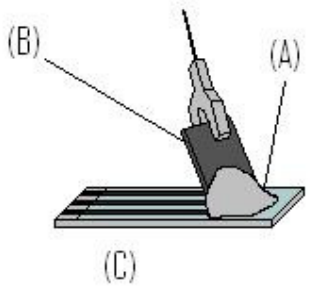

Figure 5.4 Schematic (A) 4 M KBr electrolyte, (B) Pt foil working electrode connected with crocodile clip and (C) DuPont sensor with active counter and reference electrodes

The samples were then delivered to Dr M. Kershaw (School of Applied Sciences, Cranfield) wrapped in aluminium foil. The gold strips were cut (with scissors) from the sensors before being placed in the chamber.

The samples (in an ultra high vacuum) were then irradiated with X-rays and a range of electron energies were measured emitted from the surface. The electron energy spectra were then used to identify elemental composition of the surfaces. Also, a quantitative analysis using the major elemental peaks and known instrumental sensitivity was performed by Dr M. Kershaw.

5.3 Results

5.3.1 Extraction of Inks

DuPont Gold BQ331

After extraction in acetone for 3 – 5 min, the gold BQ331 showed signs of removal from the strip surfaces. In some cases the gold extraction produced a fine suspension rendering the entire liquid phase a gold colour, in others the gold was removed in

flake like pieces. The suspension settled after several hours, leaving the strips, according to visual inspection, free of gold. However, complete removal of the gold was not always found; in some cases the gold was removed in flakes which accumulated directly at the bottom of the tube whilst some flakes were found remaining on the strip. These flakes remaining on the strip surface could not be extracted even with increased extraction times (up to 1 hr).

Extraction of Other Sensor Materials

Within a short extraction time of about 5 min, using controls, there was no evidence of PET degradation and little evidence of carbon ink dissolution. With longer 1-2 hr extractions still the PET did not appear to degrade, although this was not tested carefully with the chloroform solvent. Most of the tested carbon inks could be extracted with 1 – 2 hrs extraction time in acetone. DuPont Carbon ink R471 and Electrodag Carbon 423 SS were exceptions both extracting easily into acetone. Typically the solution was blackened with a fine suspension of carbon particles requiring 1 – 2 days to settle. For the Ercon and Gwent gold inks, both were extracted after less than 5 min stirring/shaking in acetone.

Of the low temperature solvents acetone was the most effective for removing the gold ink and in most cases the other inks also. The high boiling point screen-printing solvents removed both the carbon and gold inks easily.

Gold Powder Weight

The gold powder from 8 strips after acetone extraction weighed 15.6 (±0.1) mg. However some deposits of gold were still present on the strips where the bases rested in the sample tube. These were carefully scraped and added to the foil. The weight was then 16.6 (±0.1) mg. Some residues of the gold powder could not be removed from the tube/strips; it is difficult to judge how much gold remained; less than 15 % (negative bias on result) was estimated. Although the carbon tracks appeared intact some black carbon was visible in the gold deposit. Gold is 8.6 times as dense as

carbon graphite so although the maximum volume of carbon would be equal to gold volume (for same thickness of ink and ink polymer loading), the maximum error would be only about 10 %; but since observational evidence suggests only a small fraction of the carbon desorbed this uncertainty is probably less than 5 % (positive bias on result). There may be some insoluble polymer and/or additives in the residue also, suggested by the coalescing of the deposit. However, the density of organic materials is likely to be low in comparison with the gold. Therefore per strip there is about 2.2 (± 0.2) mg of gold powder.

5.3.2 FTIR study of Ink Extracts

With a 1 - 2 min dry time, no significant peaks were seen with the acetone control or PET in acetone control. Therefore, the polypropylene tips, tubes and PET substrate showed no signs of leaching detectable materials (such as plasticizers), within the limits of sensitivity. A low-level spectrum of peaks with poor definition was obtained for the carbon ink (BQ221) after short extraction times (not shown).

The gold ink BQ331 extract produced a clear spectrum as shown in Figure 5.5, attributed to the polymer in (or acetone soluble part of) BQ331, with some contribution from the underlying carbon. Spectra were obtained also for the carbon (after 2 hr extraction), Ag/AgCl reference ink (5 min extraction) and insulation ink for batch D^+.

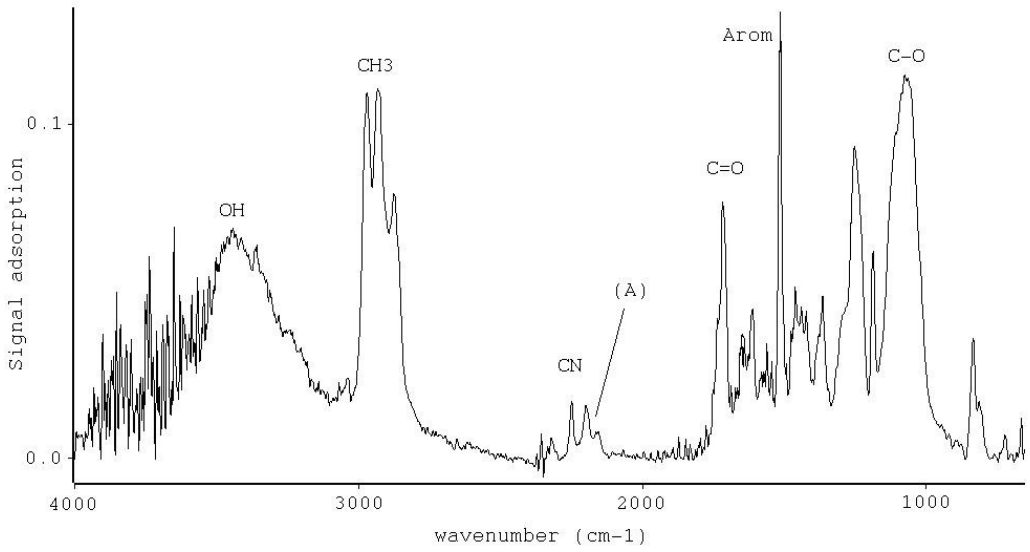

Figure 5.5 Acetone extract of BQ331 from Batch D+ DuPont sensors for range 600 to 4000 cm-1 by FTIR-ATR

In Figure 5.5 the exact peak wavelengths are not given, to avoid disclosure of the polymer. BQ331 is a mixture of aliphatic and aromatic compounds with reasonable hydrophilicity as seen in the OH groups. The noise above 3500 cm^{-1} is attributed to water vapour. The polymer also contains oxygen groups being strong in ether groups and having some C=O. A nitrile (CN) group is also visble close to peaks marked 'A', discussed in Section 5.3.3. The insulation ink of batch D^+ had a spectrum very similar to the BQ311. Minor difference included no CN or peak 'A'. The C= O peak was much weaker and one or two peaks in the 600-1200 cm^{-1} showed differences. The silver reference ink, BQ164 and carbon counter ink, BQ221 produced clear spectra (not shown). The carbon ink for batch D^+ (BQ221) was aliphatic containing with C=O, C-O and some amine groups indicating a general polyester/urethane. The silver ink extract was matched to a polymer in the library but the identity will be withheld.

Spectra for BQ331 were also obtained with methanol, toluene and deuterated chloroform solvents (not shown). The same principal peaks were observed. The methanol extracted OH groups were stronger and equivalent C=O weaker. It is possible that small quantities of the solvents remain trapped in the polymer film after evaporation contributing to some distortion. Toluene and ethyl acetate produced weaker spectra. The deuterated chloroform extract produced a spectrum higher in

CH_3. The aromatic component was weakly visible. Perhaps the chloroform was extracting further components either from the gold ink, carbon/PET, or even the polypropylene tubes.

Spectra for gold ink BQ331 were acquired for 6 batches of DuPont sensor, as shown in Figure 5.6 (spectra were normalised to height of aromatic peaks at about 1500 cm^{-1}). Although the normalised spectra are similar, the peaks shown in the demonstration sample have the best definition. The nitrile peak occurs in some spectra. The peaks close to the nitrile peak marked 'A' in Figure 5.5 occur at different levels: in D^+ and the demonstration sample peak A is large; whereas in the batch JA-JD these peaks are significantly less.

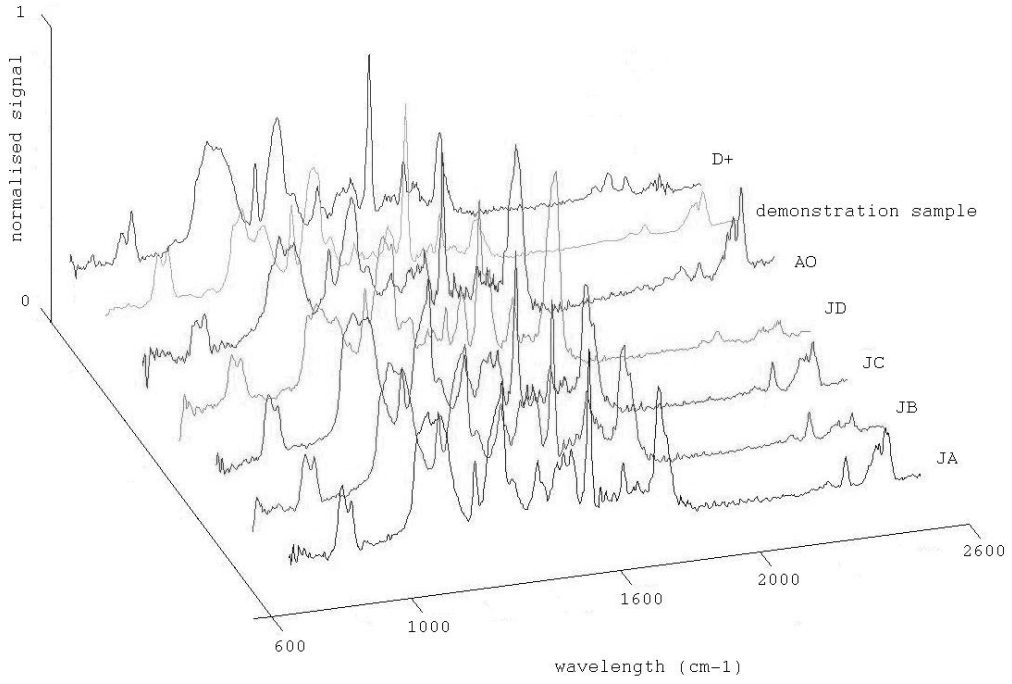

Figure 5.6 Spectra for BQ331 by FTIR ATR for 6 different batches of DuPont Sensor

Spectra for the underlying carbon inks were compared, as shown in Figure 5.7, based on 2 hr extraction time, except R471 which required only 5 min extraction. The nitrile peak has a correlation with the gold spectra except in batch JC. The nitrile peak component is probably solubilising more easily and contributing to the gold spectra.

Carbon ink BQ242 contains significant aromatic content whereas the other inks do not. All appear to contain C=O and C-O groups.

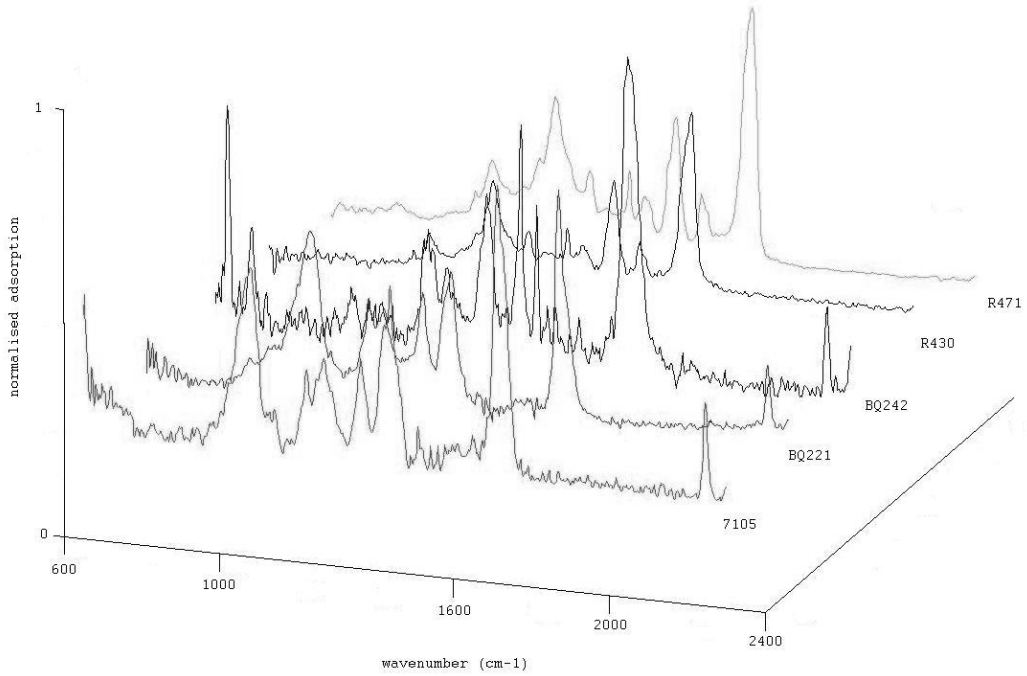

Figure 5.7 Spectra for 5 carbon inks by FTIR ATR as used in DuPont sensors

Other screen-printed inks were also tested by FTIR ATR: the Acheson Electrodag Carbon 423 SS and Electrodag Ag/AgCl 6038 SS. The carbon ink was similar in composition to the DuPont R471. The Electrodag Ag/AgCl ink was matched to a spectrum in the library, but the identity will be withheld. Both inks extracted easily into acetone (<5 min).

Samples of Ercon Gold ink and Gwent gold ink were also studied; the spectra are shown in Figure 5.8. The Gwent gold spectrum was matched with a polymer in the library, but the identity will be withheld. The Ercon gold ink was found to have a similar spectrum to both the Electrodag Carbon 423 SS and DuPont Carbon R471.

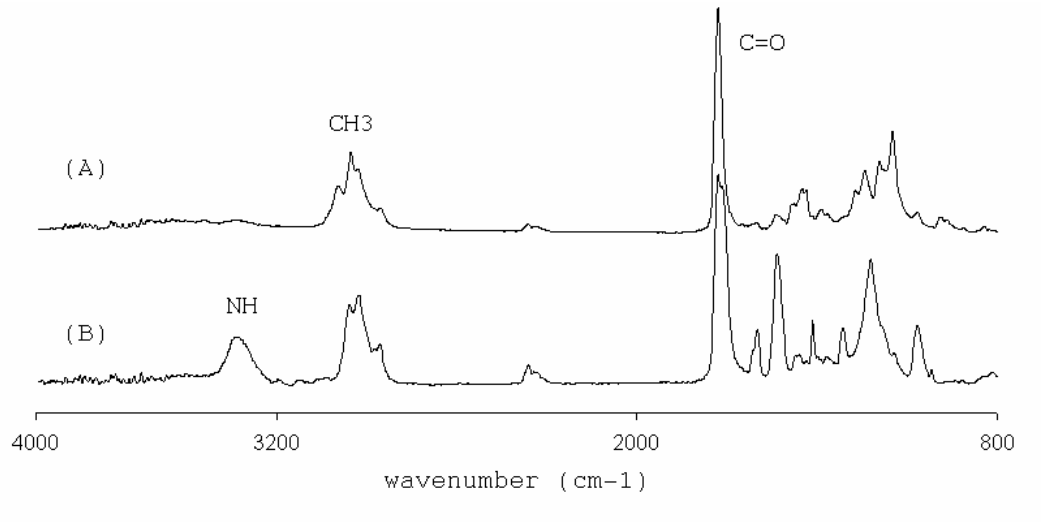

Figure 5.8 Spectra for (A) Gwent gold Ink and (B) Ercon gold ink by FTIR ATR with 5 min extraction into acetone

5.3.3 Spectral comparison of BQ331 with Polymer X

BQ331 could not be matched with any spectra in the electronic library. The available FTIR spectra with SigmaAldrich catalogue (www.sigmaaldrich.com, accessed 2007) were searched manually for possible candidates. Also, various patents were considered for a polymer expected to give a spectrum like that of BQ331. A polymer suspect (polymer X) was obtained (from an undisclosed supplier) and extracted into acetone so as to acquire a spectrum.

The spectrum from an extract of polymer X and BQ331 (demonstration sample Figure 5.6) are compared in Figure 5.9. Peak details, both major and minor, matched well across the spectrum. Some exceptions were seen: two peaks occurring about 2200 cm^{-1} in the BQ331 spectrum did not occur in the polymer X. These peaks are referred to as peak 'A'. There were also some peak differences in the 1000 cm^{-1} region.

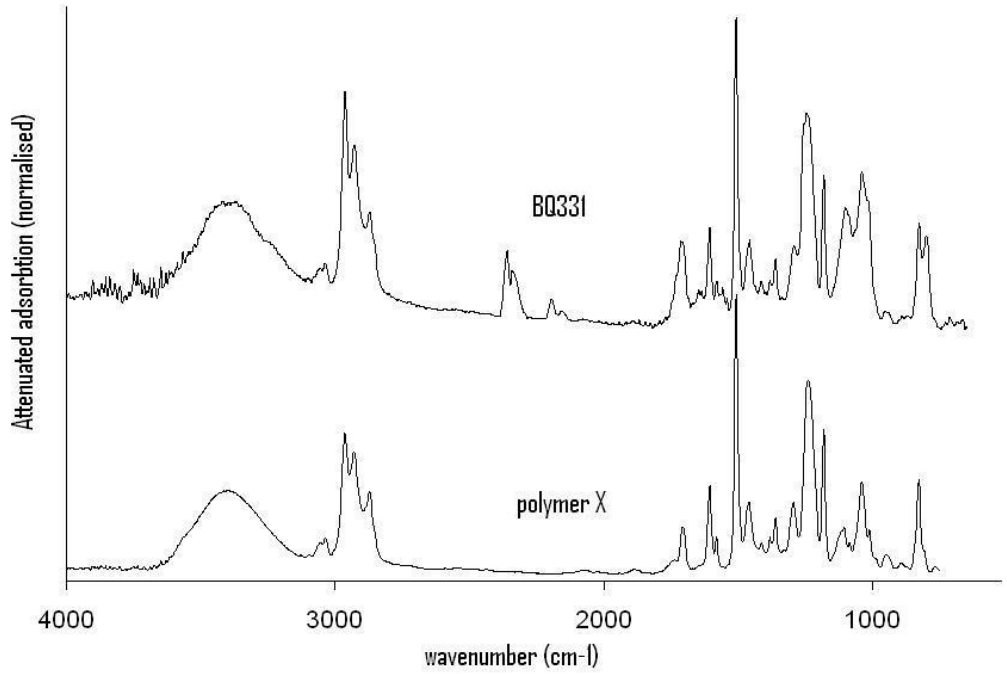

Figure 5.9 FTIR ATR spectrum for BQ331 (demonstration sample) after 5 min extract ion in acetone compared with spectrum for several mg of polymer X in 1.5 ml acetone, 5 min extraction.

5.3.4 Chloride ion electrolyte effect on polymer spectrum

The FTIR ATR spectra for BQ331 (from batch AO) with and without electrochemical cycling in 4 M HCl and 4 M KBr were compared. No difference was seen in the spectra. A rough calculation based on a 50 µA peak with base width 0.2 V in CV with scan rate 0.05 V/s has total charge 0.1 mC, equivalent to about 1 nmol of electrons transferred from chemical in solution (or on the electrode surface) to the electrode. On the other hand, if the ink is about 20 µm thick and has 0.13 cm^2 area with approximately half this volume taken by polymer, and a density about 1.2 g/cm^3 the mass of polymer is about 0.2 mg. The polymer is made up primarily of carbon, hydrogen and oxygen. From the structure of polymer X, the fractions (by weight) of C, O and H were calculated as 0.68, 0.22 and 0.1 respectively. For an individual electrode this is equivalent to 13, 3 and 20 µM. If all the electrons transferred were associated with a single peak containing, for example, O only 1 nmol out of 3 µmol could be expected to change. One or more of the peaks in the BQ331 spectrum may change by up to about 0.03 %.

5.3.5 Crosslinking Agent Effect and Chloride Ion Interference

The ink extraction technique was refined so that spectra from individual electrodes could be obtained. A single strip of BQ331 was cut from the DuPont sensors and added to a 200 µl polypropylene centrifuge tube, to which 150 µl of acetone was added. Extraction was aided, as previously, with an automatic stirrer/ shaker. 50 µl samples were added to the ZnSe crystal surface. For assessing peak A, improved signal to noise ratios were obtained by using a nitrogen cooled MCT detector. In one experiment, 8 sensors from DuPont (batch AO) were subjected to cyclic voltammetry for 40 scans. Standard parameters were used (Table 2.3) with a 4 M HCl electrolyte. The extent of interference was recorded by measuring the area under the primary interference peak. After electrochemical cycling the gold strips were cut and subjected to FTIR ATR individually.

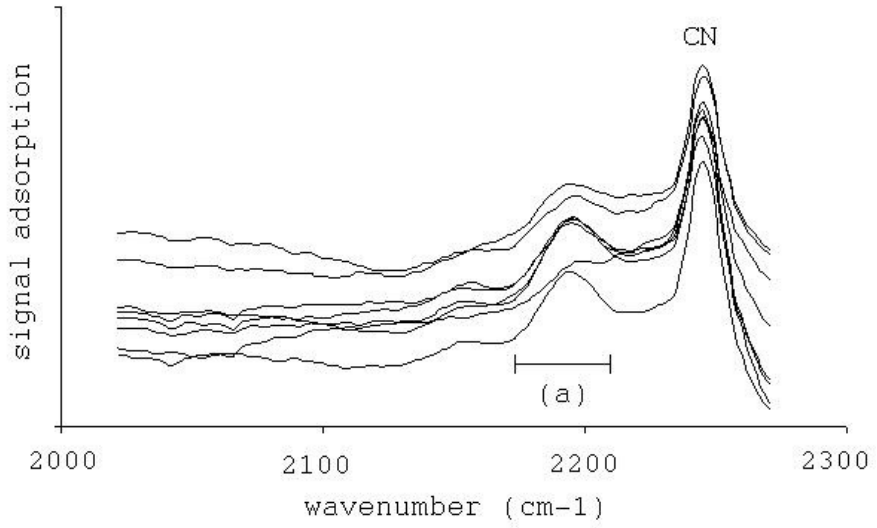

Figure 5.10 FTIR ATR using the Nitrogen cooled MCT detector. Peak assigned to curing agent in BQ331 (batch AO) for eight individual electrodes after CV in 4 M HCl, marked with range of integration shown (a)

The noise level was measured as peak to peak height in the vicinity of the curing agent peak.The signal to noise ratio (peak A height/noise height) for the DTGS and MCT detectors when running with equivalent parameters (32 one-second scans) was 3.5 and 21 respectively. Figure 5.10 shows the peak for 8 sensors after cycling in 4 M

HCl. Figure 5.11 shows the primary peak interference increasing with scan number for each electrode, marked with the area of the curing agent peak seen in Figure 5.10. No correlation was found.

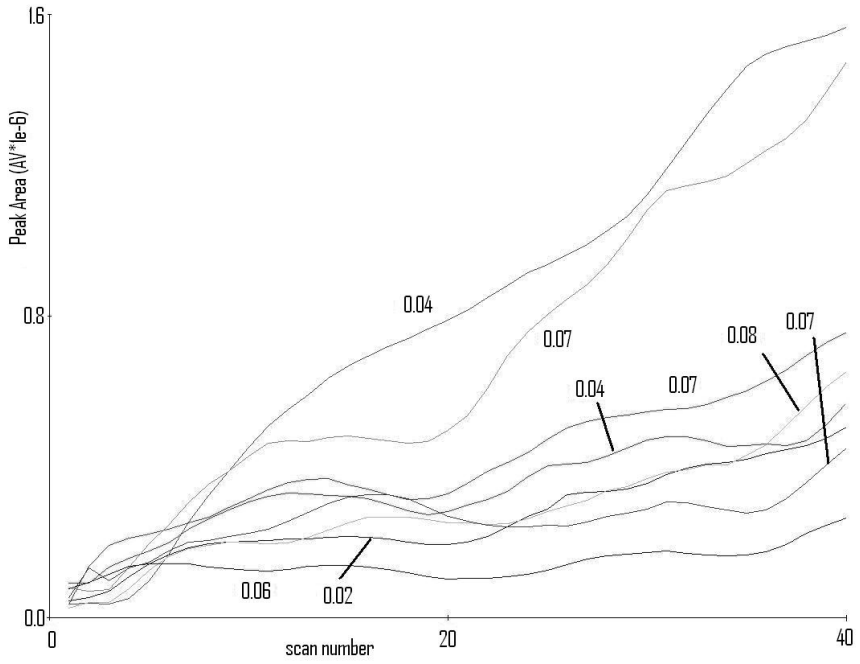

Figure 5.11 Interference (primary 0 V peak) for 8 individual DuPont sensors (batch AO) cycled in 4 M HCl, 40 scans, with area of curing agent peak (as measured by FTIR ATR), shown in Figure 5.10, marked for each sensor

5.3.6 NMR analysis: Cl^- ion effect on polymer extract proton spectrum

The possibility of chloroform selectively extracting BQ331 polymer (batch AO) was checked and found to be adequate, by visual inspection of the dissoluted gold with intact carbon remaining. 1 dimensional spectra for the three samples were obtained with a 2.5 hr acquisition time, to aid signal to noise ratios, in the proton region. The largest signals due to trace water and non-deuterated chloroform were identified, marked ‘s’ in Figure 5.12. The cycled and non cycled BQ331 spectra were so similar that they coincide in Figure 5.12.

Some peak assignments could be made comparing proton NMR spectra for similar compounds in the literature. But these references cannot be disclosed due to the confidentiality of polymer X. Aromatic peaks were identified in common with all three samples, close to 7 ppm shift. The signal magnitude of the polymer X was significantly larger than the BQ331 extracts indicating < 1 mg polymer dissolved per electrode. Peaks in 0 – 2 ppm region of the BQ331 extracts showed more complexity than for the polymer X, indicating quantities of other compounds. Polymer X may also have less fine detail due to relatively increased viscosity expected from the higher signal magnitude. One significant peak, as seen in Figure 5.12 was identified in the BQ331 spectra associated with a methyl silane (occurring at 0 ppm since the reference compound is also methyl silane): very few other peaks occur at this shift. Peaks close to the noise level are not visible in Figure 5.12. Much detail was visible in the BQ331 extract spectra (an example of which is given in Figure 5.13). The cycled and non-cycled spectra were compared for every peak visible above the background noise: no difference could be found.

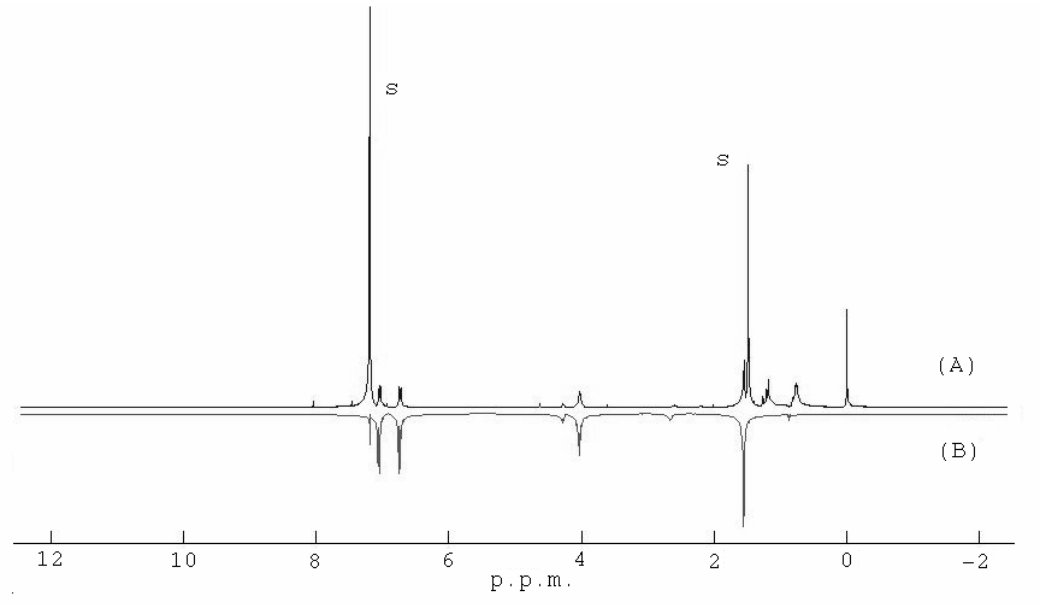

Figure 5.12 NMR spectra after 2.5 hr acquisition for (A) BQ331 chloroform extract and (B) polymer X extract (upside-down for clarity)

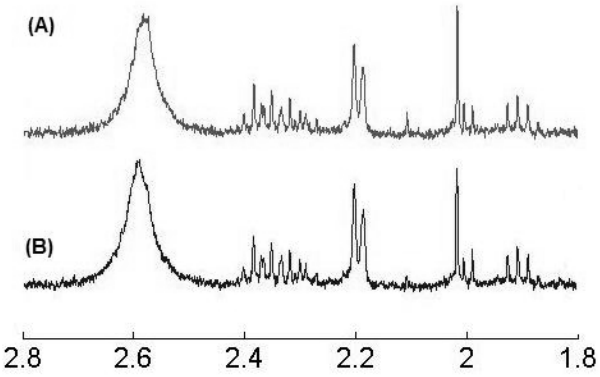

Figure 5.13 Detail of Figure 5.12 comparing the non electrochemically cycled extract (A) with the electrochemically cycled electrode extract (B) in the range 1.8 to 2.8 ppm

5.3.7 The Silane Component

The methyl silane peak was thought to arise from a polydimethylsiloxane (silicone oil) - a common polymer and sometimes flow agent used in screen-printing ink formulations (e.g. Burns *et al.*, 1995). The BQ331 FTIR spectrum was re-examined to test this assumption. Figure 5.14 shows that the silicone oil can explain two peaks found in the BQ331 not otherwise explained by the polymer X spectrum. The Silicone oil does not explain the peaks previously assigned to the curing agent (peak A).

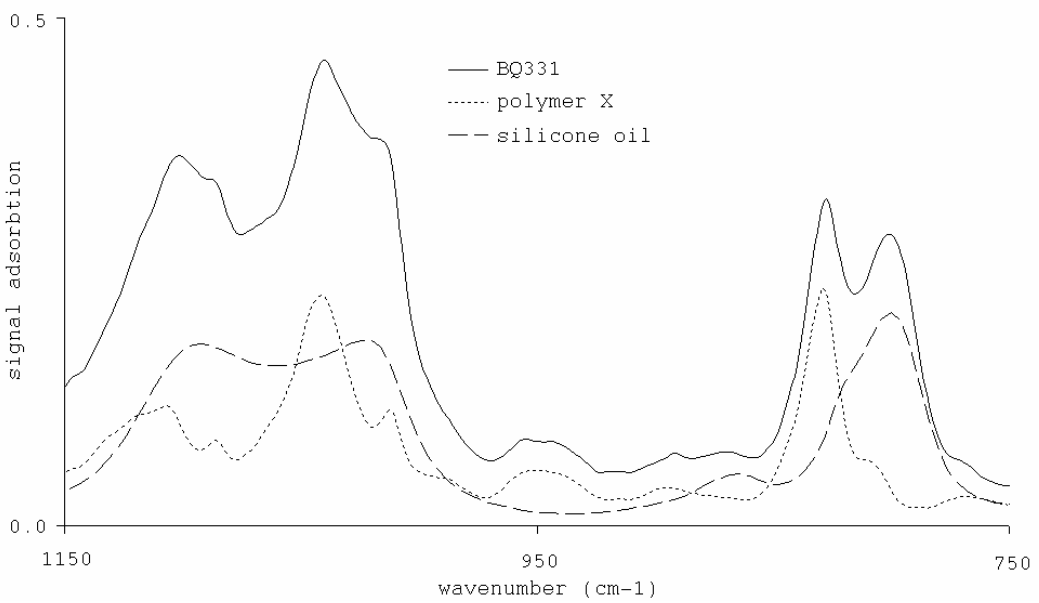

Figure 5.14 Comparison of BQ331 and polymer X acetone extracted FTIR spectra with the library PDMS spectrum

5.3.8 Reflectance Spectroscopy: Aqueous Solubility of BQ331

Having noticed that the interference seen on the DuPont sensors could be detected with standard electrodes (as described in Section 4.3.6) it was known that the interferent must be soluble. So after electrochemical cycling on DuPont sensors, samples (about 100 µl) of HCl were added to a plastic substrate and placed on a hot plate at about 100 °C, to evaporate the water/acid.

A film could be seen on the surface. In another experiment a small square of platinum foil was used as the substrate. In 1 M HCl the film was evident after ~ 10 drops were sequentially added and evaporated; for 4 M HCl about 5 drops were needed for an equivalent film; and in concentrated HCl 1 drop only was necessary. Controls were used to test for the effect of PET alone, carbon ink, silver and Ercon gold, none of which produced a visible residue. 1 and 4 M HNO_3 also produced a weak film. Higher concentrations of HNO_3 caused the polymers in the sensor to bubble indicating oxidative digestion. Also it was found that the residual films formed with and without the electrochemical cycling with 4 M HCl showing that the solubility is a chemical process alone. The platinum was used to test the residue by reflectance spectroscopy

using the platinum as the reflective surface (described in Section 5.2.5). Establishing a clear spectrum for the residue on the platinum was difficult due to the highly localised, variable signal and uncertainty as to the optimal focal point. However, with persistence, a reasonable signal was obtained with a number of peaks, including OH, CH_3, aromatic and fingerprint region peaks, matching the BQ331 spectrum, as shown in Figure 5.15. The solubility is further investigated with electrochemical experiments: see Figure 6.10.

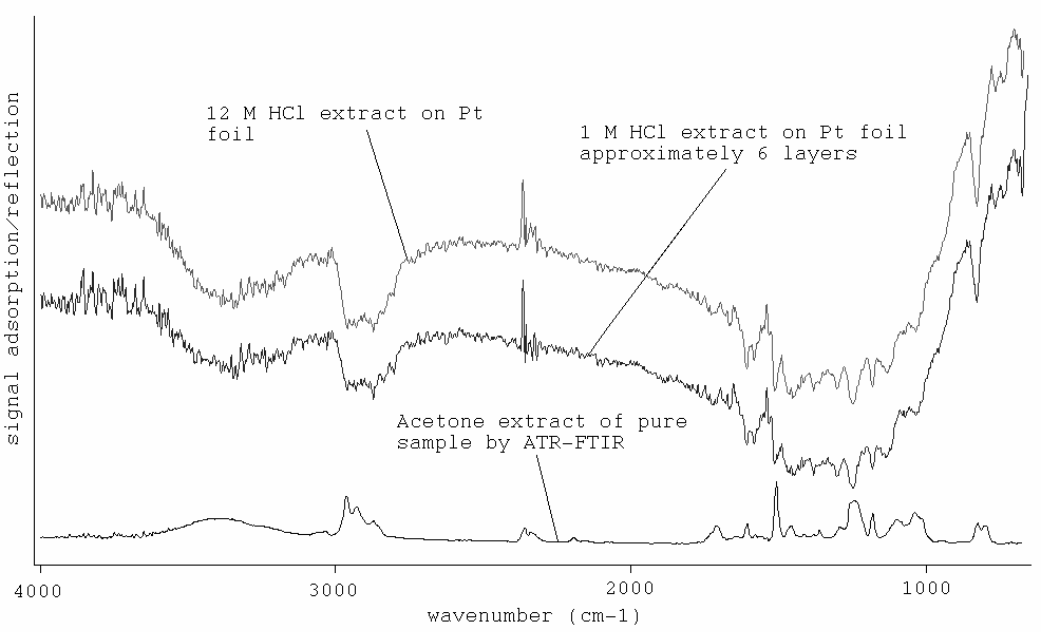

Figure 5.15 Comparison of FTIR ATR spectrum of BQ331 and FTIR reflectance spectroscopy of residual films on platinum foil as indicated (peaks face downwards) using DuPont Sensors (Batch D^+)

5.3.9 *In House* Polymer type effect on Electrochemical Interference

A number of polymer powder composite electrodes (preparation described in Section 5.2.6), all made via solvent processing, were tested in aggressive Cl^- and Br^- electrolytes. Figure 5.16 shows the cyclic voltammograms in 4 M HCl of these sensors. Standard CV parameters were used (Table 2.3) except that only ten scans were recorded and a wider scan range as indicated. The hand painted electrodes

showed considerable variation probably due to the manual application technique. However, all show a peak at 0 V to some degree. A peak was also seen at 0.5 V on some electrodes.

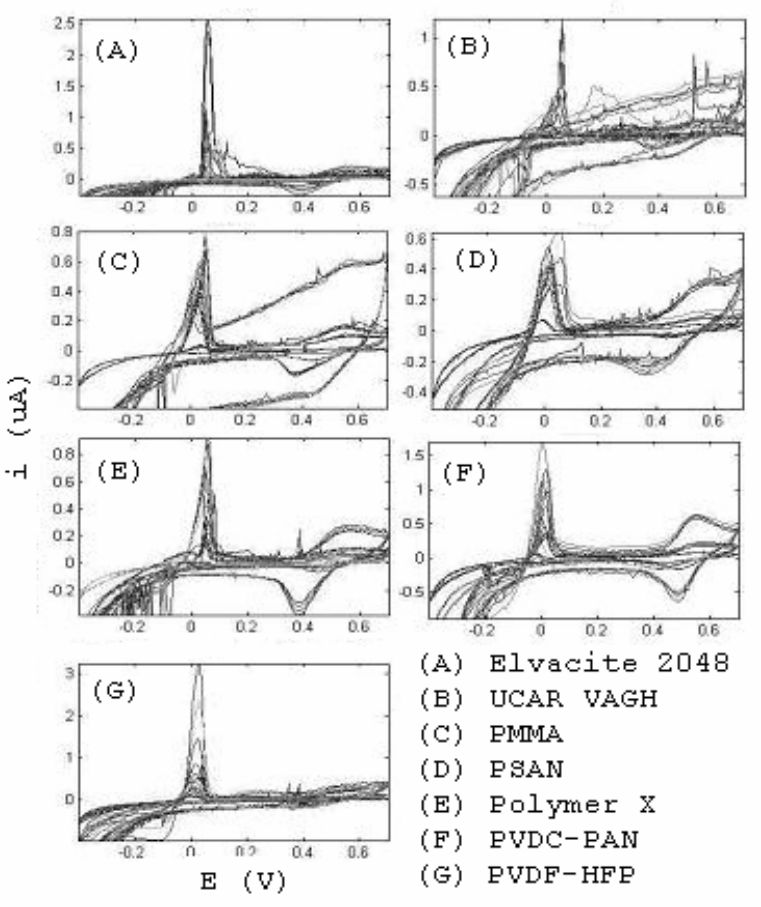

Figure 5.16 CV in 4 M HCl of Polymer-carbon powder composite electrodes hand painted onto screen-printed carbon substrates.

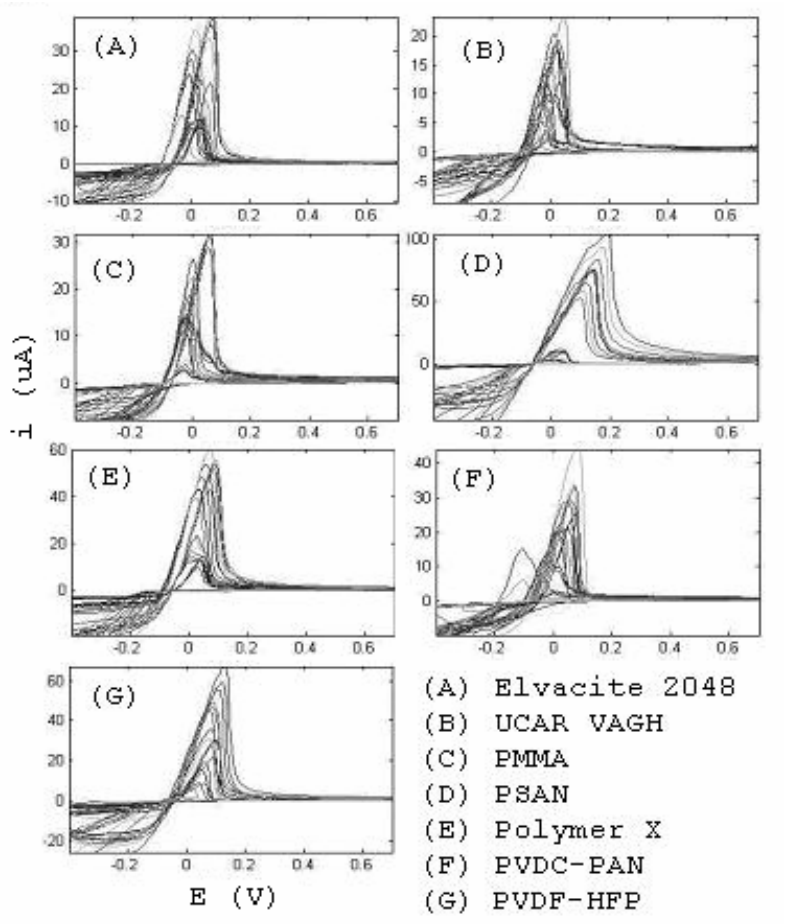

Figure 5.17 CV in 4 M KBr of electrode substrates of Figure 5.16.

As shown in Figure 5.17, cyclic voltammetry in 4 M KBr revealed the same large peaks as seen with the DuPont sensors (Figure 4.12).

5.3.10 X-ray Photoelectron Spectroscopy

The energy spectra for the DuPont gold strips, with and without cycling in 4 M KBr are shown in Figure 5.18, as is the spectrum for the Pt foil. Expected peaks included carbon 1S (281 to 292.7 eV), oxygen 1S (525.8 to 538.6 eV), Pt (66.7 to 79.0 eV) and Au (84.3 to 95.1 eV). Since the electrolyte was neutral (not expected to dissolve the polymer) the quantity of carbon on the platinum surface is more than expected.

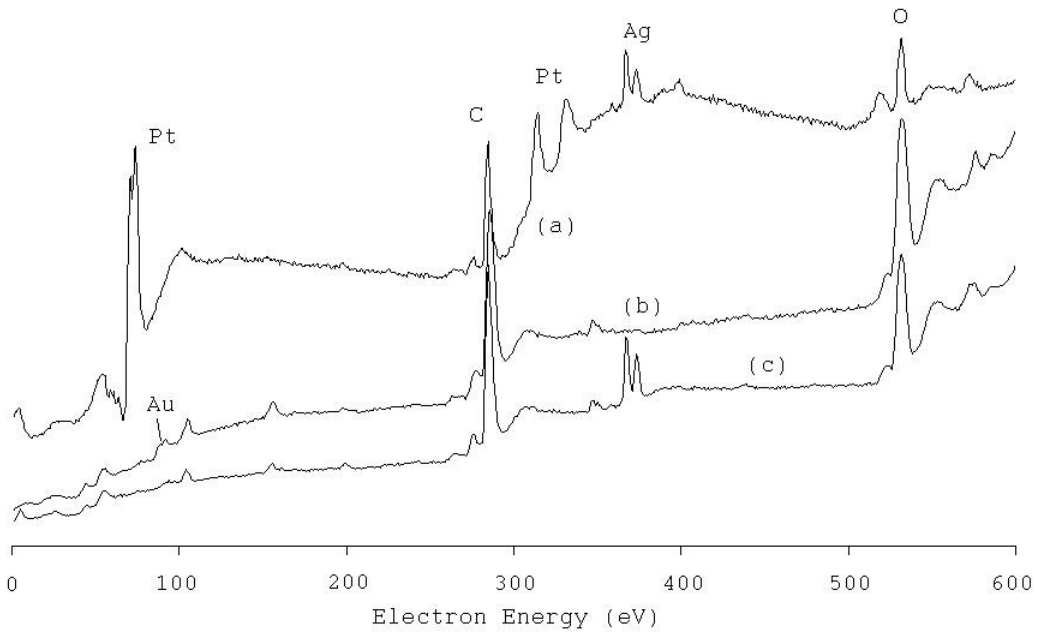

Figure 5.18 XPS spectra for binding energies between 0 and 600 eV for a BQ331 sample fresh (b) and BQ331 sample after electrochemical cycling in 4 M KBr (c). Also spectra for the platinum after cycling in 4 M Kbr in proximity to a DuPont sensor (a)

The Au peaks for BQ331 samples are surprisingly weak considering that the gold constitutes the majority of the ink. Since the X-ray penetration is only a few nanometers it is possible that a thick (relative to penetration) surface active agent was covering the surface. A small Si (2p5) peak (99.2 to 107.6 eV) was visible (accounting for about 3% composition) as would be expected for the silicon flow agent (Sections 5.3.6 and 5.3.7). Also a small peak for Ca (343.1 to 352.5 eV) was registered (quantified about 1.5 %). The purpose for Ca is unknown.

The major spectral feature observed was the presence of silver on both the platinum and the BQ331 sample cycled in the electrolyte, not present on the fresh BQ331 sample. Silver is characterised by two peaks with binding energy 367 and 373 eV. The peaks are approximately of equal magnitude with the 367 eV slightly larger. The silver identification is unambiguous. Quantified analysis using the available peaks and relative sensitivity factors for the XPS instrument indicated that the silver was present between 2 and 4 % of the surface (valid for penetration depth of less than 10 nm, for both gold and polymer surfaces).

5.4 Discussion

5.4.1 Spectroscopic Investigation

In assessing the unknown behaviour of the electrodes, the opportunity was taken to look at the inks directly by whatever means possible. However, there was a risk that because the ink formulations were proprietary the information gained from such experiments would not be publishable (or at least compromised). This is reflected by the necessity to withhold the identity of some compounds, at least one supplier and several references in Section 5.3.

The techniques chosen for the study were amongst those directly available including optical microscopy, gas chromatography mass spectroscopy (GC-MS), FTIR ATR, and Raman spectroscopy. The basic Raman technique is inherently weaker, and signals for thin polymer films either as extracts or as the printed inks revealed no clear spectra. However, the PET substrate (125 µm thick) could be detected. Surface enhanced Raman spectroscopy would have been an option; the films cast onto specially roughened gold or silver film could greatly increase sensitivity. However, this technique is more technically challenging.

GCMS was also tried but persistent problems with carrier gas purity and buildup of contamination products hindered the acquisition of useful results. GC/MS was used to look for volatiles generated from the inks before or after experiments with interference. If polymer or ink additives were breaking down during electrochemical cycling producing low weight molecules, these may be picked up by the highly sensitive MS. Chloride containing organics would have been relevant due to the Cl^- ion dependence of the interference. However, difficulties were encountered achieving consistent background levels: (i) in the helium, levels of oxygen, nitrogen and water which fluctuated after a series of unexpected power cuts and (ii) general organic products accumulated associated with the day-to-day laboratory conditions were ubiquitous. The GC/MS was out of service for several months.

Although the intention with both the FTIR and NMR was to find a change in composition or interfering product directly, useful information on ink composition was obtained which was used when preparing *in house* ink formulations. After the previous techniques had failed to find the cause of the electrochemical interference, XPS was thought to be useful due to its elemental characterisation and specificity for the electrode surface. From this experiment, the cause of the interference was identified.

5.4.2 Extraction of Inks

The extraction of inks was successful for isolating ink components for analysis when the materials and extraction time were selected carefully. BQ331 is a curable ink (DuPont Microcircuit Materials, 2001); with sufficient crosslinking the entire gold strip would be expected to be insoluble. However, smearing of the gold ink with a number of common solvents (including acetone, toluene and methanol) had been noted. If the crosslinking was spatially non-uniform through the strips, variation in solubility would be expected. Typically a solvent-processable polymer is crosslinked with a suitable agent which renders the polymer insoluble. This variable crosslinking could explain why some BQ331 strips left insoluble flakes of gold attached to the strip surface whilst others formed a fine suspension.

The extraction process could be used to effectively isolate the powder component. A mass of 2.2 (± 0.2) mg for gold powder per strip was measured. The gold needs to be highly pure to avoid associated copper and silver metals, and processed to form the particle size distribution required. This measured quantity compares well with a theoretical estimate given in Table 5.2. Although the precise cost depends on scale of manufacture and gold price, it is probably less than 50 p per electrode based on the values given in Table 5.2.

Table 5.2 Estimation of cost for gold in a single screen-printed sensor

Parameters	Value	Unit
gold ink area (one strip)[a]	0.15	cm^2
gold ink thickness	1.7×10^{-3} [b]	cm
gold ink volume	2.6×10^{-4}	cm^3
volume fraction gold powder	0.5[c]	
gold powder volume	1.3×10^{-4}	cm^3
gold density	19.3	g/cm^3
gold powder mass (one strip)	2.5	mg
screen-printing waste fraction	0.5[d]	
cost of gold by market value (one strip)[e]	0.07	£
cost of gold with processed powder value (one strip)[f]	0.23	£

[a]according to metal sensor design in Figure 2.1.– smaller with microband design; [b]value taken from Table 6.1 on page 251; [c]assumption based on polymer and powder ratio; [d] ink lost smeared on screen, mixing vat and tools - applies to screen-printing in general (Gilleo, 1996); [e]according to market in January 2008 of about 14.2 £/g; [f]price based on 5 g quantity of 1.5 – 3 micron gold flake, 99.96 % purity, from AlfaAesar (Lancashire, England). Cost would be less for larger quantity but also subject to change in market value.

5.4.3 FTIR Analysis

It was found that the FTIR ATR technique applied to screen-printed ink extracts could be informative as regards to ink formulation and potential causes of interference. Spectra were obtained for BQ331 from a number of batches (Figure 5.6). Similarly a number of carbon inks (Figure 5.7) were analysed as well as Ercon and Gwent gold inks (Figure 5.8). Although the information was useful, the identities of products, where known, could not be disclosed.

5.4.4 Composition of BQ331

The main functional groups of the FTIR spectra from BQ331 were compared with the expected FTIR peaks for a number of screen-printable formulations described by Chan and Kuty (2000). From this an educated guess was made. Polymer X was identified (Figure 5.9)

The supplier of polymer X advised about crosslinking agents according to curing conditions: phenol >190 °C, urea > 150 °C, melamine > 130 °C and a further agent,

'A', which can be crosslinked at room temperature (or activated at higher temperatures when suitably prepared) that will remain undisclosed. The agent crosslinks the OH groups as visible in the spectrum (Figure 5.5). The peaks occurring about 2200 cm^{-1} in the BQ331 spectrum not seen in the pure polymer X, can be attributed to agent 'A'. Few organic groups occur in this region beside CN which could explain these peaks; but the peak pair is not most typical of chemicals similar to 'A'. An example was found in the literature showing that the typical peaks for this agent can shift wavelength and split under some circumstances. This reference must be withheld to maintain confidentiality. The assignment can only be made to crosslinking functionality, rather than molecular identity. When agent A crosslinks some C=O bonds will also be expected: the C=O in BQ331 is larger than for the polymer X sample. The compound of peak A is reactive so that its presence in the ink formulation, may indicate, in this case Cl^- induced interference. Differences in the peak A level between DuPont batches were noted and visible in Figure 5.6.

A further component was recgonised from the NMR (Figure 5.14) and subsequent FTIR-ATR analysis (Figure 5.14) as a silicone oil. A patent for screen-printable formulations describing the principle of this combination of components could not be disclosed.

5.4.5 Polymer Degradation Hypothesis

No effect could be seen in the FTIR ATR spectra of BQ331 as a result of scanning in 4 M HCl or 4 M KBr. No effect could be seen in the NMR proton spectra due to scanning in 4 M KBr. Also no correlation was found between the primary interference scanning in 4 M HCl and subsequent extraction and analysis of the levels of curing agent (peak A) in the the strips (Figure 5.11). It should be conceded that these techniques are probably too insensitive to measure small chemical changes (0.03 % as calculated in Section 5.3.4) in the bulk material, so the result is not surprising.

As regards the influence of the curing agent peak, it is possible that a number of factors determine the peak shape, area and baseline level in the FTIR signal. Also the

critical factor is likely to be the curing agent close to the powder-polymer interface, where as the agent as measured by FTIR indicates bulk polymer concentration. The uniformity of the agent dispersion within the ink possibly has spatial variability down to the micro scale. To continue the experiments more work would be needed to assess the FTIR peak, peak area and baseline response. Correlations could, therefore, be tried for each of the three interference peaks seen. A simpler way to investigate the issue would be to obtain some of the curing agent (or similar agent) and add to DuPont or *in house* sensors to look for an increase in interference. However, this avenue of investigation was not pursued.

Another possible method to look at the extent of crosslinking in a prepared formulation is to use a hardness test. ASTM D3363 (ASTM International, 2005) provides a standard method for measuring film hardness using normal graphite pencils between 6B and 6H. Starting with the hardest, the pencil is held at 45 ° to the film surface and a 6.5 mm mark is made. Each pencil is tested until the pencil is too soft to make an impression. The method is used to determine the cure of coatings, since highly crosslinked surfaces have a greater hardness. The method has some subjectivity according to the operator. According to the DuPont gold ink literature BQ331 has hardness equivalent to a 2H pencil. If the film is much softer than this then insufficient crosslinking could be the reason.

Evidence in favour of the polymer degradation hypothesis includes the solubility of BQ331 polymer (Figure 5.15) where it was previously known that the electrochemical interference was also soluble (Figure 4.20). On the other hand, the FTIR work has shown that C=O, C-O, NH, CN and OH groups are common to many inks (Figure 5.6, Figure 5.7 and Figure 5.8). Several polymer powder composites were handpainted onto screen-printed substrates with similar polymers (such as polymer X, Elvacite 2048, UCAR VAGH and PSAN and at least one with lower numbers of functional groups (PVDF-co-HFP). However, the results of cycling in 4 M HCl (Figure 5.16) and 4 M KBr (Figure 5.17) showed all polymer compositions were susceptible to electrochemical interference. Significantly the fluoro polymer should contain only C-

C, C-H and C-F bonds, but experienced interference no less than the other formulations in 4 M KBr.

The *in house* polymer powder formulations show that a polymer additive (such as the curing agent of peak A) is not necessary to cause the interference. If the polymer is degrading then the action appears not to involve any particular functional group unless it be C-C ot C-H. It is possible that the interference was coming from the PET substrate or the Electrodag inks in the *in house* formulations. Otherwise the polymers are probably not degrading.

5.4.6 XPS: Silver Contamination

XPS was chosen due to its ability to analyse specifically the sample surface. The clear implication was that silver had arrived at the working electrode (Figure 5.18) surface as a result of the electrochemical procedure. There is a possibility that when the gold strip was cut, that a flake of silver removed from the reference strip onto the gold. However, this reason cannot account for the Ag found on the platinum foil. It is possible that silver was present on the platinum as a result of improper cleaning prior to the electrochemical cycling. However, this reason could not be used with the DuPont strips.

The fact that silver is used for a reference electrode is due to the ease with which it reacts with chloride. Silver present on the working electrode would give rise to a large peak at 0 V in either Br^- or Cl^- assuming that the reference strip sets the potential by the same reaction. The fact that Br^- displaces Cl^- ions at the reference electrode could be seen by the colour change of the strip when KBr (4 M) was added indicating the reaction:

$$AgCl + Br^- \leftrightarrow AgBr + Cl^- \text{ (fast)} \qquad \mathbf{58}$$

The primary interference peak is typically close to 0 V. The spike peak is also close to 0 V implying a connection. After an online search (www.google.com, accessed 2007), it was found the silver forms complexes at high halide concentrations:

$AgCl(s) + nCl \leftrightarrow AgCl_{n+1}^{-n}(aq)$ **59**

$AgBr(s) + nBr \leftrightarrow AgBr_{n+1}^{-n}(aq)$ **60**

The coordination number of the Cl^- ion is thought to lie in the range 2 - 5 with $AgCl_4^{3-}$ most likely at > 1 M concentrations. Uncertainty exists due to the need to assign accurate individual ion activities at high concentration (as was the case for Cu, As and Hg speciation in high Cl^- ion solutions: Figure 1.8, Figure 1.9 and Figure 1.10). The solubility of silver in chloride solution (according to Forbes, 1911, Jonte and Martin, 1952) is shown graphically in Figure 5.19. It is well known that silver chloride has a particularly low solubility product seen in the range 0.001 to 0.01 M Cl^- where the solubility is less than 1 µM, with the ions present as Ag^+ and Cl^-. But this value increases, as $AgCl_n^{-(n+1)}$ complexes become favourable, to as high as 3 mM, for Cl^- above 4 M. The cation, e.g. Ca^{2+}, H^+, or Na^+ has little effect. Silver ions even at 1 µM in a test solution for metal ions at nM concentrations could also be problematic.

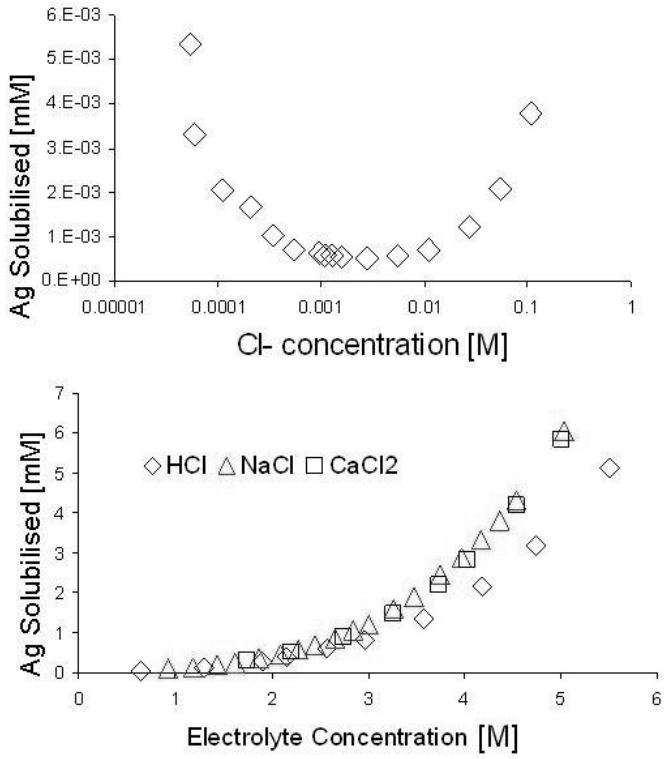

Figure 5.19 Solubility of silver via complexation in low-high Cl^- ion media. Graphs drawn in Microsoft Excel from tabulated data (Forbes, 1911; Jonte and Martin, 1952)

The speciation of Ag chloride complexes can be predicted with thermodynamic data by Helgeson (1969) as cited by Sella and Bauer (1990). Sella and Bauer used an electrochemical method to determine the single ion activities of H^+ and Cl^- in HCl electrolytes for high concentrations (1 – 10 M HCl). The potential of the Ag/Ag^+, H/H_2 and Cl/Cl_2 redox couples were observed with variation in HCl concentration and a new value for the formation of $AgCl_4^{3-}$ was derived. A stable reference potential was provided by a metallocene redox couple presumed to be independent of the electrolyte conditions. According to Henderson (1969) the log equilibrium constants $\log\beta_1$ = 3.31, $\log\beta_2$ = 5.25, $\log\beta_3$ = 5.25 and $\log\beta_4$ = 5.51. In the range 2 – 10 M HCl, Sella and Bauer (1990) conclude that $AgCl_4^{3-}$ is the dominant complex: the $\log\beta_4$ constant should be modified to a value of 5.1. As Figure 5.20 shows $AgCl_2^-$ species dominates the solubilised silver for concentrations about 0.05 to 1 M HCl.

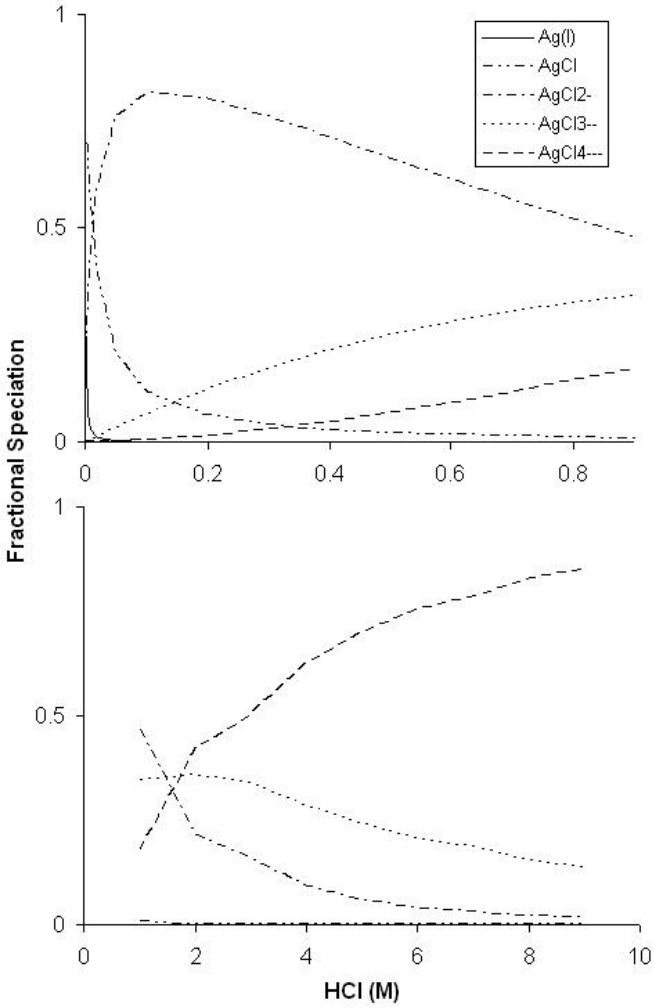

Figure 5.20 Speciation of Silver in HCl acid solutions using equilibrium constants given by Sella and Bauer (1990) and Henderson (1969)

5.4.7 Solubility of BQ331/Polymer X

The solubility of BQ331 in concentrated HCl (Figure 5.15) may explain the background current drift seen with the electrochemical signal in 4 M HCl electrolytes (for example, Figure 4.4 and Figure 4.5). The baseline current would be expected to vary with the standing time of the electrode in the electrolyte prior to the electrochemical test. This solubility could be explained as being due to the BQ331 hydroxyl groups in Figure 5.5. Other inks such as the carbon-based inks do not show this behaviour.

5.5 Conclusion

Evidence for the voltammetrically induced breakdown on the BQ331 polymer is weak. The choice of polymer in a screen-printable ink appears to have little effect on the interference. The effect of PET degradation could not yet be ruled out; it would be possible to prepare electrodes on ceramic substrates instead. It has not been possible to explain the electrochemical interference of Chapter 4 as being due to changes in polymer structure and additives.

The interference was clearly identified by XPS as silver. backed up by studies in the literature. So the exposed reference electrode is the problem particularly as the Cl^- ion levels exceed 1 M HCl. Since the electrochemical interference was composed of three distinguishable peaks (Figure 4.10), it is still necessary to ascertain whether silver is the cause of these. In addition some of the salient components of the DuPont gold ink have been identified. The ink is slightly soluble in strong acids contributing to a rising baseline in 4 M HCl, not ideal for arsenic analysis in this electrolyte. In general, the outlook for preparing an ink formulation suitable for a commercial arsenic sensor has been improved.

Chapter 6 The Spike Peak and Further Developments with DuPont Sensors

6.1 Introduction

Having identified silver (in Chapter 5) as the probable cause of the background peaks seen during As(III) and Hg(II) determination (in Chapter 4), this chapter concerns, firstly the verification of silver as the problem, mitigation thereof and reassessment of As(III) determination. In addition a microband design is introduced for improved As(III) sensitivity.

6.1.1 Underpotential Deposition

Sub-monolayer quantities of the metal at the surface exhibit an alloy effect (Herzog and Arrigan, 2005). For example silver on gold forms a monolayer consisting of a silver-gold film. The energy of the bound valence electrons in the silver is modified by the presence of the gold – thus an altered stripping potential is seen (compared with bulk silver stripping). Since the silver and gold have a high affinity the electrons are more closely bound causing the sub monolayer to strip at a potential higher than the bulk phase stripping. Lorenze *et al.* (1971) showed the underpotential deposition effect of silver on gold electrodes in non-Cl^- ion systems (1 M $HClO_4$). The peaks of interest occur at significantly high potentials, associated with the Ag/Ag^+ electrochemistry. A two further redox couples are seen +240 and +670 mV positive of Ag/Ag^+ bulk peak. The shape of these peaks relative to the main stripping peak is highly characteristic of the interference seen on either the DuPont screen-printed gold (Figure 4.10) or a gold disk electrodecycled in close proximity to a silver strip (Figure 4.20) in high Cl^- electrolytes. The main difference is the large shift in potential. Cl^- ions were not used and no spike peak was observed in the work of Lorenze *et al.* (1971). According to Kolb *et al.* (1974) based on a wide survey of metal on metal deposition the data could be split into two categories: those with and those without chloride ions in the electrolyte. The metallic substrates included Pt, Au, Ag and Cu. The effect of chloride adsorption (< 20 % of the surface) to the electrode surface was found to reduce the potential of the monolayer stripping. Cl^- adsorption also reduces

the potential of the point of zero charge of the electrode surface. It was not possible to find, in the literature an example of underpotential deposition for Ag on Au in high Cl^- ion electrolytes.

6.1.2 The Spike peak

Voltammetric peaks usually have a minimum width associated with the thermal distribution of energies irrespective of diffusion or kinetic considerations (as seen in Figure 1.2). Peak widths narrow also if several electrons are exchanged per molecule. Atypical peak shapes can result from coulombic repulsion between surface adsorbed electroactive species. In general a number of complex effects may occur during electrochemical experiments such as spontaneous oscillations, stochastic peaks and sharp spikes. Such effects can be seen when dynamic processes occur between active and passivating processes.

For example, the formation of hydrogen at negative potentials causes bubbles which block electroactive surface areas. When the bubbles reach a critical size buoyancy effects overcome surface tension effects the bubbles leave the electrode surface. The complex nature of the process leads to erratic current profiles classed as a temporal instability (Hamann *et al.*, 2007).

The adsorption of both organic and inorganic layers to electrode surfaces is known to cause sharp peaks in voltammograms. Sulphide phases on mercury (Benucci and Schariker, 1985), heptyl viologen on mercury (Arihara *et al.*, 2000), thiourea with halide ions as first noted by Frumkin as cited by Hills and Silva (1982) on mercury electrodes, thiols, tymine, camphor, uridine, coumarin, guanine and adenine on various electrodes (BuessHerman, 1994).

Some adsorbates form condensed phases on electrode surfaces characterised by distinct phase changes. Self assembly of these phases depends on the solvent-surfactant and electrode. It is possible that a suitable potential step applied to the electrode can induce the phase change. The kinetics depend on nucleation and growth

processes which can lead to deterministic or stochastic behaviours. The peaks are associated with dips in the electrode-electrolyte capacitance (BuessHerman, 1994). Sharp peaks are also observed for single crystal metallic electrodes.

Some of these spike phenomena depend on halide concentrations, such as for thiourea on mercury, where spike peaks were seen for chloride > 0.3 M, ascribed to coadsorption (Hills and Silva, 1982).

BQ331 is known to include a surface active agent on the gold particles helping to aid polymer powder affinity thereby allowing a greater proportion of powder to be included in the ink composition whilst retaining viscosity requirements for printing. Whilst most deposited organic layers passivate an electrode, some may facilitate electron transfer with suitable steric conditions depending on adsorbate size and presence of functional groups (BuessHerman, 1994).

Whilst the unknown surface active agent maybe causing the spike peak seen in chloride (or bromide) media the spike peak has been seen in a number of carbon inks both commercial and *in house.* The spike peak typically occurs at about +0.05 V (vs Ag/AgCl) on the forward sweep and at about -0.05 V on the reverse sweep. On carbon inks the spike shows a higher degree on stochastic behaviour – one or more sharp spikes are seen on the reverse scan. The potential of occurrence may change with each scan but typically occur for the reverse scan at potentials more negative than -0.05 to about - 0.2 V.

On the other hand, a spike peak was noticed by Kroger and Turner (1997). Biosensors with low temperature screen-printed inks on polyester substrates were initially printed with silver tracks and one of several carbon ink working electrodes. On at least two of the carbon sensors, cycled in 0.1 M KCl and 0.1 M phosphate buffer spike peaks were evident. The connection with chloride was noted and silver was suspected as the cause. However when the electrodes were reprinted with carbon tracks (no silver) the spike peak was still evident. Fig 5 in the paper (Kroger and Turner, 1997) shows the

spike peaks with a 4 μA forward peak and stochastic reverse peak with many spikes between -0.1 and -0.5 V, the largest at -0.1 V.

6.1.3 Mitigation of Silver Interference

A possible method involves immobilising the silver with a membrane such as Nafion; the Nafion prevents negatively charged ions from penetrating the electrode/electrolyte barrier. Both the Cl^- ions and the Ag-Cl complexes would be expected to be negatively charge. If the barrier was complete the refernce electrode would not be expected to function. But if the passage of ions is reduced by several orders of magnitude the electrode would still function and the silver would remain precipitated.

It is possible to use non-silver based electrodes. Reference systems such as hydrogen and chlorine couples are too complicated for simple test systems (Hamann *et al.,* 2007). Pb, Cu and Hg are also used in reference electrodes sytmes normally with a complexing anion such as Cl^-, Br^- or SO_4^{2-}. But these metals will also form soluble complexes for high concentration Cl^- ion electrolytes. For some experiments, particularly those in non aqueous electrolytes quasi reference electrodes such as platinum and gold are sometimes used. Ideal reference electrodes are non-polarised. Quasi reference electrodes can offer non-polarised behaviour within its potential window. The system may rely on a relatively minor reaction, or upon the oxidation/reduction wave in the electrolyte. The weakness or instability of these reactions may allow the potential to drift.

When redox mediators, such as potassium ferrocyanide, are used in solution at high levels the ferrocyanide/ferricyanide couple adequately sets the potential with otherwise inert electrodes such as carbon. Dilleen *et al.* (1998) used screen-printed electrodes to detect silver (complexed with ammonium thiocyanate) in photographic emulsions. The pseudo reference electrode utilised carbon ink. Since the emulsion contained quantities of redox active compounds the carbon ink was sufficient.

As shown in Figure 6.1, the standard glass capillary reference electrode incorporates a ceramic Vycor plug, through which only slow ion seepage is possible. Thus high Cl^- ion electrolytes could be used over short time frames with the reference electrode separated by a physical barrier.

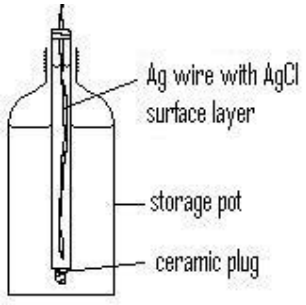

Figure 6.1 Storage of glass capillary Ag/AgCl electrode

However, the storage electrolyte is usually saturated KCl or NaCl (e.g. Bioanalytical Systems, 2002-2005), in which silver is soluble. Over a longer time period the inner and pot electrolytes equalise presumably saturating the pot with several mM of Ag (see Figure 5.17). The silver could easily be carried on to sensitive experiments. If such an electrode were to be used for arsenic determination, a storage (and inner) electrolyte of 0.01 M KCl (or NaCl) would help to minimise silver contamination to less than 1 µM.

6.1.4 Screen-printed Microelectrode

Chang and Zen (2006a and 2006b) describe a method to make ultramicroelectrodes from screen-printed strips. Screen-printed electrode thickness is 5 - 30 µm, about adequate for convergent diffusion. The working electrode is sandwiched between two insulating layers with just the ink edge exposed. Screen-printers cannot print with accuracy below 100 µm. Thus to provide the appropriate surface, the sandwiched layer is cut. Similarly, Authier *et al.* (2001) made screen-printed microband electrodes using a scapel to cut through a sandwich of conductive layers. By using high-impact PS for the insulation ink and substrate, the electrodes were found to be more reproducible when cut. Craston *et al.* (1991) constructed microband electrodes using

high temperature screen-printed inks on alumina cut with a diamond saw. The electrodes were tested with vitamin B, vitamin C and paracetamol and despite high levels of impurities were deemed good for electroanalysis. Similarly (but not involving screen-printed electrodes) Welford *et al.* (2001) describe inexpensive methods for making microband electrodes by laminating foils with polymeric masks. Cutting the surface could provide renewed surfaces.

Wang *et al.* (1993) used ultramicroarrays constructed with screen-printed electrodes. First covering the working electrode with an insulation layer, micro gaps were ablated with a laser. The sensors were purchased from Ecosse Sensors (Edinburgh, UK) and the details of fabrication were not given. The sensors were used with mercury film for sensitive trace metal detection.

The method of Chang and Zen (2006a and 2006b) used electrodes where the working, counter and reference electrode were superimposed in multilayer sandwich separated by insulation ink. How the electrodes are sliced is not discussed in detail other than the generalisation that machine cutting would be more reproducible than manual cutting. The sensors are used for nitrite and iodide sensing applications.

It is interesting that Salaun *et al.* (2007) used a gold microwire of 5 μm diameter for electrochemical analysis of As(III) and As(V). The particular advantage being that the electrodes could be used with potentials more negative than those usually associated with gold based analytical methods. Generated bubbles of hydrogen were not observed adhering to the smooth curved microwire surface as would be the case on planar electrodes. Consequently the background currents after depositions at potentials as low as -1.2 V were still compatible with trace analysis. As(V) reduces to As(0) at pH 1 at these potentials. Although some arsine is also generated, the technique is promising for facile speciation of arsenic, without the need for chemical prereduction of As(V).

6.2 Materials and Methods

6.2.1 Materials

In addition to previous electrode sensors, DuPont (DuPont Microcircuit Materials, Bristol, UK) prepared a batch of sensors (October, 2007) with: BQ164 (5874) (as standard); 5870 with 80:20 Ag/AgCl; and E107255 -45 B with an unknown silver ratio. Samples of each silver ink were also prepared solo on PET sheets.

Table 6.1 DuPont Sensors Received October 2007

	Product	Approximate Thickness[a] (μm)
Carbon[b]	7102	6
Gold[b]	BQ331	17
Encapsulation[b]	5036	6
Group 1	5874	25
Group 2	5870	24
Group 3	E107255-45B	17
Group 4	no Ag	0

[a]reported by DuPont; [b]used for sensor groups 1-4; All layers were Infrared dried at 130 °C; Samples of each silver ink were prepared as separate strips, also

6.2.2 Spike Peak Study

A macro was setup in GPES software to conduct repeat scans with 30 s deposition phases for each of 10 – 40 scans taken consecutively. A 1 M HCl solution was used as electrolyte; this was considered optimum for spike incidence without the large primary interference peak. Gold, carbon and platinum disk electrodes were used for working and counter electrodes; a standard Ag/AgCl glass capillary electrode sufficed for the reference. The schematic for this experiment is given in Section 2.3.5 and Figure 2.5. *In house* printed commercial and i*n house* formulated inks were prepared as described in Sections 2.4.1 and 2.4.3.

6.2.3 XPS measurements

XPS was conducted as described in Section 5.2.7, except that the dwell time was increased to improve signal to noise ratios over selected areas of the energy spectrum.

6.2.4 Mitigation of Silver Experiments

Nafion films were applied to screen-printed reference electrodes from 5 % solutions in a mixture of alcohols. About 10 µl was added and spread across the reference electrode with the pipette tip. Screen-printed substrates include both DuPont sensors and *in house* printed electrodes using Electrodag carbon and Ag/AgCl inks as described in Section 2.3.3. Cyclic voltammetry was based on standard parameters (Table 3.4), but with scan ranges as indicated. 20 scans were saved automatically and loaded into Matlab and displayed in 3 dimensions (see Section 2.3.8). No Electrode pretreatment was used. For studying the interference 4 M KBr was used being most direct for producing strong electrochemical peaks. 4 different silver inks were compared for reactivity to addition of 4 M KBr. For this a 200 µl drop of 4 M KBr was added to screen-printed silver strips and allowed to stand for about 5 minutes before being adsorbed with paper towel. The colour change was compared.

For experiments using non silver reference electrodes, the silver printed strip was removed from the sensors. Standard gold, platinum and carbon disk electrodes were added according to Figure 6.2. In one case screen-printed gold was used as reference for which the setup of Figure 5.4 (on page 218) would be more appropriate.

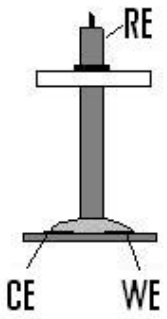

Figure 6.2 Schematic for substitute reference electrodes

Standard CV parameters were used (Table 2.3). The scan range had to be altered for each reference electrode.

6.2.5 Preparation of Microband Electrodes

DuPont sensors were cut by various methods including scissors, Stanley knife, roller cutter and CO_2 laser. The cut was made so as to leave only a gold edge exposed which would be about 20 µm thick (if cut cleanly), as shown in Figure 6.3. Using the existing design the gold is printed on top of a carbon layer so that both inks are exposed at the edge.

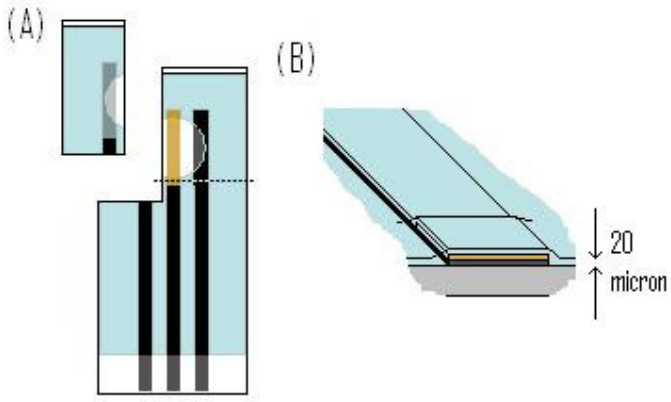

Figure 6.3 Schematic for preparation of microband electrodes (A) removal of silver track and dotted line indicating cut along tracks to leave a sandwiched gold layer shown in (B)

Scissors used were ordinary stainless steel nail scissors (obtained in local pharmacy), disposable razor blade, roller cutter (Avery, Precision Cutter 460 N, such as can be obtained from Solution Centre, Reading, UK) with apporx. 5 cm diameter blade and CO_2 laser (Fenix Laser Maker, Synrad, Inc., Banbury, UK).

Optical microscopy was used to study the edges. The sensor edges were cut again from the electrode giving about 5 mm height with the gold on the top exposed edge. These pieces were taped to a glass slide to hold steady in an upright orientation, as shown in Figure 6.4.

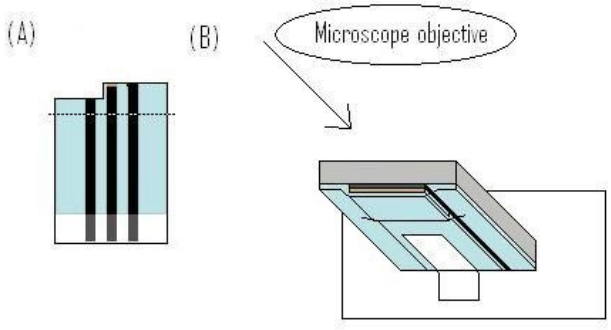

Figure 6.4 Preparation for microscope inspection. Cut as shown in (A) and tape to glass slide in (B) to hold upright

6.2.6 Electrochemistry with Microband Electrodes

The microband design requires that the electrodes be submerged into a beaker. The removal of silver requires that a separate reference electrode be provided.

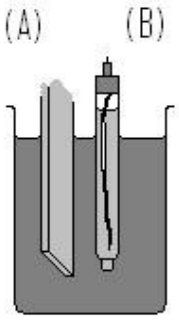

Figure 6.5 Schematic for microband electrode (A) in beaker of electrolyte with a glass capillary Ag/AgCl reference electrode (B)

For the calibration of arsenic in pure and river water samples a setup, as shown in Figure 6.6, was used. The Electrodag-Nafion reference electrode was reused, rinsed with pure water but not wiped, for up to 30 experiments. The magnetic stirrer was not used during electrochemical determination.

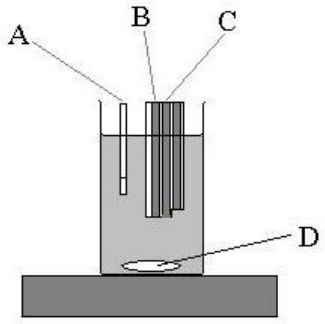

Figure 6.6 Schematic for As calibration with A Electrodag carbon – Electrodag silver silver chloride single track electrode with Nafion layer reference electrode; B/C Microband Sensor with silver removed, B carbon counter electrode and C gold working electrode; and D magnetic stirrer to mix after additions of As(III)

6.3 Results

6.3.1 Screen-printed Silver with Nafion Membrane

The electrodes, with and without Nafion film were tested by cyclic voltammetry in 4 M KBr. Figure 6.7 and Figure 6.8 show the result of cycling in 4 M KBr for four electrodes; the electrodes in this case were the i*n house* printed strips printed with Electrodag Carbon and Electrodag Silver inks (Section 2.3). With the Nafion film, the interference is almost entirely (< 5 %) eliminated. The electrode with the largest residual interference also exhibited some specks of exposed silver, upon inspection.

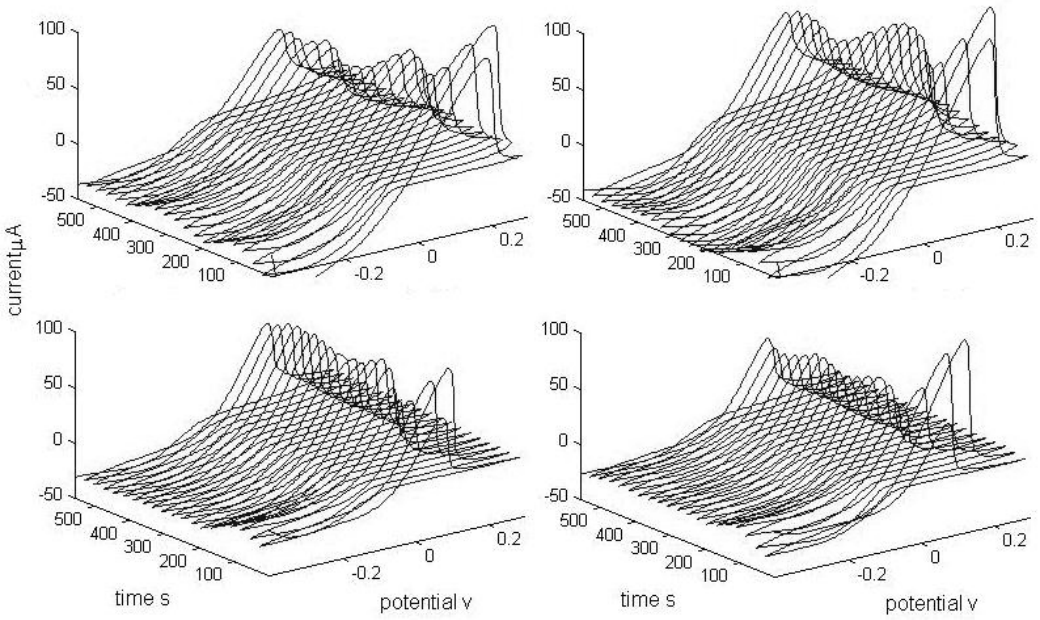

Figure 6.7 Electrodag carbon strips with Electrodag silver strips cycled in 4 M KBr

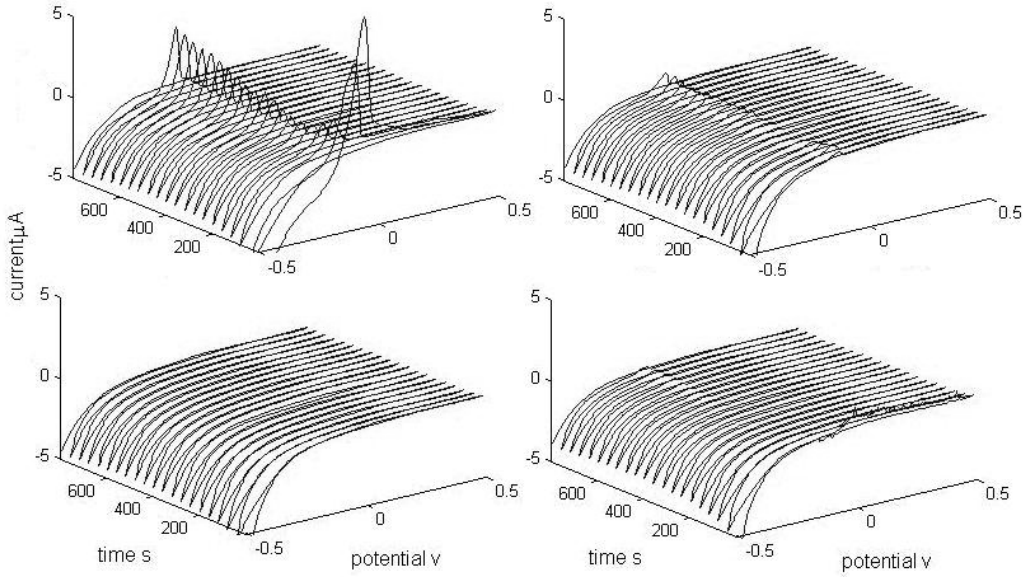

Figure 6.8 Electrodag carbon strips with Electrodag silver strips covered in a Nafion film cycled in 4 M KBr

Nafion films were also applied to the DuPont strips, but the reduction of interference was only about 50-60 %. After several attempts, it was thought that the film permeability must have been compromised on the DuPont strip, and that this was due to the physiochemical properties on the surface of the silver.

By Inspection, the Nafion film on the DuPont silver ink (BQ164) could not be seen as a separate layer as it could on the Electrodag silver. It is possible that the Nafion solution is partly absorbed or percolates into the DuPont silver preventing a separate layer formation.

Using a Nafion film, the silver interference (in a 4 M KBr electrolyte) could be entirely eliminated. Whilst this applied to Electrodag 6038 Ag/AgCl only a 50-60 % reduction in interference was possible with DuPont BQ164 Ag/AgCl.

The Electrodag silver contains 90:10 Ag to AgCl ratio whereas the DuPont ink contains a 65:35 % ratio. The DuPont ink changes colour when 4 M KBr is applied attributed to the formation of AgBr; but the change of colour of the Electrodag silver

was slight. It was hypothesised that the silver salt loading in the ink directly affects the susceptibility to halide reactions.

For the consideration of Nafion as a practical solution to the silver problem, several silver inks were studied. The silver inks were compared visually after reaction with droplet of 4 M KBr, as shown in Figure 6.9. Strips were exposed between 1 and 5 min; the apparent reaction took place in less than 30 seconds. The Electrodag silver showed only slight change in colouration - in Figure 6.9A the black colour is the carbon ink showing from below. The 80:20 and 65:35 silver inks reacted strongly, as shown in Figure 6.9B and Figure 6.9C. The 65:35 ink formed a darker colour after reaction. The distribution of material (presumably AgBr) accumulated more at the drop edges. The E107255-45 B silver ink was a darker colour before reaction (as shown in Figure 6.9D). Application of the KBr solution caused further darkening of the surface. The results indicate the degree of reaction correlated to the Ag/AgCl loading in the ink. This can be attributed to a fast substitution reaction of Br^- for Cl^-. There is probably also a slow oxidation of silver for which an electron acceptor, such as dissolved oxygen, is needed.

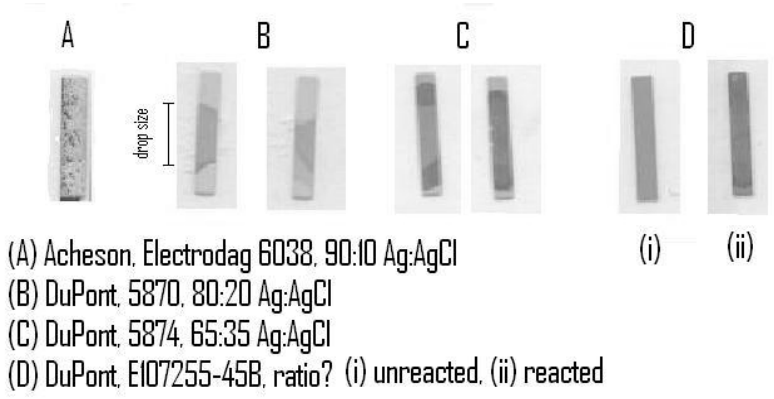

Figure 6.9 The effect of 4 M KBr applied as a single drop for about 5 min, on 4 Ag/AgCl ink formulations as indicated

6.3.2 Non Silver Reference Electrode

A standard gold electrode was used as a reference electrode with DuPont sensors from which the silver strip had been removed. The electrodes were cycled in 4 M HCl. Good stability was found after several initial scans. The voltammograms were shifted negatively compared to the Ag/AgCl reference by about 400 mV; the measured potential 0 V corresponding to the oxidative wave about 0.5 - 0.6 V (vs Ag/AgCl) suggesting the Au/AuCl couple. However, when the reference electrode was removed and replaced from the electrolyte, strong potential drift occurred and a different stable point was found. The DuPont screen-printed gold strip was also tried in place of the standard gold. The same problem occurred. With platinum, the potential drift was more severe. Carbon gave the poorest stability as reference electrode.

Using an Au reference electrode with the silver strip removed, DuPont sensors were cycled in 4 M HCl, as shown in Figure 6.10A. The primary interference has been removed. The spike and possibly secondary peak (going by the shape at about -0.2 V in Figure 6.10A, and 0.1 V in Figure 6.10B) are still present. The effect of the solubility of the ink accounts for the widening background currents as the electrolyte percolates to a greater gold particle surface area. In 4 M NaCl (Figure 6.10B) the background widening is not seen as expected since the solubility is pH not Cl^- dependent.

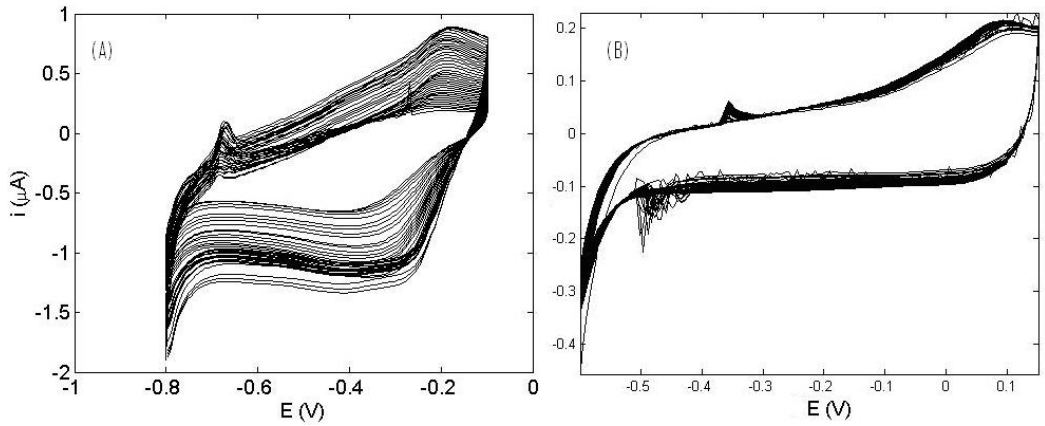

Figure 6.10 Standard cyclic voltammetry with DuPont sensor printed without silver strip using an Au refernce electrode. (A) Scan range -0.8 to -0.1 V in 4 M HCl And (B) Scan range -0.6 to 0.2 V in 4 M NaCl

6.3.3 Experiments to Identify the Cause of the Spike Peak in Screen-Printed Electrodes

Due to the low quantity of material to be detected a surface detection procedure such as EDX or XPS was unlikely to identify the compound, clearly. Initially a probe was constructed to investigate inks by proximity. Where the spike peak was found to occur the introduction of longer potential deposition steps at negative potentials were found to increase the spike effect where as the spike tended to decrease with standard cyclic scanning. Initially the DuPont sensor surface was tested with exposed silver, gold, carbon, insulation and PET substrate: a spike peak could be obtained after a number of scans. The PET substrate was tested alone, then the insulation, carbon ink and silver inks.

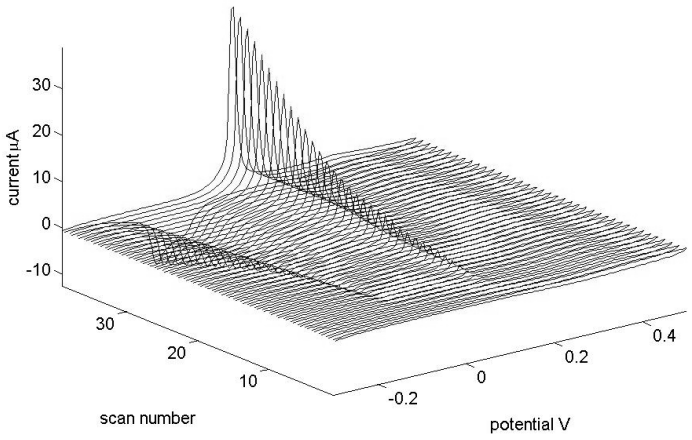

Figure 6.11 Probe of DuPont Sensor: 30 s depositions for each of 40 scans at -0.3 V, cycled in 1 M HCl on a DuPont sensor with exposed PET substrate, carbon, insulation, silver and gold inks. Working electrode: standard gold disk, counter electrode: standard platinum disk and reference electrode: glass capillary Ag/AgCl.

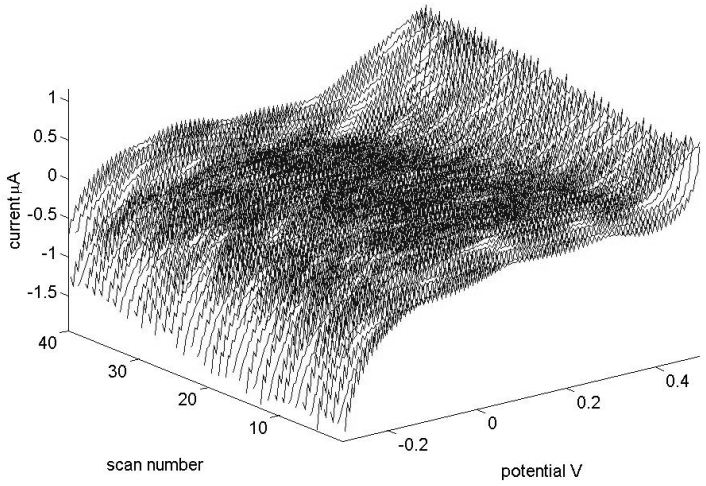

Figure 6.12 Probe of DuPont insulation ink alone with experimental parameters of Figure 6.11

Figure 6.11 implies that the DuPont sensor causes some interference sourced from some material on the screen-printed sensor surface. Figure 6.12 shows that the interference is not coming from the insulation ink.

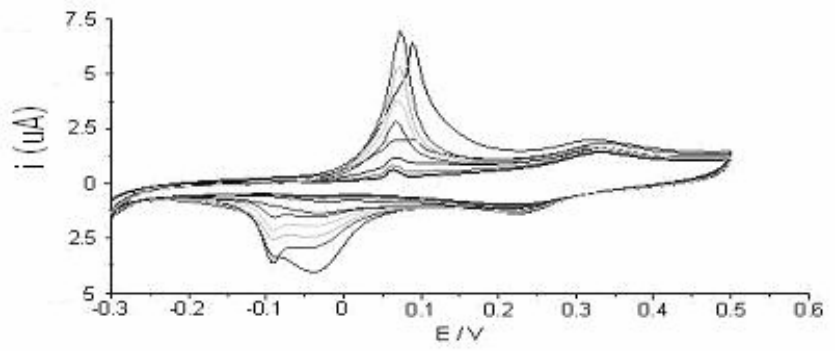

Figure 6.13 Changing the deposition times manually during study of the spike peak on gold working electrode cycled in 1 M HCl in proximity to an exposed DuPont sensor

Figure 6.13 shows that a large (> 10 µA) spike peak could be 'converted' to a wider peak typical of a bulk silver peak. Note also the underdeposition potential stripping peak of silver at 0.25 – 0.35 V. The evidence for silver as the cause of the spike peak is strong.

Where a sharp spike occurs from the first scan, for example with screen-printed DuPont gold and Electrodag 423 SS carbon working electrodes the contamination must be present before diffusion could occur. A probe of the carbon Electrodag implies that interfering species given from the electrode are minimal (Figure 6.14).

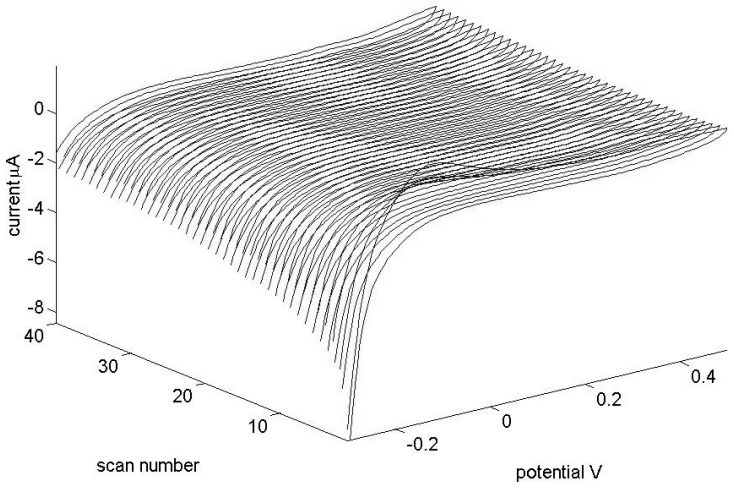

Figure 6.14 Probe of Electrodag Carbon on PET substrate: Experimental parameters as for Figure 6.11

With the inclusion of the Electrodag silver ink to the experiment of Figure 6.14 the spike peak was found building with scan number.

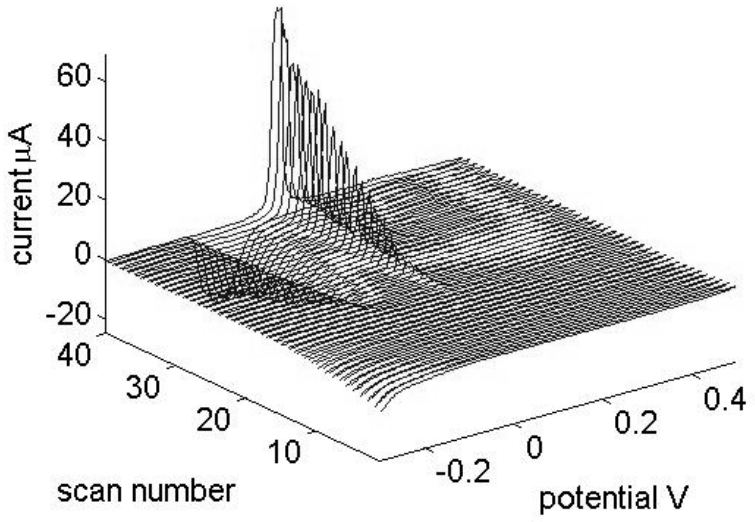

Figure 6.15 Probe of Electrodag Carbon and Silver inks on PET using experimental parameters of Figure 6.11

A small quantity of silver was apparent in the XPS spectra of one of the two DuPont surfaces tested as shown in Figure 6.16. The Silver (peaks at 367 and 373 eV) was near the detection limit of XPS equivalent to about 0.1 % coverage of the top 5 – 10 nm.

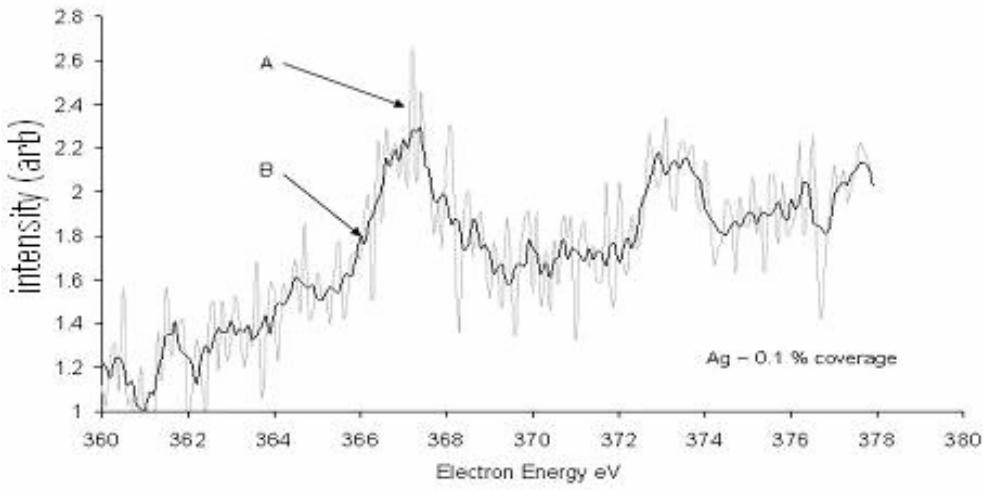

Figure 6.16 XPS spectra after extended dwell time for silver with uncycled Dupont gold surface: (A) original data and (B) data after 5 point smoothing

However, DuPont Microcircuit Materials (Bristol, UK) prepare and print inks in clean room (dust-free) conditions and silver contamination of the gold formulation would not be expected either during ink preparation or during printing. Further proof of silver as opposed to some organic moiety would be needed, to be sure. For example the Electrodag silver may contain a surfactant which solubilises deposits on the working electrode in a condensed phase and so causes sharp peaks. The peaks at 0 V may come from some silver leakage form the glass capillary reference electrode.

However, the proximity of silver and working electrode inks using the standard screen-printed electrode design suggests that cross contamination could easily occur. A further batch of electrodes was printed at DuPont with PET substrate, gold, carbon and insulation layers as usual. The silver was not printed. The hope was that the spike peak would be eliminated since the opportunity for spatter of silver during printing had been removed. However, the spike peaks were still seen in this batch. The printing unavoidably would have used the same screens, possibly squeegee, and preparation facilities. Unfortunately it is not possible, due to time and access constraints (to the facilities at DuPont) to examine the printing process more carefully.

A carbon ink was prepared carefully (avoiding any material or tool possibly contaminated with silver), *in house* using polymer X carbon flake formulation as described in Section 2.4.3. Well-adhered tracks were obtained, but coverage was variable (due to manual conditions, dust, clogging, and applied pressure) such that the track length resistance varied from 2 to > 10 kΩ. Gaps could be observed when the electrode sheets were held up to the light.

Some electrode samples were cycled in 1 M HCl using a glass capillary Ag/AgCl reference electrode. It was found that a spike would build after a couple of scans on the printed carbon electrode, unless the glass capillary reference electrode was rinsed in pure water. Excessive rinsing caused the reference electrode to lose stability presumably due to high impedance of pure water trapped in the ceramic frit. The carbon electrodes were repeatably clear of the spike, for example Figure 6.17(A). The spike peak seen was only the forward peak and the reverse peak was absent. On

further screen-printed polymer X/carbon samples Electrodag silver was hand painted to use as reference. Cycling in 1 M HCl showed a build up of the spike peak and again only for the forward peak. To eliminate the chance of a surfactant in the silver ink causing the spike peak, a silver ink was prepared by mixing 25 % polymer X in γ-butyrolactone with silver powder 2:5 by weight ratio (silver is about 4.9 times as dense as carbon); no silver chloride was included. The silver ink formulation was hand painted to the polymer X/carbon screen-printed electrodes to act as reference. As shown in Figure 6.17B, the spike peak was seen to build up after several scans. However since the electrode system was fabricated entirely *in house*, the ink components were known – the role of surfactant could be ruled out. The only extra component in the system that could cause the spike peak was the silver. Thus the silver must be the cause of the spike. However this spike phenomenon apparently only includes the forward spike – the reverse peak and the stochastic behaviour seen on some electrodes could possibly only be coincidence.

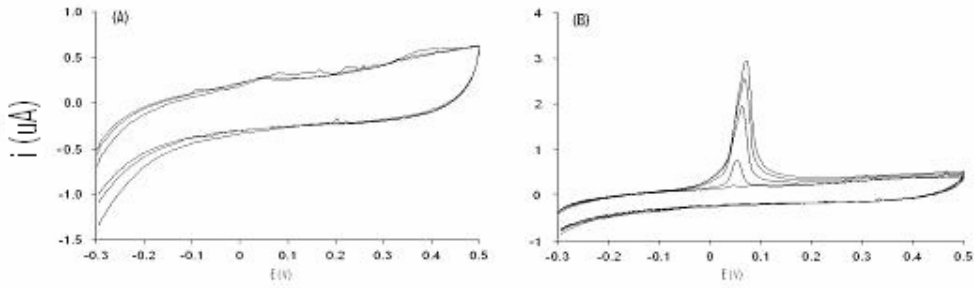

Figure 6.17 Polymer X/carbon flake electrodes cycled in 1 M HCl (5 cycles): (A) rinsed glass capillary electrode as reference no printed or painted silver; (B) hand painted polymer X/ Ag powder reference strip

In one final experiment a clean carbon electrode was printed with polymer X/carbon ink as mentioned previously. In 1 M HCl electrolyte with a rinsed Ag/AgCl glass capillary reference the electrode was cycled and no spike peak was seen (Figure 6.18A solid line). A 1 mM $AgNO_3$ solution was prepared by diluting a 1000 ppm $AgNO_3$ stock solution. 2 µl of this solution was pipetted to the carbon working electrode surface. Subsequent cyclic voltammetry in 1 M HCl showed almost complete depolarisation ascribed to the Ag/AgCl reaction, as shown in Figure 6.18A

(dot-dashed line). The electrode was washed with concentrated HCl and wiped with Nuffield Blue towel and the silver reaction reduced until peaks were about 30 µA with a rounded shape, as shown in Figure 6.18(B). Washing with HCl again reduced the peaks to about 10 µA now with a spike like shape, (Figure 6.18B solid line). As a control, HCl washing and wiping with Nuffield Blue was applied to a clean carbon electrode (Figure 6.18A dashed line) – no interference was found to result.

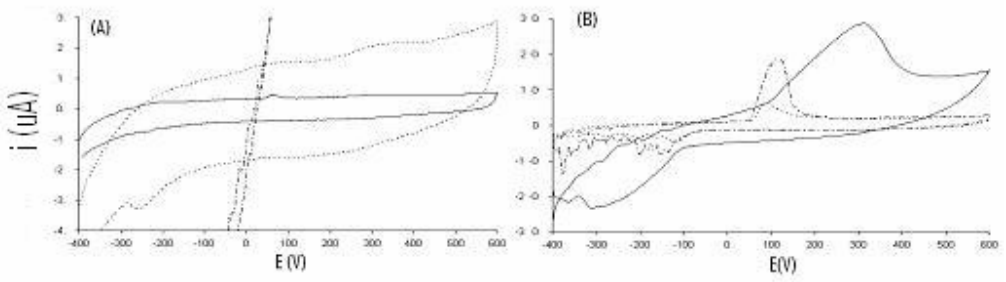

Figure 6.18 Polymer X/ carbon screen electrodes cycled in 1 M HCl with a rinsed Ag/AgCl glass capillary reference electrode. (A) clean electrode (-); HCl washed electrode (- -); and 2 µl of 1 mM $AgNO_3$ added (-.-); (B) silver added electrode after 1 washing with HCl (-); after two washes (--); and a new electrode with silver applied and washed twice in HCl(-.-)

Figure 6.18B (dot-dashed line) shows another electrode to which silver was added and then washed in HCl. The silver is clearly the cause of the forward and the reverse spike peak, as well as the stochastic behaviour. The variety of shapes adopted by the silver contamination has also been shown highlighting the need to avoid this phenomenon during reproducible analysis procedures.

6.3.4 Preparation of Microband Electrodes

Microband DuPont sensors were prepared by cutting the sensors such that the exposed edge was sandwiched between the PET substrate and the insulation layer above, as shown schematically in Figure 6.3. In the previous studies of Chang and Zen (2006a and 2006b) little is described with regard to controlling the surface quality, evidently critical in the mass production of sensors. A blunt pair of scissors would have a greater shear effect, dragging the material such as the gold and the insulation layer

down across the PET surface. Brittle substrate or inks could cause flaking exposing macro sized regions of ink surface.

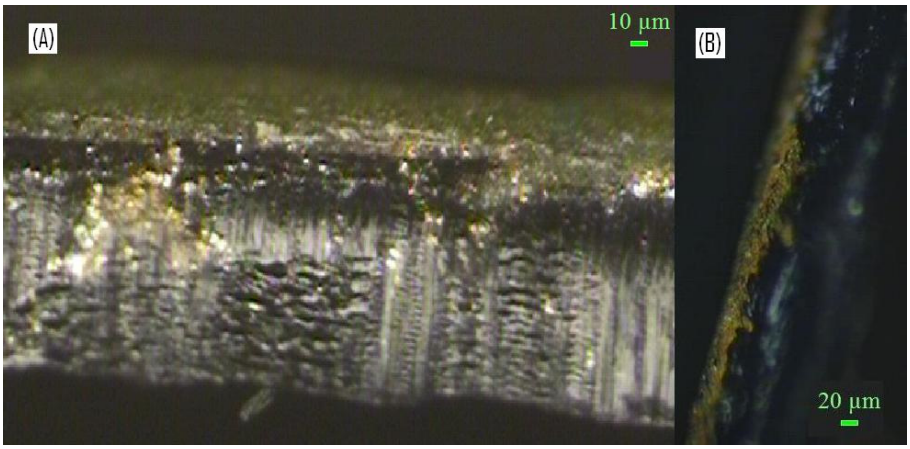

Figure 6.19 DuPont sensor gold ink edge cut with (A) Stanley knife and (B) scissors, both with downward cut on the gold edge.

Figure 6.19 shows the ink edges for Stanley knife (A) and scissor cut (B). Both examples show the effect of shear force dragging the ink downwards. A greater amount of gold ink is apparently exposed with the scissor. With the Stanley knife, the insulation layer (green) is covering the gold. The quality of these surfaces would be affected by the sharpness of the blade, as well as cut orientation.

Several cuts were made and variation was apparent between sensors. Since the taped samples (schematic in Figure 6.4) for observation were not fixed, the sensors could be observed from several angles, as shown in Figure 6.20. The angle did not affect the visible gold exposed at the surface. However along a single electrode, the exposed gold varied from being almost covered by the insulation shroud to being highly exposed.

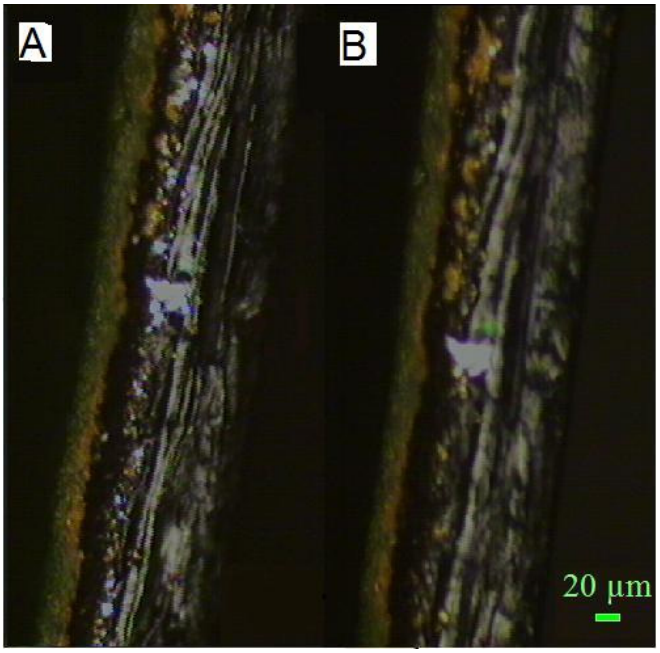

Figure 6.20 Observation of gold surface with slight lean toward (A), and lean away from (B), the microscope objective

A roller cutter, such as those used for paper trimming was considered. A circular blade is mounted on to a rail and constrained to move smoothly along fixed trajectory and held closely to a long flat blade on the roller cutter base. Thus the cut should benefit from consistent parallel and transverse angle of attack. The whole outer rim of the blade is used so that wear on an individual blade section is lessened. One cut could be used to prepare a single row of eight electrodes. Figure 6.21 shows the schematic of the roller cutter: due to asymmetry the cut on the outer and inner blade edge would be expected to have different levels of friction and shear force.

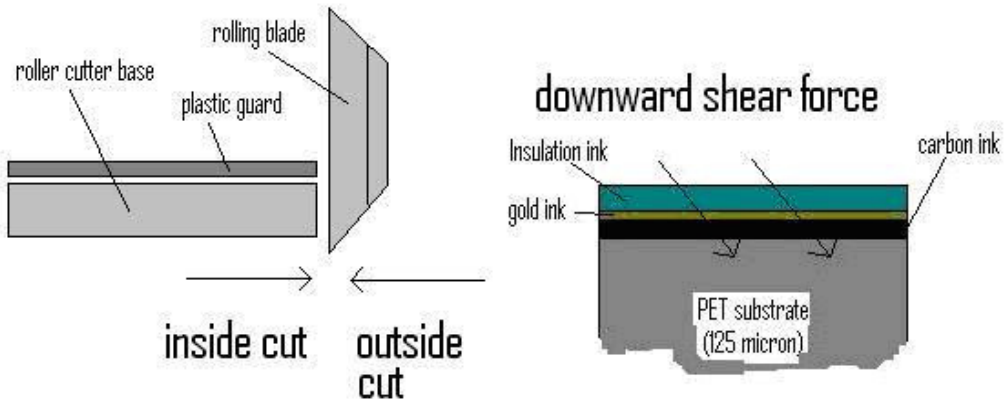

Figure 6.21 Schematic of the roller cutter and cut sensor edge

Shear force maybe reduced by using a vertical blade kept as sharp as possible. One way to avoid frictional forces altogether would be to use a laser. A CO_2 laser marker operating at 15 % (of a 25 W maximum) the minimum power needed for a complete cut was used to prepare microband surfaces. The laser focuses a narrow spot of infrared light (10.6 μm) on the sample. The precise width of the laser spot is not known. The cut lasted less than 1 second for a single electrode.

Incidence of the infrared light caused an initial flash attributed to temporary ignition of the polymeric material. A plume of vaporised materials was seen to rise from the cut. Inspection of the electrode surface is shown in Figure 6.22. The PET was blackened due to charring. The surface edge was not flat as with the sliced edges. The gold and insulation inks apparently receded from the edge. The surface was not stable since wiping caused a change in the available gold surface area, as shown in Figure 6.22B.

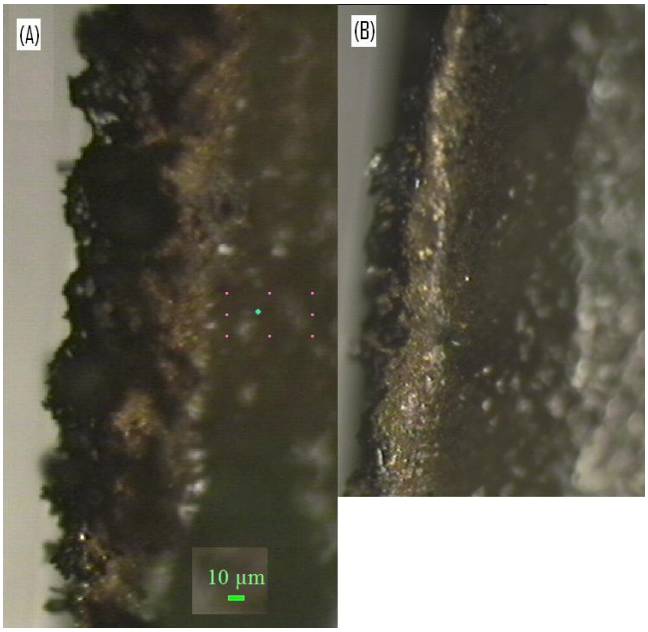

Figure 6.22 Top-down image of CO_2 laser treated DuPont working electrode edge, as prepared (A), and after wiping (B)

The roller cutter was found to give the most repeatable surface. A triplicate sensor surface is shown in Figure 6.23; these sensors were cut with the gold surface faced upwards and used the inside edge of the blade as indicated in Figure 6.21.

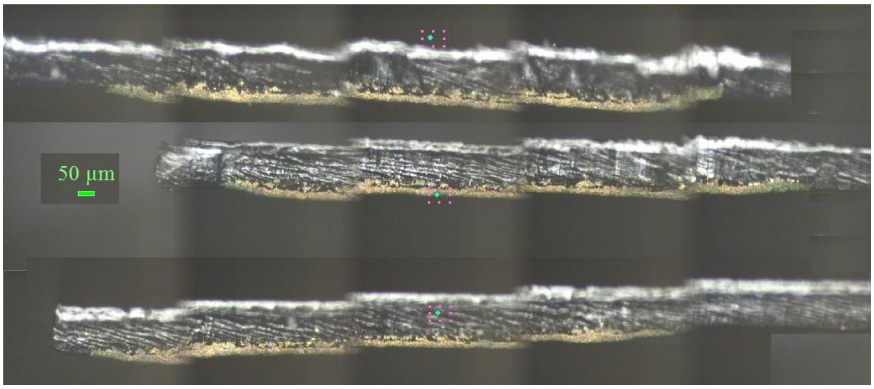

Figure 6.23 Triplicate of DuPont edge sensors with inside roller cut: 5 images per electrode showing the entire edge

6.3.5 Electrochemistry of Microband Electrodes

The microband electrodes were tested in 5 mM potassium ferrocyanide solution (with 0.1 M NaCl) and an acetate buffer solution pH 4.5, as shown in Figure 6.24. For these examples, the working, counter and reference electrode were cut as microbands – the electrode was inserted vertically into a beaker containing about 10 ml of electrolyte. The size of the current is small as 100 nA for the redox buffer and < 1 nA for the acetate buffer attributed to the low electrode surface area. The basic background capacitive currents as measured in an acetate buffer are very low. The ferrocyanide buffer shows sigmoidal profile due to convergent diffusion. Repeatability of the ferrocyanide limiting currents (+ 100 nA and -300 nA) for 3 electrodes was good.

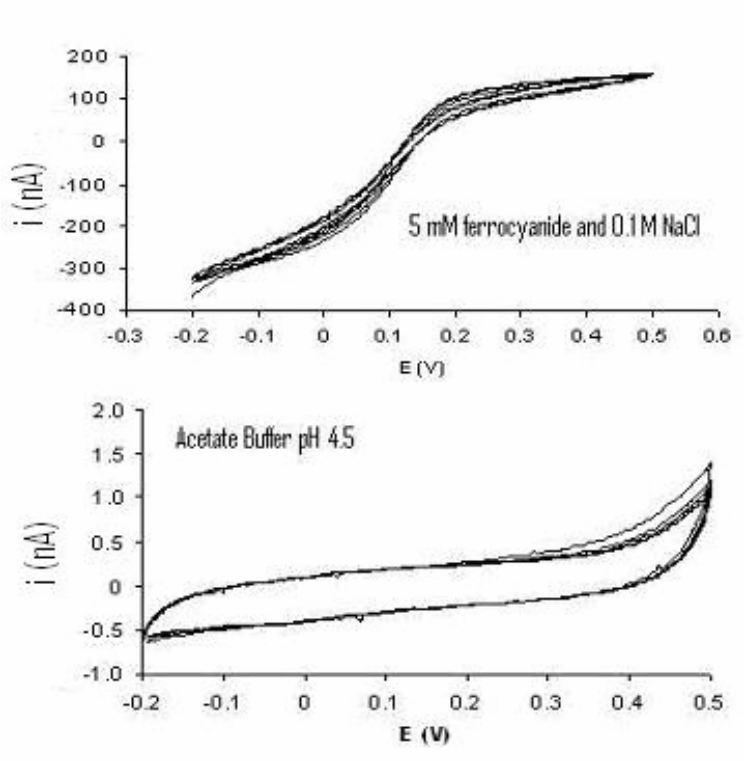

Figure 6.24 DuPont microband sensor prepared as for Figure 6.23 electrochemically cycled with standard redox couple and with standard buffer as indicated. Scan range as indicated, 5 scans for each and scan rate 50 mV/s, no electrochemical pretreatment

Although the capacitive currents would reduce, the redox behaviour of BQ331 would be expected to be consistent with macro electrodes. In acids a rising baseline would be

expected due to polymer solubilisation (as seen in Figure 5.5). A rising baseline can be seen in Figure 6.25 where a microband sensor has been cycled in 4 M HCl. A gold reference electrode has been used to avoid any silver interference; the location of the 0 V point in comparison to the voltammetric profile shows that the gold reference is operating close to the oxidation wave, probably due to the Au/Au-Cl complex couple. The background current level is significantly higher than the acetate buffer, about one order of magnitude in the cathodic limit, attributed to the evolution of hydrogen in the strong acid.

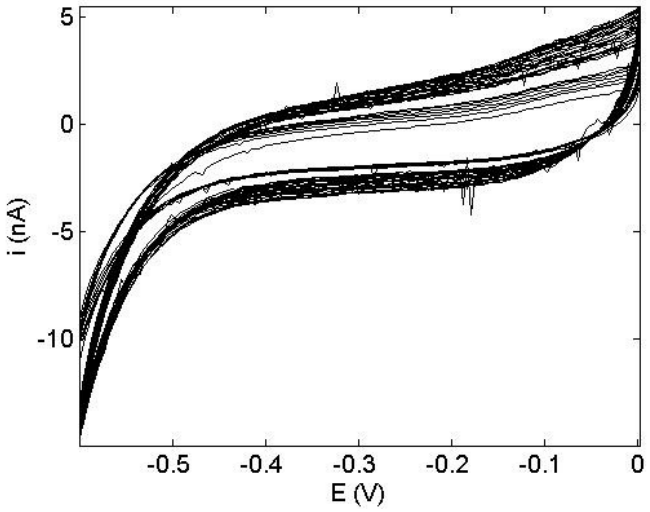

Figure 6.25 Microband DuPont gold working electrode scanned in 4 M HCl with a gold disk reference electrode (silver reference strip removed), the cycle was paused between scans 10 and 11 for about 10 min. Scan range as indicated, otherwise CV parameters as given (Table 2.3)

The microband electrodes were first tested with As(III) with 1 M HCl facilitating a reliable arsenic peak. For 200 ppb As(III) in solution a good peak was registered. However, the reproducibility was poor and electrode saturation was thought to be the cause. A 20 ppb concentration of As(III) registered a 1 to 2 nA peak at about 0.15 V with 30 s deposition at -0.3 V, as shown in Figure 6.26. No residual silver was seen on 5/6 electrodes tested, the silver interference on the 1/6 resulted in a peak > 1000 nA, evidence for localisation of silver on the gold surface. A small peak at 0.15 V was also registered for an As solution prepared to 1 ppb using longer 6 min deposition. However silver contamination was in evidence, increasing with each experiment. The

reference electrode used was a glass capillary housed Ag/AgCl wire with a Vycor frit stored in saturated NaCl solution (as shown in Figure 6.1). With the high Cl^- ion content, solubilised Ag complexes would be expected (Figure 5.20); the rinsing of the glass house before testing had only a temporary effect as seen with the 6 min depositon times.

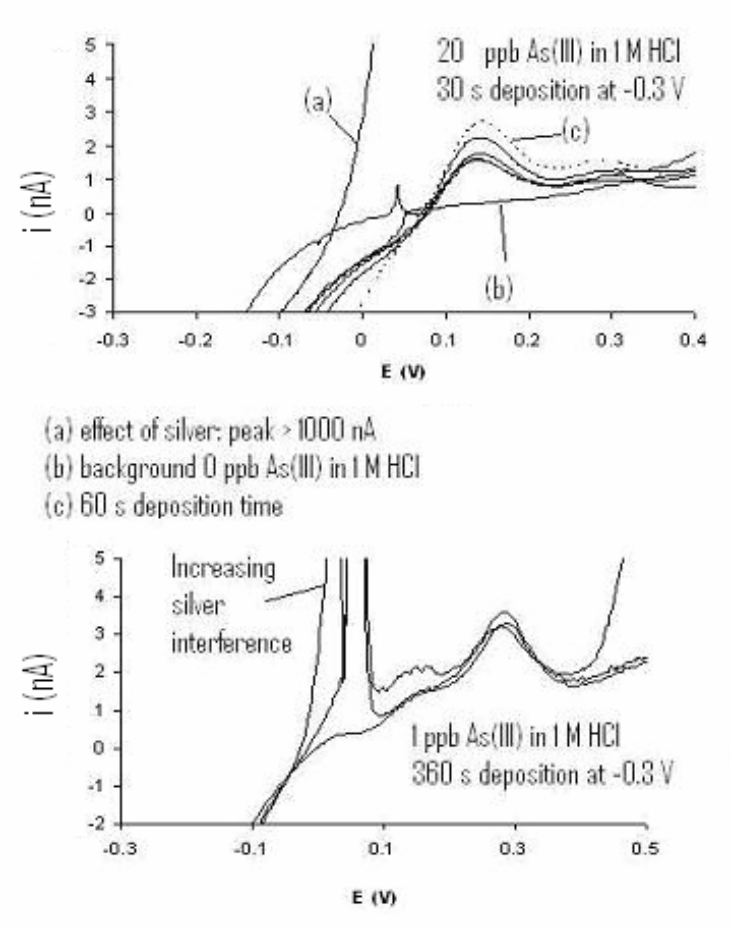

Figure 6.26 Voltammetry of As(III) prepared in 1 M HCl on DuPont Microband electrodes with silver strip removed and reference provided by a rinsed glass capillary Ag/AgCl (stored in saturated NaCl). Scan rate 100 mV/s.

Arsenic was then analysed by ASV in 4 M HCl. The background currents were significantly higher, particularly for the cathodic regions. An approximate 1 nA peak for As was seen after 60 s deposition, as shown in Figure 6.27. In this case the Autolab showed sinusoidal interference presumably due to electrical mains

interference with amplitude about 2 nA peak to peak. The voltammograms shown in Figure 6.27 have been smoothed with 5 point average. The addition of 100 ppb Cu(II) did not affect the As(III) peak. With a 180 s deposition time the As(III) for 5 ppb was as large as 4 nA (not shown).

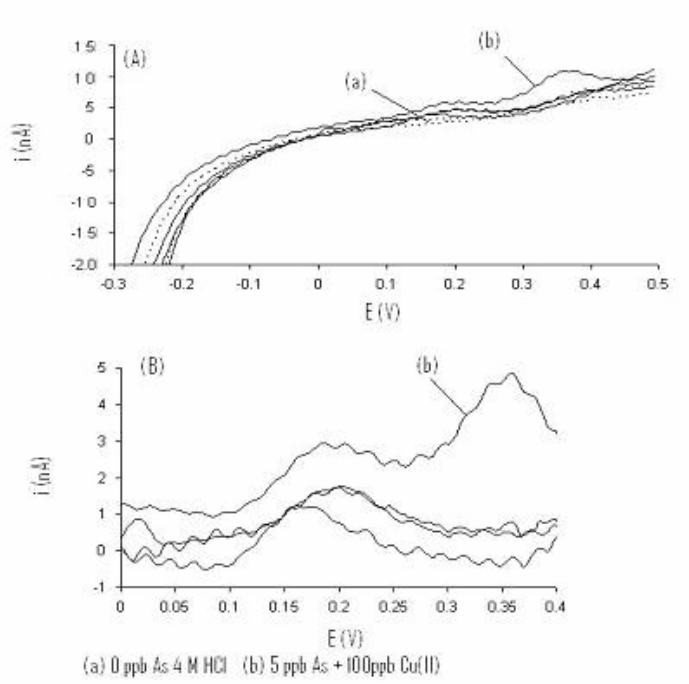

Figure 6.27 Anodic stripping voltammetry with microband electrodes of: (A) 5 ppb As in 4 M HCl (3 repeats), dotted voltammograms show background and voltammogram marked (b) contains 5 ppb As and 100 ppb Cu(II) as indicated. (B) background subtracted shown As peaks. Reference electrode: glass capillary Ag/AgCl stored in 0.01 M NaCl.

A calibration for As(III) was produced between 0 and 20 ppb. A 180 s deposition at -0.3 V (vs Nafion covered Ag/AgCl strip) and stripped at 100 mV/s. peaks heights were calculated as shown in Figure 6.28.

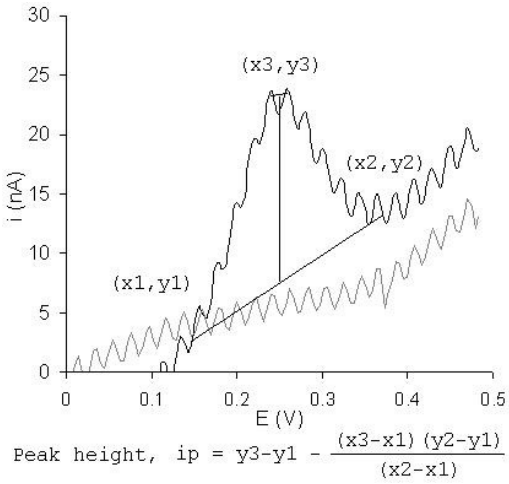

Figure 6.28 Calculation of As(III) peak height using linear stripping voltammetry

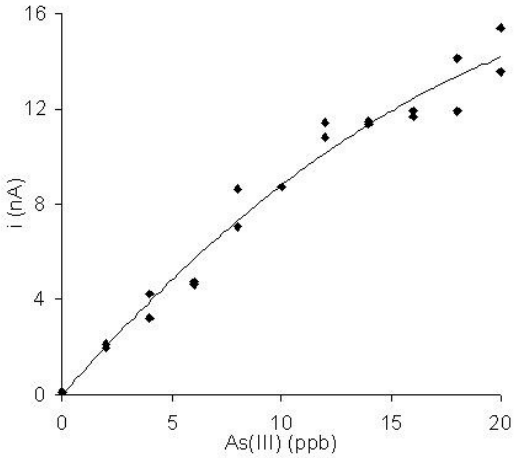

Figure 6.29 Calibration curve for As(III) between 0 and 20 ppb based on peak height with calculation as given in Figure 6.28. Deposition at - 0.3 V for 180 s then linear strip at 100 mV/s

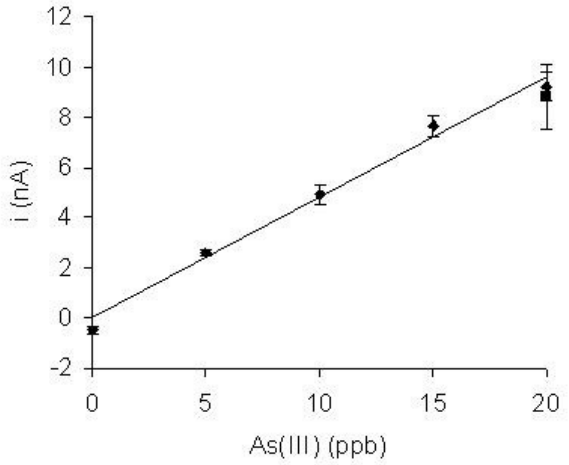

Figure 6.30 Calibration curve for As(III) additions to River Water (River Ouse, Bedford, UK) (diamonds) and comparison with pure water sample (square).

As stripping was tried with excewss interfering metal ions Cd, Cu, Pb, Fe, Cr, Zn and Bi. Cu, as already discussed is the most problematic ion likely to occur. These metals were test at levels of between 100 and 500 ppb with 10 ppb As(III). Only Bi was found to overlap the As peak (Figure 6.31). Bi is not likely to occur at this level in drinking water.

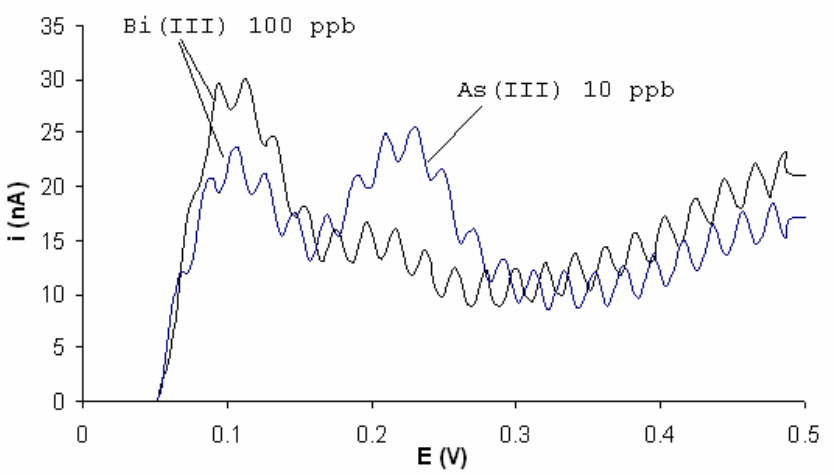

Figure 6.31 ASV with 4 M HCl with 100 ppb of Cr(VI), Zn(II), Fe(II) and Bi(III) with and without 10 ppb As(III). Depostion 180 s at -0.3 V and stripping at 100 mV/s

The electrochemical acitivity of As(V) on the gold microband sensors was tried. The deposition potential was varied from -0.3 to -0.7 V. A peak was seen below -0.5 V.

Reproducibility based on 6 repeats gave a range of peak areas of upto 150 % for the same level of arsenate. The formation and adhesion of hydrogen bubbles could be seen with each test covering a portion of the electrode surface.

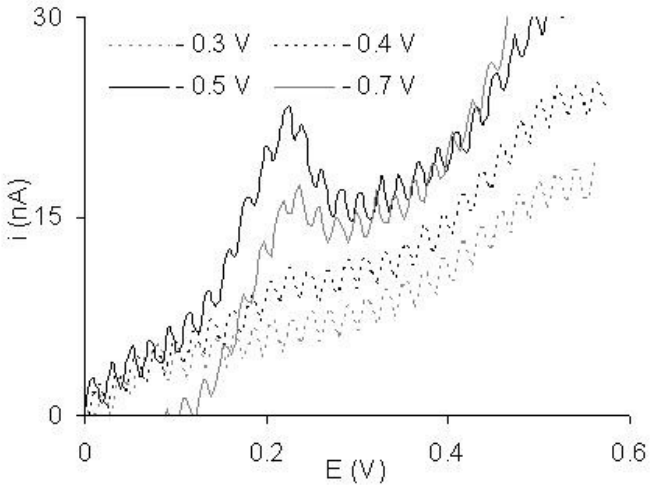

Figure 6.32 ASV with 100 ppb As(V) in 4 M HCl with deposition 180 s at potential indicated and stripping at 100 mV/s

6.4 Discussion

6.4.1 Identification of Interferences

Three electrochemical interference peaks were seen in Chapter 4 (Figure 4.10C). The primary peak, with the largest peak areas, corresponds to the highest charge exchanged and would be ascribed to the majority of the silver seen in the XPS experiment (Section 5.3.10). In Cl^- ion electrolytes this peak occurs above about 2 M Cl^- ion concentration. Referring to the literature (Lorenze *et al.* 1971, Kolb *et al.* 1974, Herzog and Arrigan, 2005), the secondary peak could be ascribed to stripping of a monolayer silver from the gold surface (as described in Section 6.1.1). This peak is not evident on carbon, at least within the range of potential studied (typically < 0.5 V vs Ag/AgCl), and only weakly present on Pt (for example see Figure 4.20). The basic interpretation is that silver has a high affinity for gold, so stripping of a

monolayer of silver from gold, where a surface alloy forms, takes a greater energy than for bulk silver; therefore, the peak is seen at more positive potentials. This peak appears largest at Cl^- ion concentrations above 1 M but does not increase as the primary peak does attributed to gold surface saturation.

The spike peak appears to demonstrate some complex behaviour behaviour such as stochastic reduction (particularly on carbon electrodes) and changeable shape (Figure 6.13). A number of experiments were needed to prove that the spike peak was coming from silver, eventually achieved by the addition of silver salt to an otherwise clean carbon screen-printed electrode (Figure 6.18). This experiment showed that the oxidation and reduction peaks, as well as the stochastic behaviour could all be stimulated by silver (although, the formation of Ag-Cl complexes may play a part in some of these behaviours). It was demonstrated that the spike peak can result from solubilisation of silver in 1 M HCl from a reference electrode (Figure 6.17). Also it was found that the glass capillary reference electrodes stored in saturated NaCl could cause silver to solubilise and generate a spike peak.

It appears that the spike peak has been used by researchers for analytical methods. Saterlay *et al.* (2000) used boron doped diamond electrodes for the analysis of Ag. The reaction was controlled by the use of low Cl^- ion levels (12.5 mM KCl in 0.5 HNO_3) which were found to produce a sharp spike at about 100 mV (vs SCE) deemed good for Ag sensing purposes. It was thought that the transition from rounded (0.4 V) to sharp (about 0.1 V) stripping peaks correlated to the transition in Ag-Cl complex from AgCl to $AgCl_2^-$. Although this work clearly supports the conclusion that silver causes the spike peak, the interpretation of the rounded and spike seems too simple to apply to the results in this thesis. The relationship between spike and round is more complex and can be dependent on time of deposition such as Figure 6.13 and Figure 6.15. The larger body of work supports the complex relationship between crystalline and monolayer formation at the gold surface. Perhaps the spike formation is more stable at a boron doped electrode than at a polycrystalline gold, platinum or carbon electrode. Also the silver monolayer formation of boron doped diamond would be expected to be different to that of gold. More work could be done to study the spike

peak behaviour in detail looking at the quantitative changes with Cl^- ion concentration, controlled levels of silver with a specially prepared silver reference.

A convincing explanation for the peak behaviour could be made by drawing an analogy to a study on PbO_2 deposition. Laitinen and Watkins (1975) studied the electrochemical stripping of lead from an antimony doped tin electrode. A spike peak with stochastic behaviour was observed. The spike was attributed to crystalline formation of PbO_2 with complex kinetics associated with nucleation and growth. Where PbO_2 was adsorbed as a monolayer the peak was broad. It is possible that the formation of AgCl crystals on the electrode surface particularly with the carbon lends to nucleation and crystal growth which strips with a stochastic type behaviour. The charge interactions between AgCl crystals cause the narrow peak.

The sharp peak (about 85 mV vs Ag/AgCl) and rounder peak at about 0.4 V noted by Navritil *et al.* (2003) when Cl^- ions exceeded 0.15 M was due (according to the results in this thesis) to silver contamination from the reference electrode.

6.4.2 Methods to avoid Silver Solubilisation and Interference

The most direct way to avoid silver interference would be to preclude the use of silver from the sensor. Then, a different reference system is needed. Of the carbon, platinum and gold quasi reference electrodes which were tried in 4 M HCl. Gold, only, produced a reasonably stable potential with scanning and none were reproducible when the reference was removed and replaced into the electrolyte. A quantitative test based on stripping voltammetry will require that the potential of deposition is reproducible. The potential of the gold reference suggests the Au/AuCl couple, and so the potential could be stabilised by the addition of $AuCl_3$ to the electrode. Inevitably some gold salt will enter the solution. This is not necessarily a problem since many researchers have intentionally added $AuCl_4^-$ to solutions to improve the gold active area on deposition and improve As(III) oxidation on stripping (Munoz and Palmero, 2005). The question remains whether the Au/AuCl electrode would be rapid and stable enough for ASV.

The Nafion film result implies that complete elimination of silver interference is possible, assuming that complete films can be applied. A change in silver ink would be necessary to act as substrate to a stable film with the DuPont sensors, the Electrodag 6038 SS would be suitable.

With the presense of the film, interference is seen, (Figure 6.8), the peak is shifted by approximately 100 mV (in comparison to electrodes without a film) in the negative direction which is stable with time. The Nernst Equation can be used to provide a rough value for the reduction in Br^- ions reaching the reference electrode surface. Assuming a one electron transfer and room temperature a 50, 100, 150 and 200 mV negative shift equates 7, 52, 380 and 2800 fold reduction in Br^- ion activity respectively. So going by concentration (neglecting the activity of Br^- ions in this 4 M electrolyte), the effective concentration at the reference electrode is about 4/52 equal to 0.08 M. In addition the Nafion film would be expected to block passage of any soluble AgBr complexes formed at this effective concentration.

In a meeting with DuPont the possibility of preparing reference electrodes with Nafion films was raised. The common precursor of Nafion 117 dissolved about 5 % in a mixture of alcohols, having low viscosity, and with the possible degradation effect of alcohol on screens and squeegee, would not be printable. However, were the viscosity to be increased, thicker films would result and increasing barrier properties of the Nafion film. If the Br^- ions were entirely blocked the reference would not be stable. Therefore further ink development would be needed; it is not clear how the issue would best be approached.

In general, higher loadings of AgCl give a greater stability to the reference electrode, due the ability to maintain potential with transient influxes of both negative and positive currents (Chan, 1998). It is also possible that these inks can cause a low level of Cl^- ions in other wise non-Cl^- ion electrolytes providing the stability seen, for example in Figure 4.13. High AgCl loaded inks can be used in two electrode systems due to the ability to maintain stable potential whilst passing currents (Chan, 1998).

An Arsenic sensor using high HCl electrolytes needs to minimise Ag interference, a conclusion which is clear from Chapter 4. A sensor using anodic stripping voltammetry also needs a stable potential reference system for a consistent deposition potential. Reducing the AgCl loading in the silver probably reduces the quantity of Ag-Cl complexes formed within the time frame (for As analysis by ASV, i.e. several minutes) which maybe useful for one-shot sensors. If the AgCl was to be eliminated from the reference altogether, the stability of the potential would be risked.

Finally the practical means of avoiding silver solubilisation in electrochemical experiments was to use a glass capillary Ag/AgCl reference electrode where a ceramic frit offers a physical barrier to the diffusion of silver. The reference electrode stored in silver solubilising saturated NaCl demonstrated rising silver interference (Figure 6.26) but appeared more stable when the storage electrolyte was 0.01 M NaCl (Figure 6.27), as would be expected from the solubility chart for silver (Figure 5.19). The lower ion content of the electrolyte results in an increased reference electrode impedance which could threaten the potential stabilisation. However, a non silver complexing salt could be used (> 1 M concentration) to supplement the conductivity.

6.4.3 Residual Silver in the Electrodes

There is some evidence that silver is found in some screen-printed electrodes as a residual:

1. The spike and secondary peak can be seen even at Cl^- > 1 mM (Figure 4.19), where solubility of Ag is in the low µM level (Figure 5.19).

2. The XPS measurement of an unused DuPont sensor detected a low level silver (Figure 6.16)

3. Measurements using gold reference electrodes still showed the spike peak (Figure 6.10) despite silver being entirely removed from the system.

In general the interference could occur when gold ink is prepared, printed or handled (after printing). So to find out the whole process would have to be considered. As part of the Batch of sensors provided in November 2007 (Table 6.1) one batch of sensors was prepared without printed silver. However, this batch still demonstrated the residual silver. Further investigation would be needed to find where this contamination was occurring.

Results from electrochemistry (1 M HCl) of the microband design (Figure 6.26) appear to suggest that the residual silver is localised on the ink surface. In addition, in 4 M HCl electrolyte the residual silver is not observed perhaps implying solubilisation of the residual silver from the working electrode before electrochemical deposition. The silver residual would be a problem in 1 M HCl of either planar (refer to Section 4.3.7) or microband electrodes (Figure 6.26), but the frequency and severity is different between these cases. The silver residual appears to be less of a problem in 4 M HCl which could be attributed to solubilisation away from the working electrode; more tests would be needed to confirm the reliability of this conclusion.

6.4.4 BQ331 polymer solubilisation

In addition to the spectroscopic evidence of polymer solubilisation in HCl electrolytes (Figure 5.15), further evidence in Figure 6.10 and Figure 6.25 show rising baselines expected if the polymer is dissolving and exposing more gold surface. Figure 6.10 supports the view that the solubilisation is H_3O^+ induced, also suggested by the OH group content of the polymer X (Figure 5.5).

The ink would be better formulated not to include soluble polymer such as the Ercon gold ink formulation (spectra Figure 5.8B). However the larger particle aggregates used in the Ercon formulation (as seen in Figure 3.17) may lead to less reproducible edge thickness, since the width of an aggregate could be larger than the mean ink thickness.

6.4.5 Microband electrodes and Arsenic determination

Low level arsenic(III) sensitivity has been demonstrated with the microband design (Figure 6.26 and Figure 6.27) and in the absence of silver contamination. By this it is meant that arsenic at levels lower than the limit set by the US EPA and guidline limit set by the WHO of 10 ppb for total arsenic in drinking water. By using 4 M HCl and demonstrating tolerance to copper a good case has been made in light of the literature (Jagner *et al.,*1981, Huang *et al.,*1988, Huang and Dasgupta, 1999)

Two further possible methods for preparation of the microband sensors have been found since this work was conducted. One method involved using a drill to create a hole through a sandwhich of inks (Rawson *et al.,* 2007, Hyland *et al.,*2005). The other involves ultrasonic cutting to provide clean surfaces as proposed by Hyland *et al.,* (2005).

With the microband sensor, the first factor is to get a reproducible cut, which has been best attained in the laboratory with a roller cutter. The second factor is to measure As(V). It is not clear whether chemical or electrochemical reduction would be best. The motive to develop the microband design came after consulting Saluan *et al.* (2007) where arsenic(V) was electrochemically reduced with a gold fiber at extended deposition potentials. Clearly the wish would be to reproduce this method with the screen-printed microband. At present the gold is printed on top of carbon so that the microband has carbon and gold exposed at the edge. An improvement to the design would have gold printed onto the PET directly and an insulation layer on top. The background currents resulting from capacitive effects should then be reduced. A cost advantage would be realised by the smaller quantity of gold ink required per electrode in the microband design, although this may be offset by the new requirements set by providing a suitable reference electrode.

Although the work shown is preliminary, interest was shown by a leading supplier of diagnostic sensors, based on these results and two patent applications covering the work. A screen-printed sensor could, in the first instance, be used to substitute for

existing gold electrodes, avoiding the necessity to reinvent an entire electrochemical procedure for As(III) and As(V) chemically reduced.

6.5 Conclusion

All three outstanding interference peaks with the DuPont electrodes have been identified as resulting from silver contamination. XPS identified the problem directly, and electrochemical procedures were used as confirmation.

The silver comes from two sources: (i) exposed silver strips dissolved by formation of Ag-Cl complexes in electrolytes with Cl^- > 1 M and (ii) the Ag can be present as residual on working electrodes particularly with screen-printed electrodes where silver is printed in close proximity to the working electrode.

Three methods have been considered to prevent the solubilisation of silver interference: Nafion film immobilisation, non silver reference electrode or the use of a glass capillary Ag/AgCl reference electrode. Although the experiments performed were not exhaustive, the glass capillary has provided consistent results if stored in 0.01 M NaCl electrolyte (Ag solubility is less than 1 μM in Figure 5.19).

To prevent residual silver, more the process (preparation and printing) needs to be considered to find when and how the silver contamination arises. However, the problem appears to be mitigated using the preferable 4 M HCl by solubilisation.

Evidence both spectroscopic and electrochemical indicates that the polymer in BQ331 is soluble; causing a rising baseline in the electrochemical signal when working in 4 M HCl. Improved sensor performance would therefore be expected with a change in formulation.

A modified design for a microband sensor has been used, in conjunction with silver mitigation, to detect levels of arsenic(III) below the USEPA regulated and WHO

guideline limit of 10 ppb in drinking water. Several ways of preparing this sensor including knife, scissor, roller and CO_2 laser cutting have been attempted with the roller cutter giving reasonable reproducibility. The use of a drill or an ultrasonic cutter has yet to be tried and could lead to better defined edges. Also, an improvement to this design would omit the carbon layer from underneath the gold at the sensor edge.

The silver mitigation method is still open to improvements as is the microband edge preparation. In terms of the commercial application of the sensor a method for arsenic(V) is needed. Adapting the electrochemical method of Salaun *et al.,* (2007) would be preferable if possible as opposed to the separate chemical reduction procedures typical in the literature which need heating for 10 or more minutes (Munoz and Palmero, 2005, Cavicchioli *et al.,* 2004).

Chapter 7 Final Conclusions

7.1 Thesis Results Compared to Objectives

The objectives for this PhD, given in Section 1.11.1 were divided into three sets.

7.1.1 Objectives Set 1, Conclusions

The first major issue was the inability to repeat the electrochemical determination of As and Hg reported by Cooper (2004). The detailed electrochemical characterisation of the sensors showed a clear Faradaic type interference involving halide ions. The interference was found to be soluble.

As a consequence many of the initial objectives had to be disregarded. Only gold screen-printed electrode methods were considered, since there was not enough time to return to carbon based sensors with bismuth or mercury films. There was also no opportunity to study metal ion extraction from water and soil matrices, or to investigate methods for As(V) reduction due to time limitations.

The objective of bringing together a multi ion sensor (alluded to in Section 1.11.1) was dropped in favour of purpose built single ion sensors.

7.1.2 Objectives Set 2, Conclusions

The focus with the second set of objectives was to find out why a high HCl electrolyte could not be used and if this was inherent in the sensor materials. Chapter 4 and 5 were spent trying to assess the interference.

After testing of polymer extracts by FTIR ATR and NMR the polymer appeared to be unchanged as a result of aggressive electrochemical cycling. No correlation could be found between the cross linking agent in BQ331 and interference. And incidence of the interference appeared to be largely in dependent of working electrode ink used.

The ink BQ331 was found to be soluble in HCl acid solutions as confirmed by electrochemical current baseline increases with time indicative of capacitive increases; FTIR measurement of the polymer extracted in HCl solution; and by the prevalence of OH groups in the FTIR spectrum.

XPS showed silver was contaminating the working electrodes. This was clearly supported by a subsequent literature search with the formation of silver halide complexes ($AgCl_n^{n-1}$). Thus the interference was explained essentially nullifying the hypothesis polymer degradation.

The electrochemical interference took the form of three peaks referred to as the primary, secondary and spike peaks. The primary peak was attributed to bulk silver stripping to halide complexes. The secondary peak is highly likely to be sub monolayer stripping of the silver from the gold surface. The electrochemistry of the spike peak is interesting showing atypical peak shape and stochastic behaviours in some cases. This was proved to be silver as well, and a possible explanation was given based on an analogy with other work in the literature.

Further investigation showed that the silver must be resulting from two distinct sources: (i) as already noted via solubilisation of the reference strip and (ii) through residual contamination of printed strip.

This finding should have some wider relevance because the spike peak has often been seen by researchers whether on carbon or gold screen printed electrodes (at least, anecdotally), but no clear explanation for it was reported in the literature previously.

It is also surprising that Ag/AgCl reference electrodes are commonly stored in saturated KCl or NaCl electrolytes when this solubilises Ag. No reference or warning of this could be seen in the literature.

The above points show some success in linking physical/ chemical properties of the sensor with performance. Further efforts for sensor characterisation identified a common factor in screen-printed design glossed over in other projects. This project argues and demonstrates that the Nicholson method cannot be used to measure the electron transfer rate constant at screen-printed surfaces unless the effect of electrode resistance is considered. Furthermore good practice would be to note the electrode resistance for general potentiometric and voltammetric studies since the potential set by the potentiostat the actual potential of the working electrode will be different. These oversights may be minor in the context of previous projects (focusing on mechanisms of biological systems) but represent one aspect of experimental variability which could be controlled. This aspect is important when moving from academic studies to commercial viability for maintaining batch to batch performance.

A model for electrode characterisation by the method of Nicholson was extended to rough (fractal) surfaces was successfully completed and generated a number of predictions. Screen-printed electrodes for the sensors (used at Cranfield University, at least), have well defined roughness in the up to about 30 μm. The model extension is superfluous under typical working conditions. But since the model has theoretical interest, it would be worth validating it experimentally (with correct conditions to reduce the diffusion layer thickness to less than 30 μm), and if not experimentally then confirming with an explicit simulation.

Investigations showed that the commercial gold inks could vary by both gold particle size and dispersion as well polymer solubility. Further effects of chemical affinity between particles and powders in ink formulations, having profound effects on printability and electron transfer were observed; but little/no headway was made in understanding these effects. In addition the inclusion of surface active agents on particle surfaces almost certainly affects electron transfer but this could not be studied since the identity of this component in BQ331 was unknown.

Thus, the attempt to link physical and chemical properties with electrode performance has met with some success. But it is opened ended. The main reason for inhibited sensor performance was identified.

7.1.3 Objectives Set 3, Conclusions

Silver mitigation was optimised (according to available means and time constraints). Nafion membrane prepared over the reference electrode could prevent silver solubilisation and provide a stable potential. However, the present manifestation cannot be printed and effectiveness was compromised on the DuPont silver (BQ164) attributed to poor membrane integrity. Further work would be needed to improve printability and control thickness. Also Nafion is expensive and toxic.

Non silver electrodes (including gold, platinum and carbon reference electrodes) tested lack sufficient stability for stripping analysis. Glass capillary reference electrodes could be used, only if the storage electrolyte would be changed (recommended 0.01 M NaCl, with a preferably non halide co-salt to keep conductivity high). This method was found to be the best.

The sensors, working with a modified design could successfully detection As(III). A new microband design enabled a greater sensitivity and 5 ppb was detected in the desirable 4 M HCl electrolyte. This was below the WHO and US EPA limit of 10 ppb. The limit would be expected to be lower than 1 ppb As(III) (with appropriate deposition time and full elimination of silver).

The issue of concern is the confidence in the microband preparation procedure. The roller cutter has provided, within laboratory conditions, reproducible electrochemistry. A number of parameters would affect the viability of manufacturing this type of sensor design, which will require further study.

7.2 Objective and Motivation for Further Work

The rational was constructed during the course of this project so is presented at this juncture, considering the continuation of this project. The financial justification is based on the observation of the scale of arsenic contamination in drinking water, although full justification would require sales figures for existing colorimetric kits (according to advice Dr R. Pirzad, private communication).

The Arsenic problem is one of the largest environmental contamination issues and is frequently at the forefront of concern in drinking water and industrial residues. In 2007, Prof. P. Ravenscroft of Cambridge University used the figure of 137 million people being at risk of arsenic contaminated water supplies (as cited by Bagchi, 2007). Whilst this figure is probably an overestimate based on an extrapolation, the problem of arsenic analysis warrants a systematic study. The electrochemistry of As is the subject of more than 200 papers and the mechanism is clearly simple to implement for *in situ* analysis. Several general problems need to be addressed to provide a viable sensor in a self contained kit: (i) simple electrode-electrolyte system, (ii) electrode renewal between tests (iii) As(V) detection and (iv) metal interference, particularly Cu(II). Screen-printed electrodes tackle the second issue directly, and most conveniently of all electrode embodiments available. The DuPont sensors, have the advantage of already being mass manufacturable.

Since the colorimetric methods only effectively achieve 2-5 ppb sensitivity with an (expensive) spectrometer and 10-30 min reaction time, the electrochemical technique could boast sensitivity and time advantages. In addition, the electrochemical method could boast lower toxicity (colorimetric method generates arsine and uses mercuric bromide). The disadvantages of the electrochemical method would be: that the colorimetric method is already established; and that material selection of the electrochemical sensor needs to be carefully done to ensure decent performance.

The one issue that needs to be addressed is the microband preparation: can it be relied upon or would an ultrasonic cutter, freeze-fracture or drill preparation be preferable? As an academic study this has low priority, but for commercialisation is critical.

At the first stage, screen-printed gold can substitute for existing gold surfaces, alleviating the need to reinvent As(III) and As(V) electrochemical procedures. But in the long run, As(V) reduction needs to be as simple as possible, since the chemical reduction of As(V) with elevated temperatures and separate solution would be inconvenient *in situ*. Adaption of the electrochemical reduction method of Saluan *et al.,* (2007) would be good for this reason.

The glass capillary reference electrode may be sufficient initially for the sensors. But, a longer term solution would preferably be self-contained. Thus, revisiting Nafion would appear advantageous.

Another design modification would remove the carbon layer from underneath the gold at the exposed edge, since the carbon would contribute to the capacitive current, but not the As(III) signal. Small currents are a concern for the microband design. A new portable potentiostat would need to be made for these measurements. In addition to microband preparation, changing the top insulation ink could be used to modify the effect of shear force on the as prepared surface.

References

Ahmad, K, Wrong Test Used for Checking Arsenic Contamination of Wells in Bangladesh, Lancet, 360 (9347), 2002, 1757

Alegret, S, Rigid Carbon-Polymer Biocomposites for Electrochemical Sensing: A Review, The Analyst, 121 (12), 1751-1758, 1996

Amador-Hernandez, J, Fernandez-Romero, JM, Luque de Castro, MD, In-Depth Characterised of Screen-Printed Electrodes by Laser-Induced Breakdown Spectrometry and Pattern Recognition, Surface and Interface Analysis, 31 (4), 313-320, 2001

Arcand, GM, Distribution of Tripositive Arsenic Between Hydrochloric Acid Solutions and b, b' – Dichlorodiethyl Ether, Journal of the American Chemical Society, 79, 1865, 1957

Arihara, K., Kitamura, F., Ohsaka, T. and Tokuda, K., Adsorption Structure of the Heptyl Viologen Cation Radical on a Mercury Electrode Surface: Voltammetric and *in situ* infrared Reflection Adsorption Spectroscopic studies, Journal of Electroanalytical Chemistry 488, 117-124, 2000

Arnold, JP, Johnson, RN, Polarography of Arsenic, Talanta, 16, 1191-1207, 1969

Ashcroft, F., Life at the Extremes: The Science of Survival, Flamingo, Florida, 2000

ASTM international, West Conshohocken, PA, US, ASTM D 3363 -05, Standard Test Method for Film Hardness by Pencil Test, Book of Standards, volume 6.01, 408-410, 2005

Authier, L, Grossiord, C, Brossier, P, Limoges, B, Gold Nanoparticle-Based Quantitative Electrochemical Detection of Amplified Human Cytomegalovirus DNA using Disposable Microband Electrodes, Analytical Chemistry, 73 (18), 4450-4456, 2001

Bagchi, S, Arsenic Threat Reaching Global Dimensions, Canadian Medical Association Journal, 177, (11), 1344-1345, 2007

Baker-Austin, C., Dopson, M., Wexler, M., Sawers, R.G., Stemmler, A., Rosen, B.P., Bond, P.L., Extreme Arsenic Resistance by the Acidophilic Archaeon 'Ferroplasma Acidarmanus' Fer1, Extremophiles 11(3), 425-434, 2077

Bello-Rodriguez, Development of Biosensors for the Determination of Metals in Water and Soil Extracts, PhD Thesis, Cranfield University, 2004

Bott, AW, Practical Problems in Voltammetry 3: Reference Electrodes for Voltammetry, Bioanalytical Systemes, West Lafyette, IN, USA, website: www.currentseparations.com/issues/14-2/cs14-2d.pdf, accessed 2008 published 1995

Bott, AW, Practical Problems in Voltammetry 4: Preparation of Working Electrodes, Bioanalytical Systemes, West Lafyette, IN, USA, website: www.currentseparations.com/issues/16-3/cs16-3b.pdf, accessed 2008 published 1996

Bard, A., Faulkner, L., Electrochemical Methods: Fundamentals and Applications, 2nd Ed., Wiley, New York, 2001

Bard, AJ, Faulkner, L, Electrochemical Methods: Fundamentals and Applications, 2nd Ed, New York, Wiley, 2001

Bard, AJ, Parsons, R, The Encyclopedia of Electrochemistry of the Elements, Marcel Dekker: Volume 7 Inorganic Chemistry, New York, 1973

Bard, AJ, White, MC, Polarography of metal-Pyrogallol Complexes, Analytical Chemistry, 38, 61-63, 1966

Barile, F, Cao, Z, Hardej, D, Li, Y, Trombetta, LD, Thrush, MA, 2004 *Clinical Toxicology:* Principles and Mechanisms – Chapter 24 Metals, CRC Press LLC Florida

Barker, DJ, Brewin, DH, Dahm, RH, Hoy, LRJ, The electrochemical Reduction of Polytetrafluoroethylene, Electrochimica Acta, 23 (10), 1107-1110, 1978

Benucci, C, Schariker, BR, Effect of Temperature on the Formation of two Dimensional Sulphide Phases on Mercury, Journal of Electroanalytical Chemistry, 190, 199-212, 1985

Berg, M, Tran, HC, Nguyen, TC, Pham, HV, Schertenleib, R, Giger W, Arsenic Contamination of Groundwater and Drinking water in Vietnam: A Human Health Threat, Environmental Science and Technology 35 (13), 2621-2626, 2001

Bioanalytical Systems, Frequently Asked Questions: EC Electrodes, BioAnalytical Systems, inc., 2002-2005, accessed 2007 www.bioanalytical.com/products/ec/faqele.html#Storage

Bioanalytical Systems, Inc., Indiana, USA, BAS 100B/W version 2, Instruction Manual, 1996

Birch, S, Bolbot, JA, D'Costa, E, Higgins, JI, Electrochemical Metal Anaylsis, US Patent 5672257 (also published as WO9428405), assigned to Cranfield Biotech, Ltd, filed 1994 and published 1997

Bisquert, J., Compte, A., Theory of the Electrochemical Impedance of Anomalous Diffusion, Journal of Electroanaytical. Chemistry, 499 (1), 112-120, 2001

Blake, D.A., Jones, R.M., Blake, R.C., Darwish, I.A., Yu, H., Antibody-Based Sensors for Heavy Metal Ions, Biosensors and Bioelectronics, 16 (9-12), 2001, 799-809

Bolbot, J, Cooper, J, Saini, S, Setford, SJ, Dudeney, RH, Method and Apparatus For Elemental Analysis, WO/2007/000583, assigned to Cranfield University, filed 2005, published 2007

Bontidean, I, Berggren, C, Johansson, G, Csoregi, E, Mattiasson, B, Lloyd, JR, Jakeman, KJ, Brown, NJ, Detection of Heavy Metal Ions at Femtomolar Levels using Protein-Based Biosensors, Analytical Chemistry, 70 (19), 4162-4169, 1998

Borole, DD, Kapadi, UR, Kumbhar, PP, Hundiwale, DG, Influence of Inorganic and Organic Supporting Electrolytes on the Electrochemical Synthesis of Polyaniline, Poly(o-toluidine) and their Copolymer Thins Films, Materials Letters, 56 (5), 685-691, 2002

Bowers, GM, Kirkpatrick, RJ, High-Field ^{75}As NMR Study of Arsenic Oxysalts, Journal of Magnetic Resonance, 188 (2), 311-321, 2007

Branch, S, Ebdon, L, O'Neill, P, Determination of Arsenic Species in Fish by Directly Coupled High-Performance Liquid Chromatography-Inductively Coupled Plasma Mass Spectrometry, Journal of Analytical Atomic Spectrometry, 9 (1) 33-37, 1994

BuessHerman, C, Self-Assembled Monolayers at Electrode Metal Surfaces, Progress in Surface Science, 46, (4), 335-375, 1994

Burns, KG, Jezequel, H, Gould, NP, Radiation-Curable Ink Compositions Comprising a Solid N-vinyl Monomer, US Patent 5395863, assigned to Sericol Ltd., Kent, UK, filed 1993 and published 1995

Cairney, T., Hobson, D., Contaminated Land, E & FN Spon, London, 1998

Cass, AEG, Francis, DG, Hill, HAO, Aston, WJ, Higgins, IJ, Plotkin, EV, Scott, LDL, Turner, APF, Ferrocene-Mediated Enzyme Electrode for the Amperometric Determination of Glucose, Analytical Chemistry, 56, 667-671, 1984

Cauchi, M, Data Anlysis Tools for Safe Drinking Water Production, PhD Thesis, Cranfield University, Cranfield Health, 2006

Cavicchioli, A., La-Scalea, M. A., Gutz, I. G. R., Analysis and Speciation of Traces of Arsenic in Environmental, food and Industrial Samples by Voltammetry: A Review, Electroanalysis 16 (9), 697-711, 2004

Cepria, G, Alexa, N, Cordos, E, Castillo, JR, Electrochemical Screening Procedure for Arsenic Contaminated Soils, Talanta 66 (4), 875-881, 2005

Chan, MS, Kuty, D., Pepin, J., Parris, N., Potts, R., Reidy, M., Tierney, M., Uhegbu, Jayalakshmi, Y., Materials for Fabricating Biosensors for Transdermal Glucose Monitoring, Clinical Chemistry, 45, 1689-1690, 1999

Chan, M-S, Kuty, DW, Thick Film Conductor Composition for Use in Biosensors, US Patent 6042751, assigned to E.I. du Pont de Nemours and Company, Wilmington, DE, USA, filed 1998 and published 2000

Chan, MS, Thick Film Compositions for Making Medical Electrodes, US Patent 5928571, assigned to E.I. du Pont de Nemours and Company, Wilmington, DE, USA, filed 1998 and published 1999

Chan, M-S, Thick Film Compositions for Making Medical Electrodes, US Patent 5851438, assigned to E.I. du Pont de Nemours and Company, Wilmington, DE, USA, filed 1997 and published 1998

Chang, JL, Zen, JM, Disposable Screen-Printed Edge Band Ultramicroelectrodes for the Determination of trace Amounts of Nitrite Ion, Electroanalysis 18 (10), 941-946, 2006a

Chang, JL, Zen, JM, Fabrication of Disposable Ultramicroelectrodes: Characterization and Applications, Electrochemistry Communications 8 (4): 571-576, 2006b

Chatterjee, A, Das, D, Mandal, BK, Chowdhury, TR, Samanta, G, Chakraborti, D, Arsenic in Ground-Water in 6 Districts of West-Bengal, India-The Biggest Arsenic Calamity in the World .1. Arsenic Species in Drinking-Water and Urine of the Affected People, Analyst 120 (3), 643-650, 1995

Cheah, K, Simon, GP, Forsyth, M, Effects of Polymer Matrix and Processing on the Conductivity of Polymer Blends, Polymer International, 50 (1), 27-36, 2001

Cheng, Z, van Geen, A, Seddique, AA, Ahmed, KM, Response to Comments on “Limited Temporal Variability of Arsenic Concnetration in 20 Wells Monitored for 3 years in Araihazar, Bangladesh”, Environmental Science and Technology, 40, 1718-1720, 2006

Compte, A., Metzler, R., The Generalized Cattaneo Equation for the Description of Anomalous Transport Processes, Journal of Physics A-Mathematical and General, 30 (21), 7277-7289, 1997

Cooper, J, Electrochemical Method for the Rapid *In Situ* Screening of Metals in Soil and Water Samples, PhD Thesis, Cranfield Institute of Bioscience and Technology, Bedfordshire, UK, 2004

Craston, DH, Jones, CP, Williams, DE, Microband Electrodes Fabricated by Screen-printing Processs: Applications in Electroanalysis, Talanta, 38 (1), 17-26, 1991

Cui, G., Yoo, J.H., Lee, J.S., Yoo, J., Uhm, J.H., Cha, G.S., Nam, H., Effect of Pre-treatment on the Surface of Screen-Printed Carbon Paste Electrodes, The Analyst, 126 (8), 1399-1403, 2001

Cullen,W.R., Reimer, K.J., Arsenic Speciation in the Environment, Chemical Reviews, 89 (4), 713-764, 1989

Dai, X, Compton, RG, Detection of As(III) via Oxidation to As(V) using Platinum Nanoparticle Modified Glassy Carbon Electrodes: Arsenic Detection without Interference from Copper, Analyst 131 (4), 516-521, 2006b

Dai, X, Nekrassova, O, Hyde, ME, Compton, RG, Anodic Stripping Voltammetry of Arsenic(III) using Gold Nanoparticle-Modified Electrodes, Analytical Chemistry, 76, (19), 5924-5929, 2004

Dai, XA, Compton, RG, Direct Electrodeposition of Gold Nanoparticles onto Indium Tin Oxide Film Coated Glass: Application to the Detection of Arsenic(III), Analytical Sciences 22 (4), 567-570, 2006a

Davidson, CM, Duncan, AL, Littlejohn, D, Ure, AM, Garden, LM, A critical evaluation of the three stage BCR sequential extraction procedure to assess the potential mobility and toxicity of heavy metals in industrially-contaminated land, Analytica Chimica Acta, 363, 45-55, 1997

DEK, Screens and Product Range, DEK International, website: www.dek.com, accessed 2008, last updated 2007

Deltombe, E, de Zubov, N, Pourbaix, M, Atlas of Electrochemical Equilibria in Aqueous Solution (1st English Ed), Pergammon Press, New York, 1966

Dilleen, JW, Sprules, SD, Birch, BJ, Haggett, BGD, Electrochemical Determination of Silver in Photographic Solutions using Fixed –Volume Single-Use Sensors, Analyst 123 (12), 2905-2907, 1998

Dorfman, RJ, Thick Film Conductor Compositions for use in Membrane Switch Applications, US Patent 6939484, assigned to EI du Pont de Nemours and Company, Wilmington, DE, USA, filed 2003 and published 2005

Down to Earth, Arsenator: The World's Only Digital Arsenic Tester Prove Handy in India? Press release, published June 2004, accessed 2008 at: http://www.downtoearth.org.in/full6.asp?foldername=20040630&filename=news&sec_id=4&sid=37

Duan, G.L., Zhu, Y.G., Tong, Y.P., Cai, C., Kneer, R., Characterisation of Arsenate Reductase in the Extract of Roots and Fronds of Chinese Brake Fern, an Arsenic Hyperaccumulator, Plant Physiology, 138 (1), 461-469, 2005.

DuPont Microcircuit materials, Bristol, UK, BQ331 Gold Conductive Composition: Polymer Thick Film Composition, published 2001, accessed 2007, website: http://ap.stop.dupont.com/MCM/en_US/PDF/datasheets/BQ331.pdf

DuPont Microcircuit Materials, Online guide: DuPont Biosensor Materials, 2006, accessed 2007, website: www2.dupont.com/MCM/en_US/PDF/biosensor-H9156101.pdf

Eftekhari, A., Kazemzad, M., Keyanpour-Rad, M.,Influence of Atomic-Scale Irregularities in Fractal Analysis of Electrode Surfaces, Applied Surface Science, 239 (3-4), 311-319, 2005

Eftekhari, A., Kazemzad M., Keyanpour-Rad M., A Practical for Sensing Surface Nanostructures in Electrochemical Experiments, Surface Review and Letters, 13(5), 703-710, 2006

Eftekhari, A., Limitations of Electrochemical Methods for Surface Analysis at Small Fractility Scales, Surface Review and Letters, 2006

Ehrreich, JE, Novel Electroconductive Compositions and Powder for use Therein, US Patent 4319920, assigned to Ercon, Inc., USA, filed 1980 and published 1982

Ekino, S, Susa, M, Ninomiya, T, Imamura, K, Kitamura, T, Minamata Disease Revisited: an Update on the Acute and Chronic Manifestations of Methyl Mercury Poisoning, Journal of Neurological Sciences, 262 (1-2), 131-144, 2007

Ellis, D.R., Gumaelius, L., indriolo, E., Pickering, I.J., Banks, J.A., Salt, D.E., A Novel Arsenate Reductase from the Arsenic Hyperaccumulating Fern Pteris Vittata, Plant Physiology 141 (4), 1544-1554, 2006

Environment Agency, Soil Guideline Values, available: www.environment-agency.gov.uk/subjects/landquality, accessed 2008, published 2002

EPA Review, Monitoring Arsenic in the Environment: A Review of Science and Technologies for Field Measurements and Sensors, US EPA/ National Service Center for Environmental Publications, Cincinnati, OH, USA, 2004

EPA, Drinking Water Contaminants, website: www.epa.gov/safewater/dwh/c-ioc/lead.html, accessed, 2008, published 2006

Fahrenfort, J, Attenuated Total Reflection: A New Principle for the Production of Useful Infra-Red Reflection Spectra of Organic Compounds, Spectrochimica Acta, 17, 698-709, 1961

Ferguson J.F., Gavis, J., Review of Arsenic Cycle in Natural Waters, Water Research 6 (11), 1259, 1972

Feeney, R, Kounaves, SP, Voltammetric Measurement of Arsenic in Natural Waters, Talanta, 58 (1), 23-31, 2002

Fifield and Haines, Environmental Analytical Chemistry, Blackwell Science, London, 2000

Flanagan, JB, Margel, S, Bard, AJ, Anson, FC, Electron Transfer to and from Molecules Containing Multiple, Noninteracting Redox Centres. Electrochemical Oxidation of Poly(vinylferrocene), Journal of the American Chemical Society, 100 (13), 4248, 1978

Fogg, AG, Pirzad, R, Moreira, JC, Davies, AE, Improving the Performance of Screen-Printed Carbon and Polished Platinum and Glassy Carbon Voltammetric Electrodes by Modification with Poly(L-Lysine), Analytical Proceedings Including Analytical Communications, 32, 209, 1995

Forbes, GS, The Solubility of Silver Chloride in Chloride Solutions and Existence of Complex Argentichloride Ions, Journal of the American Chemical Society, 33, 1937, 1911

Forrow, NJ and Bayliff, SW, A Commerical Whole Blood Glucose Biosensor with a low Sensitivity to Hemocrit Based on an Impregnated Porous Carbon Electrode, Biosensors and Bioelectronics 21, 581-587, 2005

Francesconi, K.A., Kuehnelt, D., Determination of Arsenic Species: A Critical Review of Methods and Applications, 2000-2003, The Analyst, 129(5), 2004, 373-395

Friebolin, H., Basic One- and Two-Dimensional NMR Spectroscopy, 4th Ed, Wiley-VCH, Morlenbach, Germany, 2005

Furst, A., Bioassay of Metals for Carcinogenesis: Whole Animals, Environmental Health Perspectives, 40, 83-91, 1981

Gao, Q, Cui, XQ, Yang, F, Ma, Y, Yang, XR, Preparation of Poly(thionine) Modified Screen-Printed Carbon Electrode and its Application to Determine NADH in Flow Injection Analysis systems, Biosensors and Bioelectronics, 19 (3), 277-282, 2003

GEM, Papers Published with Acknoweldgment to GEM Ltd., www.g-e-m.com last update 2000, accessed 2008

Ghosh, D, Deb, A, Patra, KK, Sengupta, R, Bera, S, Double Health Risk in Arsenic Contaminated Drinking Water - Evidence of Enhanced Alpha Radioactivity, Water Air Soil pollution, 187, 81-87, 2008

Gilleo, K., Polymer Thick Film, International Thompson Publishing, Inc., New York, USA, 1996

Gilmartin, MAT, Ewen, RJ, Hart, JP, Honeybourne, CL, Voltammetric and Photoelectron Spectral Elucidation of the Electrocatalytic Oxidation of Hydrogen-Peroxide at Screen-Printed Carbon Electrodes Chemically-Modified with Cobalt Phthalocyanine, Electroanalysis 7 (6), 547-55, 1995b

Gilmartin, MAT, Hart, JP, Patton, DT, prototype, Solid-Phase, Glucose Biosensor, Analyst, 120 (7), 1973-1981, 1995a

Glicksman, H.D., Kodas, T.T., Majumdar, D., Method for Making Gold Powders by Aerosol Decomposition, US Patent 5616165, Assigned to E.I. Du Pont de Numours and Company, Delaware, USA; and The University of New Mexico, filed: 1995 and published: 1997

Go, J.-Y., Pyun, S.-I., A Review of Anomalous Diffusion Phenomena at Fractal Interface for Diffusion-controlled and Non-Diffusion-Controlled Transfer Processes, Journal of Solid State Electrochemistry, 11 (2), 2007, 323-334

Go, J.-Y., Pyun, S.-I., Hahn, Y.D., A Study on Ionic Diffusion Towards Self-Affine Fractal Electrode by Cyclic Voltammetry and Atomic Force Microscopy, Journal of Electroanalytical Chemistry, 549, 2003, 49-59

Gong, Z, Lu, X, Ma, M, Watt, C, Le, CX, Arsenic Speciation Analysis, Talanta, 58 (1), 77-96, 2002

Gunzler, H, Gremlich, HU, *in* IR Spectroscopy: An Indroduction, Chapter 6, Qualitative Spectral Interpretation, Wiley VCH, New York, 2002

Guo, Y, Guadalupe, AR, Screen-printable Surfactant-Induced Sol-gel Graphite Composites for Electrochemical Sensors, Sensors and Actuators B: Chemical, 46 (3), 213-219, 1998

Gwent Electronic Materials, Ltd., Pontypool, UK, Gold Polymer Paste C2041206D2, website: www.gwent.org, accessed 2007, published 2005

Hamann, CH, Hamnett, A, Vielstich, W, Electrochemistry, 2nd Ed, Wiley-VCH, Weinheim, Germany, 2007

Hammadi, A, Electrical Conductance, Density abd Viscosity in Mixtures or Alkali-Metal Halides and Glycerol, International Journal of Thermophysics, 25 (1), 89-111, 2004

Hart, JP, Crew, A, Crouch, E, Honeychurch, KC, Pemberton, RC, Designs and Developments of Screen-Printed Carbon Sensors/Biosensors for Biomedical, Environmental and Industrial Analyses, Analytical Letters, 37 (5), 789-830, 2004

Hasegawa, H, Sohrin, Y, Matsui, M, Takeda, N, Ueda, K, Chemical Speciation of Inorganic and Methylarsenic(III) Compounds in Aqueous Solutions, Applied Organometallic Chemistry 16 (8), 446-450, 2002

He, P., Faulkner, L.R., Intelligent, Automatic Compensation of Cell Resistance, Analytical Chemistry, 58, 517-523, 1986

He, Y, Zheng, Y, Locke, DC, Cathodic Stripping Voltammetric Analysis of Arsenic Species in Environmental Water Samples,Microchemical Journal 85 (2), 265-269, 2007

Heitkemper, DT, Vela, NP, Stewart, KR, Westphal, CS, Determination of Total and Speciated Arsenic in Rice by Ion Chromatography and Inductively Coupled Plasma Mass Spectrometry, Journal of Analytical Atomic Spectrometry, 16, 299-306, 2001

Herzog, G, Arrigan, DWM, Determination of Trace Metals by Underpotential Deposition-Stripping Voltammetry at Solid Electrodes, Trends in Analytical Chemistry, 24 (3), 208, 2005

Hills, G., Silva, F., Phase Transformations in Adsorbed Layers of Thiourea and Halide Ions on Mercury, Journal of Electroanalytical Chemistry 137, 387-392, 1982

Hobby, A, Technical Information on Screen-printing: 'Print Thick Film Hybrids', Applications Manager, DEK Printing Machines Ltd, available www.g-e-m.com, accessed 2007, published 1997

Holak, W, Determination of Arsenic by Cathodic Stripping Voltammetry with a Hanging Drop Electrode, Analytical Chemistry 52 (13), 2189-2192, 1980

Honeychurch, KC, Hart, JP, Kirsch, N, Voltammetric, Chromatographic and Mass Spectral Elucidation of the Redox Reactions of 1-Hydroxypyrene Occurring at a Screen-printed Electrode, Electrochimica Acta, 49 (7), 1141-1149, 2004

Honeychurch, KC and Hart, JP, Screen-Printed Sensors for Monitoring Metal Pollutants, Trac Trends in Analytical Chemistry, 22 (7), 456-469, 2003

HopenhaynRich, C, Biggs, ML, Fuchs, A, Bergoglio, R, Tello, EE, Nicolli, H, Smith AH, Bladder Cancer Mortality Associated with Arsenic in Drinking Water in Argentina, Epidemiology 7 (2), 117-124, 1996

Horst, F, Basic One- and Two- Diensional NMR Spectroscopy, Wiley VCH, Weinheim, Germany, 2005

Hostetler, MJ, Wingate, JE, Zhong, CJ, Harris JE, Vachet, RW, Clark, MR, Londono, JD, Green, SJ, Stokes, JJ, Wignall, GD, Glish, GL, Porter, MD, Evans, ND, Murray, RW, Alkanethiolate Gold Cluster

Molecules with Core Diameters from 1.5 to 5.2 nm: Core and Monolayer Properties as a Function of Core Size, Langmuir, 14, 17-30, 1998

Huang, D, Liao, F, Molesa, S, Redinger, D, Subramanian, V, Plastic-Compatible Low Resistance Printable Gold Nanoparticle Conductors for Flexible Electronics, Journal of the Electrochemical Society, 150 (7) G412-G417, 2003

Huang, H, Dasgupta, PK, A Field-Deployable Instrument for the Measurement and Speciation of Arsenic in Potable Water, Analytica Chimica Acta, 380 (1), 27-37, 1999

Huang, H, Jagner, D, Renman, L, Flow potentiometric and Constant-Current Stripping Analysis for Arsenic(V) without prior chemical reduction to Arsenic(III), Analytica Chimica Acta, 207, 37-46, 1988

Hutton, C, Bryce, DW, Russeau, W, Glass, HJ, Jenkin, LET, Corns, WT, Stockwell, PB, Aqueous and Solid-Phase Speciation of Arsenic in Cornish Soils, Mineralogical Magazine, 69 (5), 577-589, 2005

Hyland, M, Lorimer, K, Dobson, PJ, Askew, HF, Microband Electrode Manufacturing Method, Patent WO/2005/121762, assigned to Oxford Biosensors Ltd, Oxford, UK, filed and published 2005

Islam, FS, Gault, AG, Boothman, C, Polya, DA, Charnock, JM, Chatterjee, D, Lloyd, JR, Role of Metal-Reducing Bacteria in Arsenic Release from Bengal Delta Sediments, Nature 430 (6995): 68-71, 2004

Jagner, D, Potentiometric Stripping Analysis – A Review, Analyst, 107 (1275), 593-599, 1982

Jagner, D, Josefson, M, Westerlund, S, Determination of Arsenic(III) by Computerised Potentiometric Stripping Analysis, Analytical Chemistry, 53(13), 2144-2146, 1981

Jaunakais, I, Jaunakais, LM, Lewis, CB, Arsenic Analysis, US Patent 6696300, assigned to IND Test Systems Inc., (US), filed 2001 and published, 2004

Jiage, L, Nagaosa, Y, Cathodic Stripping Voltammetric Determination if As(III) with *in situ* plated bismuth-film electrode using the catalytic hydrogen wave, Analytica Chimica Acta, 593 (1), 2007

Jonte, JH, Martin, DS, The Solubility of Silver Chloride and the Formation of Complexes in Chloride Solution, Journal of the American Chemical Society, 74, 2052, 1952

Jurado, JR, Moure, C, Duran, P, Rodriguez, M, Linares, A, Acosta, JL, The Electrical and Morphological-Studies of Polymeric Composites based on Carbon-Black, Journal of Materials Science, 26 (15), 4022-4025, 1991

Jurica, L, Manova, A, Dzurov, J, Beinrohr, E, Broekaert, JAC, Calibrationless Flow-through Stripping Coulometric Determination of Arsenic(III) and Total Arsenic in Contaminated Water Samples after

Microwave Assisted Reduction of Arsenic(V), Fresenius Journal of Analytical Chemistry, 366, 260-266, 2000

Kabata-Pendias, A, Trace Elements in Soils and Plants, 3rd Ed, CRC Press, Boca Raton, Florida, USA, 2001

Kadara, R, Development of Electrochemical Sensors for Heavy Metal Ions and Detection in Environmental Samples, PhD Thesis, Cranfield University, 2004

Kalleder, A, Kreutzer, R, Mennig, M, Schmidt, H, Method and Compositions for Printing Substrates, US Patent 6863923, assigned to Inst Neue Mat Gemein GMDH, Germany, filed 2000 and published 2005

Kaufman, T, White, P, Dindal, A, Willenberg, Z, Riggs, EPA: Environmental Technology Verification Report: Industrial Test Systems, Inc. Quick™ II Test Kit, website: www.epa.gov/etv/vt-ams.html#atk, accessed 2008 published, 2003

Kim, M.J., Nriagu, J.O., Haack, S., Arsenic Species and Chemsitry in Groundwater of Southeast Michigan, Environmental Pollution, 120 (2), 2002, 379-390

Kissinger, P.T., Heineman, W.R., Laboratory Technique in Electroanalytics Chemistry 2nd, Marcell Dekker Inc., New York, 1996

Kodas, T.T., Hampden-Smith, M.J., Caruso, J., Skamser, D.J., Powell, Q.H., Chandler, C.D., Gold Powders, Methods for Producing Powders and Devices Fabricated from Same, US Patent 6830823, Assigned to Superior Micropowders LLC, new Mexico, USA, filed: 2000 and published 2004

Kolb, DM, Przasnyski, M, Gerischer, H, Underdeposition of Metals and Work Function Differences, Journal of Electroanalytical Chemistry, 54, 25-38, 1974

Kopanica and Novotny, Determination of Traces of Arsenic(III) by Andoic Stripping Solutions, Natural Waters and Biological Material, Analytica Chimica Acta, 368 (3), 211-218, 1998

Kroger, S, Turner, APF, Solvent Resistant Carbon Electrodes Screen-printed onto Plastic for use in Biosensors, Analytica Chimica Acta, 347, 9-18, 1997

Laitinen, HA, Watkins, NH, Cathodic Stripping Coulometry of Lead, Analytical Chemistry, 47, 1352, 1975

Lamm, SH, Engel, A, Krus, MB, Feinleib, M, Byrd, DM, Lai, SH, Wilson, R, Arsenic in Drinking Water and Bladder Cancer Mortality in the United States: An Analysis on 133 US Counties and 30 years of Observation, Journal of Occupational and Environmental Medicine 46 (3), 298-306, 2004

Lamm, SH, Engel, A, Penn, CA, Chen, R, Feinleib, M, Arsenic Cancer Risk Confounder in Southwest Taiwan Data Set, Environment Health Perspectives, 114 (7): 1077-1082, 2006

Lamm, SH, Kruse, MB, Arsenic Ingestion and Bladder Cancer Mortality-What do the Dose-Response Relationships Suggest About Mechanism? Human and Ecological Risk Assessment, 11, 433-450, 2005

Lane, P., Peto, M., Blackstone's Guide to the Environment Act, 1995, Blackstone, London, 1995

Lane, W, Newton, HV, Hill, MJM, The Use of Screen-printed Electrodes in the Electrochemical Analysis of Electroactive Species, European Patent 0969281, assigned to University College, Cork, Irland, published 2000

Larsen, E.H., Pritzl, G., Hansen, S.H., Arsenic Speciation in Seafood Samples with Emphasis on Minor Constituents – an Investigation using High-Performance Liquid-Chromatography with Detection by Inductively-Coupled Plasma-Mass Spectrometry, Journal of Analytical Atomic Spectrometry 8 (8), 1075-1084, 1993

Latimer, WM, Oxidation States of the Elements and Their Potnetials in Aqueous Solutions 2nd Ed, Prentice-Hall, Inc, New York, 1952

Lee, S.I., Pyun, S.I., Determination of the Morphology of Surface Groups Formed and PVDF-binder Materials Dispersed on Graphite Composite Electrodes in Terms of Fractal Geometry, Journal of Electroanalytical Chemistry, 556, 72-82, 2003

Li, ZL, Wu, TH, Niu, ZJ, Huang, W, Nie, HD, *In Situ* Raman Spectroscopic Studies on the Current Oscillations during Gold Electrodissolution in HCl Solution, Electrochemistry Communications, 6 (1), 44-48, 2004

Lide, DR, (Editor) and 28 other authors, CRC Handbook of Chemistry and Physics 84th Ed CRC Press: Section 8 Analytical Chemistry: p8-20, Electrochemical Series, Florida, 2003

Lomborg, B, The Skeptical Environmentalist, English 1st Ed, Cambridge University Press, 2001

Lopez, A, Torralba, R, Palacios, MA, Camara, C, Generation of AsH_3 from As(V) in the Absence of KI as Prereducing Agent: Speciation of Inorganic Arsenic, Talanta, 39 (10), 1343-1348, 1992

Lorenz, WJ, Moumtzis, I, Schmidt, E, Studies on Adsorption of Metal Ions on Gold Electrode with Triangular Voltage Sweep Method, Journal of Electroanalytical Chemistry, 33 (1), 121, 1971

Lux, F, Models Proposed to Explain the Electrical Conductivity of Mixtures made of Conductive and Insulating Materials, Journal of Materials Science, 28 (2), 285-301, 1993

Ma, L.Q., Komar, K.M., Tu, C., Zhang, W., Cai, Y., Kennelley, E.D., A Fern that Hyperaccumulates Arsenic, Nature 409, 579, 2001

McLaren, RG, Crawford, Studies on Soil Copper. I. The Fractionation of Copper in Soils and Soil Components, Journal of Soil Science, 24, 172-181, 1973

Meites, L, Polarographic Characteristics of +3 and +5 Arsenic in Hydrochloric Acid Solutions, Journal of the American Chemical Society, 76, 5927, 1954

Metzler, R., Klafter, J., The Random Walk's Guide to Anomalous Diffusion: a Fractional Dynamics Approach, Physics Reports, 339, 2000, 1-77

Miller, WP, Martens, DC, Zelazny, LW, Effect of Sequence in Extraction of Trace Metals from Soils, Soil Science Society of America, 50, 598-601, 1985

Morgado, J, Moons, E, Friend, RH, Cacialli, F, De-mixing of Polyfluorene-Based Blends by Contact with Acetone: Electro- and Photo-luminescence Probes, Advanced Materials, 13 (11), 810-814, 2001

Morrin, A, Killard, AJ, Smyth, MR, Electrochemical Characteristics of Commerical and Home-Made Screen-Printed Carbon Electrodes, Analytical Letters, 36 (9), 2021-2039, 2003

Mulligan, CN, Yong, RN, Gibbs, BF, Remediation technologies for metal-contaminated soils and groundwater: an evaluation, Engineering Geology, 60, 193-207, 2001

Munoz, E., Palmero, S. Analysis and Speciation of Arsenic by Stripping Potentiometry: a Review. Talanta 65 page 613-620, 2005

Nascimento, V.B., Lucio, A., Electrodes Manufactured for "Silk-Screen", Quimica Nova, 21 (5), 1998

Navratil, T, Kopanica, M, Krista, J, Anodic Stripping Voltammetry for Arsenic Determination on Composite Gold Electrode, Chemia Analityczna, 48 (2), 265-272, 2003

Newman, JD, Turner, APF, Home Blood Glucose Biosensors: A Commercial Perspective, Biosensors and Bioelectronics, 20 (12), 2435-2453, 2005

Newman, JD, White, SF, Tothill, IE, Turner, APF, Catalytic Materials, Membranes, and Fabrication Technologies Suitable for the Construction of Amperometric Biosensors, Analytical Chemistry, 67 (24), 4594-4599, 1995

Ni, Y, Wang, L, Kokot, S, Voltammetric Determination of Butylated Hydroxyanisole, Butylated Hydroxytoluene, Propyl Gallate and *Tert*-butylhydroquinone by use of Chemometrics Approaches, Analytica Chimica Acta, 412, 185-193, 2000

Nicholson, R.S., Shain, I., Theory of Stationary Electrode Polarography: Single Scan and Cyclic Methods Applied to Reversible, Irreversible, and Kinetic Systems, Analytical Chemistry, 706-723, 1964

Nicholson, R.S., Theory and Application of Cyclic Voltammetry for Measurement of Electrode Reaction Kinetics, Analytical Chemistry, 37 (11), 1351-1355, 1965a

Nicholson, R.S., Some Examples of the Numerical Solution of Nonlinear Integral Equations, Analytical Chemistry, 37 (6), 667-671, 1965b

Nickson, R, McArthur, J, Burgess, W, Ahmed, KM, Ravenscroft, P, Rahman, M, Arsenic Poisoning of Bangladesh Ground Water, Nature, 395, 338, 1998

Nies, D.H., Microbial Heavy Metal Resistance, Applied Microbiol technology, 51, 730-750, 1999

Noh, MFM, Electrochemical Sensors Development for Toxic Heavy Metals, PhD Thesis, Cranfield University, UK, 2005

Noh, MFM, Tothill, IE, Development and Characterisation of Disposable Gold Electrodes, and their use for Lead(II) Analysis, Analytical Bioanalytical Chemistry, 386, 2095-2106, 2006

Nriagu, J.O. (Ed), Arsenic in the Environment, Part 1: Cycling and Characterization, 1994, John Wiley & Sons, Inc., New York

Nyikos, L., Pajkossy, T., Diffusion to Fractal Surfaces, Electrochimica Acta, 31, 1347-1350, 1986

Oldham, K.B., Diffusive Transport to Planar, Cylindrical and Spherical Electrodes, Journal of Electroanalytical Chemistry, 41, 351-358, 1973

Osbourne, M.D., Seddon, B.J., Dryfe, R.A.W., Lagger, G., Loyall,U., Schafer, H., Girault, H.H., Excimer Laser-Induced Electrochemical Activity in Carbon Ink Films. Journal of Electroanalytical Chemistry, 417, 5-15, 1996

Osman, M.A., Atallah, A., Suter, U.W., influence of Excessive Filler Coating on the Tensile Properties of LDPE-Calcium Carbonate Composites, Polymer, 45, 1177-1183, 2004

Pajkossy, T., Borosy, A. P., Imre, A., Martemyanov, S.A., Nagy, G., Schiller, R., Nyikos, L., Diffusion Kinetics at Fractal Electrodes, Journal of Electroanaytical. Chemistry. 366, 69-73, 1994

Pajkossy, T., Electrochemistry at Fractal Surfaces, Journal of Electroanalytical Chemistry, 300, 1-11, 1991

Pajkossy, T., Nyikos, L., Diffusion to Fractal Surfaces II: Verification of Theory, Electrochimica Acta, 34, 171-179, 1989a

Pajkossy, T., Nyikos, L., Diffusion to Fractal Surfaces III: Linear Sweep and Cyclic Voltammograms, Electrochimica Acta, 34, 181-186, 1989b

Pal, A, Nayak, B, Das, B, Hossain, MA, Ahamed, S, Chakraborti, D, Additional Danger of Arsenic Exposure Through Burning of Cow Dung Cakes Laced with Arsenic as a Fuel in Arsenic Affected Villages in Ganga-Meghna-Brahmaputra Plain, Journal of Environmental monitoring 9 (10), 1067-1070, 2007

Palintest, Ltd, Gateshead, UK, website: www.palintest.com, accessed 2007, website publish date and author unknown

Pfaendner, R, How Will Additives Shape the Future of Plastics?, Polymer Degradation and Stability, 91, 2249-2256, 2006

Piech, R, Bas, B, Niewiara, E, Kubiak, WW, Determination of Trace Arsenic on Hanging Copper Amalgam Drop Electrode, Talanta, 72 (2), 762-767, 2007

Planer-Friedrich, B., Lehr, C., Matschullat, J., Merkel, B.J., Nordstrom, D.K., Sandstrom, M.W. Speciation of Volatile Arsenic at Geothermal Features in Yellowstone National Park, Geochimica et Cosmochimica Acta, 70 (10), 2006, 2480-2491.

Prasad, KS, Chen, JC, Ay, C, Zen, JM, Mediatorless Catalytic Oxidation of NADH at a Disposable Electrochemical Sensor, Sensors and Actuators, B: Chemical, 123 (2), 715-719, 2007

Proccacia, I., Grassberger, P., Measuring the Strangeness of Strange Attractors, Physica D: Nonlinear Phenomena, 9 (1-2), 189-208, 1983

Prudenziati, M, Handbook of Sensors and Actuators: Thick Film Sensors, Elsevier Science, Amsterdam, 1994

Pud, AA, Surface Electrochemical Reactions and the Subsequent Degradation of Solid-Phase Poly(Ethylene Terephthalate) at a Cathode, Polymer Degradation and Stability, 30, 181-193, 1990

Quevauviller, P Operationally Defined Extraction Procedures for Soil and Sediment Analysis 1. Standardisation, Trends in Analytical Chemistry, 17 (5), 289-298, 1998

Rahman, MW, Chowdhury, UK, Mukherjee, SC, Mondal, BK, Paul, K, Lodh, D, Biswas, BK, Chanda, CR, Basu, GK, Saha, KC, Roy S, Das, R, Palit, SK, Quamruzzaman, Q, Chakraborti, D, Chromic Arsenic Toxicity in Bangladesh and West Bengal, India - A review and Commentary, Journal of Toxicology- Clinical Toxicology 39 (7): 683-700 2001

Rahman, A, Vahter, M, Ekstrom, EC, Rahman, M, Mustafa, AMG, Wahed, MA, Yunus, M, Persson, LA, Association of Arsenic Exposure during Pregnancy with Fetal Loss and Infant Death: A Cohort Study in Bangladesh, American Journal of Epidemiology, 165 (12), 1389-1396, 2007a

Rahman, MA, Hasegawa, H, Rahman, MM, Islam, MN, Miah, MAM, Tasmin, A, Arsenic Accumulation in Rice (Oryza Sativa L.) Varieties of Bangladesh: A Glass House Study, Water Air and Soil Pollution, 185 (1-4), 53-61, 2007b

Ramirez, P, Andreu, R, Calvente, JJ, Calzado, CJ, Lopez-Perez, G, Electrochemical Formation and Electron Transfer Through Self-Assembled Monolayers of 4-Mercaptophenol on Mercury, Journal of Electroanalytical Chemistry, 582 (1-2), 179-190, 2005

Rao, VK, Sharma, MK, Pandey, P, Sekhar, K, Comparison of Different Carbon Ink based Screen-Printed Electrodes towards Amperometric Immunosensing, World Journal fo Microbiology biotechnology, 22, 1135-1143, 2006

Rauret, G, Lopez-Sanchez, JF, Sahuquillo, A, Rubio, R, Davidson, C, Ure, A, Quevauviller, P, Improvement of the BCR three step sequential extraction procedure prior to the certification of new sediment and soil reference materials, Journal of Environmental Monitoring, 1, 57-61, 1999

Ravens, DAS, The Chemical Reactivity of Poly(ethylene terephthalate): Heterogeneous Hydrolysis by Hydrochloric Acid, Polymer, 1, 375, 1960

Ravenscroft, P, Predicting the Global Distribution of Natural Arsenic Contamination of Groundwater, Proceedings of a Symposium: Arsenic – The Geography of a Global Problem, Royal Geographical Society: Arsenic Conference, 29th August 2007, presentation available: www.geog.cam.ac.uk/research/projects/arsenic/, accessed 2008

Rawson, FJ, Purcell, WM, Xu, J, Cowell, DC, Fielden, PR, Hart, JP, Fabrication and Characterisation of Novel Screen-Printed Tubular Microband Electrodes, and their Application to the Measurement of Hydrogen Peroxide, Electrochimica Acta, 52, 7248-7253, 2007

Rosen, B.P., Biochemistry of Arsenic Detoxification, Febs Letters 529 (1), 86-92, 2002

Sadana, RS, Determination of Arsenic in the Presence of Copper by Differential Pulse Cathodic Stripping Voltammetry at a Hanging Mercury Drop Electrode, 55, 304-307, 1983

Salaun, P, Planer-Friedrich, B, van den Berg, CMG, Inorganic Arsenic Speciation in Water and Seawater by Anodic Stripping Voltammetry with a Gold Microelectrode, Analytica Chimica Acta 585, 312-322, 2007

Salimi, A, Hyde, ME, Banks, CE, Compton, RG, Boron Doped Diamond Electrode with Iridium Oxide for Amperometric Detection of Ultra Trace Amounts of Arsenic(III)

Salt, DE, Blaylock, M, Kumar, NPBA, Dushenkov, V, Ensley, BD, Chet, I, Raskin, I, Phytoremediation – A Novel Strategy for the Removal of Toxic Metals from the Environment using Plants, Biotechnology 13 (5), 468-474, 1995

Samanta, G., Chowdhury, T.R., Mandal, B.K., Biswas, B.K., Chowdhury, U.K., Basu, G.K., Chanda, C.R., Lodh, D., Flow Injection Hydride Generation Atomic Spectrometry for Determination of Arsenic in water and Biological Samples from Arsenic-Affected Districts of West Bengal, India, and Bangladesh, Microchemcial Journal, 62 (1), 174-191, 1999

Saterlay, AJ, Marken, F, Foord, JS, Compton, RG, Sonoelectrochemical Analysis at a Highly Boron Doped Diamond Electrode, Talanta, 53 (2), 403-415, 2000

Savarimuthu, X, Hira-Smith, MM, Yuan, Y, von Ehrenstein, OS, Das, S, Ghosh, N, Mazumder, DNG, Smith, AF, Seasonal Variation of Arsenic Concentration in Tubewells in West Bengal, Journal of Health Population and Nutrition, 24 (3), 277-281

Sbarato, VM, Sanchez, HJ, Analysis of Arsenic Pollution in Groundwater Aquifers by X-ray Fluorescence, Applied Radiation and Isotopes, 54 (5), 737-740, 2001

Schifano, V, Macleod, C, Hadlow, N, Dudeney, R, Evaluation of Quicklime Mixing for the Remediation of Petroleum Contaminated Soils, Journal of Hazardous Materials, 141 (2), 395-409, 2007

Seah, MP, A Review of the Analysis of Surfaces and Thin Films by AES and XPS, Vacuum, 34 (3-4), 463-478, 1984

Sebkova, S, Navratil, T, Kopanica, M, Graphite Composite Electrode in Voltammetry, Analytical Letters, 38, 1747-1758, 2005

Sekine, T., Ishii, T., Studies of the Liquid-Liquid Partition Systems. VII. The Solvent Extraction of Mercury(II) Chloride, Bromide, Iodide and Thiocyanate with Some Organic Solvents, Bulletin of the Chemical Society of Japan, 43 (8), 2422, 1970

Sella, C, Bauer, D, Determination of the Hydrogen Ion and Chloride Ion Activities in Hydrochloric Acid, Hydrometallurgy, 23 (2-3), 353-364, 1990

Sella, C, Mendoza, RN, Bauer, D, Distribution of Arsenic(III) Between Hydrochloride-Acid Solutions and an Aromatic Solvent – effect of a Salting-Out Agent such as Calcium-Chloride, Hydrometallurgy 27 (2), 179-190, 1991

Shankar, PN, Kumar, M, Experimental Determination of the Kinematic Viscosity of Glycerol-Water Mixtures, Proceedings: Mathematic and Physical Sciences, 444, 573-581, 1994

Sherman, D.M., Complexation of Cu^{+} in Hydrothermal NaCl Brines: Ab *initio* Molecular Dynamics and Energetics, Geochimica et Cosmochimica Acta, 71(3), 714-722, 2007

Simm, AO, Banks, CE, Wilkins, SJ, Karousos, NG, Davis, J, Compton, RG, A Comparison of Different types of Gold-Carbon Composite Electrode for Detection of Arsenic(III), Analytical and Bioanalytical Chemistry, 381 (4), 979-985, 2005

Smedley, P.L., Kinnigburgh, D.G., A Review of the Source, Behaviour and Distribution of Arsenic in Natural Waters, Applied Geochemistry, 17 (5), 517-568, 2002

Smith, AH, Goycolea, M, Haque, R, Biggs, ML, Marked Increase in Bladder and Lung Cancer Mortality in a Region of Northern Chile due to Arsenic in Drinking Water, American Journal of Epidemiology, 147 (7), 660-669, 1998

Smith, AH, Lingas, EO, Rahman, M Contamination of Drinking-Water by Arsenic in Bangladesh: a Public Health Emergency, Bulletin of the World Health Organisation 78 (9): 1093-1103, 2000

Smith, AH, Lopipero, PA, Bates, MN, Steimaus, CM, Public Health – Arsenic Epidemiology and Drinking Water Standards, Science, 296 (5576), 2145-2146, 2002

Smith, MG, Laplace Transform Theory, D. van Nostrand, London, 1966

Soignet, SL, Maslak, P, Wang, ZG, Jhanwar, S, Calleja, E, Dardashti, LJ, Corso, D, DeBlasio, A, Gabrilove, J, Scheinberg, DA, Pandolfi, PP, Warrell, RP, Complete Remission after Treatment of Acute Promyelocytic Leukaemia with Arsenic Trioxide, New England Journal of Medicine, 339 (19), 1341-1348, 1998

Song, YS, Muthuraman, G, Zen, JM, Trace Analysis of Hydrogen Sulfide by monitoring As(III) at a Poly(L-Lactide) Stabilized Gold Nanoparticles Modified Electrode, Electrochemistry, 8 (8), 1369-1374, 2006a

Song, YS, Muthuraman, G, Chen, YZ, Lin, CC, Zen, JM, Screen-printed Carbon Electrode Modified with Poly(L-Lactide) Stabilized Gold Nanoparticles for Sensitive As(III) Detection, Electroanalysis, 18 (18), 1763-1770, 2006b

Song, Y, Swain, GM, Development of a Method for Total Inorganic Arsenic Analysis using Anodic Stripping Voltammetry and a Au-Coated, Diamond Thin-Film Eelctrode, Analytical Chemistry, 79 (6), 2412-2420, 2007

Sposito, G, Lund, LJ, Chang, AC, Trace Metal Chemistry in Arid-Zone Field Soils Amended with Sewage Sludge. I-Fractionation of Ni, Cu, Zn, Cd and Pb in Solid Phases, Soils Science Society of America, 46, 260-264

Stohs SJ, Bagchi, D, Oxidative Mechanisms in the Toxicity of Metal-Ions, Free Radical Biology and Medicine, 18 (2), 321-336, 1995

Strawn, D., Doner, H., Zavarin, M., McHugo, S., Microscale Investigation into the Geochemistry of Arsenic, Selenium, and Iron in Soil Developed in Pyritic Shale Materials, Geoderma, 108 (3-4), 237-257, 2002

Strømme, M., Niklasson, G. A., Granqvist, C. G., Voltammetry on Fractals, Solid State Communications, 96, 151-154, 1995

Stulikova, M, The Deposition and Stripping of Mercury on a Glassy Carbon Rotating Disk Electrode, Electroanalytical Chemistry and Interfacial Chemistry, 48, 33-45, 1973

Styblo, M, Del Razo, LM, Vega, L, Germolec, DR, LeCluyse, EL, Hamilton, GA, Reed, W, Wang, C, Cullen, WR, Thomas, DJ, Comparative Toxicity of Trivalent and Pentavalent Inorganic and Methylated Arsenicals in Rat and Human Cells, Archives of Toxicology 74 (6), 289-299, 2000

Sun, YC, Mierzwa, J, yang, MH, New Method of Gold-Film Electrode Preparation for Anodic Stripping Voltammetric Determination of Arsenic (III and V) in Seawater, Talanta 44, 1379-1387, 1997

Svancara, I, Vytras, K, Bobrowski, A, Kalcher, K, Determination of Arsenic at a Gold-Plated Carbon Paste Electrode using Constant Current Stripping Analysis, Talanta, 58 (1), 45-55, 2002

Swash, P, Field Evaluation of the Wagtech Arsenator: Myanmar 2003, Royal School of Mines, Imperial College, London, UK, website: www.physics.harvard.edu/~wilson/arsenic/measurement/field-eval-wagtech-arsenator.html, accessed 2008 published 2003

Tan, KL, Woon, LL, Wong, HK, Kang, ET, Neoh, KG, Surface Modification of Plasma-Pretreated Poly(tetrafluoroethylene) Films by Graft-Copolymerisation, Macromolecules, 26 (11), 2832-2836, 1993

Tchounwou, P.B., Patlolla, A.K., Centeno, J.A., Carcinogenic and Systemic Health Effects Associated with Arsenic Exposure – A Critical Review, Toxicologic Pathology, 31, 575-588, 2003

Tessier, A, Cambell, PGC, Bisson, M., Sequential Extraction Procedure for the Speciation of Particulate Trace Metals, Analytical Chemistry, 51 (7), 844-851, 1979

The New Dutch List, The Ministry of Housing, Spatial Planning and Environment (Netherlands), available: www.contaminatedland.co.uk/std-guid/dutch-l.htm#KEYWORD-ONE, accessed 2008, published 1996

Thornton, J., Beckwith, S., Environmental Law, Sweet and Maxwell, London, 1997

Thundiyil, JG, Yuan, Y, Smith, AH, Steinmaus, C, Seasonal Variation of Arsenic Concentration in Wells in Nevada, Environmental Research, 104 (3), 367-373, 2007

Tierney, MJ, Highly Catalytic Screen-Printing Ink, US Patent 7018568, Assigned to Animas Technologies LLC, West Chester, PA, USA, filed 2002, published 2006

Towlson, SM, Flexible Thick Film Conductor Composition, US Patent 5653918, assigned to DuPont, US, filed 1996 and published 1997

Turner, AFP, Newman, JD, Tigwell, LJ, Warner, PT, Biosensors: A Global View, Proc 9th World Congress on Biosensors 2006, Toronto Canada, 031, Elsevier, 2006

Turyan, I and Mandler, D, Self-Assembled Monolayers in Electroanalytical Chemistry – Application of Omega-Mercaptocarboxylic Acid Monolyaers for Electrochemical Determination of Ultralow Levels of Cadmium(II), Analytical Chemistry, 66 (1), 1994

Turyan, I, Mandler, D, Selective Determination of Cr(VI) by a Self-Assembled Monolayer-Based Electrode, Analytical Chemistry, 69 (5), 894-897, 1997

UNICEF, Evaluation of Water Quality Monitoring and Purification Products under Long Term Agreement (Performance Evaluation of Wagtech Arsenator), study conducted by Shriram Institute for industrial Research, Delhi, India, published: 2006; available: www.wagtech.co.uk/UserFiles/File/Water%20Cat/ArsenatorEvaluation.pdf, acessed 2008

US EPA Method 7063, Arsenic in Aqueous Samples and Extracts by Anodic Stripping Voltammetry (ASV),www.epa.gov/sw-846/pdfs/7063.pdf, accessed 2008, published 1996

Usmani, AM, Diagnostic Biosensor Polymers, Chapter 1 Diagnostic Polymers and Coatings, American Chemical Society, Washington DC,

van den Berg, CMG, Determination of Copper, Cadmium and Lead in Seawater by Cathodic Stripping Voltammetry of Complexes with 8-Hydroxyquinoline, Journal of Electroanalytical Chemistry, 215 (1-2), 111-121, 1986

Vasconcellos, A. R., Ramos, J. G., Gorenstein, A., Kleinke, M.U., Cruz, T.G.S., Luzzi, R. Statistical Approach to Non-Fickian Diffusion, International Journal of Modern Physics B, 20, 4821-4841, 2006

Voltammetric Measurement of Arsenic in Natural Waters. Feeney, R., Kounaves, S.P., Talanta 58 (1), page 23-31, 2002

Wang, J, Method and Apparatus for Trace Metal Testing, US Patent 5292423, Assigned to New Mexico State University Technology Transfer Corporation, Las Cruces, New Mexico, USA, Filed 1992 and published 1994

Wang, J, Sol-Gel Materials for Materials Biosensors, Analytica Chimica Acta, 399, (1-2), 21-27, 1999a

Wang, J, Analytical Electrochemistry, 2nd Ed, New York, Wiley VCH, 2000

Wang, J, Bismuth-Based Electrochemical Stripping Analysis, US Patent 6682647, Assigned to New Mexico State University, Technology Transfer Corporation, Las Cruces, New Mexico, USA, Filed 2001, published 2004

Wang, J, Stripping Analysis at Bismuth Electrodes: A review, Electroanalysis, 17 (15-16), 1341-1346, 2005

Wang, J, Tian, BM, Screen-Printed Stripping Voltammetric Potentiometric Electrodes for Decentralised Testing of Trace Lead, Analytical Chemistry, 64 (15), 1706-1709, 1992

Wang, J, Lu, J, Tian, B, Yarnizky, C, Screen-printed Ultramicroarrays for *On-site* Stripping Measurements of Trace Metals, Journal of Electroanalytical Chemistry, 361, (1-2), 77-83, 1993

Wang, J, Tian, B, Mercury-Free Disposable Lead Sensors Based on Potentiometric Stripping Analysis at Gold-Coated Screen-Printed Electrodes, Analytical Chemistry 65 (11), 1529-1532, 1993b

Wang, M., Zhang, Y., Muhammed, M., Ions in Aqueous Solutions III. The System Cu(I,II)-Cl⁻e at 298.15 K, Hydrometallurgy, 45, 53-72, 1997

Wang, J, Pamidi, PVA Sol-Gel-Derived Gold Composite Electrodes, Analytical Chemistry, 69 (21), 4490-4494, 1997a

Wang, J, Tian, B, Nascimento, VB, Angnes, L, Performance of Screen-printed Carbon Electrodes Fabricated from Different Carbon Inks, Electrochimica Acta, 43 (23), 3459-3465, 1998

Wang, J, Jianmin, L, Kirgoz, UA, Hocevar, SB, Ogorevc, B, Insights into the Anodic Stripping Voltammetric Behavior of Bismuth Film Electrodes, Analytica Chimica Acta, 434, 29-34, 2001

Wang, J, Musameh, M, Carbon Nanotube Screen-Printed Electrochemical Sensors, Analyst, 129 (1-2), 2004

Wei, H., Sun, J., Xie, Y., Lin, C., Wang, Y., Yin, W., Chen, G., Enhanced Electrochemical Performance at Screen-Printed Carbon Electrodes by a New Pretreatment Procedure.Analytica Chimica Acta, 588 (2), 297-303, 2007

Welford, PJ, Freeman, J, Wilkins, SJ, Wadhawan, JD, Hahn, CEW, Compton, RG, Laminated Microelectrodes: A Simple Approach to the Construction of Inexpensive Microelectrodes with a Variety of Geometries, Analytical Chemistry, 73 (24), 6088-6092, 2001

Wenzel, WW, Kirchbaumer, N, Prohaska, T, Stingeder, G, Lombi, E, Adriano, DC, Arsenic Fractionation in Soils using an Improved Sequential Extraction Procedure, Analytica Chimica Acta, 436 (2), 309-323, 2001

WHO, Media Center Factsheet: Arsenic in Drinking Water, website: www.who.int/mediacentre/factsheets/fs210/en/ accessed 2008 last revised: 2001

Williams, SC, Yon-Hin, B, Blair, N, Electrodes and their use in Assays, US Patent 6309535 assigned to Cambridge Sensors Ltd., Cambridge, UK, filed 1999 and published 2001

WOS, Web of Science, website: wos.mimas.ac.uk, last updated and accessed 2008

Zen, JM, Chen, PY, Kumar, AS, Flow Injection Analysis of an Ultratrace amount of Arsenite using a Prussian Blue-Modified Screen-Printed Electrode, Analytical Chemistry, 75 (21), 6017-6022, 2003

Zhang, HL, Han, SJ, Viscosity and Density of Water + Sodium Chloirde + Potassium Chloride Solutions and 298.15 K, Journal of Chemical Engineering Data, 41, 516-520, 1996

Zhang, HX, Uusinaki, A, Leppavuori, S, Karjalainen, P, Phase-Transition Revealed by Raman-Spectroscopy in Screen-Printed Lead-Zirconate-Titanate Thick-Films, Journal of Applied Physics, 76 (7), 4294-4300, 1994

Zheng, Y, Stute, M, van Geen A, Gavrieli, I, Dhar, R, Simpson, HJ, Schlosser, P, Ahmed, KM, Redox Control of Arsenic Mobilisation in Bangladesh Groundwater, Applied Geochemistry, 19 (2), 201-214, 2004

Publications

Since some of the findings in this thesis have been patented and talks are proceeding, as of the time of writing, to support the full commercialisation of the electrodes papers have not been submitted to Journals.

Bolbot, J, Cooper, J, Saini, S, Setford, SJ, Dudeney, RH, Method and Apparatus for Elemental Analysis, WO/2007/000583, assigned to Cranfield University, filed 2005, published 2007

Dudeney, R, Setford, SJ, Newman, JD, Tothill, IE, Method to Prevent Silver Contamination in Sensors, Patent Application No. 0715466.9, filed 09 08 2007

Dudeney, R, Newman, JD, Tothill, IE, Method to Improve Signal to Noise Ratio in Screen-printed Gold Sensors, Patent Application No. 0722865.3, filed 22 11 2007

Dudeney, R, The Nicholson Method Extended to Rough Electrode Surfaces, paper *in preparation*

Appendices

A1. Patent Publication

METHOD AND APPARATUS FOR ELEMENTAL ANALYSIS

Document Type and Number: Wipo Patent WO/2007/000583
Application Number: PCT/GB2006/002348
Filing Date: 06/26/2006 Publication Date: 01/04/2007
Assignee:
CRANFIELD UNIVERSITY (Silsoe Bedfordshire MK45 4DT GB)

Bolbot, John Anthony (55 Partridge Piece, Cranfield Bedfordshire MK43 0BL, GB)

Cooper, Joannne (2 Willow Way, Shefford Bedfordshire SG17 5JY, GB)

Saini, Selwayan (16 Sandhill Close, Millbrook Bedfordshire MK45 2JD, GB)

Setford, Steven John (55 Queens Drive, Bedford Bedfordshire MK41 9BP, GB)

Dudeney, Richard (9 Wendy Crescent, Guildford, Surrey GU2 9RP, GB)

International Classes: ***G01N27/30***; ***G01N27/416***; ***G01N27/42***

Attorney, Agent or Firm: Stuart, Ian (Mewburn Ellis LLP, York House 23 Kingswa, London Greater London WC2B 6HP, GB)

Method and apparatus for elemental analysis

Technical Field

This invention relates to a method and apparatus for elemental analysis, particularly the electrochemical detection and trace level quantification of metals and metal-like species. It particularly relates to a method of and apparatus for electrochemical stripping analysis.

Background Art

The classical electrochemical method for detection of metals and metal-like species in solution is stripping analysis, which can be of two fundamental types, amperometric or potentiometric. Examples of these techniques include, but are not limited to, anodic stripping voltammetry (ASV) and potentiometric stripping analysis (PSA). Examples of species which can be detected using these techniques may include; antimony, arsenic, bismuth, cadmium, copper, gallium, germanium, gold, indium, lead, mercury, silver, thallium, tin, zinc and chromium and certain non-metallic species that may be directly determined by amperometic or voltammetric means. Such species may be referred to as metals hereafter.

Both ASV and PSA involve the preliminary electrochemical deposition of the analyte metals onto a working electrode surface. Inherent in this process is a pre-concentration effect, at, or in the immediate vicinity of, the electrode surface region. In both ASV and PSA, electrochemical deposition is a reductive process and is achieved by poising the working electrode potential such that a cathodic (reducing) current is effected between the working electrode and analyte species. After reductive deposition the metals are re-oxidised; this process results in their re-solution and is consequently called "stripping" - the metals being stripped back into solution from the electrode. Monitoring and quantifying the stripping process is the way in which the metals are identified and analysed;

the way in which the stripping is effected is the basis for the difference between ASV and PSA.

In ASV, after metal deposition, the potential is moved in a positive direction and the current is monitored. Each deposited metal is oxidised (stripped) at a characteristic potential (the stripping potential) and the value of this potential can be used to identify the metal. At the stripping potential, a current change can be recorded (the stripping current) which is an anodic current concomitant with the metal oxidation and proportional to its concentration. Consequently, by measuring stripping potentials and stripping currents, metals can be identified and quantified. If the potential is *swept* to a more positive potential, the metals are stripped sequentially and a series of stripping current peaks are obtained, each at a metal-specific stripping potential. The precise value of the stripping potentials depends upon the assay conditions and the type of electrode used.

PSA differs from ASV in that, after reductive deposition, the metals are allowed to re-oxidise either electrochemically or by way of chemical oxidants and the concomitant change in electrode potential is monitored. A typical result is a plot of (falling) potential against time (or some derivative thereof) in which the metals are characterised by periods in which the potential decay is slowed or arrested. The potential at which each such event occurs is characteristic of a particular metal (stripping potential) and the duration of the event (transition time) is proportional to the metal concentration.

A mercury electrode is conventionally used for both types of metal stripping analysis. The mercury electrode can be pre-formed from metallic mercury, as is the case with the classical mercury hanging drop electrode, or it can be formed *in situ,* during the deposition phase of the assay, by electrochemical reduction of soluble mercury ions at the surface of an electrode of some other material (such as carbon). Because the mercury is deposited at the same time as the analyte metals, this procedure is called co-deposition and patents exist for two different ways of doing this on screen-printed carbon

electrodes (US 5292423 and WO 94/28405). In the first of these, the analyte sample is mixed with a solution of soluble mercury ions before the assay is begun. In the second, a dry layer containing a soluble mercury salt is coated across the surface of the electrode and is hydrated by the analyte sample when it is introduced.

Several types of electrode have been described for stripping voltammetry; these include gold, platinum, glassy carbon and wax-impregnated graphite, carbon paste and screen-printed carbon. The carbon-based electrodes can be electroplated with gold for the same purpose.

Examination of the prior art indicates that solid metal electrodes have been well utilised for the trace determination of metals by voltammetric or potentiometric means. Furthermore, prior art exists relating to the use of screen-printed carbon electrodes, utilised in conjunction with mercuric films or electroplated gold for the measurement of trace metals. In such cases, it is evident that the electrodes must either be pre-dosed with materials to provide the requisite metal deposition surface, or appropriate reagents must be added to the measurement solution to allow the real time *in situ* creation of the deposition surface in conjunction with the metals deposition process. Such methods have clear drawbacks in that mercury containing materials are required, posing a potential environmental issue and also a user-toxicity danger which renders the method less amenable to decentralised field-based usage. Additionally, the use of carbon working electrodes in conjunction with mercury containing materials, restricts the applicability of the method with respect to the determination of, for example, mercury itself and also other metals, such as arsenic, that would be stripped back into solution at potentials more electropositive than elemental mercury, at a given carbon working electrode.

The relatively limited potential window offered by the carbon electrode, utilised in conjunction with mercury films for metal deposition, prevents the measurement of mercury and metals that undergo stripping at more positive potentials than mercury. Thus, the method becomes limited with respect to the total number of

different metals it can be used to detect. Screen-printed electrode assemblies that are not reliant on metal deposition films such as elemental mercury, therefore offer the possibility of wider potential windows and hence the determination of a wider number of metal species. Such screen-printed assemblies therefore may serve as useful screening tools for the semi-quantitative evaluation of the total metal content of a sample.

Patent EP 0 969 281 describes the use of electrode assemblies incorporating screen-printed gold working electrodes for measurement of electroactive species by means of electrochemical stripping analysis. The invention is described as an alternative means of measuring electroactive species using screen-printed electrodes without the requirement for mercury films. However, we have appreciated that the commercially available gold inks as used in EP 0 969 281 contained metal species such as bismuth oxide and copper oxide, to act as fluxes to promote metal binding and improve flow properties, and copper to assist in wire bonding. Consequently, background voltammograms exhibited numerous interfering peaks due to the presence of these metal species and other unidentified additives. In most cases, means of quantitatively determining metallic analytes required the use of complex data conversion algorithms.

As described earlier, carbon screen-printed electrodes require the use of mercuric ions in the sample solution, which, on application of the electrochemical depositioning technique, are reduced to elemental mercury, thus forming a mercury film at the electrode surface to facilitate the amalgamation of metal analytes in the test solution. The potential of the electrode, in the case of anodic stripping voltammetric techniques, is then increased to more positive potentials, resulting in the stripping of these metals from the electrode surface and hence the subsequent analyte determination. Whilst this approach is satisfactory for determination of those metals that are oxidised at potentials lower than for mercury, scanning of electrode potential above this value, will strip mercury from the electrode, hence providing a significant background signal and preventing the analytical determination of metals at, or above this potential.

This has long been identified as a problem, hence the interest shown in gold electrodes, since no mercury film is required (metals can directly deposit onto the gold surface due to gold's preferential surface properties in this respect). However, EP-A-0 969 281 does not address this issue, since other metal species are required in the ink formulation in order to allow formulation and acceptable depositioning of the ink. Thus, in certain cruicial respects, it is clear that there is no benefit to the ink used over and above that offered by carbon. described herein is the use of inks without the addition of metallic species to allow metals determination - which may be considered an advantage over the prior art.

Metal detection by electrochemistry requires acidic conditions, which the electrodes must endure. Low temperature polymer electrodes proposed for different applications (for example, bioligand immobilisation), do not necessarily fulfil this function. The use of highly inert polymer materials within the gold ink formulations defined here lend the ink particularly suitable properties with respect to acid resistance.

Analysis of the literature identifies numerous applications in which it is desirable to be able to measure trace levels of heavy metals in field locations, without recourse to centralised analytical facilities. This may be achieved through the use of low cost and hence single-use disposable electrodes. Given these demands, the prior art does not provide evidence of low-cost electrode assemblies being used for trace metal determination in which no form of electrode surface adulteration to facilitate deposition (preconcentration) of metal analyte species is required and in which the voltammograms obtained were sufficiently devoid of ink-derived interferents that significantly distort the analyte-specific voltammetric response.

Disclosure of the invention

The invention comprises a method for determining trace metals that involves the provision of a plurality of flat printed electrodes, with at least one of the said flat printed electrodes serving as a

site for deposition of target metal analyte species. This working electrode is produced from a formulation not requiring, and not containing, additional metal species to serve as fluxes, bonding assistants, etc. In particular it is free from Cu and Bi species. Thus there is no requirement for subsequent electrode adulteration to facilitate metal analyte deposition. Our system can exhibit voltammetric profiles that are sufficiently devoid of background ink-derived interferents to allow sufficiently accurate quantitative data to be obtained. Samples may be subsequently analysed for heavy metal content with said plurality of electrodes. At least one of the flat screen-printed electrodes serves to provide a reference potential, being for example an Ag/AgCl reference electrode. At least one of the electrodes is fabricated from a screen-printed or otherwise deposited film of a noble metal ink containing negligible electroactive interferents, such as a gold ink of a suitable formulation.

Our preferred noble metal "ink" composition, unlike numerous previous attempts to prepare gold-based screen-printed sensor assemblies for metal determination, does not require firing at relatively high temperatures (typically several hundred degrees). These previously screen-printed gold inks have required firing because they have contained metal species that, on being heated, promote adhesion of the gold film to the underlying substrate material. Examples of these metallic species include copper, bismuth and lead. These materials are either frit or oxide based in order to confer advantageous adhesion properties to the ink formulation. Our formulations are essentially free of such metals.

Preferably, the ink contains polymer materials based on epoxy resins, polyvinyls, polyesters or polyurethanes. These polymer materials confer adhesion properties onto the particles of gold or other noble metal that specifically allow the metal films to be adhered to the underlying substrate at lower temperatures without the need for added copper and lead frits and/or oxides , and subsequent high temperature treatment, to facilitate the adhesion process.

The noble metal inks are preferably based on micron-dimension metal particles (typically 2-4 μm) dispersed in polymer materials (specifically chemically inert resins, typified by chemical species such as polyvinyls, polyesters and polyurethanes, these polymers removing the need to add metallic species, specifically copper and lead (either frit or oxide based) in order to promote adhesion of the metal films to underlying substrate surfaces). The removal of the need to add these metallic adulterants therefore removes the need to heat treat the metal films at high temperature in order to melt said adulterants and facilitate the metal ink-substrate adhesion process. Therefore such polymer based inks may be adhered to substrate surfaces without the need for an elevated temperature curing process.

It is to be recognised that this class of noble metal ink does not contain metallic adulterants and therefore such inks have superior properties with respect to the trace level and repeatable determination of metal species by appropriate electrochemical means. Given the prior art, it would have been concluded that low temperature curable screen-printable inks are not compatible with metals detection (c.f. EP-A-0969281), but the non-obvious step of examining the field, liaising with ink manufacturers and identifying a class of screen-printable lower temperature curable inks that does not exhibit interferences with respect to metals determination, was followed.

A further inventive aspect to this disclosure is the realisation that if the ink can be cured at low temperature, then the range of substrate materials onto which the ink may be deposited, may be extended. For example, it is possible to print onto heat labile materials such as plastics (as opposed to ceramics usually employed with high temperature curable inks). Thus a new class of low-cost mass-manufacturable devices, based on the low temperature curable properties of the gold inks, and devoid of metallic ink formulation interferents has been created.

The sample analysis procedure for the determination of heavy metal content may be voltammetric or potentiometric or any other electrochemical stripping method. The use of a deposition step may

be used to preconcentrate target metal species upon one or more electrodes. Tests may be performed by applying appropriate volumes of test solution to the plurality of electrodes, which may be as little as microlitre volumes if desired. Alternatively, the electrode plurality may be submerged in a test solution. Samples may be tested with or without stirring (or other method of agitation, such as shaking or sonication) as required and with or without deaeration as required.

The invention may enable the provision of disposable single-use electrodes for trace metal detection.

The invention may enable the provision of an apparatus or instrument, to which the electrodes can be connected, for applying, measuring and manipulating the electrical potentials and currents required for the analysis. Furthermore, the apparatus or instrument may be sufficiently compact to be easily portable.

The invention may enable the provision of a trace metal testing apparatus that is compatible with the usage of small (microlitre) volumes of sample. The approach is compatible with the determination of samples that have not been de-aerated, stirred or otherwise manipulated to facilitate the measurement process.

The invention may enable the use of low-cost electrodes for metal determination. The low cost and ease of mass manufacture of the devices may mean that the electrode assembly may be for single use or may be reused if desired. Disposability has the added advantage of removing the requirement to regenerate or clean fouled or otherwise altered electrode surfaces which is a further encumbrance when working with traditional electrode materials.

Use of the invention may lead to simplicity and rapidity of the assay procedure, which allows the apparatus to be readily used in decentralised or field locations without recourse to centralised facilities or complex data treatment procedures to account for background ink-derived interferent effects. However, the invention may be used within centralised locations if required.

Desirably the invention makes use of screen-printable inks that can be dried or cured and hence stabilised onto a variety of backing substrates that can be subsequently used for the intended measurement purpose.

Desirably use is made of low temperature curing gold inks that do not require elevated temperatures to form stable structures for subsequent usage within liquid sample solutions. Low temperature curing offers the advantage that the apparatus may employ backing substrates, e.g. plastic materials, that may otherwise become deformed or otherwise damaged when subjected to elevated temperature conditions. Ink curing may be achieved by simple forced-air convection.

The sample to be analysed may be extracted or pre-treated by appropriate physico-chemical means before it is brought into contact with the electrodes.

The benefit of the invention resides in the fact that the noble metal ink selected to fabricate the working electrode is prepared in such a manner that electroactive species are either not employed, or used to a minimal extent, to formulate the ink with the requisite physico-chemical properties for its intended use. As a consequence, the ink preparation will therefore not give rise to significant interfering peaks in the electroactive profiles obtained when performing electrochemical stripping analysis. This approach differs from the prior art in that clear potential windows are offered by the superior ink formulations used, thereby removing the need to subsequently treat, or otherwise account for, the voltammetric data obtained in order to obtain meaningful quantitative information. The invention described herein further extends the technical field by virtue of the fact that superior noble ink working electrode ink formulations, coupled to the non-requirement for mercury, as is necessary for screen-printed carbon electrodes, significantly extends the interferent-free potential window towards higher positive potentials. Thus, for the first time, screen-printed electrodes can be used to accurately determine more electropositive metals such as arsenic.

Screen-printing inks may be made by the dispersal of a conductive material in a non conducting polymeric matrix. Metal-containing inks are often formulated by the dispersal 0.1-10 µm, preferably 0.5-5 µm particles into a polymeric matrix. The particles maybe spherical, irregular, flake, or fibre shaped. Other possible conductive species may include platinum, palladium and gold. The polymer itself must perform several tasks: solvated, it provides a consistent viscous paste forming a suspension when mixed with the conductor; once cured at temperatures below 200 °C, it must be chemically and electrochemically inert; and be reasonably strong and flexible to avoid cracking. Therefore, because of these complex requirements polymeric formulae include several different components. Polymer matrices suitable for screen-printing inks should be chemically inert and may include epoxy resins, polyvinyls, polyacrylics, polyesters and polyurethanes.

Another means by which the metallic screen-printable inks may be formulated is by the employment of metal conductor particles of suitably reduced dimensions, typically in the nanometer range, but of other dimensions if appropriate for the application. Preferred particles have sizes in the range 0.1 to 1000 nm, more preferably 0.1 to 100 nm, most preferably 0.5-5 nm. Preferably, such particles would exhibit regular shapes with a narrow size distribution Such reduced dimension structures, and aggregates thereof, exhibit significantly lowered melting and sintering temperatures, with or without encapsulation with shorter-chain alkanes, in comparison to their larger scale counterparts. Melting/sintering temperatures may, at least in part, be dictated by the size of the metallic particles. Curing temperature of less than 150°C are possible, allowing formation of conducting films on heat labile substrates if required. Curing of the metal containing medium results in the formation of a continuous, conducting metal film on the substrate surface.

Such structures and corresponding aggregates may be formulated into pastes suitable for subsequent printing or other suitable deposition method by adulteration of the metallic structure surfaces. An example would be the use of suitable agents containing two moieties, the first moiety being able to associate itself with the metal surface in question, coupled to a second moiety that is orientated

away from the surface structure. Such manipulation would effectively result in the encapsulation of the metallic components of the mixture.

The choice of the primary moiety will depend upon the metal species in question. For example, certain metals such as gold and certain alloys such as gold-silver alloys are able to bind to compounds containing thiol moieties to form stable complexes.

The choice of second moiety will be dependent upon compatibility with those other reagents required to formulate the metallic paste as will be discussed in subsequent sections of this disclosure. However, the purpose of the second moiety is to allow integration of the metallic particulates into these other materials required to form a matrix of the required functional characteristics and consistency for subsequent depositioning. In a preferred embodiment of the invention, the second moiety will exhibit a chemistry compatible with carrier solvents used to formulate the preparation. Given that such carrier solvents are primarily non-aqueous or non-polar in nature, typically exhibiting a basic aliphatic or aromatic hydrocarbon structure, the second moiety of the metal binding species will be similarly aliphatic or aromatic in nature. In a preferred embodiment, such structures would include aliphatic structures based on dodecane, octane, hexane or butane structures. The carrier solvent would preferably exhibit similar structural features, typical solvents therefore including dodecane, octane and hexane although aliphatic solvents such as toluene may also be considered. Thus, overall, when using such a strategy, the metal particles are effectively encapsulated by the double-moiety compound, thereby facilitating metal particle suspension in the matrix for subsequent routine depositioning.

Many materials used for metals depositioning exhibit properties consistent with the intended depositioning process. For example, formulations intended for screen-printing may be of a particular viscosity range, whilst formulations intended for spray depositioning may exhibit an alternative viscosity range. Appropriate selection of the associating agent may aid this aspect of the formulation

procedure. The selected derivatisation agent may also be used to alter the solubilisation properties of the metallic species, such that the metallic paste may be introduced to a carrier solvent to allow formulation of pastes of the desired consistency and viscosity for depositioning purposes. Such carrier solvents would typically be non-polar in nature but may alternatively exhibit greater polarity, depending upon the given demands of the depositioning process.

Specifically, the metallic pastes used to fabricate one or more structures within the screen-printed electrode assembly may contain nano-structured metallic particles, which may be present in the form of clusters.

Alternatively, the metallic pastes used to fabricate one or more structures within the screen-printed electrode assembly may contain micro-structured metallic particles which may be present in the form of individual particulates or clusters.

Specifically, the metallic species present may be gold.

The metallic species may be spherical, irregular, flake or fibre shaped

The metallic pastes used to fabricate one or more structures within the screen-printed electrode assembly may be dispersed within a non-conducting polymer matrix which may consist of one or more polymeric species.

The polymer species should be chemically inert and may include epoxy resins, polyvinyls, polyacrylics, polyesters and polyurethanes.

Preferably, the polymer matrix should provide a consistent paste of the desired viscosity, to allow compatibility with the depositioning method of choice.

Preferably the polymer matrix should exhibit properties such that is forms a stable and physico-chemically resistant paste on being heat treated at temperatures of less than 200°C.

Preferably the polymer matrix is chemically and electrochemically inert, being of reasonable flexibility and strength to avoid cracking or other similar structural damage when employed within the constraints of the usual device measurement procedure.

Alternatively, the metallic pastes used to fabricate one or more structures within the screen-printed electrode assembly may be enveloped by a suitable encapsulating agent.

The encapsulating agent may comprise of one or more reagents containing a metal specific surface active chemistry that is able to associate itself with the metallic structures and containing a second moiety allowing subsequent solubilisation of the complex in a suitable carrier solvent.

Specifically, the encapsulating agent may contain a second moiety that may be hydrocarbon-based to facilitate solubilisation of the metallic complexes in suitable non-polar solvents or solvents of intermediate polarity.

Specifically, the encapsulating agent may contain a thiol derivative.

Specifically, the encapsulating agent may be a thiol derivative and the metallic species be composed of gold.

Specifically, the encapsulating agent may be a thiol derivative incorporating a hydrocarbon moiety, which may be a linear or branched hydrocarbon structure. The hydrocarbon structure may for example be, but not necessarily be limited to, an alkane.

The carrier solvent would typically be a solvent of sufficient volatility to be volatilised during the metal curing process.

The encapsulating agent may also be removed, wholly or in part, during the volatilisation procedure. The encapsulation agents may also enhance adhesion of the metallic particles to the substrate material.

The curing process may be enhanced by the use of UV curing agents within the metallic paste formulation.

Such formulations may include other adulterants as necessary in order for the ink formulation to achieve optimum performance with respect to the end application, particularly with respect to formulation handling and depositioning, and subsequent performance during the measurement process.

A plurality of screen-printed electrode structures may be fabricated. Such an architecture may consist of one or more working (noble metal) electrodes, one or more screen-printed reference electrodes, most likely of the Ag/AgCl type, and one or more counter or auxiliary electrodes as required. In its simplest format, the electrode assembly would consist of one noble metal (gold) electrode of superior ink formulation and hence free of significant electrochemical interferents and one reference electrode, both screen-printed.

The above assembly may be used for trace level determination of heavy metals in solution and provides both qualitative and quantitative information.

In one embodiment of the invention, the noble metal material, specifically gold material of superior ink formulation and hence free of significant electrochemical interferents, may require high temperature curing to allow formation of a stable gold electrode preparation suitable for the intended end usage in liquidic solutions. In such situations, all other materials used to fabricate the electrode assembly, including the backing substrate material should be resistant to the applied heat. In such instances ceramic material or other suitable backing substrate may be considered.

In a more preferred embodiment of the invention, the noble metal material, specifically gold material of superior ink formulation and hence free of significant electrochemical interferents, may not require high temperature curing to allow formation of a stable gold electrode preparation suitable for the intended end usage in liquidic solutions. In such situations, a lower requirement for thermal stability of all materials used in the electrode assembly preparation is evident. This allows electrode assemblies to be printed onto heat labile backing materials, e.g., plastic-based materials such as polyester or polyvinyl chloride, provided adequate material adhesion can be achieved.

The low cost and ease of mass manufacture of the screen-printed noble metal electrodes of superior ink formulation and hence free of significant electrochemical interferents, renders them simple to use and disposable. Such an approach (1) removes issues associated with extensive electrode preparation steps (electroplating of gold), (2) negates the use of mercuric salts in electrode preparation, undesirable from both environmental and toxicological viewpoints, and (3) removes the need to account for significant interfering peaks within voltammograms. Overall, therefore, this approach is conducive to usage of such devices in decentralised locations with a simplified measurement technology.

The test method may be voltammetric (to include anodic stripping voltammetry which may include linear voltammetric waveforms, normal pulse voltammetric waveforms or square wave voltammetric waveforms including cathodic stripping voltammetry or any other electrochemical stripping analysis procedure), or may consist of a potentiometric stripping analysis procedure.

The screen-printed noble metal provides a surface suitable for the accumulation of metals from the test solution during the sample deposition step whilst not engendering significant interference factors. The inherent physico-chemical properties of the material allow heavy metals to be preconcentrated from solution onto the electrode surface throughout the deposition process. To a certain extent, prolongation of the deposition step influences the extent of

heavy metal deposition at the electrode surface(s). The preconcentration step may also be in the form of an adsorptive accumulation step.

Samples may be applied as droplets of any suitable volume, most likely microlitre volume, directly onto the active electrode assembly such that all of the active areas of the exposed parts of the screen-printed electrode elements are in contact with said sample solution. The solution may be deaerated as required.

Alternatively, sample-electrode assembly contact may be achieved through suspending the electrode assembly in the sample solution to be measured. The solution may be stirred and/or deaerated as required.

The invention may be used to assess the heavy metal content of any liquidic solution. Specifically, the invention may be used to determine the heavy metal content of urine or any other body fluid, biomaterial or other material from which a liquid same can be prepared, such as hair samples, water, drinking water, waste water, process water and other waters; soil and sediment liquid extracts, liquid components of foods, such as heavy metals in fish products and liquid traps in which heavy metal species are collected from gaseous samples, including exhausts and emissions. Heavy metals may include Bi, Cu, Cd, Zn, Ni, Pb, Hg, V and Sn.

The screen-printed gold electrodes can be used to detect and quantify metals in biological fluids and materials such as urine, blood, saliva, hair, skin, nails and teeth. This may be particularly useful in the *medical diagnosis* of potentially harmful levels of any metal or metals in the human body or any part of the human body. In this respect, it may be especially useful for screening populations of individuals for their content of any metal or metals. It may also find application in the monitoring of populations deemed to be at some risk of exposure to a particular metal or metals, for example, populations of workers whose occupation may carry some risk of such exposure.

Use of screen-printed gold electrodes of superior ink formulation, and hence free of significant electrochemical interferents, for detection or quantification of metals in biological materials need not be restricted to the field of medical diagnosis or the assessment of human health. There is also an important application in testing biological materials which are intended for human consumption as *foodstuffs*. The source of these materials may be animal (for example; cattle, sheep, pigs, poultry, fish and milk) or plant (for example; vegetables, fruit, grain). The metals present in, or contaminating the biological materials under test, may have accumulated during the lifetime of the relevant organism or may have been introduced after slaughter or harvest by way of cooking, storage, transport, processing, preservation or packaging.

Screen-printed gold electrodes of enhanced electrochemical performance may also be used for detection/quantification of metals in *animal feeds* (such as grain products, fish products, offal and other abattoir products, human food waste) and also plant fertilizers or other soil fertility enhancers such as sewage or silage or organic or inorganic wet or dry composite preparations or treatments. One application of such use might be the prevention of metals accumulation in humans by way of investigation or monitoring of potential or actual pathways of human food borne metal contamination.

Another application of this technology in relation to metals detection in biological materials could concern testing non-food materials of a *biological origin or else containing some component of a biological origin*. Such materials frequently have direct or indirect human contact or useage and in some circumstances it may be deemed necessary to determine their metals content, possibly in order to assess their potential toxicity or risk to human health. Examples are cosmetics (for example, shampoos, soaps, cremes and perfumes), medicines or medical preparations (for example linctuses, pills, lotions, ointments, tonics), paper or cardboard packaging for food or other materials, clothing, bedding, soft furnishings, furniture, flooring, carpeting, wallpaper, paint, varnish, panelling or tiling.

The invention allows both quantitative and qualitative information to be obtained regarding the heavy metals composition of a sample.

The quantitative and qualitative information obtained by the method allows the simultaneous detection of two or more metals in the same test solution. The invention has use as a method for providing an indication of the total heavy metals content of a given sample.

The device may be used in combination with other electrode materials, such as carbon inks, to allow more complex measurements to be performed.

Further, the method can be combined with appropriate data treatment procedures, such as chemometrics and machine learning, to allow complex voltammetric or potentiometric profiles to be interrogated with respect to the qualitative and/or quantitative composition of the solution under test.

The measurement procedure utilises the unadulterated surface of the screen-printed electrode element of enhanced electrochemical performance as a means of direct deposition and pre-concentration of metals from solution. The method is therefore not limited with respect to the potential window otherwise dictated by the use of additional deposition films, such as mercury. The method is therefore amenable to measuring those metals undergoing oxidation at more electropositive potentials and is therefore more useful as a means of semi-quantitatively determining the total metal content of a sample.

The measurement procedure and electrode assembly can be under the control of a measurement apparatus that is both portable and simple to use, if necessary containing on-board software to allow requisite measurements to be performed, analysed and stored as appropriate. The device may be capable of performing both stripping voltammetric and potentiometric stripping analysis as required.

Brief Description of drawings

Fig 1(a) is an anodic stripping voltammogram (“ASV”) showing detection of mercury (“Hg”) and a blank (“B”) at a screen-printed gold electrode.

Fig 1(b) is an ASV corresponding to Fig 1(a) determined with a solid gold disc electrode.

Fig 2(a) shows a set of ASVs for different mercury concentrations (i), and a corresponding graph (ii) of peak area vs concentration.

Fig 2(b)(i) and (ii) correspond to Fig 2(a)(i) and (ii) for a smaller range of concentrations (10-400µg/l).

Fig 3(i) and (ii) correspond to Fig 2(a)(i) and (ii) for experiments with longer deposition times.

Fig 4(i) and (ii) correspond to Fig 2(a)(i) and (ii) but relate to the determination of arsenite.

Fig 5 shows a set of ASV, for mixtures of arsenite and mercury.

Fig 6(i) and (ii) correspond to Fig 2(a)(i) and (ii) and were determined for solutions of reduced arsenate.

Figs 7, 8 and 9 show ASVs for Cd, Pb and Cu respectively.

Fig 10 is a schematic view of an apparatus embodying this invention.

Fig 11, 12 and 13 shows cyclic voltammograms of potassium hexacyanoferrate solutions using gold ink screen-printed electrodes formed in three different ways.

Modes for carrying out the Invention

The preferred device consists of a plurality of planar electrodes screen-printed, or deposited by an analogous method such as stencil depositing, onto a suitable supporting material. Trace metal analysis is achieved through the application of suitable voltammetric or potentiometric stripping procedures. Electrochemical measurements were performed using either a computer controlled Autolab PGSTAT-10 (Eco Chemie, Utrecht, Netherlands) with a general-purpose electrochemical software operating system (GPES3) or a hand-held PalmSens electrochemical analyser (Palm Instruments BV, Utrecht, Netherlands).

Many voltammetric and potentiometric stripping analyses have been performed either by applying discrete volumes of test solution directly to the planar electrode assembly or by suspension of the assembly in the test solution, typically of 2-20 ml capacity. The preferred measurement protocol involves the application of microlitre or multiple microlitre volumes of test solution directly to the plurality of printed planar electrodes. Alternatively the electrode assembly may be suspended in test solutions (held within test cells if so required). However the first approach, not requiring immersion, is well suited to simple, rapid decentralised testing operations. Stripping analyses (voltammetric and potentiometric) were performed using the PGSTAT-10 device. A number of voltammetric experiments were performed using the PalmSens electrochemical analyser.

The electrode assembly may be fabricated by any suitable printing process that involves the deposition of conducting and insulating preparations, as appropriate, onto suitable supporting substrates. The preferred embodiment of the device involves the use of screen-printing techniques to sequentially deposit the requisite electrode assembly preparation materials onto selected substrates.

The screen-printed electrodes used to illustrate the applicability of the invention consisted of a planar 3-electrode assembly 8 (see Fig 10). The electrode strips comprised 3 electrodes – a working electrode 10 fabricated from a proprietary printable gold-containing preparation formulated to contain minimum quantities of electroactive

interferents within the specific potential window necessary to quantitatively determine the analyte of interest, carbon counter electrode 12 and Ag/AgCl reference electrode 14. For the purposes of these examples, the ink used was Du Pont gold ink BQ331 throughout, with ink BQ164 used for the reference electrode, either BQ225 or BQ242 used for the counter electrode, and BQ425 used for the 'encapsulant' layer. However, any ink formulated to provide a voltammetric response with minimal interference may be used, including those fabricated using suitably sized gold particles and aggregates coupled to appropriate encapsulant technologies. Underlying conducting tracks 16 were fabricated from the same carbon ink as the counter electrode. The backing substrate 18 was based on a plastic (polyester) material. The uppermost printed layer 20 consisted of an insulation shroud with a circular aperture (target area) 22 to allow exposure of the working, reference and counter electrodes to the test solution whilst protecting the underlying conducting tracks from the test solution. The hydrophobic nature of the insulation shroud allowed application of appropriate volumes (typically 100 microlitre) of test solution to the target area such that the solution was contained within the circular aperture and directly over the exposed portions of the printed electrode elements (Fig 10 actually shows the assembly 8 immersed in a test solution 24 in a vessel 26). An optional stirring means (stirrer bar 28 and magnetic stirrer unit 30) and a deaerating means (tube 32 for bubbling nitrogen) are shown in phantom. The electrodes 10, 12, 14 are connected to an electrochemical analysis operating system 34.)

Most experiments were performed using the 3 electrode elements. A number of experiments were performed using only a 2 electrode system in which the counter electrode was excluded from the circuit and its function was performed instead by the Ag/AgCl reference electrode, which was in this case working as both counter and reference electrode. The working electrode was always placed in direct proximity to the reference electrode.

Conventional electrodes were used for comparative analysis and included a platinum (Pt) wire counter electrode and Ag/AgCl solid reference electrode.

All solutions were prepared using HPLC grade water. The metal-containing test solutions were atomic absorption standard solutions purchased from commercial organisations. High purity standard/stock solutions of 1000 mg l^{-1} were used to prepare 50 mg l^{-1} working standards for each analyte of interest. Standard mixtures were prepared at the required concentration, in 0.1 M potassium chloride (KCl) and 2-4M nitric acid (HNO_3) for subsequent ASV analysis. Potassium chloride served a dual purpose as a supporting electrolyte, and to stabilise the reference potential of the Ag/AgCl electrode. Nitric acid was used to obtain a low and relatively constant pH and ensure the solubilisation of the analytes being determined. Urine samples were collected from a healthy volunteer.

The preferred anodic stripping voltammetry (ASV) and potentiometric stripping analysis (PSA) procedures will now be described. Both types of procedural method involved a common deposition stage followed by the relevant stripping steps. In a typical procedure one hundred microlitre volumes of test solution containing nitric acid and supporting KCl electrolyte were applied to the 3 electrode assembly, forming a solution bead bounded by the edge of the electrode target area. The exact test solution volume may be varied according to experimental requirements. Metals were deposited from solution onto the gold working electrode by application of a suitable deposition potential (varied according to the analyte of interest as illustrated in the examples to follow) for a fixed period of time (again varied according to the analyte of interest and preferred detection limit as illustrated in the examples to follow). Experiments were usually performed on non-deaerated and non-agitated samples. In another type of embodiment of the procedure, the electrode assembly may be suspended in a suitable volume of test solution, containing nitric acid and supporting KCl electrolyte, within an electrochemical cell. The sample may be deaerated and agitated if so desired. (See Fig 10.)

All stripping steps were performed on quiescent solutions. In the voltammetric procedure, the potential was scanned, usually (but not necessarily) with a differential pulse waveform, from the depositioning potential to a more positive potential, at a fixed scan rate. The scan was stopped at a potential dependant upon the

analytes of interest, as illustrated in the examples to follow. Potentiometric stripping was performed by application of a constant oxidation current, typically in the region of 1 microAmp, but this may be varied according to application.

In a typical procedure, each printed electrode assembly was used once before disposal. Such an approach is possible given the ease and low-cost of mass manufacture of the screen-printed electrode assemblies.

Example 1

The electrochemical detection strip (approx. 1cm x 3.5cm) was screen-printed on polyester (125µm) and comprised 3 electrodes; gold (working electrode); carbon (counter electrode); Ag/AgCl (reference electrode). An example of the utility of this invention is indicated by the following case of metal detection; in this case, mercury in aqueous solution. Figure 1 compares stripping voltammograms for an unstirred and non-deaerated solution containing 100µg/l mercury and a reagent blank at a screen-printed gold electrode (Figure 1(a)) and a solid gold disk electrode (Figure 1(b)). Since ultra-pure solutions were used to prepare the test solutions, the blank response profile clearly demonstrates minimal interferences, demonstrating (i) the quality of the test preparations and (ii) the superior voltammetric performance of the gold electrode formulation when compared to the prior art, and also when compared to the solid gold disk electrode. Further (a) used a screen-printed Ag/AgCl reference electrode, while a conventional Ag/AgCl electrode was employed in (b). Metal deposition was carried out at +0.2V for 30 seconds before the potential was swept to +0.7V. A differential pulse waveform of 20 mV/s scan rate and amplitude of 50 mV was applied. The gold screen-printed electrode of the invention exhibits a well-defined stripping response for mercury and low background current. A short (30 seconds) preconcentration time allows quantification in the micrograms per litre range. Comparison to the more traditional solid gold disc electrode indicates that the gold screen-printed electrodes of this invention are less affected by the use of unstirred and non-deaerated solutions, exhibiting lower background currents.

Example 2

A screen-printed detection strip as used in Example 1 was connected (in a flat, horizontal position) to an electrochemical analyser and a drop (100µl) of suitably pre-treated sample (containing mercury) placed across the three electrodes. Figure 2(a) illustrates differential pulse anodic voltammetric stripping responses for gold screen-printed electrodes for unstirred and non-deaerated solution of increasing mercury concentrations, from 0-2000 µg/l. Metal deposition was carried out at +0.2V for 30 seconds before the potential was swept to +0.7V, stripping out the mercury at around 0.4V. Stripping peak areas were calculated and plotted against the mercury concentration in µg/l (parts per billion). In this analysis, each electrode was used once and discarded. Fourteen concentration increments from 0-2000 µg/l resulted in a linear calibration plot with a correlation coefficient of 0.9971.

Linearity was maintained in the concentration range of 0-400 µg/l yielding a correlation coefficient value of 0.9989 (Figure 2(b)). An LOD, calculated according to the IUPAC convention (S/N = 3) using a 20µg/l mercury solution was calculated as 2.7 µg/l following 30 s depositioning. The reproducibility was estimated from a series of 10 successive measurements of a 10 and 100 µg/l mercury solution. Mean I_p values of 0.05µA and 0.0044µA with RSD of 8.4% and 9.1% for 100 and 10 µg/l mercury respectively, were achieved using a deposition time of 30 seconds. The efficacy of the ink preparation, with respect to absence of interfering voltammetric peaks is clearly apparent.

Example 3

To achieve a lower limit of detection, the mercury deposition time was increased to 120 s. All other parameters were identical to those in Example 2. Figure 3 shows linearity was maintained in the range 0-10µg/1, yielding a correlation coefficient value of 0.9989. A limit of detection, calculated according to the IUPAC convention (S/N = 3) using a 10µg/l mercury test solution was calculated as 0.15 µg/l. The use of gold screen-printed electrodes in this invention has provided

a low cost technique for the detection of Hg. The experimental protocol is simple to perform, allowing semi-skilled personnel the ability to rapidly measure Hg in field conditions.

Example 4

Figure 4 illustrates the applicability of the gold screen-printed electrodes to the analysis of Arsenite (As^{3+}). The gold screen-printed electrode was connected to the analyser and a 100µl sample droplet placed onto the gold screen-printed electrode such that is completely covered the 3-electrode assembly. A differential pulse waveform of 20 mV/s scan rate and amplitude of 50 mV was applied. Figure 4 illustrates the voltammetric stripping responses for gold screen-printed electrodes for unstirred and non-deaerated solution of increasing arsenite concentrations, from 0-800 µg/l in 4 M HCl supporting electrolyte. Metal deposition was carried out at 0V for 30 seconds before the potential was swept to +0.5V, stripping out the arsenite at around 0.15V. Stripping peak areas were calculated and plotted against the arsenite concentration in µg/l (parts per billion). In this analysis, each electrode was used once and discarded. The calibration plot was linear with a correlation coefficient value of 0.9939. A relative standard deviation of <10% was obtained (n=6) at each arsenite concentration. The limit of detection, calculated according to the IUPAC convention (S/N = 3) using a 50µg/l arsenite test solution was calculated as 1 µg/l. The gold screen-printed electrode of the invention exhibits a well-defined stripping response for arsenite and despite the short (30 seconds) deposition time allows quantification in the micrograms per litre range. Examination of the blank response indicates no interfering species are present.

Example 5

Figure 5 illustrates stripping voltammograms of an unstirred and non-deaerated solution containing equal concentrations of arsenite and mercury in the range of 0-800 µg/l in 4 M HCl supporting electrolyte. Metal deposition was carried out at 0V for 30 seconds before the potential was swept to +0.7V, stripping out the arsenite at around

+0.15V and mercury at +0.4V. The calibration plot was linear with a correlation coefficient value of 0.9824 and 0.9885 for arsenite and mercury respectively. The gold screen-printed electrode of the invention exhibits a well-defined stripping responses and good resolution between the stripping peaks of arsenite and mercury at these concentrations.

Example 6

The measurement of both arsenite (As^{3+}) and arsenate (As^{5+}) is important for environmental toxicity studies. For the speciation measurement of As^{5+}, a pre-reduction step, to reduce As^{5+} to As^{3+}, henceforth referred to as As^{5+}_{RED}, is necessary. This was performed by adding 0.1ml 20% v/v cysteine to test solutions containing As^{5+}, and heating at 75°C for 10 minutes. The reduction procedure was simple and rapid (10 min) to perform and by using a commercially available portable heating system, could easily be carried out under field conditions. Following reduction of $As^{5+} \rightarrow As^{5+}_{RED}$ a calibration plot (Figure 6) of the As^{5+}_{RED} stripping response versus its concentration in the range of 0-800 µg l^{-1}, in 1 M HCl supporting electrolyte, yielded a correlation coefficient value of 0.9852. Metal deposition was carried out at -0.3V for 30 seconds before the potential was swept to +0.5V, stripping out the As^{5+}_{RED} at around 0.25V. A RSD of ≤15% was obtained (n=6) at each concentration increment. The limit of detection, calculated according to the IUPAC convention (S/N = 3) using a 100µg/l As^{5+}_{RED} test solution was calculated as 42 µg/l. The voltammograms illustrated in Figure 6 show a different shape of signal was obtained when analysing the pre-reduced As^{5+}_{RED} than the original trivalent As^{3+}. The stripping peaks obtained were broader and shifted to more positive potentials. These preliminary findings have demonstrated the applicability of the sensor to determining the less toxic As^{5+} when speciation studies are necessary.

Example 7

Metals such as cadmium, lead, and copper are generally measured by amalgamation in a mercury film electrode. In this instance, the metals are deposited directly onto the bare gold screen-printed

working electrode, providing a mercury free procedure. The gold screen-printed electrode was connected to the analyser and a 100µl sample droplet was placed onto the gold screen-printed electrode such that completely covered the 3-electrode assembly. A differential pulse waveform of 20 mV/s scan rate and amplitude of 50 mV was applied. Figure 7 illustrates the voltammetric stripping response for 200 µg/l lead, while Figure 8 shows the response of 1mg/l cadmium solution; both in 0.1M KCl and 1%v/v nitric acid supporting electrolyte, at the gold screen-printed electrodes. Reagent blanks are also shown. Metal deposition was carried out at -1.1V for 165 seconds before the potential was swept to 0V, stripping out lead at around -0.2V and cadmium at around -0.3V. Figure 9 illustrates stripping voltammograms for copper (0.2-1mg/l) following a 30 second deposition at 0V. The gold screen-printed electrode of the invention exhibits a wide potential window, with well-defined stripping responses for these metals at both negative (lead and cadmium) and positive (copper) potentials. These preliminary findings have demonstrated the applicability of the gold screen-printed electrodes to determining a range of metals environmentally important metals. Again, an absence of interfering peaks, across the more negative potential window examined, is evident on examination of Figures 7 and 8.

Example 8

A sample of fresh urine was spiked with a solution of mercuric nitrate such that it contained 100 ppb mercury. The concomitant urine dilution was 1 %. This spiked urine was then diluted tenfold with a solution of 6% (v/v) nitric acid containing 0.1M KCl. An unspiked urine sample was also diluted in the same way. Aliquots (5 ml) of both spiked and unspiked acidified urine were then sealed in 20 ml screw-top glass Universal containers and autoclaved for 15 min at 120°. After cooling, samples were tested for mercury content by placing 100µl on the target area of a gold screenprinted electrode which was held horizontally and connected to an Autolab electrochemical workstation programmed to perform the ASV analysis. The three mercury-containing urine samples all showed a pronounced stripping peak at approximately 0.375 V, the two urine samples lacking mercury showed no stripping peaks. ASV parameters were as

follows: deposition potential, 0.2V; deposition time, 30s; modulation time, 0.05s; interval time, 0.5s; final potential 0.7V; step potential, 0.00495V; modulation potential 0.04995V.

Example 9

Evaluation of alternative gold ink preparation methods

Gold preparations of three alternative formulations, varying with respect to encapsulant properties were used to fabricate the screen-printed 3-electrode assembly. Preliminary cyclic voltammetry investigations using 0.1mM hexacyanoferrate showed clear reversible electrochemical behaviour for all formulations (Figures 11-13). All sensors exhibited the expected symmetrical shape characteristic of a reversible redox reaction, with an increase in peak currents (I_p) with increasing scan rate (v). At low v (20 mV/s), the anodic to cathodic peak separation (ΔE_p) varied from approximately 100-130 mV for the 3 preparations studied. Similar measurements performed with a solid-state gold disk electrode yielded a peak to peak separation of 70 mV.

Using the slopes obtained from plots of anodic *I*p versus square root of scan rate ($v^{1/2}$) for 0.1mM ferrocyanide, the *Randles-Sevcik* equation was applied and the active surface areas were calculated as; 0.1255, 0.1287 and 0.1203 cm^2 for the three gold ink formulations studied. Comparing these values to the overall geometric area of the working electrode of 0.14cm^2 (0.7 x 0.2 cm), suggests *ca.* 85-90% of the printed gold surface is actively used for deposition. This suggests the gold ink has a high gold content, contaning a relatively low amount of co-formulants required for successful depositioning and curing of the gold structures.

Claims

1) A method of electrochemical stripping analysis comprising:

(a) causing an analyte element to be deposited from a solution onto a working electrode;

(b) causing the deposited element to be re-dissolved while monitoring the potential of the working electrode and optionally the electrical current also;

wherein said working electrode is a screen-printed electrode containing a solid noble metal as conductor;

characterised in that said electrode is printed using a printing composition containing noble metal particles in a curable resin composition free from metallic compounds other than the nobel metal itself. Specifically, the ink formulation is free of copper, bismuth, lead and compounds thereof.

2) A method according to claim 1 wherein said electrode is printed and cured at a temperature below 200°C.

3) A method according to claim 1 or claim 2 wherein said curable resin composition comprises one or more of epoxy resins, polyvinyls, polyacrylics, polyesters and polyurethanes or similarly chemically inert polymer.

4) A method according to any preceding claim wherein said printing composition contains no metallic species apart from said noble metal particles.

5) A method according to any preceding claim wherein said noble metal particles have sizes in the range 0.1-10μm.

6) A method according to claim 5 wherein said particles have sizes in the range 0.5-5μm.

7) A method according to claim 6 wherein said particles have sizes in the range 2-4μm.

8) A method according to any preceding claim wherein said noble metal is gold, platinum, palladium or a gold-silver alloy.

9) A method according to claim 8 wherein said noble metal is gold.

10) A method according to any preceding claim wherein the analyte is arsenic or a heavy metal.

11) A method according to any preceding claim wherein, in addition to said working electrode, there is a screen-printed reference electrode.

12) A method according to claim 11 wherein there is also a screen-printed counter electrode.

13) A method according to any preceding claim wherein the or each electrode is deposited on a non-conductive substrate.

14) A method according to any preceding claim which employs a technique selected from anodic stripping voltammetry, cathodic stripping voltammetry and potentiometric stripping analysis or derivations thereof.

15) Apparatus for carrying out a method according to any preceding claim comprising a plurality of screen-printed electrodes (10,12,14) whereof one is said working electrode (10), coupled to an electrochemical analysis operating system (34).

Abstract

Electrochemical stripping analysis employs screen-printed electrodes (10,12,14) including a working electrode (10) produced from a composition in which the conductive component is a noble metal (e.g. gold), preferably of particle size 2-4 μm, and the vehicle is based on a polymeric resin (e.g. epoxy, polyvinyl, polyacrylic, polyester or polyurethane). The formulation is such that there is no need for potentially-interfering metal species such as copper, lead and bismuth either in the free metrallic state or in the form of oxides. Furthermore it is curable at a low temperature (below 200°), allowing the use of plastic substrates.

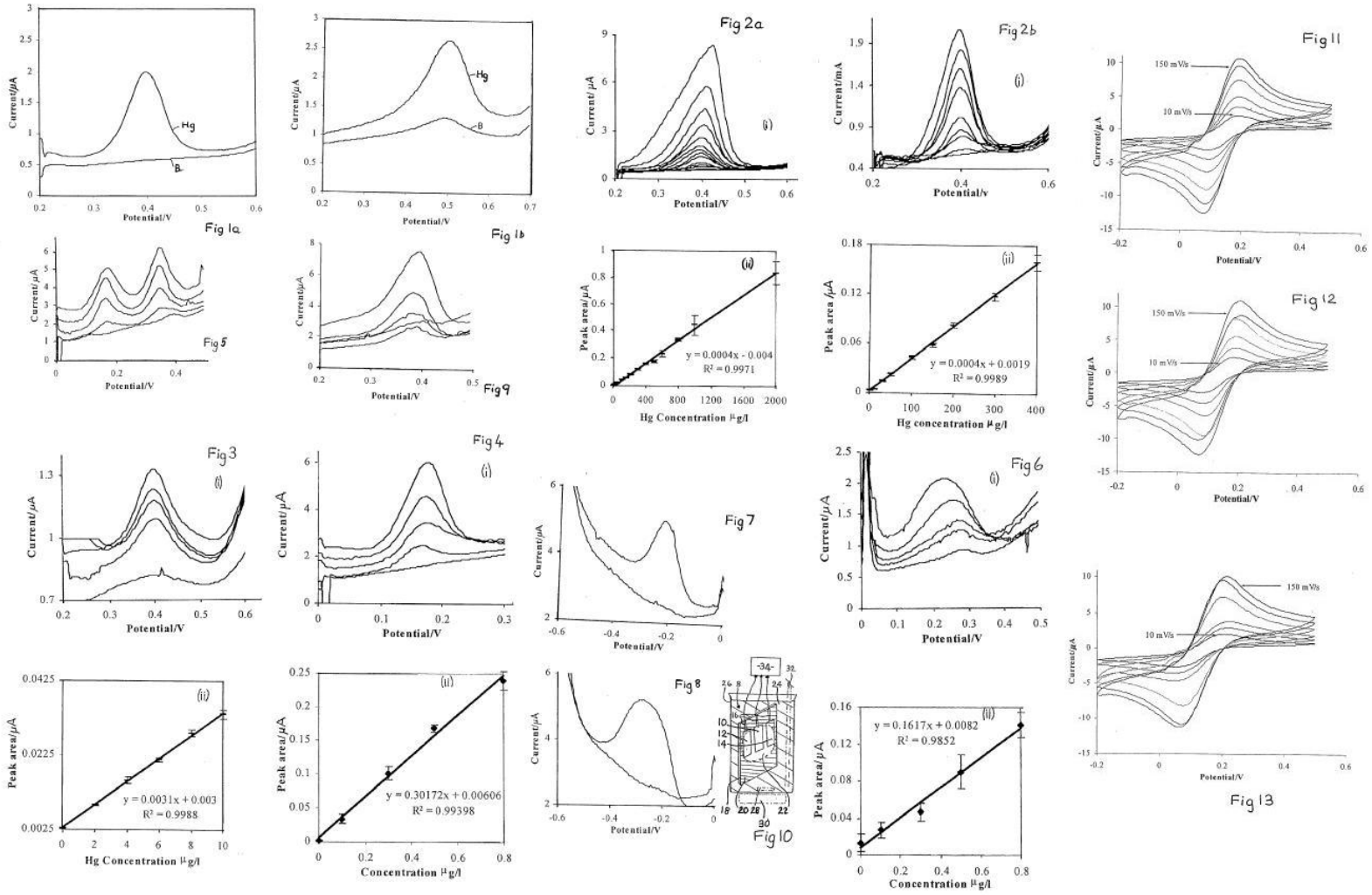
Fig 1a
Fig 1b
Fig 2a
Fig 2b
Fig 11
Fig 5
Fig 9
Fig 12
Fig 3
Fig 4
Fig 7
Fig 6
Fig 8
Fig 10
Fig 13
Potential/V
Current/μA
Hg
B
Peak area/μA
Hg Concentration μg/l
Concentration μg/l
y = 0.0004x - 0.004
R² = 0.9971
y = 0.0004x + 0.0019
R² = 0.9989
y = 0.0031x + 0.003
R² = 0.9988
y = 0.30172x + 0.00606
R² = 0.99398
y = 0.1617x + 0.0082
R² = 0.9852
150 mV/s
10 mV/s

A2. Matlab Script for Voltammetric Simulation

```
% quasi reversible peak simulation with fractional diffusion
%this is going to take a long time maybe 24 hours

%L = [0 0 0];
for epsilon = 1.5;
for ks =10^-6;
%A. (work within SI units)
%1. [R] J/Kmol ; [T] K ; [F] C/mol ;
R = 8.314; T = 297; F = 96485;
%2. [C] mol ; [D] m^2/s; [E] V; [v] V/s;


formal = 0;
Do = 7.63*10^-10; Dr = 6.32*10^-10;
gamma1 = (Do/Dr)^0.5;
alpha = 0.5;
scans = 4;
%ks = 0.00004;
ne = 1;
v = 0.05;
dE = 0.004;
Ei = -0.8; Ef = 0.8;
offset =  (0.5*(Ei+Ef)-Ei)+0.2;
Cri = 10^0;
Coi = Cri*exp(ne*F*(Ei-formal)/(R*T));
to = 0; tend = (Ef-Ei)*scans/v;
N = (Ef-Ei)*scans/dE;
A = 1.4*10^-5;
%3. [lambda] s;
lambda = (Ef - Ei)/v;
a = ne*F*v/(R*T);
psi = (gamma1^alpha)*ks/((pi*a*Do)^0.5);
delta = a*tend/N;
ns = a*lambda/delta;
X = zeros(round(N),8);chi =zeros(round(N),1);

for n = 1:N;
    y = delta*n;
    t = y/a;


    j = fix(n/ns); beta = factor(j+1);
    if beta(1) ~= 2; E = Ei + v*(t-j*lambda);
    Slambda = exp(a*(t-j*lambda)); end;
    if beta(1) == 2; E = Ei + v*((j+1)*lambda - t);
    Slambda = exp(a*((j+1)*lambda - t)); end;

    sgc = Slambda*gamma1*(Coi/Cri);
    mod = (delta/a)^(epsilon/2)*2*...
        ((pi*a)^0.5)/(epsilon*gamma(epsilon/2));
    denominator =((sgc^alpha)/psi) + mod*(1+sgc);

        if  n==1;
            chi(1) = 1/denominator;
            summ =1;
        elseif  n==2;
            numerator=1-mod*(1+sgc)*(2^(epsilon/2)-1)*chi(1);
            chi(n)=numerator/denominator;
            summ = 1;
        else
            summ = (n^(epsilon/2))*chi(1)-chi(n-1);
                for i = 1:(n-2);
                    summ = summ + ...
                        ((n-i)^(epsilon/2))*(chi(i+1)-chi(i));
                end;
            numerator=1-mod*(1+sgc)*summ;
            chi(n)=numerator/denominator;
        end;

    current = (-(10^6)*chi(n)*ne*F*A*Cri*(pi*Do*a)^0.5);

    X(n,1:8)= [n j E Slambda chi(n) sgc summ current];


end;

clear R T F Coi Cri Do Dr Ei Ef to tend N lambda
clear  gamma1 delta n y t j beta E Slambda numerator
clear denominator i sgc summ N chi A current

number = fix(length(X)/round(ns));
%find maxima and minima for forward and reverse scan
mx = zeros(number,3);
for i = 1:number;
m=((i-1)*round(ns))+1; n=i*round(ns);
%deficit in method here
mx(i,1:2) =[max(abs(X((m+ns/2):n,8)))...
    find(abs(X((m+ns/2):n,8))==max(abs(X((m+ns/2):n,8))))+m];
end; clear i m n
mx(:,3) = X((mx(:,2)+ns/2),3);
peakseparation = mx(3,3)-mx(4,3);
figure;
plot(X(:,3),X(:,8)); axis tight;
ylim([-1.1*mx(4,1) 1.1*mx(3,1)]);
string = (strcat('\DeltaEp=',num2str(peakseparation));...
strcat('k=',num2str(ks));...
strcat('\psi=',num2str(psi));...
strcat('\alpha=',num2str(alpha));...
strcat('n=',num2str(ne));...
strcat('v=',num2str(v)));
title(string);
%L = [L; psi peakseparation epsilon];
clear Z formal offset
end;
end;
%L(1,:) = [];
%semilogx(L(:,1),L(:,2),'.');
%ylabel('\DeltaEp V'); xlabel('\Psi');
clear dE a alpha ks psi string v ne
```

A3. Matlab Script for Electrode Surface Reconstruction

```
%data loaded as structural array 'BQ331', this data is loaded into a rank 3
%matrix, 'X', the first index is for image number, 1:32. The second and
%third are for the x-y information for each (binary) image
for i = 1:32;
    X(i,:,:) = (i/255)*double(BQ331(i).cdata);
end; clear i;

%%
%The single rank 2 matrix is designated 'F'
F = zeros(346,508);
%average of input data, selects each point indivually and runs through
%32 images, counting total vaue with 'c' and counting number of points with
%'d'
for i = 1:346;
for j = 1:508; c = 0; d= 0;
    for k = 1:32;

        Fk = X(k,i,j);
        if Fk ~= 0;
           c = c + Fk; d = d+1;  F(i,j)= c/d;
        end;

    end;
end;
end;
clear c d;

%%
%Interpolation for zero elements uses 24 nearest neighbours, no weighting.
%Does not interpolate zeros in outermost two rows/columns
for i = 3:343;
for j = 3:505;
    if F(i,j) == 0;
F(i,j)=(1/24)*(...
F(i-2,j-2)+ F(i-2,j-1)+ F(i-2,j)+ F(i-2,j+1)+ F(i-2,j+2)+...
F(i-1,j-2)+ F(i-1,j-1)+ F(i-1,j)+ F(i-1,j+1)+ F(i-1,j+2)+...
F(i,j-2)+ F(i,j-1)+ F(i,j+1)+ F(i,j+2)+...
F(i+1,j-2)+ F(i+1,j-1)+ F(i+1,j)+ F(i+1,j+1)+ F(i+1,j+2)+...
F(i+2,j-2)+ F(i+2,j-1)+ F(i+2,j)+ F(i+2,j+1)+ F(i+2,j+2)...
);

    end;
end;
end;
clear i j

%%
%smoothing algorithm uses 24 nearest neighbours
for i = 3:343;
for j = 3:505;

F(i,j) =(1/24)*(...
F(i-2,j-2)+ F(i-2,j-1)+ F(i-2,j)+ F(i-2,j+1)+ F(i-2,j+2)+...
F(i-1,j-2)+ F(i-1,j-1)+ F(i-1,j)+ F(i-1,j+1)+ F(i-1,j+2)+...
F(i,j-2)+ F(i,j-1)+ F(i,j+1)+ F(i,j+2)+...
F(i+1,j-2)+ F(i+1,j-1)+ F(i+1,j)+ F(i+1,j+1)+ F(i+1,j+2)+...
F(i+2,j-2)+ F(i+2,j-1)+ F(i+2,j)+ F(i+2,j+1)+ F(i+2,j+2)...
);

end;
end;
clear i j

%%
%Delete outer most rows/columns
F = F(3:343,6:505);
%%
%Surface dimension calculation
a = size(F);
S = mean(F(:));
for L = [5:5:80 100 140 160];
    b = fix(a/L);
    c = 0;
    d = [];
    for j = 1:b(1);
        for k = 1:b(2);
        d(j,k,:,:) = F((L*(j-1)+1):L*j,(L*(k-1)+1):L*k);
        s = mean(d(j,k,:));
        n = (squeeze(d(j,k,:,:)) - s).^2;
        n1 = sum(n(:))/length(n(:));
        c = c + n1;
```

```
81          c = c + n1;
82          end; clear k;
83      end; clear j;
84      W(L/5,1) = (c/(b(1)*b(2)))^0.5;
85      W(L/5,2) = L/1;
86      W(L/5,3) = b(1)*b(2);
87  end; clear i;
88
89  %%
90  %Surface map plotted in Matlab
91  %Application using orignal colour images to super impose a single in-focus
92  %image onto the 3D map
93   Fk = round(F);
94   V = zeros(324,464,3);
95   V = uint8(V);
96   for i = 1:28;
97       for j = 1:324;
98       for k = 1:464;
99               if Fk(j,k) == i;
100                 V(j,k,:) = BQ331colour(i).cdata(j,k,:);
101             end;
102      end;
103      end;
104  end;
105
106  clear j k i;
107  Vd = double(V) + 1; Vd = Vd/256;
108  surf(F,Vd*1.3,'linestyle','none');
109  zlim([0 50]); axis off; light; lighting gouraud; material dull;
110 %%
111
112  Y = zeros(332,476);
113 for i = 1:28;
114     for j = 1:332;
115     for k = 1:476;
116         if Y(j,k) ==0;
117            Y = Y + (double(BQ331(i).cdata));
118         end;
119     end;
120     end;
121 end;
122     clear i; Y = Y/255;
123 imagesc(Y); figure(gcf)
```

A4. Organo Metallic Ink

This experiment although yielding a reasonably important conclusion: that the commercial gold inks used in this study, the polymeric DuPont, Ercon and Gwent gold are not produced by this type of method. However, the experiment is quite involved and could be considered a detour from the main theme of the project.

Hostetler *et al.* (1998) showed that controlled sizes of gold nanoparticle could be achieved with alkanethiol encapsulation with sizes between 1.5 and 5.2 nm, equivalent of about 110 to about 4800 Au atom clusters with a 10 – 20 % deviation in size. The core sizes were determined by high-resolution transmission electron microscopy and small angle x-ray scattering. Further analytical techniques such as FTIR, FT NMR, MS, and XPS were used to probe the encapsulated particles which had ligands numbering about 53 to 520 per core. A dividing line between effectively flat self assembled monolayer (SAM) formation associated with planar gold surfaces and 3 dimensional SAM formation was found for core sizes about 4.4 nm, despite the relatively high radius of curvature at this size. Two factors determine the change in SAM bonding: (i) the number of surface defects is greater for smaller nano particles leading to a larger density of thiol bonding sites and (ii) the radius of curvature gives a decresing density in the alkane chains as they extend from the surface. Evidence for (ii) was shown using NMR by comparing neighbouring bond correlations. FTIR was used to study the alkane chain ordering (using methylene stretches about 2920 cm^{-1}), from 3D to 2D SAM, and the change at about 4.4 nm core size was noted, with greater ordering for larger cores. With XPS the Au(I) thiol bond with reference to the $Au_{f7/2}$ peak showed increased binding energy for the smaller clusters. The molecular Au-thiolate complex has a higher binding energy than the bulk gold thiolate complex. However, the bonding was mostly metallic. UV/vis spectroscopy showed metallic characteristics for the higher core sizes.

Huang *et al.* (2003), using the methodology of Hostetler *et al.* (1998) showed that the gold nano particles could be melted at temperatures lower than 200 °C down to a

minimum 120 °C producing continuous films of gold with resistance about 70 % of pure gold. The process was used to printed high conductivity patterns on plastic substrates using inkjet printers. The adhesion of the layers to PET sheets was reasonable, but dependent on the processing conditions. It was thought that some alkane thiols remained between the gold and the PET and deposition at temperatures close to thiol sublimation aided adhesion. Three distinct events were observed, for the thiol sublimation where the particles turned from black to gold colour, coalescence – forming a film and for good conductivity. Four thiol encapsulants were tested: dodecane-, octane-, hexane-, and butane- thiol. The thiol sublimation occurred at the lower temperature of 120 °C for butanethiol when 5 nm Au particles were encapsulated. In this case 120 °C was sufficient for coalescence and conduction. With 1.5 nm particles encapsulated with butanethiol 127 °C for sublimation and 133 °C for conduction was necessary. The authors report being able to print 1 µm thick tracks with excellent conductivity, with the encapsulated particles dissolved in toluene and the substrate maintained at elevated temperature to evaporate solvent quickly.

Evidently, this could be a powerful method for the design of printed electrodes, especially micro array applications. When discovered, it was thought that this method would account for the gold ink used by DuPont. So an effort was made to produce this type of ink following the procedure of Huang *et al.,* (2003) to be deposition on carbon screen-printed electrodes.

Reagents

All reagents, of analytic grade quality, were obtained from SigmaAldrich (Poole, UK) unless otherwise stated.

Method

The techniques and methods for organic chemistry preparation were made possible with the help of an associate G. Saint Pierre. In brief, nano particle preparation was as follows. 0.25 g gold salt ($HAuCl_3$), was dissolved into 25 ml HPLC water producing a

yellow solution after 10 min stirring. Separately 1.5 g tetraoctylammonium bromide was added to 80 ml of toluene and stirred for 5 min. The tetraoctylammonium bromide functioned as the phase transfer catalyst to carry the gold from the aqueous to organic phase via electrostatic interaction as shown in Figure 0.1 (A). The two solutions were stirred together for 40 min, then transferred to a separation funnel and shaken vigorously for 5 min. The aqueous phase was drawn slowly from the funnel. The organic phase was then removed and the aqueous returned to the funnel with 20 ml fresh toluene. The process was repeated three times to remove as much as possible of the gold from the aqueous phase indicated by the colour of the aqueous solution (yellow to clear with washing). The toluene phase had turned orange-brown. The toluene gold complex mixture was stirred for 10 min before the thiol encapsulant was added. Butanethiol was used in two ratios of gold:thiol – 12:1 (6.5 µl) and 1:4 (312 µl) expected to produce 5 and 1.5 nm particles respectively. To reduce the bulk gold from the trivalent state 0.38 g of sodium borohydride dissolved in 25 ml of HPLC water was added to the organic phase. Figure 0.1(B) shows the encapsulated particles. The aqueous phase was then separated from the organic phase very slowly (about 3 hr) in a funnel. The particles were then filtered from the toluene using a ceramic frit, filter paper and a bench top vacuum pump. The black/golden powders were washed with toluene and acetone. After air drying the particles were transferred to a beaker with 2 ml toluene ready for 'printing'.

Standard *in house* carbon (Electrodag 423 SS) screen-printed electrodes with reference strips (Electrodag 6038 SS) were used as substrates. An immunosensor design was used with circular working electrode area, for easier application of drops. Unfortunately the design chosen suffered from thin track design, so resistance was high. The particles in toluene were pipetted, 2-3 µl per drop, to the working electrode surface. The particles did not dissolve in the toluene so particulate densities were variable on application; increased densities were noticed near to drop edges. For other electrodes a paintbrush was used to apply the ink, although this result in some wastage by ink adsorption on to the bristles. The electrodes were fired at 140 °C for 30 – 60 minutes expected to be hot enough to sublimation the butanethiol, coalesce and render conductive both the 1.5 and 5 nm particulates according to Huang *et al.* (2003).

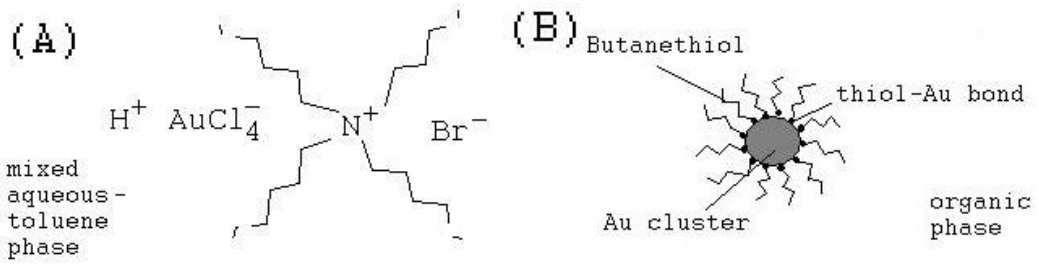

Figure 0.1 (A) The Gold salt and tetraoctylammonium bromide transfer agent in the mixed organic/aqueous phase; (B) the nanoclusters of gold encapsulated by butanethiol in the toluene phase

Results and Discussion

The Prepared films were studied under the microscope. The 1.5 nm showed clear continuous films, shown in Figure 0.2(A). The gold ink seems to have formed pools due to the surface roughness of the ink substrate allowing ridges of carbon to show through. In Figure 0.2 (B) the gold of the 5 nm was not so clear - the surface looks particulate, but 5 nm particles are well below the 0.3 µm limit for visible light – a higher resolution technique such as SEM would be needed to check for indication of melting.

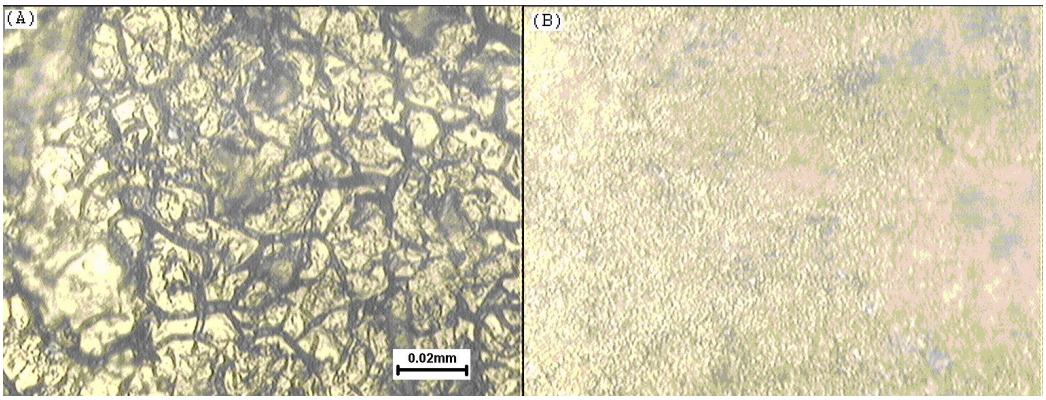

Figure 0.2 Electrode surface after application of (A) 1.5 nm gold particles; (B) 5 nm gold particles

The quality of adhesion was variable some flaking was noticed. Electrodes were sonicated in methanol removing a portion of the gold swiftly indicating improved adhesion would be needed.

The electrodes were subjected to electrochemistry. 1 mM potassium ferrocyanide in 0.1 M NaCl electrolyte was used to test the electroactivity. In hindsight it was realised that the impedance was > 10 kΩ: resistance correction, increase scan range or reduced ferrocyanide concentration should have been used. Figure 0.3 shows that the gold is electroactive. The electrodes were tested in 500 ppb of As(III) and Hg(II) in 4 M HCl with the standard DPASV procedure. As shown in Figure 0.4, two small peaks (<1 μA) appear near to the expected peak potentials for As and Hg. The bare carbon shows a peak 0.1 to 0.2 V, not expected for As(III). It is doubtful that this peak is As(III) since accumulation of trivalent arsenic on carbon is weak. The peak 0.3-0.4 V could be Hg(II). However the peak is small for 500 ppb concentration. The peak pattern has some resemblance to the primary and secondary interference peaks seen with the DuPont sensors in 4 M HCl (for example compared with Figure 4.10B). The background values for the gold covered surfaces were much larger than the carbon only surfaces (not shown).

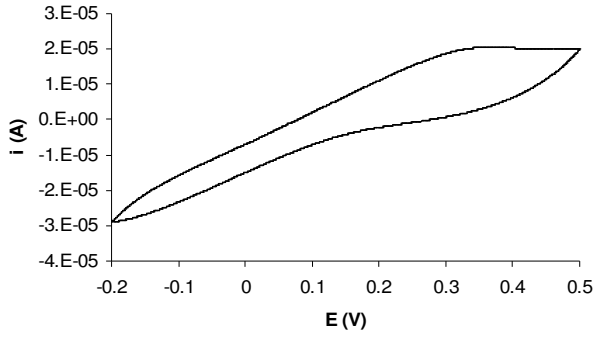

Figure 0.3 1.5 nm particle prepared electrodes with 1 mM potassium ferrocyanide in 0.1 M NaCl at 50 mV/s

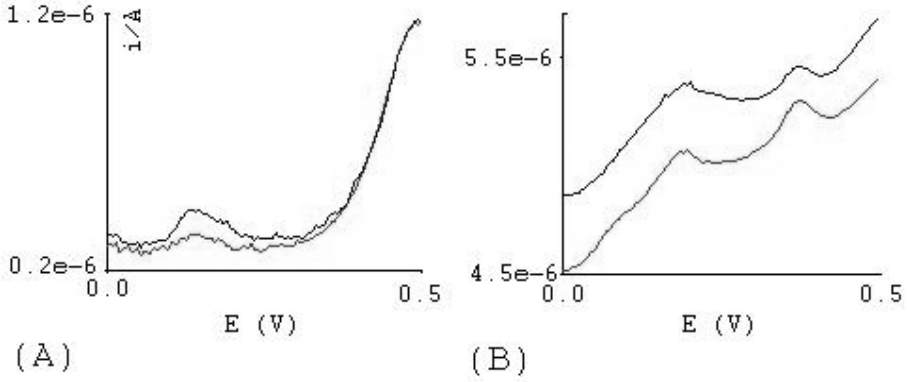

Figure 0.4 Electrodes tested in 500 ppb As(III) and Hg(II) in 4 M HCl tested: (A) on bare carbon and (B) 1.5 nm gold particle modified carbon electrodes, 2 examples for each

Conclusions

A more detailed investigation could be pursued to tests curing conditions and gold prepareation. Evidently improvements could be made directly to the assessment of the gold surfaces such as selecting low impedance tracks and further controlled experiments with As and Hg. However, several issues surrounding the method are clear. A more fundamental issue, is that the encapsulated particles in toluene either need to be dissolved properly or a thickening agent added to provide a uniform dispersion. Also, the adhesion was not stable enough, with flaking seen, more development would be needed. As shown in Figure 3.18, A microscopic view of the DuPont sensor shows that these sensors were constructed with particulate (about 1 μm diameters) material, as opposed to a melted layer. In retrospect the usual mode of screen-printing involves a micro powder dissolved in a viscous resin (Gilleo, 1996) confirms this view. Although the nano particle technique is novel, investigating the methods of screen-printing gold formulations are going to improve the understanding of the DuPont sensors.